HOW TO MEND A BROKEN HEART: MASSIVE ENDOCYTOSIS AND THE ROLE OF LIPIDIC FORCES IN MEMBRANE TRAFFICKING

APPROVED BY SUPERVISORY COMMITTEE

Stephen C. Cannon, M.D., Ph.D., Committee Chair

Donald W. Hilgemann, Ph.D., Advisor

Helen L. Yin, Ph.D., Program Chair

P. Robin Hiesinger, Ph.D.

Joseph P. Albanesi, Ph.D.

DEDICATION

For my family:

For wonderful daughter Helaena, who constantly reminds me of the beauty of science

For beautiful son Logan, who constantly reminds me of the complexity of science

For my lovely wife Christina, who constantly reminds me to graduate

For my Mom, who constantly reminds me her son is a doctor now

For my Dad, who I am constantly reminded of and miss dearly

HOW TO MEND A BROKEN HEART: MASSIVE ENDOCYTOSIS AND THE ROLE OF LIPIDIC FORCES IN MEMBRANE TRAFFICKING

by

MICHAEL FINE

DISSERTATION

Presented to the Faculty of the Graduate School of Biomedical Sciences

The University of Texas Southwestern Medical Center at Dallas

In Partial Fulfillment of the Requirements

For the Degree of

DOCTOR OF PHILOSOPHY

The University of Texas Southwestern Medical Center at Dallas

Dallas, Texas

November, 2011

Acknowledgements

Without argument, the contributions made to my dissertation and life could not be understated without mentioning my mentor and friend, Dr. Donald Hilgemann. His patience, understanding and constant desire for exploration reminded me how wonderful science can be. He can remember every single experiment ever done and immediately help you make it better. His shear dedication to science and discovery and caring nature provides incentive to all he meets to become better at what they do and strive to bring answers to this complicated world.

I would also like to thank my committee members Drs. Joseph Albanesi, Stephen Cannon, Helen Yin, and Robin P. Hiesinger. Dr. Albanesi constantly reminded me of the fun in science and brought an inspired a sense of awe in his ability to consolidate a treasure trove of literature. Dr. Cannon for his insights and keeping me from being stranded in Baltimore. Dr. Yin for always supporting and believing in me. Dr. Hiesinger to whom I could not have made it without. His coffee and advice single handedly kept me sane. His scientific prowess kept me grounded. His friendship kept me smiling and his openness to share his lab and expertise remind me of why science works.

Finally, I would like to thank my colleagues over the years. Dr. Alp Yaradanakul taught me everything and continues to inspire. Drs. Vincenzo Lariccia and Simona Magi, our Italian brethren, made our lab a family. Chengcheng Shen and Marc Llaguno for all their love and work. Sherry, Naomi, Victor, Hao-Ran, Andre, as well as Ryan, Adam, Dong and everyone else in Robin's lab were all a part of my close academic family. To Linda Patterson, our admin, if ever there were someone to slap my wrist with a ruler it would have to be her. Most important, Mei-Jung "Susan" Lin was the key to my successfully completing my doctorate. Nothing would have been accomplished without her skills at the bench. Her compassion and kindness are unmatched and if all others mentioned were members of my second family, Susan will forever be my second Mom and this thesis is as much hers as mine.

HOW TO MEND A BROKEN HEART: Massive Endocytosis and the Role of Lipidic Forces in Membrane Trafficking

MICHAEL JON FINE, Ph.D.

The University of Texas Southwestern Medical Center at Dallas, 2011

Advisor:
DONALD W. HILGEMANN, Ph.D.

Novel forms of membrane internalization defined as massive endocytosis (MEND) were characterized for mechanism and physiological significance in isolated cells and intact cardiac tissue. These non-canonical forms of membrane trafficking are related to perturbations within the outer lipid monolayer of the plasmalemma or through coupled calcium-mediated fusion and phosphatidylinositol 4,5-bisphosphate (PIP_2) signaling. Both forms of MEND do not rely on classical endocytic proteins such as clathrin or dynamin and appear independent of the cytoskeletal or extracellular matrix. A hypothesis emerged implicating lipidic driven processes as the mechanistic basis of MEND. One explanation involves lipid domain formation with excessive inward curvature from rapid accumulation of PIP_2 within the inner monolayer subsequent to

large calcium transients. Alternatively, perturbation of the outer monolayer through amphipathic detergents or modulation of lipid content also promotes inward curvature of the membrane leading to massive endocytosis. Electrophysiological and optical methods support MEND preferentially internalizing membrane of liquid-ordered (*Lo)* domains leading to the potential selection of certain proteins and markers due to physiological segregation into their respective energetically favorable domains. MEND demonstrates that lipidic reorganization of the membrane may be sufficient for rapid and selective internalization of the plasma membrane. The implications of such a novel form of endocytosis could dramatically impact numerous physiological and cellular activities. In cardiac pathologies, short-term changes in the surface membrane expression of vital ionic transporters have been implicated in hypertrophy, atrial defibrillation, and damage post myocardial ischemia. It is possible that the properties underlying MEND mechanics may be responsible for some of these acute cardiac changes. Protocols that induce massive endocytosis were performed on isolated cardiac myocytes with similar results described in the fibroblast cell lines. MEND occurs in cardiomyocytes with calcium transients. MEND also occurs upon isolation of myocytes without stimulation. While this indicates that MEND does occur in primary cells, protocols to mimic MEND in intact cardiac tissue have remained inconclusive. Cellular processes during the isolation procedures cause dramatic changes in the membrane of cardiac myocytes. Subsequently, it is likely isolated cardiomyocytes have distinct differences from unstressed intact tissue. MEND may still occur in cardiac tissue as well as other physiological systems and newer protocols to monitor membrane movements in intact tissues are currently being investigated.

Table of Contents

Prior Publications

Hilgemann, D.W., and M. Fine, 2011. Mechanistic analysis of massive endocytosis in relation to functionally defined surface membrane domains. *Journal of General Physiology* 137:155-172.

Fine, M., M.C. Llaguno, V. Lariccia, M.-J. Lin, A. Yaradanakul, and D.W. Hilgemann, 2011. Massive endocytosis driven by lipidic forces originating in the outer plasmalemmal monolayer: a new approach to membrane recycling and lipid domains. *Journal of General Physiology* 137:137-154.

Lariccia, V., M. Fine, S. Magi, M.-J. Lin, A. Yaradanakul, M.C. Llaguno, and D.W. Hilgemann, 2011. Massive calcium-activated endocytosis without involvement of classical endocytic proteins. *Journal of General Physiology* 137:111-132.

List of Figures, Tables, and Appendix

List of Abbreviations and Symbols

alkyl-TPP	alkyltriphenylphosphonium
AP2	adapter protein 2
AMP-PNP	adenylyl imidodiphosphate
ATPγS	adenosine 5′-[γ-thio]triphosphate
BEL	bromoenol lactone
BMCD	β-methylcyclodextrin
C4TPP	butyltriphenylphosphonium
C6TPP	hexyltriphenylphosphonium
C10TPP	decyltriphenylphosphonium
C12TPP	dodecyltriphenylphosphonium
Ca_v	voltage gated calcium channel
CCCP	carbonyl cyanide m-chlorophenylhydrazone
CLIC	clathrin and caveolin independent endocytosis
C_m	membrane capacitance
CsA	cyclosporine A
DAB	diaminobenzidine
DDG	dodecylglucoside
DDM	dodecymaltoside
DFMO	α-difluoromethylornithine
DMSO	dimethylsulfoxide

DPA	dipicrylamine
DTPT	ditridecylphthalate
EDA	ethylenediamine
GFP	green fluorescent protein
GTPγS	guanosine 5′-[γ-thio]triphosphate
GP	guinea pig
GUV	giant unilamellar vesicles
HMDS	hexyltriphenylphosphonium
HPCD	hydroxypropyl-β-cyclodextrin
HRP	horseradish peroxidase
L_d	liquid disordered
L_o	liquid ordered
LPC	lysophosphatidylcholine
MEND	massive endocytosis
MUNC	mammalian homologue of the unc-18 gene
Na/K ATPase	sodium potassium pump
NBD-PE	7-nitrobenzo-2-oxa-1,3-diazole phosphatidylethanolamine
NCX	cardiac sodium calcium exchanger
NFA	niflumic acid
NP-40	tergitol
NEM	N-ethylmaleimide
NTA	nitrilotriacetic acid
PC	phosphatidylcholine

PE	phosphatidylethanolamine
pHl	pHluorin
PI	phosphatidylinositol
PIP_2	phosphatidylinositiol-bis 4,5-phosphate
PH	pleckstrin homology domain
PMCA	plasma membrane calcium ATPase
PS	phosphotidylserine
SDS	sodium dodecylsulfate
SMase	sphingomyelinase
SNARE	soluble *N*-ethylmaleimide-sensitive factor attachment protein receptor
Syb	synaptobrevin
Syt	synaptotagmin
Syx	syntaxin
TMA	tetradecyltrimethylammonium
TtPP	tetraphenylphosphonium
TX100	Triton X-100

CHAPTER 1 – GENERAL INTRODUCTION

1.1 - THE PLASMA MEMBRANE

One of the fundamental requirements for life is the ability to safely interact with the environment while simultaneously controlling and maintaining internal systems. One of the earliest adaptations to maintain such internal balance with the outside environment had to be a selective semi-permeable membrane. This membrane would allow entry of desired factors such as nutrients and essential elements while blocking unwanted factors from gaining access. Additionally, membranes allowed for the origins of communication by allowing secretion of signaling elements into the outside environment and, likewise, the selective detection of these factors from other cells. This primitive barrier eventually evolved to an organelle used by all living cells known as the plasma membrane.

MEMBRANE COMPOSISTION

The modern plasma membrane is composed of a lipidic bilayer primarily consisting of phospholipids defined by a hydrophobic fatty acid tails and polar hydrophilic phosphate heads (Fig. 1). These lipids arrange themselves so that the polar heads face the outside and inside environment while the oily tails face each other forming a semi-porous bilayer barrier. In addition to phospholipids, eukaryotic plasma membranes contain a rich assortment of other compounds that have specificity for the inner or outer membrane. (Kennedy et al., 1966) For example, sphingolipids, glycolipids, and the phospholipid phosphatidylcholine (PC) populate the outer monolayer; while

phosphotidylinositols (PI) and some phospholipids like phosphatidylethanolamine (PE) and phosphatidylserine (PS) prefer the inner monolayer. (Cooper and Hausman, 2009) While there is variety from cell type to cell type, typically plasma membrane lipid composition can contain about 40% phospholipid, 30% cholesterol, 20% sphingolipids, and 5% glycolipids. (Zachowski, 1993) (Fig 1.1)

Residing amongst the lipids, the plasma membrane contains up to 50% protein. (Singer and Nicolson, 1972) These proteins have many functions such as allowing cells to migrate or attach, participate in fusion, and allow signaling both internally and cell to cell. However, one of the most important functions of membrane proteins is their ability to regulate the permeability of the membrane to various ions, nutrients, and other essential compounds. These membrane transport proteins are essential for maintaining the ion gradients required in cell signaling. (Hille, 2001) Gradients can then be used in the transport of additional ions and molecules across the membrane barrier or for establishment of the membrane potential, an electrical gradient essential to functions like synaptic transmission, muscle contraction and cellular secretion. (Alberts, 2002) Typical physiological ionic concentrations of a cell at resting potential (-80 mV) can be seen in Table 1.

PHYSIOLOGICAL ROLE OF PLASMA MEMBRANE

A prime physiological example of the role membrane transporters perform is in the regulation of calcium signaling in the heart. (Bers, 2001) Calcium is the key signaling element in the excitation-contraction coupling of cardiac myocytes. As seen in Table 1, calcium concentrations at rest are maintained at an extremely low concentration with a ration of concentrations inside and outside of the cell at nearly 1:10,000. Therefore even when a small amount of calcium gains entry through the sarcolemma, the

cardiac plasma membrane, the cell can utilize this signal to initiate the process that allows the heart to contract. Mishandling of calcium is a central to cardiac contractile dysfunction and pathophysiological heart failure. (Bers and Despa, 2006) When the heart receives an electrical signal, a shift in the membrane potential allows for the opening of voltage-gated calcium channels (Ca_v). Allowing rapid flux of calcium into the cell due to the large calcium gradient across the sarcolemma. This causes further calcium release from internal calcium stores and initiates contraction. However, the cell must rapidly return to is resting state and remove excess cytosolic calcium. While much of the calcium is pumped back into the intracellular stores, up to 30% of the free calcium is extruded through the membrane antiporter Sodium Calcium Exchanger (NCX). NCX works using the Na gradient. (Moore et al., 1993) NCX has two transport modalities consisting of a major and two minor modes for extruding calcium. (Kang and Hilgemann, 2004) The major mode permits NCX to transport three sodium ions from the outside of the cell to travel across the concentration gradient into the intracellular space and provides the free energy required to transport one calcium ion against its concentration gradient from the cytosol back into the extracellular space. This results in a net loss of calcium inside the cell and facilitates the reduction of free cytosolic calcium back to its resting concentrations allowing the myocyte to prepare for additional excitation contraction cycles. However, in order for NCX to utilize sodium gradients to extrude calcium, the cell must establish a sodium gradient where concentrations of sodium are maintained lower inside then outside of the sarcolemma. To fulfill this requirement another membrane transporter called the sodium potassium pump (Na/K ATPase) is required. Na/K ATPase provides active transport utilizing the energy released from hydrolysis of ATP to force sodium and potassium against their concentration gradients across the membrane. (Hilgemann et al., 2006; Kang et al., 2003) Maintenance of these ion gradients is paramount to the function of other membrane transporters like NCX and

establishment of physiological calcium levels and excitation-contraction. (Fig. 1.2) Without the plasma membrane barrier and the proteins involved in transmembrane molecular transport, principal cellular functions would cease to function. (Bers and Despa, 2006)

1.2 - MEMBRANE TRAFFICKING

As the environment and cellular conditions change, so to must the cellular membrane and its components. When cellular membranes are damaged they must move large amounts of plasma membrane in order to reverse the damage and prevent cellular lysis. Membrane trafficking also serves to control and regulate surface proteins. As requirements for nutrients shift, or when changes occur in the extracellular environment, cells must respond with corresponding changes in membrane transporter function and quantity. There has been a long history toward exploring different cell signaling pathways that regulate the activity of surface transporters, (Huang et al., 1998) however the regulation of how long a protein actually resides in the surface membrane as a function of altering its activity has only recently been explored. One of the problems with exploring membrane resident proteins is due to their varied half-lives ranging from minutes to days. (Benito et al., 1991; Egner and Kuchler, 1996; Egner et al., 1995; Heda et al., 2001) These proteins are either marked for degradation through typical ubiquitination processes (Egner and Kuchler, 1996) or undergo more rapid surface expression regulation through the processes of membrane insertion and retrieval. The movement of membrane and membrane proteins occurs via the action of outward moving exocytosis and inward driven endocytosis.

EXOCYTOSIS

Exocytosis occurs as new membrane from internal vesicles fuses to the plasma membrane. Fusion requires vesicle and plasma interaction between the two lipid bilayers, which is not considered an energetically favorable event on its own. (Markin and Albanesi, 2002) Due to the complexity of bilayer fusion mechanics and the need for precise timing and control of how membranes and proteins are targeted, fusion of vesicles to the membrane requires the assistance a superfamily of highly conserved eukaryotic proteins called SNARE (soluble *N*-ethylmaleimide-sensitive factor attachment protein receptor) proteins. (Jahn et al., 2003) Proteins like Synaptotagmin (Syt) utilize small increases in intracellular calcium as a signal for vesicle fusion and allow transmembrane proteins on the vesicles like synaptobrevin (Syb) and plasmalemma proteins SNAP-25 and syntaxin (Syx) to interact and allow for favorable fusion between the two bilayers. (Rizo, 2003)While much of exocytosis can be described through these SNARE mediated processes, the explanation of all the potential calcium sensors and proteins involved, as well as the biophysical interaction between the bilayers, is still actively being modeled and explored. (Chapman, 2008) (Fig. 1.3)

ENDOCYTOSIS

While exocytosis is the fundamental process allowing the outward movement of membrane, its opposing force, endocytosis, is of equal importance in the regulation of the plasmalemma. Endocytosis is the process in which the cell retrieves excess membrane, engulfs soluble extracellular molecules, recycles secretory vesicles, and internalizes membrane proteins to effect cell signaling or control membrane transporters. (Goldstein et al., 1979) The movement of lipids and membrane proteins through endocytosis is

required for cell motility, proper synaptic function in neurons, immune responses, autophagy, and cellular wound response. (Bretscher, 1984; Idone et al., 2008; Tam et al., 2010; Taylor et al., 2005; Zhang et al., 1998) The standard paradigm states that endocytosis is subdivided into four categories: clathrin-mediated endocytosis, caveolae, phagocytosis, and macropinocytosis. (Doherty and McMahon, 2009) In clathrin-mediated endocytosis, an area of the plasma membrane forms a small approx. 100nm pit of negative curvature (towards the cell lumen). This pit is coated with a clathrin coat complex thought to stabilize the membrane in an invaginated energetically unfavorable negative curvature. The clathrin-coated vesicle then incorporates the GTPase dynamin that forms a ring around the neck of the vesicle and upon hydrolysis the complex severs the vesicle free from the plasma membrane resulting in endocytosis. (Mukherjee et al., 1997)

Like clathrin, caveolin forms a cage-like structure surrounding an invaginated lipidic stalk. One of the key differences is that caveolin dependent endocytosis is linked to a form of lipid specificity. Caveolae are formed with the recruitment of individual caveolin proteins to cholesterol and dense protein rich membrane domains known as "lipid rafts". The rafts are theorized nano-scale compartmentalized domains in the plasmalemma enriched in cholesterol, sphingomyelin, and glycosyl-phosphatidyl-inositol anchored proteins. (Anderson, 1993) Caveolin sequesters this region of the membrane into coated pits and primes it for internalization. While caveolin coated vesicles are smaller then clathrin-mediated endocytosis (50-80nm in diameter), caveolin is thought to stabilize the pit allowing for dynamin hydrolysis and internalization in the same manner as clathrin. (Parton et al., 1994)

Unlike caveolae and clathrin-mediated endocytosis, phagocytosis and macropinocytosis involve internalization of large vesicles usually over 500 nm in

diameter. Phagocytosis is a receptor-mediated engulfment of large extracellular particles requiring sizeable amounts of energy in the form of ATP hydrolysis and dramatic changes in cytoskeleton. (Aderem and Underhill, 1999) This form of endocytosis in commonly seen in the immune system where white blood cells, or phagocytes, engulf of foreign bodies and bacteria for degredation. Macropinocytosis involves the movement and internalization of highly ruffled regions of the plasmalemma. A large pocket is formed when filopodia-like extensions of the membrane fold in over themselves creating large invaginations of the membrane and internalization of the membrane. (Swanson and Watts, 1995) Like phagocytosis, macropinocytosis in an energy-extensive process and requires dynamic changes in the cellular cytoskeleton and extra-cellular matrix. (Fig. 1.4)

NON-CANONICAL ENDOCYTOSIS

Recently, work has started to question the standard dogma of the four categories of endocytosis. Mutations in dynamin that block its GTPase activity do not prevent all forms of small vesicle endocytosis. (Xu et al., 2008) Additionally, membrane can internalize in potassium free conditions and after disruption of adapter protein 2 (AP-2) complexes; both of which are required for clathrin and caveolae mediated endocytosis. (Altankov and Grinnell, 1995; Ivanov, 2008) There are some forms of viral infection that utilize unknown forms of endocytosis to gain entry into cells. The mechanism by which HIV-1 typically infects $CD4^+$ T cells involves a process of receptor-mediated fusion of the viral envelope the plasma membrane. During *in utero* transmission of HIV-1 from mother to fetus, HIV-1 must cross the highly protective placental barrier. This barrier is composed of specialized epithelial cells that lack $CD4^+$ expression and cannot internalize the virion by standard mechanisms. Even without the typical tools required for infection, placental epithelium still massively internalizes the virion and traffics the infecting

particles to endosomal compartments. (Vidricaire and Tremblay, 2007) While the mechanism of internalization is unknown it is characterized by some of the same features most forms of non-canonical endocytosis exhibit; large-scale, cholesterol dependent endocytosis that is independent of the adapters clathrin, dynamin, caveolin, and some cytoskeleton components. Since the phenomena of non-canonical endocytosis, which in some systems may amount to 30% of small vesicle endocytosis, cannot be classified under the classical categories of endocytosis, they have been dubbed "CLIC" or clathrin and caveolin independent endocytosis. (Mayor and Pagano, 2007)

CALCIUM AND ENDOCYTOSIS

The notion that calcium has a significant role to play in endocytosis has been demonstrated for over 15 years. Observations in the field of membrane fusion have demonstrated that progressively larger Ca transients lead to progressively increasing endocytic responses. (Engisch and Nowycky, 1998; Smith and Neher, 1997; Thomas et al., 1994) This results in "excessive" endocytosis in which the amount of membrane internalized exceeds the amount of membrane brought to the surface such that the surface area of the cell returns below basal pre-stimulation levels. During fertilization, large sustained calcium signals lead to endocytic events and the complete internalization of surface Calcium-ATPase (PMCA) pumps that typically extrude excessive intracellular free calcium. (Bi et al., 1995; El-Jouni et al., 2008) A more generalized biological process involves a cellular stress response known as cell "wounding". During membrane rupture, the cell is flooded with excessive calcium normally kept outside the cell through the activity of membrane transporters and the impermeability of the cell membrane to calcium. (Idone et al., 2008) The cell responds to this "wound" by fusion of internalized membranes to the cell surface followed by a large internalization of the lesioned membrane. Additionally, typical endocytic compartments are internalized into acidified

compartments, however during cellular wound response, the internalized compartments are not acidified. (Cocucci et al., 2004) It is likely that calcium has many targets that could lead to non-canonical forms of endocytosis in physiological processes but the underlying mechanistic basis of adapter independent and calcium-dependent bulk endocytosis had previously failed to be demonstrated.

LIPID AND LIPID RAFT ENDOCYTOSIS

Calcium is not the only driving element that has been implicated in non-canonical forms of endocytosis. Lipidic forces and changes in the plasmalemma have the potential to drive internalization of membranes through various means. Lipids themselves have a variety of shapes that can lead to forces that promote membrane curvature. (Sprong et al., 2001) The hydrophobic fatty acid tails of lipids can be very linear as in the case of saturated lipids where no carbon double bonds are present. Likewise, unsaturated acyl tails like arachidonyl moieties have four double bonds creating tail movement and larger diameter hydrophobic regions. The hydrophilic heads of lipids also contribute to their shape. Polar heads of phosphatidylethanolamine have much smaller diameters than sphingolipids or phosphatidylcholine. (See Fig. 1.5) Localization of these lipids to either side of the membrane or at specific regions laterally can amplify their individual shapes and induce membrane curvature. (Vicogne et al., 2006) For instance, PIP_2 has a large anionic polar head and resides primarily on the inner monolayer. It is hypothesized that aggregates of this lipid may implicate dramatic shifts toward luminal curvature of the membrane. (Cremona et al., 1999; Liu et al., 2009)

Specific membrane organization of lipids is also central to the theory of lipid "raft" endocytosis. Lipid rafts are microdomains within the plasma membrane that are enriched in cholesterol and sphingolipids. (Simons and Ikonen, 1997) They are thought to be involved in the lateral compartmentalization of lipids and proteins at the cell surface. Lipid rafts were first defined based on membrane regions resistant to extraction by high concentrations of Triton X-100. (Heerklotz et al., 2003) It was assumed that these detergent-free regions were highly ordered and prevented the detergent from interchelating the individual lipids. The theory of potentially unique regions within the plasma membrane led to the hypothesis that membranes may be laterally compartmentalized. (Lingwood and Simons, 2010) Some of the first evidence supporting the raft hypothesis came from studies using artificial giant unilamellar vesicles (GUVs). It was observed that GUV's containing mixtures of phospholipids, sphingomyelins, and cholesterol spontaneously form two distinct phases; liquid disordered (*Ld*) and liquid ordered (*Lo*) states. (Veatch and Keller, 2003) The *Ld* phase is composed of highly flexible and mobile components such as unsaturated phospholipids while the *Lo* phase is characterized by its enrichment of highly packed sphingolipids, cholesterols, and saturated phospholipids. Movement within ordered domains is restricted. (Anderson and Jacobson, 2002; Mayor et al., 1994; van Meer et al., 2008) It is thought that lateral forces within these domains along with curvature created from the organization of similarly packed lipids may lead to lipid budding and decreased energy needs required for endocytosis. Model membranes like those within the GUV support the raft hypothesis, however there have been difficulties characterizing these domains *in-vivo*. The artificial domains formed in GUVs are quite large and most research on raft-induced endocytosis indicates that the membrane internalized is similar to small vesicle caveolin induced endocytosis with diameters of 60 nm or less. (Mukherjee and Maxfield, 2004) Additionally, lipid diffusion studies within biological membranes have not shown much

evidence supporting large scale changes in lateral movement of these molecules as would be indicated in the raft theory. High concentrations of Triton X-100 used to isolate lipid rafts may not be revealing distinct domains within a biological membranes but in fact creating these domains by causing lipids and proteins to aggregate into large clusters that would normally exist as much smaller dynamic domains. (Maxfield, 2002) This has led to a more refined theory involving small clusters of *Lo* and *Ld* domains that upon stimulation aggregate, inducing negative curvature toward the cell lumen facilitating endocytosis. (See Fig. 1.6) While most recent work has focused on this relationship and the known endocytic adapter caveolin, (Coskun and Simons, 2010) there still remains an enigmatic segment of adapter-independent lipid raft endocytosis.

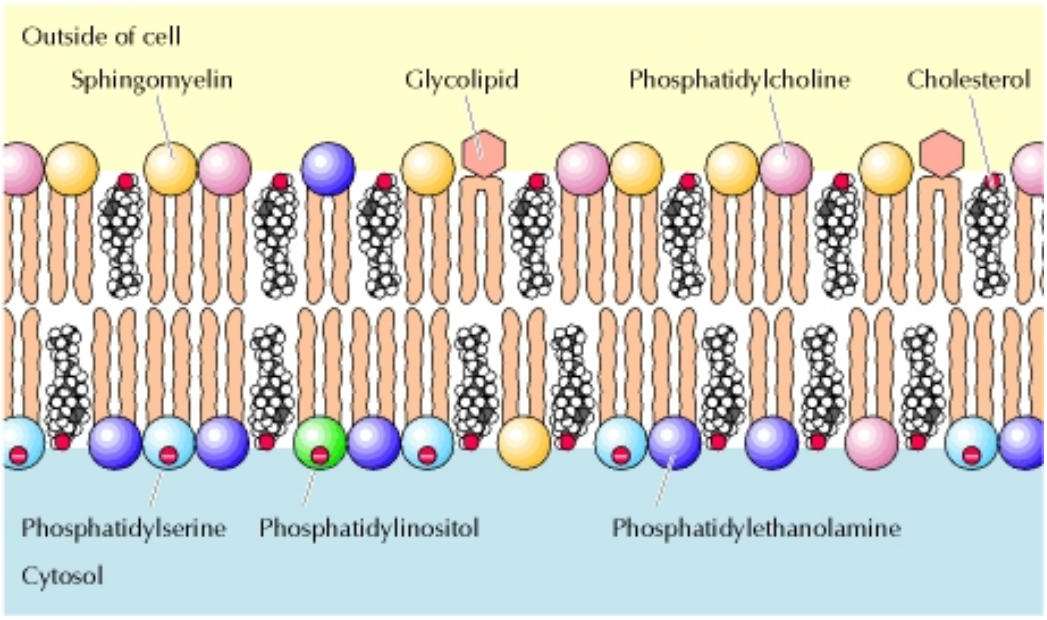

Fig. 1.1 Composition of Plasmalemma. The lipid bilayer that separates the inside and outside environment of a cell is a heterogeneous mixture of lipids. In the plasmalemma, the composition of the leaflets can be quite different with some lipids like sphingomyelin (SM), glycolipids, and PC preferring the outer leaflet, while anionic lipids like PS, PI and PE residing in the inner leaflet. The anionic composition of the inner leaflet creates a net negative charge to the inner monolayer. (Figure 12.2 of The Cell: A Molecular Approach, 2nd edition, (Cooper and Hausman, 2009))

Ion	Plasma (Extracellular)	Cytosolic
Na	130-150	20-40
K	3.5-4.2	130-145
Mg	0.8-1.4	4-20
Ca	2.1-2.7	<0.001
Cl	98-110	50-60
HCO_3	23-31	4-12

Table 1. Biological Ionic Concentration in Millimolar

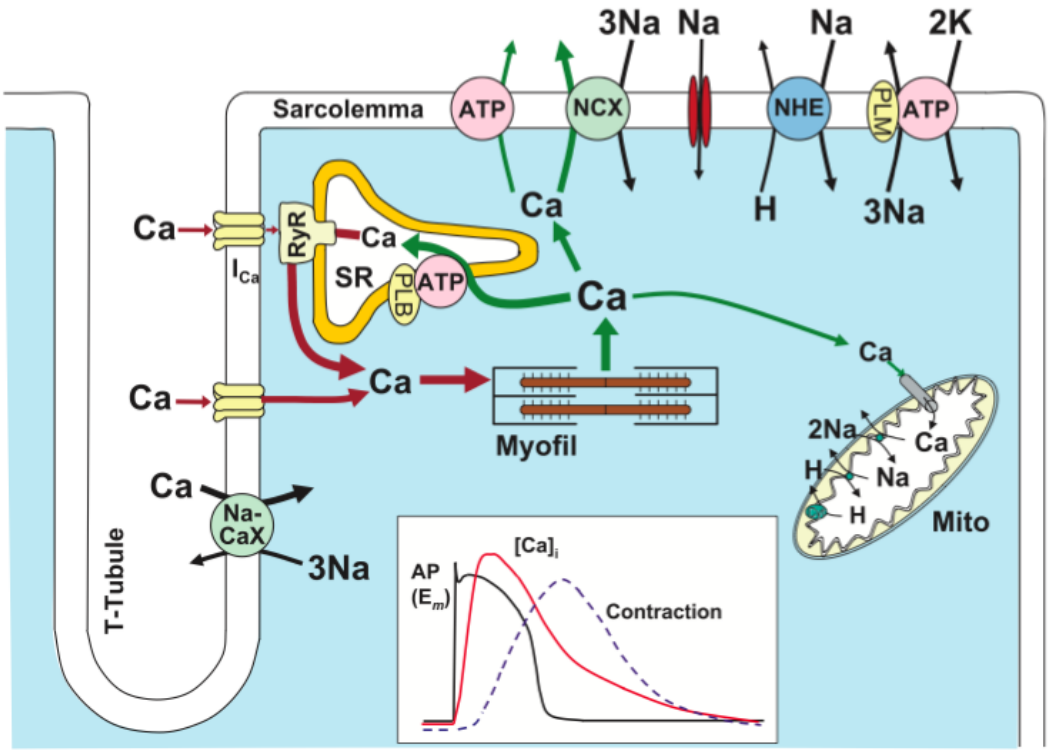

Fig 1.2 Ionic transport across the cardiac sarcolemma. Ion gradients are established against the cardiac plasma membrane in order to facilitate signaling during excitation-contraction in the heart. Membrane transporters like Ca_v, Na/K ATPase and NCX control the movement of calcium in and out of the cell. Without semi-permeable membrane barriers like the sarcolemma, signaling of this sort would be impossible to establish. (Fig. 1 of (Bers and Despa, 2006))

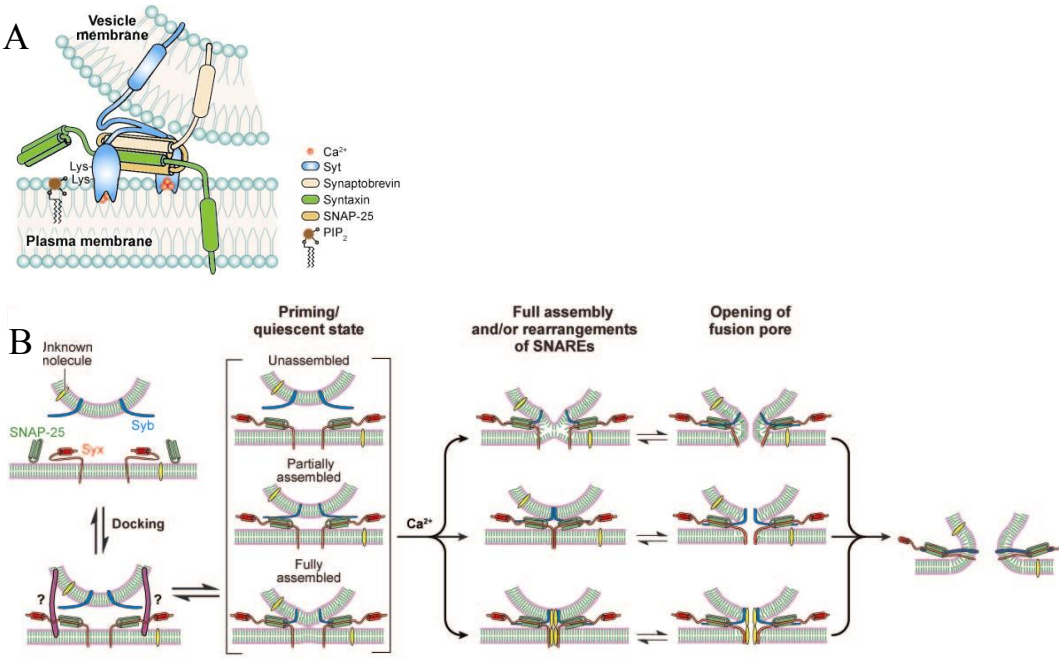

Fig 1.3 SNARE mediated exocytosis. **A.** The SNARE core machinery involved in vesicle fusion. Vesicle and plasmalemma transmembrane proteins combine following a calcium signal to initiate exocytosis. **B.** The sequence of events involved in exocytosis. Many events are known, however certain questions still remain. It is unclear how docking occurs or how syntaxin interact with the assembly and many have suggested involvement of additional unknown players such as MUNC proteins. (Dulubova et al., 1999) (Figure modified (Chapman, 2008))

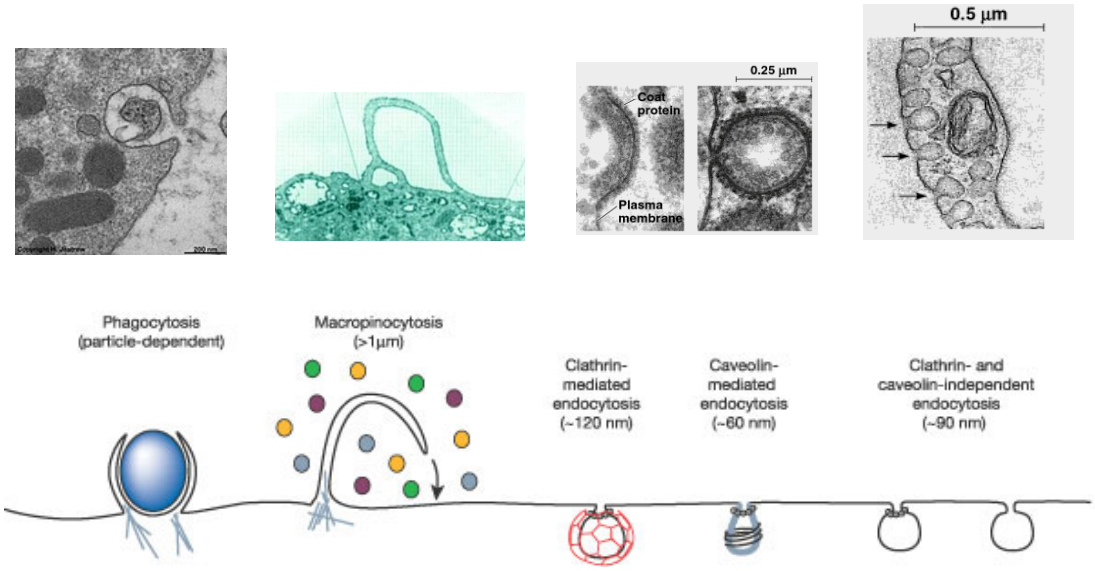

Fig 1.4 General categories of endocytosis. While the four traditional forms of endocytosis have been explored for decades, it is only recently that novel categories such as clathrin and caveolin independent (CLIC) and dynamin independent CLIC have garnered attention. EM micrographs above help visualize phagocytosis, macropinocytosis, clathrin and caveolin-mediated endocytosis respectively. (Figure modified from (Conner and Schmid, 2003)).

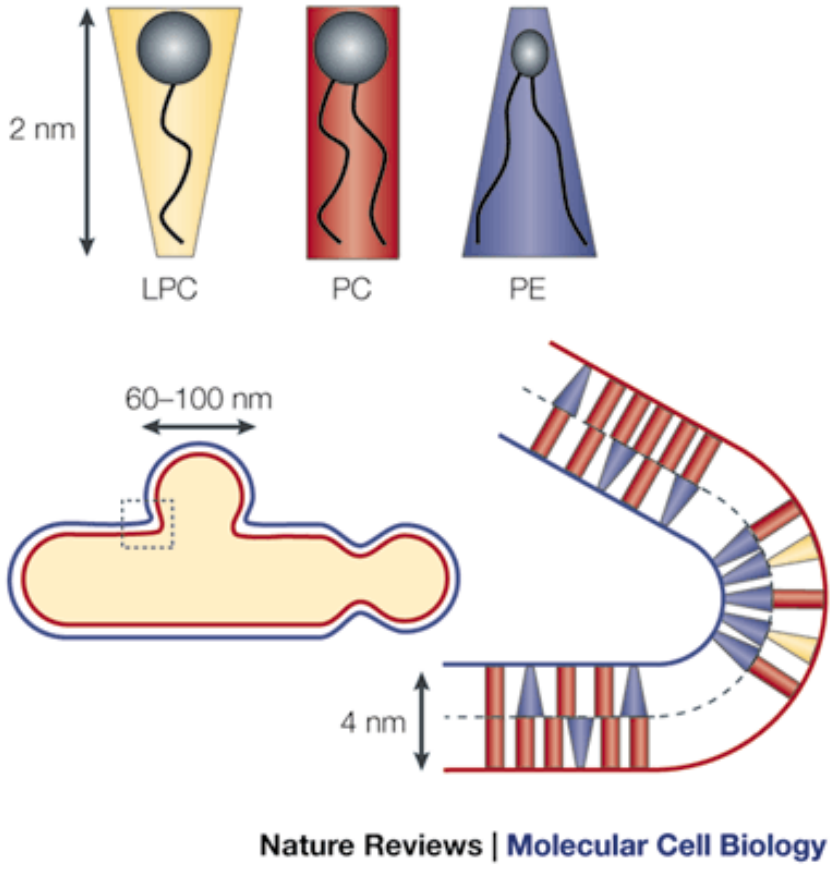

Fig 1.5 Lipid shape controls membrane curvature. The shape and saturation of lipids can contribute to their localization within the budding membrane. Unsaturated fatty acid tails, due to the increasing number of their carbon double bonds, have larger hydrophobic widths. The diameter of the phospho-head groups can also contribute to an overall cone shape. Lysolipids such as LPC and saturated lipids can have more of a inverted cone or cylindrical shape. (Figure from (Sprong et al., 2001)).

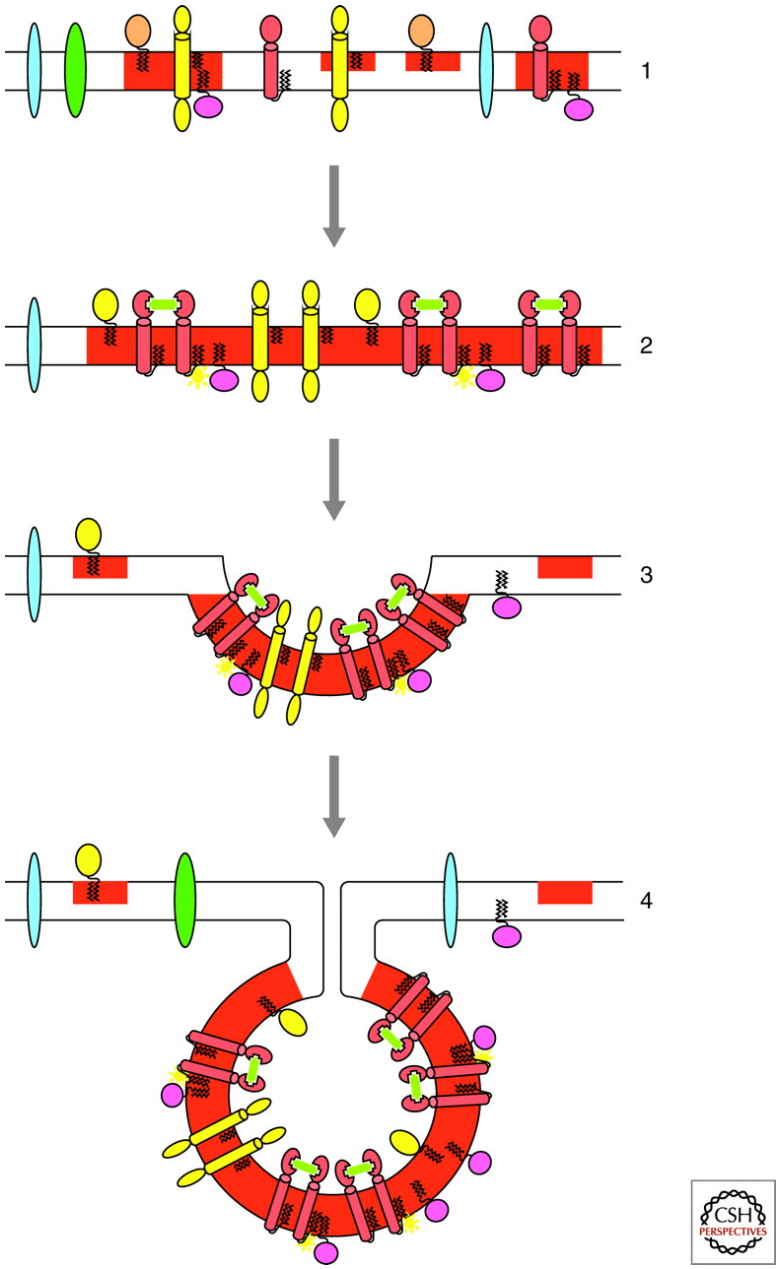

Fig 1.6 Lipid raft aggregation and domain-induced budding. Current theories suggest that lipid rafts exist as "nano-domains" in the outer monolayer that, upon stimulation, aggregate bringing together lipids and adapters. Upon further coalescence the raft reaches a critical size. This induces budding and facilitates endocytic processes. (Simons and Sampaio, 2011)

CHAPTER 2 – MASSIVE ENDOCYTOSIS (MEND)

Recent work performed by Hilgemann lab suggests a novel form of non-canonical endocytosis that is independent of classical adapters and cytoskeletal components. Large fractions of the plasma membrane can be internalized very rapidly as defined by the whole-cell patch and optical techniques utilized in the lab. This form of endocytosis has ben dubbed "Massive Endocytosis" or MEND and is the largest endocytic response on a biological system that has been defined and characterized as of publication. The following chapter serves to summarize these findings with the major texts appearing as the three published appendices at the end of this book.

2.1 – CALCIUM ACTIVATED MASSIVE ENDOCYTOSIS

Much of the work outlined in Appendix 1 centers around a novel protocol in which large intracellular calcium transients drive MEND in fibroblasts and isolated cardiomyocytes. This research originated from previous experiments in the laboratory of Dr. Hilgemann performed primarily by Dr. Alp Yaradanakul, Dr. Vincenzo Lariccia, and Dr. Tzu-Ming Wang. (Shen et al., 2007; Wang and Hilgemann, 2008; Yaradanakul et al., 2007; Yaradanakul and Hilgemann, 2007; Yaradanakul et al., 2008) While investigating large membrane fusion events evoked by reverse activation of cardiac Na/Ca exchanger (NCX1) it was observed that repeated stimulation would trigger subsequent endocytosis. (See Fig. 2.1) These experiments were performed while recording real-time surface area changes in individual fibroblasts. To study membrane surface area the lab focused on whole-cell patch-clamp recordings. Using a 4-6 μm diameter glass pipette, cells were sealed using gentle suction to pull a small amount of membrane into the pipette. The

membrane inside the pipette is ruptured allowing cytosolic access through diffusion from the pipette solutions. For the majority of my work on the subsequent papers, 20-mV square-wave voltage perturbations at 0.5 kHz were employed and recorded using our own software developed by Dr. Tzu-Ming Wang. The software allowed us to monitor cellular electrical properties as follows: 1) Membrane current measured in (nA); 2) Membrane Conductance (nS); 3) Access resistance through the pipette (MΩ); 4) Membrane Capacitance (pF). Membrane capacitance is in direct relation to the surface area of the cell and is typically considered to be $1\mu F/cm^2$ in biological membranes. Increases in capacitance indicate exocytic events while decreases demonstrate loss of surface area later shown to be endocytic through the use of fluorescent probes. After the initial publication of these fusion events, protocols were refined to try and facilitate the endocytic response. From here the work on the next three papers (Appendix 1, 2 and 3) led to a dramatic discovery and characterization of massive endocytosis in biological systems.

Dr. Vincenzo Lariccia first noticed that cells that have been depleted of nucleotides through pipette perfusion and then reperfused with 2 mM ATP and 0.2 mM GTP subsequent to a calcium transient would exhibit a consistent loss of surface area by more than 50%. However, it was not known if the membrane was "shedding" into the extracellular space or internalizing as a massive endocytic response. To determine membrane direction, with the help of Dr. Alp Yaradanakul, I employed the use of a secondary means of monitoring membrane surface area. Using confocal microscopy we combined electrophysiological data with fluorescent markers on the cell surface. If the membrane internalized during the protocol, fluorescent markers would be trapped in the cytosol. Combining these elements with the electrical properties recorded from the

patch-clamp would allow us to determine directionality of the membrane loss during the experiment.

OPTICAL PROBES VALIDATE MEND

Two forms of optical probes were used to validate MEND. FM compounds (Invitrogen) are lipophilic styryl dyes that have long been used to stain biological membranes. They have a unique property that allows them to be highly water-soluble, yet lack strong fluorescence in aqueous solution. Once bound to lipid bilayer they exhibit a strong emission spectrum that can easily be analyzed using confocal microscopy. FM dyes do not penetrate the plasmalemma and wash off rapidly allowing for their use in transient membrane labeling protocols. The ability to rapidly wash off the exposed membrane makes them ideal for studies involving endocytosis. If endocytosis does occur during application, the dye would be internalized and the fluorescence would remain after extracellular wash of the cell. As demonstrated in part A of Figure 2.2, FM dye easily fluoresces when bound to the membrane and returns to baseline upon wash. Nucleotide-reperfusion occurs during the presence of dye and is washed after the capacitive signal reaches a baseline. Resident fluorescence remains inside the cell with small fluorescent vacuole-like structures appearing over time. The remaining fluorescence trapped by MEND correlates directly with the amount of capacitance lost, indicating that membrane loss occurs nearly exclusively in the form of internalization through endocytic processes. Of interesting note is the appearance *after* MEND of the internalized vesicles forming larger trapped endosomal like compartments. The enlarged picture is a snapshot of these vesicles that appear to be much larger then the size of the vesicle theoretically internalized through capacitive step measurements. It appears that once internalized, the small vesicles can fuse with one another to form these larger complexes. For a better

view of how this happens please see the attached supplemental video for appendix 1 (Lariccia et al., 2011)

The other optical probe used to confirm internalization of membrane was achieved through stable over-expression of pHluorin tagged NCX1 protein in HEK cells. As detailed in the Appendix this cell line contains an extracellular green fluorescent protein that exhibits strong quenching of emission in mildly acidic conditions. This allows rapid detection of protein expressed on the surface of the cell by switching extracellular solutions with neutral, acidic or, alkaline-buffered conditions. In this protocol, if membrane was internalized, there should be less fluorescence shift due to extracellular pH conditions. Additionally, MEND does not appear to internalize into acidic compartments during the time course of our experiments so internalized membrane should remain fluorescent. Part B of Figure 2.2 reveals a 34% drop in fluorescence shift after MEND correlating to a relative 45% loss in capacitance. Additionally, small punctae of fluorescence remains just under the surface of the cell. Like FM dyes, fluorescently labeled proteins appear to internalize uniformly with MEND.

Once MEND was clearly defined as a large endocytic event, several additional protocols were discovered to help elucidate a mechanism behind this novel process. 1.) Without the need for nucleotide depletion, it was determined that high intracellular ATP was sufficient to induce MEND after a large calcium transient. The rate in which membrane was internalized was directly proportional to the concentration of ATP used with approx. 50% of the membrane being internalized in 60s at 8mM ATP. 2.) Without transient activation of NCX, intracellular perfusion of calcium (0.2 mM) was sufficient to cause MEND. 3.) Finally, the presence of 1mM cytoplasmic polyamine was sufficient to induce MEND during a calcium transient. This protocol did not require nucleotide and occurred within 3s of the activation of the calcium transient. Polyamines, like spermine

and spermidine, are highly regulated naturally occurring cationic compounds. While their cellular function is still unclear, they have been linked to cell growth and regulation of ion channels as well as a role in development of cancers. Their regularly spaced positive charges may have a role in DNA binding and in the case of MEND binding directly to clusters of negative charges on the inner monolayer of the plasma membrane.

MECHANISM OF CALCIUM ACTIVATED MEND

In brief, our efforts to define a unifying mechanism for calcium activated MEND have yet to be realized, however a detail of shared characteristic has led us to a hypothesis of that calcium is modulating lipid content or movement to facilitate a form of lipid driven endocytosis. In the case of nucleotide-dependent MEND, it was determined that rapid accumulation of the anionic lipid PIP_2 was sufficient to induce MEND. Nucleotide dependent MEND was blocked by an inositol-5-phosphatase (iPP5c) and MEND inhibition in the presence of GTPγS was relieved through inhibition of PLC. Calcium is not just causing increases in PIP_2 MEND was unabated in the presence of many compounds that block traditional clathrin, caveolae, and dynamin endocytosis. MEND occurred in the presence of latrunculin A, phalloidin, and colchicine; compounds that disrupt cytoskeletal components. Even though PIP_2 formation was not necessary for polyamine activated MEND, all protocols shared the characteristics of calcium dependence with independence from endocytic adapters and cytoskeletal modifiers. It is likely that cationic polyamine may bind and sequester anionic lipids like PIP_2 thus having similar effect to rapid localized PIP_2 formation.

In summary, Figure 2.3 reveals a model of how calcium may be acting on the inner monolayer of the cell membrane priming the cell for MEND. Through formation of PIP_2 aggregates or compartmentalization due to addition of anionic polyamines the

membrane undergoes specific conformational changes that favor budding and internalization that are purely lipid force driven and independent of the classical adapters required in clathrin and caveolin dependent endocytosis. It is important to note that polyamine works directly on the membrane and not through the activity of transglutaminase, an enzyme involved in modifying proteins through attachment of spermidine and spermine to downstream proteins. Additionally, the roles of dynamin, caveolin, cytoskeleton, and clathrin have been dismissed as necessary factors for internalization. This leaves us with our hypothesis that calcium is directly altering membrane properties by promoting membrane budding and creating an energetically favorable environment for lipid driven endocytosis. It is thought that calcium could activate an unknown class of proteins dubbed "scramblases". (Bevers and Williamson, 2010) These proteins facilitate the movement of lipids across the bilayer and are activated at concentrations of free calcium similar to that of ours. Processes that promote coalescence, such as long-term calcium activated PIP_2 accumulation, further facilitate short-term calcium activated "mixing" of lipids across monolayers. Increased formation and aggregation of outer monolayer *Lo* domains through the action of lipid mixing would also be possible through this mechanism. Finally, the coalesced membrane could create vectorial buds or "caps and valleys" (Minami and Yamada, 2007) that further bend to vesiculate and internalize. (Simons and Sampaio, 2011)

CHOLESTEROL AND SPHINGOMYELIN IN MEND

Similar to caveolin adapter-dependent endocytosis it appears that there is a strong role for cholesterol and sphingolipids in MEND. Typically enriched in lipid raft domains, modification of these lipids has been demonstrated to alter endocytic processes. (Simons and Ehehalt, 2002; Zhang et al., 2007) In our hands, 12 mM treatment of cholesterol chelating agent BMCD effectively blocked ATP dependent MEND. The loss

of cholesterol could prevent the ability for domains to mix effectively preventing the proper budding necessary for lipid driven endocytosis. To further substantiate the cholesterol dependence of MEND several techniques were used to enrich the membrane with cholesterol. Using cholesterol coated pipette tips as well as cyclodextrin-cholesterol complexes, membrane that we pretreated with cholesterol dramatically promoted short-term calcium dependent MEND. From this data we also determined the importance of cholesterol in the long-term roles of calcium in MEND. Reverse NCX activation in BHK cells causes a robust fusion response with no MEND, but when cholesterol complexes are applied after the transient has long subsided, MEND occurs within 2-4 minutes.

Sphingomyelin, a ceramide based phospholipid enriched in the outer monolayer of cells, has also been linked to membrane domains and endocytosis. (Bollinger et al., 2005; Ding et al., 2008; Goni and Alonso, 2009; Holopainen et al., 2000; Staneva et al., 2009; Zha et al., 1998) Bacterial sphingomyelinases (SMases) cleave sphingomyelin to produce phosphocholine and ceramide, the latter being an important signaling lipid involved in apoptosis, cell death and senescence. When applied to GUV's, SMase causes high inward curvature and membrane budding. (Goni and Alonso, 2009) This vectorialized membrane movement led to a hypothesis that we could induce MEND with application of this enzyme. Indeed, robust MEND occurs with application of SMase C. Initially, co-application of 0.5 mM calcium was needed for MEND, however it was determined that this was due to the enzymes requirement for divalent cations for activation or binding to the membrane. Co-application with manganese in the absence of extracellular calcium was sufficient to induce MEND relieving any role of calcium signaling as a potential background cause for SMase induced endocytosis..

One of the questions that arise from treatment with SMase C is the isolation of the specific action of the enzyme. Is the trigger for MEND due to the product ceramide

signaling by “flip-flopping” across the membrane or loss of the lipid sphingomyelin and rearrangement of lipid domains in the outer monolayer? In order to resolve this unknown, we acquired a form of SMase generated from brown-recluse venom known as SMase D. SMase D cleaves sphingomyelin in a similar fashion to “C”, however SMase D hydrolyzes SM to ceramide-phosphate. This lipid cannot easily flip through the membrane or act as a lipid-signaling molecule like ceramide generated from SMase C. While MEND responses were reduced with application of SMase D, MEND still routinely occurred indicating that endocytosis is NOT caused by ceramide signaling and is a result of loss of sphingomyelin. This lipidic form of endocytosis, likely driven by massive changes in domain forming lipid content was one of the key factors for looking into the properties of lipids and domains and their roles in MEND

Domains that exist in the membrane are highly dependent on their protein and lipid make-up. The fact that cholesterol can have impact on domain formation is not a new concept (Hao et al., 2001). This importance cholesterol and sphingomyelin can be visualized through topographical analysis of the lipid bilayer. Analysis shows that a large membrane superstructure on GUV’s consisting of lipids sphingomyelin and cholesterol can form as a result of the thermodynamic properties that allow three-dimensional “bending” of these lipids. (Groves, 2007) There is even evidence the role of lipids in membrane fractionization and vectoralization is more complex then the mere presence of “bending” lipids. Their particular alignment can have a huge impact on the energy a lipid bilayer has to bud in one direction of the other. Lipid chirality uniformly patterned within large domains has been postulated to produce a budding effect sufficient for caveolin like internalization. (Sarasij et al., 2007) This evidence, and the fact that we produced robust MEND in a cholesterol and sphingomyelin dependent fashion, led us directly to our hypothesis that MEND can be powered directly through lipid forces.

2.2 – AMPHIPATH-ACTIVATED MASSIVE ENDOCYTOSIS

One of the early hallmarks researchers used to separate raft and non-raft proteins was through application of non-ionic detergent triton X-100 (TX100). It was thought that lipid rafts were ordered to the degree that they were resistant to detergent solubilization. Proteins and lipids that resided in these detergent resistant membrane fractions (DRM's) were classified as raft markers while lipids and proteins that solubilized in the presence of detergent were thought to be in a disordered state. We believed that the amphipathic agents like TX100 were not in fact detecting these domains, as mounting evidence cast doubts on the effectiveness of this technique (Mukherjee and Maxfield, 2004), but could be the driving force behind their creation. This could be caused through aggregation of small groups of associated lipids that favor order, like raft-associated lipids. As detergent molecules insert into the membrane these ordered lipids get pushed together to form larger domains and eventually you have phase separation of the membrane into detergent-free ordered lipid rafts and detergent rich disordered membrane. (See Fig. 2.4)

As noted earlier, agents that change lipid content, structure, and order (cholesterol modification, SMases, and PIP_2) drive endocytic processes like MEND. However, the mechanisms by which lipid domains, membrane proteins (e.g. integrins), and membrane-associated proteins interact to drive adapter-independent endocytosis remain poorly established (Mayor and Pagano, 2007). To establish a model of how lipid domains induce endocytosis, the next step is to show how forces within the lipid bilayer alone are sufficient to drive MEND through membrane phase coalescence.

AMPHIPATHIC AGENTS INDUCE MEND

To test whether outer monolayer domain formation would induce MEND, application of sub-micellar concentrations of various amphipathic agents (compounds with both hydrophobic and hydrophilic moieties) were applied to fibroblasts under whole-cell patch clamp with real-time capacitive recording. Non-ionic detergents such as NP-40 and Triton X-100 (TX100) (<200 uM) caused robust MEND responses within seconds. After an initial increase of capacitance, likely due to amphipath binding, over 50% (n=100's) of the membrane internalized with time constants of just a few seconds. This response occurred in the absence of extracellular calcium with calcium interfering with detergent binding to the membrane. For charged detergents like sodium-dodecyl-sulfate (SDS) or triphenylphosphoniums (TPPs), MEND rapidly occurred, but only after the detergent was removed possibly due to the nature of how different detergents allow for aggregates within the lipid structure. It is possible that SDS could be blocking the final fusion event required for budding off of vesicles. In addition to non-physiological detergents, many physiological hydrophobic agents also induced MEND. Nonspecific phospholipase C inhibitor, U73122 (Horowitz et al., 2005) (5 μM) was the most effective causing on average a 35% decline in < 2 min (n=6), while the 'control compound' without phospholipase inhibitory action, U73343, was without effect (n=5). We note in this connection, that the active compound probably accumulates in the outer monolayer because it is cysteine-reactive, while the control compound is not lending credence to the notion this is a bilayer perturbing effect and not due to its inhibitory action. Two anti-proliferative amphipaths, edelfosine and tamoxifen, were effective. Edelfosine, which is an alkyl-lyso-phospholipid (van Blitterswijk and Verheij, 2008) was more effective. The physiological amphipath, lyso-phosphatidylcholine (LPC), was effective at 15 to 40 μM, concentrations that are within 2 fold of those that disrupted recordings. It is not surprising

that NP-40 and TX100 were the most responsive as they have long been used to generate detergent resistant membrane, however there were many amphipaths applied that did not induce MEND. Detergents listed in Table 2 failed to produce MEND prior to disruption of membrane seal or in excess of micellar concentrations.

OPTICAL & ELECTRICAL VALIDATION OF AMPHIPATH ENDOCYTOSIS

As in the calcium-based protocols, it was necessary to determine the directionality of capacitance loss, especially given the robust and fast responses seen. One theory is that detergents might have been causing an equal amount of membrane shedding as well as internalized endocytic surface membrane loss. We employed similar confocal experiments as described earlier. Using the washable FM dye to label the outside of the cell as an indicator of surface membrane, MEND was determined to cause total internalization or endocytosis of membrane loss. Results for electrical monitoring of capacitance loss had nearly identical corresponding increases in internalized fluorescence of FM dye. (Figure 2.5 Part A) A similar experiment where FM was NOT applied during application of detergent also displayed reduced fluorescence post-MEND of the applied dye. Both of these protocols together determine that amphipath-MEND is a unidirectional endocytic process.

AMPHIPATH MEND IS DRIVEN BY LIPIDIC FORCES

Detailed in Appendix 2 and published in the *Journal of General Physiology* requirements and dynamics of amphipath MEND are as follows: 1.) MEND is independent of classical endocytic adapters such as dynamin and clathrin. Dynamin inhibitor such as dominant negative transfection of K44A dynamin mutants and application of Dynasore had no impact. (Figure 2.5 Part B) 2.) MEND occurs robustly even in the presence of actin and microtubule cytoskeleton disrupting agents.

Latrunculin A and colchicine (Borisy and Taylor, 1967; Yarmola et al., 2000) both cause irreversible damage to the structural components of the cell and do not block MEND protocols. In fact, as seen in Figure 2.5 Part A and B Latrunculin may improve MEND response by allowing more lateral movement of membrane aggregates. 3.) Amphipath MEND is not caused by changes in PIP_2 or nucleotides (Figure 2.5 A&B). Perfusion of nucleotide free or non-hydrolysable nucleotide analogues into the cytoplasmic solution does not inhibit MEND. Application of carbachol on cells over-expressing human muscarinic receptor (BHK-NCX-hM1) activates phospholipases and depletes PIP_2 (Yaradanakul et al., 2007). Cells depleted of PIP_2 in this manner still undergo massive endocytosis. 4.) Unlike previously described Ca-based protocols, amphipath MEND requires application of perturbants solely from the outside of the cell. MEND does not occur when large amount of amphipath (>100 uM) are applied intracellularly through pipette perfusion. MEND can then occur when the same cell is extracellularly bathed in 150 uM NP-40. Taken into account all of these characteristics, it was hypothesized that amphipaths induce MEND through perturbation of the outer monolayer and is driven by lipidic forces independent of cell structure and known adapters.

REVERSIBILITY AND RECYCLING

While NP-40 induced MEND does not require nucleotides, it was noted that ATP (8 mM) allowed cellular capacitance to recover in several minutes. This reversibility of MEND led us to question if membrane internalized was recycling back to the surface in an ATP-dependent manner or ATP allowed increased fusion rates of new vesicle pools to the surface of the cell. To probe this question, we measured activity of NCX and measurement of peak current before and after MEND as well as post-recovery. By using an NTA or EGTA (20mM) buffered cytoplasmic solution that maintained relatively low calcium concentrations we minimized the effect of calcium inhibition on NCX. Brief

application of extracellular calcium (1 mM) in cells with 40 mM Na_i showed consistent NCX current activity in the range of 300 pA. After MEND this activity reduced by slightly less then amount of capacitance lost (similar to optical measurements of NCX-pHl). Over time capacitance recovered and NCX current activity recovered to approximately 80% of capacitance recovery. This indicates that membrane internalized does recycle in the presence of high ATP, however sorting does occur with loss of some of the internalized vesicles toward non-surface fractions.

MECHANISM OF AMPHIPATH MEND

Massive endocytosis of plasma membrane via perturbation of the outer monolayer of cells driven solely by forces within the lipid environment is on one hand a novel form of endocytosis explaining perhaps the very simplest concept of how membrane internalizes. On the other hand MEND could be viewed as a very complex set of relationships leading to lateral interactions of specific lipids, their resident proteins, organizations of shape size and of such diversity that it would be difficult to detail all of the characters involved. To the extent of the work to date, Figure 2.6 helps to clarify a simplistic model of how amphipaths create aggregations and lead towards inward invagination and eventual internalization of lipid domains. As discussed in detail within the papers, detergents bind more favorably to the disordered membrane (*Ld*) excluding ordered membrane into larger aggregates. As the membrane becomes more phase-separated, the larger ordered membrane buds towards the cytosolic side. Eventually the size and content of the ordered lipid bud allows for “mixing” and fusion at the boundary of the lipid stalk. The small vesicles internalize and in most cases can return back to the surface in an oxidative and ATP dependent manner or as seen in some cases fuse together in the cytosol targeted likely to early endosomes of other lipid recycling pathways.

RELATIONSHIPS OF MEND

While protocols that induce SMase, cholesterol, calcium and amphipathic MEND differ in their methodology, there is a common mechanistic theme that underlies all forms of massive endocytosis. Whether the approach is inner monolayer lipid modifications through PIP_2, high intracellular calcium and polyamine alterations, or extracellular changes in lipid composition and lateral relationships, all forms of MEND hinge on the merger of nanoscopic domains into larger domains. When PIP_2 aggregates, membrane curves inward allowing for reduced energy constraints and internalization. Calcium and polyamine can also bind to domain specific intracellular regions stabilizing them and allowing for the same reduced energy requirements. SMase and cholesterol dramatically cause shifts in the lateral movement of lipids creating larger domains that also curve toward he cytosol and induce favorable endocytic compartments. Finally, amphipaths clearly segregate lipids in the outer monolayer driving the large ordered domains to favor intracellular budding and endocytosis.

Beyond hypothetical mechanistic relationships, MEND protocols demonstrate functional coupling. While calcium is not required for amphipathic MEND, calcium transients leading to fusion strongly facilitate amphipathic MEND. Concentrations of TX100 and other detergents required for MEND are reduced by 50% when preceded by a calcium transient. One amphipath, ditridecylphthalate (DTPT), behaves similar to cholesterol enrichment. It is without effect when applied extracellularly, but induces MEND within seconds of a calcium transient. Both calcium transients and amphipaths increase the effectiveness of cyclodextrins to extract lipids from the membrane. This is a very interesting finding as it indicates a coupled relationship between perturbation of the outer monolayer and intracellular signaling leading to fusion. If cyclodextrin lipid extraction rate is an indication of membrane disorder this would indicate that these forms

of MEND rely on fundamental shifts in membrane phases and a dynamic shift toward surface disorder after MEND. With that in mind there is now selectivity among the membrane regions that are internalized through MEND, with strong evidence for a preferential internalization of liquid-ordered (l_o) domains.

SELECTIVITY OF MEND

Further evidence for membrane selectivity required the use of different probes to elicit what goes in and what stays out. The initial probe used to detect internalized membrane, FM dyes, were sufficiently distributed across the fibroblast membrane to allow for equal distribution into domains internalized and domains. Maximal binding followed capacitance shifts and was not an indicator of what kind of membrane went in. However, it was observed that another styryl dye, di-4-ANEPPDHQ, did not internalize with TX100 induced MEND. Di-4-ANEPPDHQ has been used as an optical sensor for membrane domains. In GUV's it has been demonstrated to shift emission spectra in response to different levels of membrane order. (Jin et al., 2006) It was thought we could use this probe to look for changes in emission of internalized vesicles however it's inability to internalize during MEND meant that in fibroblasts this dye did not bind to the *Lo* domains theorized to internalize. However, the probe became a good selective indicator for *Ld* membrane. As seen in Figure 2.7, the maximal binding rate (the amount of fluorescence that can be applied and washed) did not shift after MEND. Even though over 50% of the membrane was internalized, the fluorescent probe was still binding to the same disordered compartments. This is even more useful when comparing the various forms of MEND as a similar response was seen in polyamine and nucleotide dependent MEND. Di-4ANEPPDHQ was also useful in determining if calcium transients brought increased disorder to the cell surface as theorized by earlier cyclodextrin lipid extraction experiments. Indeed, after multiple calcium transients with membrane capacitance

increases of up to 80%, the dye showed a selective shift in emission to higher wavelengths (>640nm). As reported earlier (Jin et. al, 2006) this would correlate to cholesterol depletion and increased membrane disorder.

Additional optical probes used to determine membrane selectivity revealed that the ordered membrane internalized was very resistant to fluorophore labeling. Detailed results can be seen in Appendix 3, but only FM dye and the highly ordered straight chain lipid, C16:0 NBD labeled phosphatidylethanolamine had significant labeling of internalized membrane. On explanation for the lack of optical probes to define the ordered membrane is the possibility that the fluorescent molecules could interfere with the ability of the labeled lipids to form tight rigid patters associated with highly ordered membrane domains. The mere presence of a label could create enough disorder to exclude them from internalized membrane.

Another technique to determine the selectivity of MEND without the potential interference of a large fluorescent compound was the use of electrogenic probes that could be detected through transient changes in either capacitance or current. As detailed in Appendix 3 these probes also indicated preferential binding to the disordered membrane. However, they did reveal several interesting facts. 1.) Like di-4-ANEPPDHQ they indicate increased membrane disorder after calcium transients. 2.) They show high uniformity across multiple MEND protocols. 3.) In the case of electrogenic amphipath triphenylphosphonium (TPP) the alkyl chain length may effect assignment to one domain or another. For long chain TPPs (> C6) MEND causes little change in their generated currents. For C6 and C4TPP current was reduced after TX100 induced MEND by 26% and 14% respectively. While not selective for ordered membrane this indicates that shorter chain lengths may allow partial access to the membrane that is internalized.

These shorter chains would have easier access to tightly packed ordered phases and further substantiate the claims that MEND internalized *Lo* membrane.

Finally, transporter function was used as an electrogenic probe for selective MEND internalization. While not a direct indication of lipid order, the ability to selectively internalize specific proteins would have huge importance on determining the physiological parameters of MEND. To date, NCX and Na/K ATPase activities have been analyzed before and after MEND. As noted earlier, NCX function does decrease with capacitance in a relatively evenly distributed manner. This could be as a result of over expression in a fibroblast and more work will have to be done in a more endogenous fashion. For the Na/K ATPase, endogenous activity of the transporter was examined. Indeed, after TX100 induced MEND Na/K ATPase activity was over proportionally reduced with the implication that Na/K ATPase may reside in ordered phases and be regulated by *Lo* domain endocytosis.

MEND ON INTACT CELLS

Since MEND is induced through extracellular application of detergents, it is also possible to probe whether or not MEND occurs on intact cells without the perturbations caused from trypsinization or patch pipette techniques. This is keenly important in demonstrating a more physiological relevance to MEND. To examine these issues, multiple experiments were performed.

One series of experiments was to determine if the trypsin used in cell isolation might have an impact on massive endocytosis. By using cells at 90% confluence still attached to the dish, I performed whole-cell path clamp and monitored cellular capacitance. In order to keep extracellular matrix intact, the cell was patched directly on the dish with a micromanipulator and the extracellular solution switcher was then moved

to position over the cell. This minimized perturbation of the cell and maintained cell shape and integrity. As seen in figure 2.8A NCX current and TX100 induced MEND were statistically similar to results seen in isolated trypsinized cells.

Experiments carried out in Figure 2.8B and C describe how MEND can occur on cells that are not opened via whole-cell patch clamp techniques. MEND is observed on intact tissue culture when detergent is applied and washed off of an entire dish of cells. Together, both protocols demonstrate how MEND occurs in a more physiological setting by removing any aspect of perturbation by patch pipette or interference of the extracellular matrix in cell culture. The logical next step was to further demonstrate the physiological implications of MEND by applying our techniques to intact tissue and resolving if MEND works in an *in-vivo* environment.

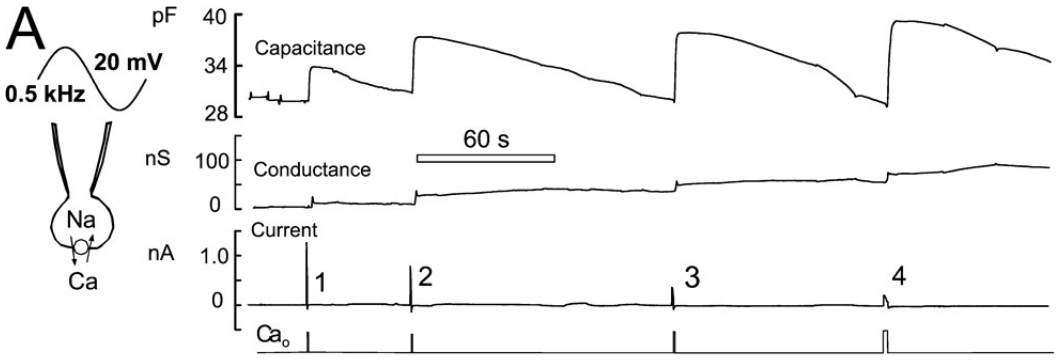

Fig 2.1 Membrane fusion and endocytosis in BHK cells constitutively expressing NCX1. 20-mV sinusoidal membrane voltage perturbations at 0.5 kHz yield real-time cellular membrane parameters. Along with membrane current and conductance, these include direct measurement of cell surface area as demonstrated by capacitance ($1\mu F/cm^2$). Exchange current is activated by briefly applying 2 mM extracellular calcium to a cell loaded with 40 mM intracellular sodium. Upon activation, the cell capacitance increases due to exocytosis. Over time these signals return to baseline due to endocytic processes, however after strong calcium signals the capacitance can drop below baseline indicating an over compensatory endocytic event. (Figure from Yaradanakul et. al., *Journal of General Physiology,* 2008).

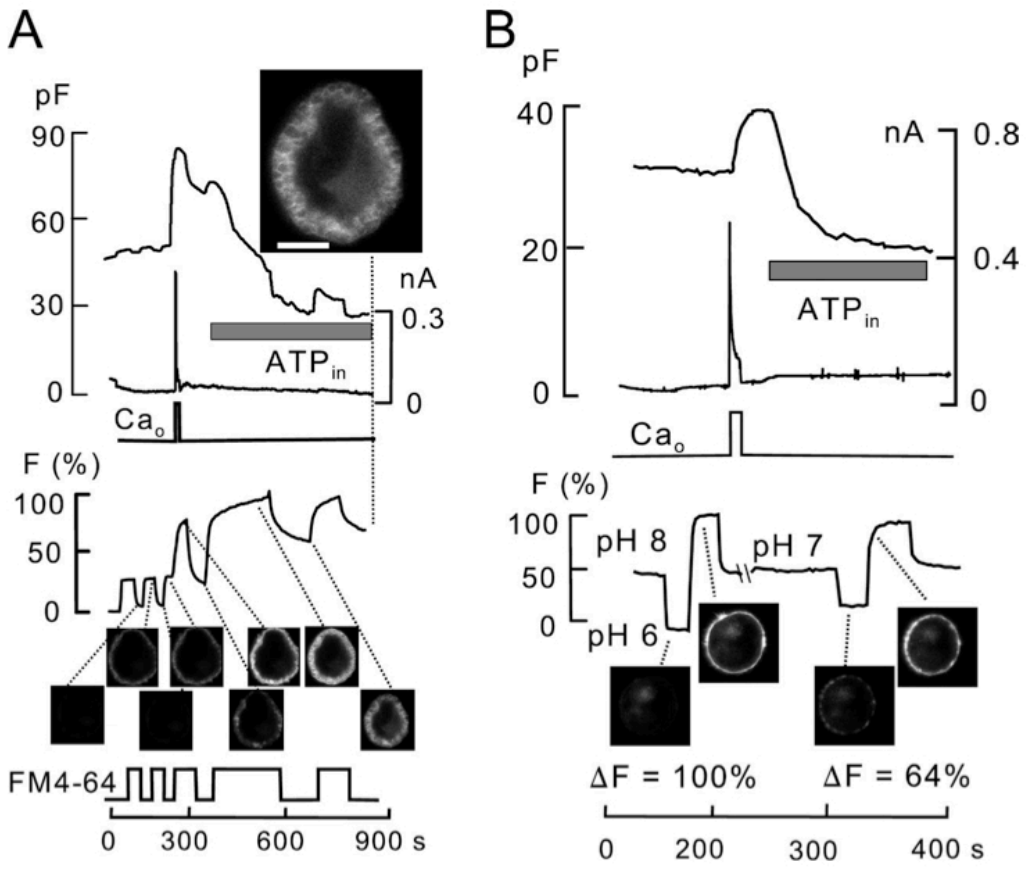

Fig 2.2 Internalization of membrane in MEND triggered by Ca and ATP reperfusion. MEND is captured by optical and electrophysiological methods indicating internalization of membrane and proteins. Styryl dye FM-4-64 (A) and pH-quenchable protein NCX1-pHluorin (B) are visualized under confocal microscopy to determine directionality of MEND. In both cases, nearly all capacitance loss is equated to internalization of optical probes. (Figure from Lariccia et. al., *Journal of General Physiology,* 2011).

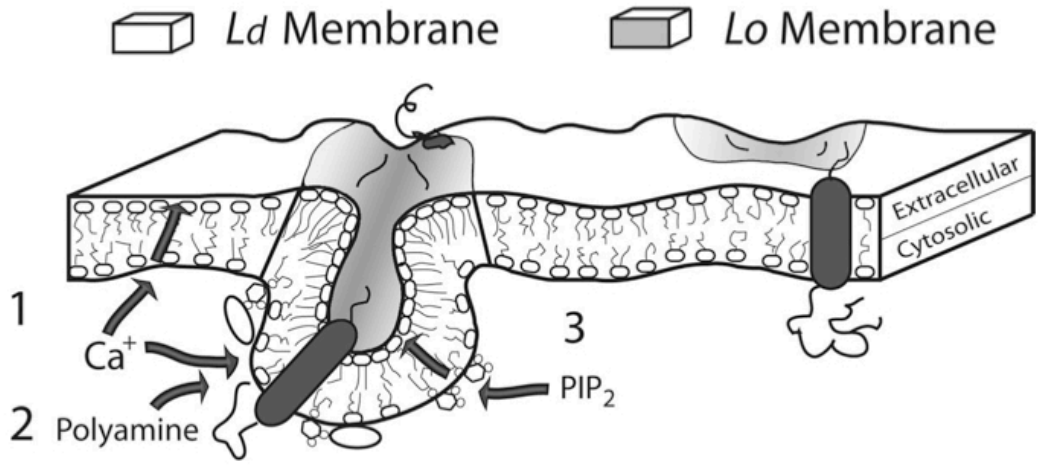

Fig 2.3 Unifying Characteristics of Ca-Activated MEND. 1.) Elevated Intracellular calcium levels prime the plasma membrane for MEND. Calcium may be acting to facilitate fusion of new membrane to the surface or by binding directly to the membrane creating changes in phospholipid properties promoting endocytosis. 2) Short polyamines like ethylenediamine or spermidine also act on the inner monolayer to facilitate MEND after large calcium transients. 3.) Formation of PIP_2 through direct perfusion or PIP kinase subsequent to calcium transients directly promotes MEND. All three factors facilitate the formation of intracellular domains promoting inward curvature and subsequent endocytosis. (Figure from Lariccia et. al., *Journal of General Physiology,* 2011).

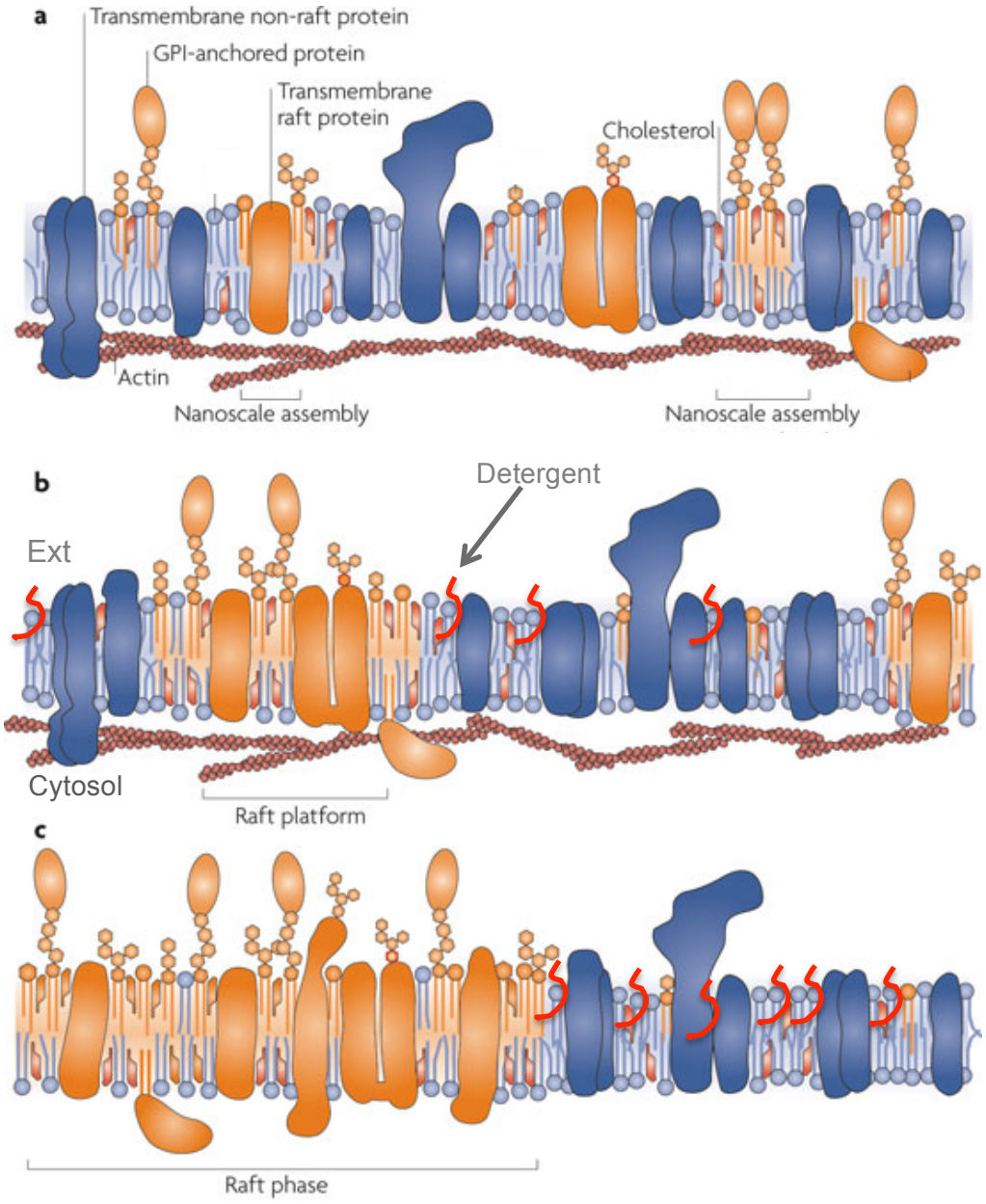

Fig 2.4 Detergent Induced Phase-Separation of the Plasma Membrane. a.) Ordered (Orange) and Disordered (Blue) lipids under normal conditions exist uniformly in the cell and aggregate into "nanoscale-assemblies" with very short lifetimes b.) After external stimuli, such as non-ionic detergents (Red), are inserted into the membrane, larger aggregates are formed eventually leading to c.) Phase separation of the plasma membrane into detergent resistant "Raft" ordered phases and detergent enriched disordered membrane. Modified from: (Simons and Gerl, 2010)

Disruptive Concentrations of 'Inactive' Detergents & Amphipaths	
Octylglucoside	90 μM
Octanesulfonic acid	46 mM
CHAPS	1.5 mM
Deoxycholate	2.0 mM
Tauro-deoxycholate	2.5 mM
Saponin	2.2 mM
β-escin	40 μM
Lipofectamine	100 μM
Sphingosine	12 μM

Table 2 Detergents and Amphipaths that do NOT induce MEND

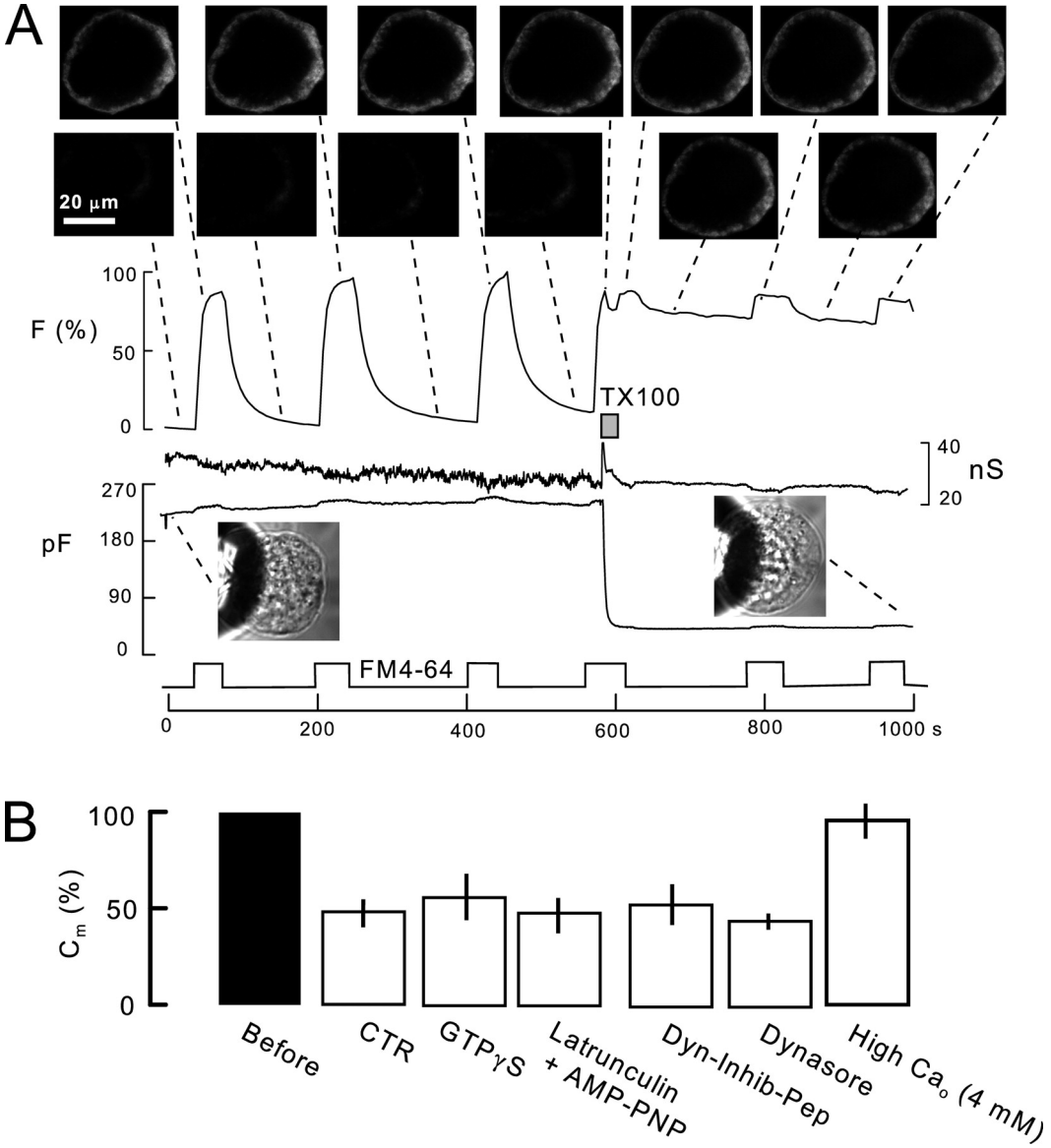

Fig 2.5 Optical and Electrical Measurements of Amphipath Induced MEND are independent of classical adapter. TX100-induced MEND does not depend on canonical endocytic proteins. (A) TX100-induced MEND after extensive disruption of cytoskeleton, phosphoinositides, and ATP-dependent processes (5 μM latrunculin with 2 μM Ca, no ATP or GTP, and 2 mM AMP-PNP). FM 4–64 was applied three times before MEND. During the fourth application, 120 μM TX100 was applied, causing a 77% MEND response. Thereafter, 85% of FM dye fluorescence was retained, and FM dye was reapplied twice. The reversible FM fluorescence amounts to 15% of pre-MEND fluorescence. (B) Further characteristics of MEND induced by 120 μM. As indicated by the open bar graphs, TX100-induced MEND was not inhibited when the cytoplasmic solution contained 0.2 mM guanosine 5′-[γ-thio]triphosphate (GTPγS), 5 μM latrunculin with 2 mM AMP-PNP, 50 μM of an unmyristolated dynamin inhibitory peptide (DynPep; Tocris Bioscience), or 0.2 mM of the organic dynamin inhibitor, dynasore. (Fine et al., 2011)

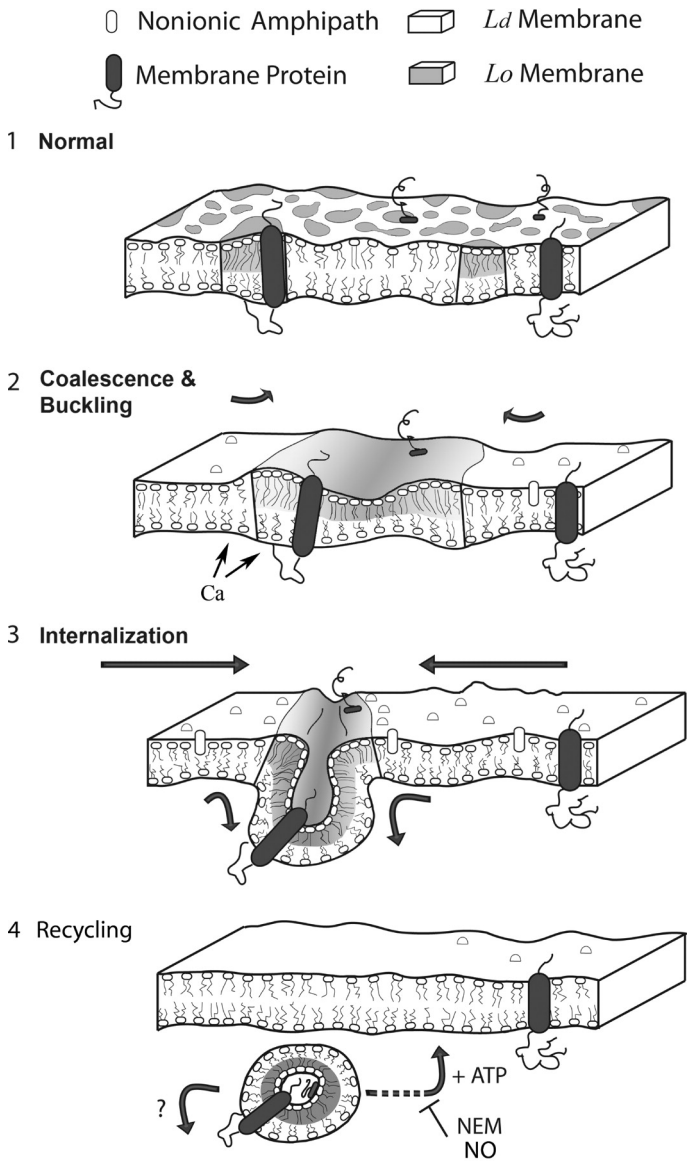

Fig 2.6 **Endocytosis driven by lipidic forces: a hypothesis**. (1) The outer monolayer consists of *Lo* and *Ld* domains of small size and equal prevalence. Lipids diffuse rapidly between domains, with affinity differences for *Lo* versus *Ld* domains being less than one log unit. Nano-scale "lipid shells" around membrane proteins (Anderson and Jacobson, 2002) need not be synonymous with *Lo* and *Ld* domains. (2) Nonionic amphipaths expand *Ld* domains and promote cap formation with buckling of the plasmalemma, which is associated with domain coalescence and protein sorting. Ca transients may trigger the generation of endocytosis-promoting lipids and their movement into the outer monolayer (Hilgemann and Fine, 2011; Lariccia et al., 2011). (3) Membrane internalization. Coalescence of *Lo* domains within expanded *Ld* domains promotes negative curvature, vesiculation, and fission without adapters or dynamins, similar to the generation of ceramide domains via SMases (Lariccia et al., 2011). Nonionic amphipaths remain in *Ld* domains at the cell surface. (4) MEND generates vesicles that follow trafficking pathways to endosomes w/recycling back to the plasmalemma via ATP dependent processes that are inhibited by NEM & oxidative stress. (Fine et al., 2011)

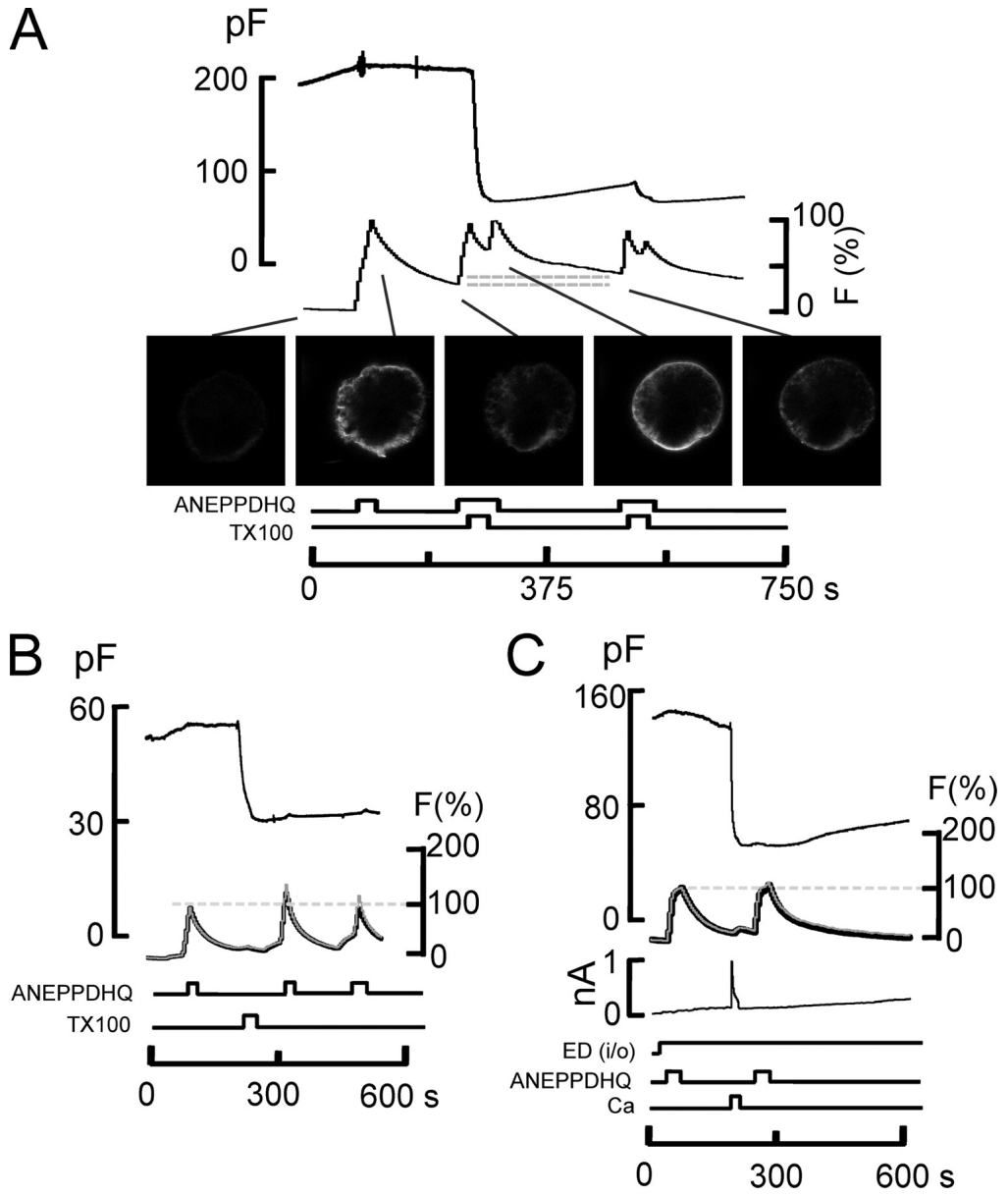

Figure 2.7 Optical Probes Show Selectivity: The styryl dye, ANEPPDHQ, does not occupy the membrane that internalizes during TX100- and Ca-activated MEND in BHK cells. (A) 10 μM ANEPPDHQ was applied before MEND and removed during the induction of MEND with 150 μM TX100 and again after MEND. The apparent binding rates of ANEPPDHQ are unchanged by the removal of >70% of the cell surface by MEND, and the amount of fluorescence internalized during MEND (i.e., does not wash off) amounts to no more than 15% of the initial labeling (see horizontal gray lines). (B) 8 μM ANEPPDHQ was applied and removed before and after TX100 (150 μM)–induced MEND while imaging at bandwidths of 500–580 nm (black) and 640 nmLP (gray). The optical records are scaled. Neither the apparent binding rates of ANEPPDHQ nor its spectral properties are changed after TX100-induced MEND. (C) Same as B, using Ca influx in the presence of polyamine, here EDA, to induce MEND. Dye signals, which approach a steady state in these records, are unchanged by MEND (Hilgemann and Fine, 2011)

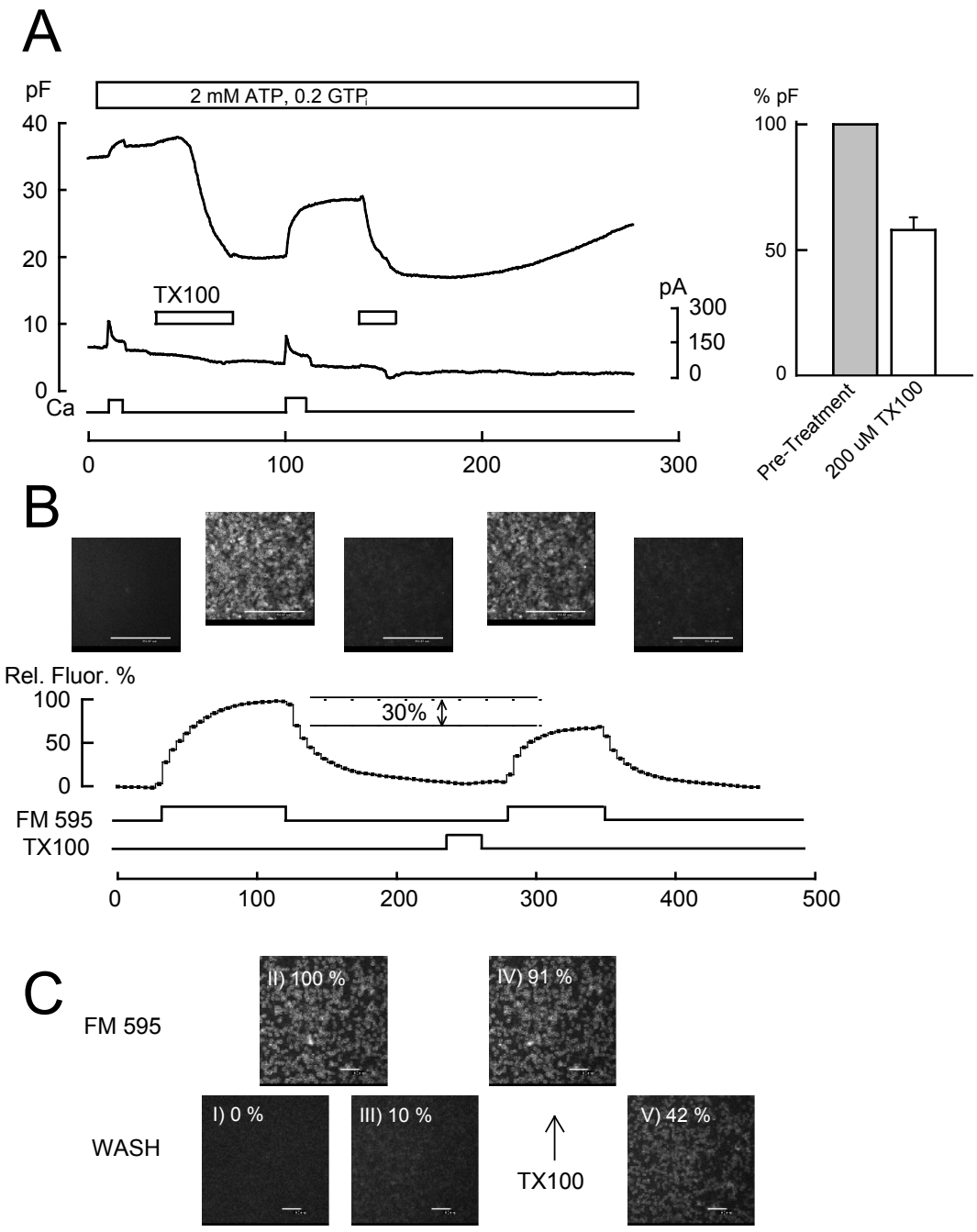

Figure 2.8 Detergent-induced MEND on attached cells: *(cont.)*

Figure 2.8 Detergent-induced MEND on attached cells:

BHK-NCX cells grown to >90% confluence on MarTek glass-bottom dishes. Cell medium was removed and replaced with standard lithium-based extra- cellular solution. No protease treatment was applied, and cells were used within 1 h of removal from incubator to prevent degradation of extracellular matrix and to keep cells firmly attached to the bottom of the dish.

(A) Electrical recording of MEND in attached cells. Typical whole cell recording of firmly attached cells using standard solutions. 2 mM Ca replaced 2 mM Mg to isolate NCX activity, and 200 μM TX100 was applied to induce MEND. Inset shows statistical values for five experiments, indicating a near 50% loss of membrane capacitance for attached cells.

(B) Membrane binding of FM dye is reduced after MEND in attached cells. As in A, cell culture medium was replaced with standard lithium-based solutions. Confocal imaging used a 20× lens and 543-nm excitation with filters set to record wavelengths above 640 nm. A solution switcher was moved to just outside the full frame recording area. Cells were bathed in standard solution, followed by the application of 5 μM FM 5–95. Dye was applied until fluorescence peak reached a plateau and washed. 200 μM TX100 was applied for 30 s to induce MEND. After a 30-s recovery, FM dye was reapplied and allowed to plateau. The maximal binding of FM was reduced by 30% after TX100 treatment. Results were similar for three other records. Bar, 350 μm.

(C) FM dye is internalized during MEND in attached cells. Protocol was as in B, with FM dye being applied and then washed to determine maximal and minimal fluorescence. FM dye was reapplied with 200 μM TX100, and then washed to determine residual or internalized fluorescence. Residual fluorescence increases >30%. I, baseline fluorescence with no treatment; II, first FM dye treatment; III, first wash pre-MEND; IV, FM dye with TX100; V, post-MEND wash. (Fine et al., 2011)

CHAPTER 3 – MEND IN CARDIAC PHYSIOLOGY

3.1 – WILDTYPE CARDIOMYOCYTE MEND

MEMBRANE MOVEMENT IN CARDIAC PHYSIOLOGY

In cardiac tissue, the specialized plasma membrane, the cardiac sarcolemma, contains an assortment of integral membrane proteins and lipid structures that are essential toward the function of the cardiomyocytes as the contractile mechanism behind cardiac output. (See Figure 1.2) The regulation and trafficking of these transporters, such as NCX and Na/K ATPase, is paramount to our understanding of cardiac physiology and pathology (Cusdin et al., 2008; Hayashi et al., 2010; Hilgemann et al., 2006). However, our understanding of these pathways remains enigmatically limited. How are cardiac transporters internalized? How does the cardiac membrane induce endocytosis? What is the role of MEND in cardiac physiology?

What is clear is that many of the hallmarks of cardiac pathology share characteristics of factors that favor MEND. Exaggerated and elevated calcium transients, activation of endogenous SMase, generation of amphipathic like lysolipids, and surface remodeling all occur during cardiac failure (Cogolludo et al., 2009; Gwathmey et al., 1987; Karliner and Brown, 2009; Mancuso et al., 2003). Increases in endogenous polyamine following myocardial hypertrophy have been observed (Caldarera et al., 1971) however their exact role in cardiac failure has yet to be elucidated. PIP_2, long demonstrated as a lipidic second messenger in the heart, has also been implicated in cardiac remodeling (Liu and Molkentin, 2011; Palaniyandi et al., 2009). The sarcolemmal t-tubule greatly increases the surface area of the cardiomyocytes and aids in the ability for the cell to maintain the fast sodium and calcium transients required for

contraction (Bers et al., 2006). This membrane in enriched in surface transporters (Despa and Bers, 2007) and recent evidence supports a massive rearrangement and loss of this structure in myocardial failure (Balijepalli et al., 2003; Wei et al., 2010). The mounting evidence that large changes in the sarcolemma are coupled directly to cardiac physiology and pathology and associated with forces that drive MEND inevitably led us to determine the role of MEND in cardiomyocytes and the intact heart.

MEND IN THE ISOLATED CARDIOMYOCYTE

We tested for the existence of MEND in adult murine cardiac myocytes, using native NCX1 to generate Ca influx and to initiate cycles of spontaneous Ca release. Wild-type hearts were quickly excised and placed in a Langendorff perfusion device that allows for the retrograde perfusion of solutions through the coronary artery. The myocytes were then perfused with collagenase to breakdown the matrix and isolate individual ventricular cardiomyocytes. The cells were then whole-cell patched following the same protocols as described for the fibroblasts and outlined in Appendix 1. Without the addition of polyamine, calcium activated MEND occurs robustly in cardiomyocytes. (See Fig. 3.1) MEND can be repeated in rat cardiomyocytes if the calcium transient is brief. Indicating a strong drive for recycling the membrane in these cardiomyocytes. Interestingly, MEND can occur without the need for large membrane fusion as typically seen in fibroblasts. Fibroblasts in cell culture tend to behave more like secretory cells and may have a larger pool of vesicles primed for release as opposed to the primary myocyte but the distinction of why MEND occurs so fast within the myocyte is still under debate. It is important to note in Figure 3.1 part D that MEND can occur spontaneously as a result of calcium release from intracellular stores. For this experiment, calcium transients were brief enough to not induce MEND but cause spontaneous contractions as a result of the sarcoplasmic reticulum calcium release. This

is the basic mechanism behind contractility in the physiological setting. During the spontaneous release cycle, the cardiomyocytes undergoes MEND. This is an indication that MEND may occur at near-physiological calcium concentrations during excessive excitation contraction conditions within the isolated cardiomyocytes and may have strong physiological implications for its role in the membrane movement of cardiac tissue.

CAFFEINE AND MEND

An additional method to test whether physiological release of calcium from sarcoplasmic stores could induce MEND in the isolated cardiomyocytes would be to treat cells with caffeine. Caffeine is an agonist for ryanodine receptors on the sarcoplasmic reticulum facilitating calcium activated calcium release. Intracellular calcium from treatment of caffeine would be due solely to levels released from within the cell an not from the reverse activation of NCX. To test whether MEND could occur through this more physiological manner we whole-cell patched isolated cardiomyocytes and briefly activated reverse NCX. These small and brief transients were intended to facilitate loading of calcium into the sarcoplasmic reticulum through SERCA and did not induce MEND. Figure 3.2 shows how MEND can occur with treatment of 5 mM caffeine subsequent to these brief transients. MEND amounts to a roughly 40% of cellular capacitance. It is important to note that this only indicates that isolated cardiomyocytes are highly sensitive to calcium and MEND, as it is not possible to rule out any long term effects the calcium transients may have had on the sarcolemma. Additionally, this protocol proved difficult to repeat as calcium transients are not consistent from cell to cell and can easily lead to MEND themselves or be so low as to not load the calcium stores inside the cell.

MOUSE VERSUS GUINEA PIG

While calcium activated MEND occurred routinely in murine cardiomyocytes, the ability to reproduce these protocols in isolated guinea pig cardiomyocytes proved much more difficult. Calcium transients observed in GP cardiomyocytes was much smaller, but even application of TX100 could not induce MEND consistently. One of the key differences in guinea pig cells was their unusually small capacitance. Typical murine capacitances observes were 150-300 pF but most guinea pig myocytes were less than 100 pF. Additionally, it was observed that in some freshly isolated GP cardiomyocytes the capacitance values would drastically fall over the course of 30-60 seconds after returning the cells to 37° C from their initial RT bath. This would occur without any other perturbation to the cell. To further explore this phenomena, a series of experiments were performed to determine if the sarcolemma in guinea pigs might be undergoing a "pre-conditioning" like MEND event prior to isolation. Pre-conditioning is the phenomena in cardiac physiology that allows a subset of cardiac cells to survive repeated ischemia-reperfusion events in cardiac failure models. The mechanisms behind which some cells can handle the excessive calcium load that occurs during reperfusion of cardiac tissue following periods of ischemia is highly debated, but there is some evidence that membrane retrieval of cardiac transporters such as NCX1 may help the cell prevent the rapid influx of calcium that leads to hypercontractility and apoptosis.(Hausenloy and Yellon, 2010; Hilgemann et al., 2006; Kang and Hilgemann, 2004)

Perfused guinea pig hearts were subjected to 2 mM of the anti-oxidant N-Acetylcysteine along with 10 μM K_{ATP} blocker Glyburide during isolation in an effort to mimic protocols that would block pre-conditioning (Dhalla et al., 2000; Grover et al., 1992). While there was a trend showing increased NCX activity and some cells responding with small losses of capacitance, the procedures failed to significantly reduce

capacitance in a manner related to MEND in murine cardiomyocytes. Interestingly, the treatment *did* improve the ability for TX100 induced MEND, but the level of endocytosis was still much smaller than typical, with very fast recovery of membrane to basal levels. An alternative protocol to block pre-conditioning with α-difluoromethylornithine (DFMO) treatment was intended to decrease intracellular polyamine levels and has been demonstrated to reverse the isoproterenol-induced pre-conditioning that elevates endogenous polyamines (Bartolome et al., 1982). Here again, the exchange current was larger and there was a tendency to internalize membrane, but not to significant levels. Amphipath MEND with TX100 also worked however membrane losses were usually less than 10%. Overall, treatment to block pre-conditioning failed to significantly increase the capacitance of isolated guinea pig myocytes and did not increase the likelihood of calcium-induced MEND.

It is likely that the isolation of guinea pig myocytes causes large scale changes in the sarcolemma that are not entirely associated to pre-conditioning phenomena. Recent work has also stressed these differences as an artifact of the isolation procedure but nevertheless an example of large-scale membrane movements. Dr. Susan Howett, PhD of Dalhousie University, Halifax, Nova Scotia, Canada has been working on this phenomena and along with some unpublished data from both of our labs noticed increases in calcium sensitive punctae that are blocked with treatment of the organic anion transporter inhibitor probenecid. (Data Unpublished) Figure 3.3 shows some of the differences between isolated murine and guinea pig cardiomyocytes when labeled for extended periods with the fluorescent membrane probe di-4-ANEPPS. Labeling of all cardiomyocytes was difficult and required up to 10 fold higher concentrations of probe than normally utilized in fibroblasts, however labeling of t-tubule structures does occur in murine cardiomyocytes and partial to nearly absent in the guinea pig. (Figure 3.3)

Another difficulty with the guinea pig myocyte originated from the inconsistency of labeling with dye. While, t-tubule labeling was always more sporadic when compared to murine myocytes, their partial presence in some guinea pig myocytes would indicate that MEND should be detectable in some cells if indeed this was a necessary factor. However, there was never evidence of MEND when monitored whole-cell. Additionally, if MEND was occurring during the isolation process then it would be possible to detect this internalization through membrane probes applied while the whole heart is perfused and treated. Fluid markers, carboxyfluorescein, and membrane markers, di-4-ANEPPS, did not accumulate into compartments when applied before and during the isolation. Carboxyfluorescein, which does not penetrate the membrane, was found evenly distributed throughout the cytosol as if isolation created a leak pathway for entry. ANEPPS dye had only non-specific labeling that was the same for mouse and guinea pig indicating no increased uptake for the guinea pig. It is possible that the ANEPPS probe is selectively isolated from the membrane being internalized, as seen in our fibroblast work (Appendix 3), thus preventing us from visualizing the internalized membrane. Unfortunately, FM dye binding on the cardiomyocyte was very poor in our hands and could not be used for such determination.

There is a strong possibility that the cardiomyocyte lipidic environment, especially within the t-tubule region, is highly ordered and densely packed. This phase difference would make labeling far more difficult than in traditional fibroblasts and could be one of the factors that favors fast MEND in the cardiomyocytes. The increased difficulty in labeling guinea pig myocytes could indicate these cells have an even higher propensity for internalization and t-tubule remodeling occurring during the process of isolation that cannot be stopped using traditional blockers of pre-conditioning. While more work needs to be done to determine if there is species-specific changes in the heart

that may promote MEND, these differences only further substantiated our need to develop protocols that can allow us to follow the surface membrane and determine if there is indeed MEND specific trafficking of surface transporters.

3.2 – TRANSGENIC α-MHC NCX-pHL MOUSE

BACKGROUND

With the establishment that calcium can induce massive endocytosis within the wild-type murine cardiomyocytes, the next step was to follow the membrane movement similar to the work performed on fibroblast cells. In fibroblasts, we employed the use of an extracellular pHluorin tag attached to the glycosylation site on NCX1.1. The pHluorin probe is a fluorescent GFP derivative that exhibits strong pH sensitivity. At low pH, the molecule is quenched. Under normal physiological conditions (pH 7.4) the pHluorin molecule is highly fluorescent unless sequestered into an acidified compartment. As seen in appendix 1 and 2, the pHluorin probe we established was very useful in correlating MEND and NCX internalization within the stable HEK cell line through comparisons of fluorescence shifts as extracellular pH is manipulated. Therefore, three factors favored use of these protocols for analyzing membrane trafficking and MEND in the heart: 1) NCX1.1 is a cardiac resident protein. 2) The membrane regulation of cardiac NCX is currently unknown although, during cardiac pathologies, it is hypothesized to undergo membrane retrieval. 3) We have already established that the NCX-pHl fusion protein generates a functional assay for MEND in isolated and intact cells. However, cardiomyocytes are not easily transfected like fibroblast cells and the induction of expression through lentiviral infection is neither consistent nor cost effective.

In order to establish viable and consistent expression of NCX1.1-pHl in primary cardiomyocytes, we produced several transgenic lines through microinjection of our transgene construct under the control of the α-myosin heavy chain promoter (α –MHC). This promoter induces expression shortly after birth, specific to the ventricles of the heart. Interestingly, there was an additional trace amount of atrial expression in several of the generated lines that could be quantified on western blot and optically visualized. Initial western blots (data not published) established on two of the transgenic lines indicate over-expression above endogenous NCX from 10-15 fold with a 4-5 fold increases in expression in the atrium. There was no expression of our fusion protein in brain, kidney or liver. Additional determinations will need to me made on the remaining lower expression transgenic lines

Transgenic over-expression of NCX1.1 had been established over ten years ago through the work of Dr. Ken Philipson, Ph.D. While lacking the extracellular fusion tag, they described their 9-fold overexpressing transgenic lines as having no myocardial hypertrophy or failure (Adachi-Akahane et al., 1997; Baumer et al., 1998). In addition, they measured force of contraction after application of isoproterenol. Isoproterenol activates β_1-receptors on the heart, inducing positive inotropic effects leading to increased calcium transients and force of contraction. There was no significant difference in the force of contraction when compared to wildtype and and no compensatory changes in the sarcoplasmic reticulum calcium handling proteins SERCA and calsequestrin or changes in calcium transient magnitude. Further analysis did reveal some increase in contractile force as compared to wildtype in response to application of strong sodium channel agonist BDF 9148. This is likely a result of increased reverse activation of NCX after loading the cells with sodium. Dr. Philipson's initial research establishing only mild phenotypes of cardiac over-expression of NCX enabled us to pursue transgenic

overexpression of NCX1.1-pHl as a viable model for monitoring MEND and NCX trafficking in the heart without risk of complicating cardiac pathophysiologies.

FUNCTIONAL CARDIAC PHENOTYPE

In addition to the extracellular pHluorin tag our transgenic lines exhibit some phenotype anomalies when compared to the original Philipson lines. Over the course of several months we noticed that some the mice appeared to respond abnormally when handled for cardiac extraction. Multiple homozygote high expression lines would seize and go unconscious as we placed them in the anesthesia boxes. In addition, there was an increased rate of unexplained death. I characterized several months of data and discovered that two of the three transgenic lines monitored had similar responses substantiating the potential that this was due to over-expression of NCX and not through genotypic artifacts that can occur during the creation of transgenic lines. While mortality rates overall not extreme when taken over the whole population, Table 3.1 shows the data collected for the unexplained early deaths in the transgenic lines.

To determine if there was the potential of an unforeseen cardiac failure model in our transgenic lines we worked with Dr. Herman May in establishing basic echocardiograph data on our transgenic lines. Observed morphogenic differences were increases in left ventricular diameter during diastole (Average mm of n=4; 29.5 control, 32.7 trangene line 297, 38.8 transgene line 282) and systole (4.9 control, 7.1 transgene 297, 10.5 transgene 282). Inner diameter was not significantly different and fractional shortening was reduced but not significant. Surprisingly, heart rate observed through echo showed average decrease from 666 bpm in control to 585 in the 297 line and 473 in 282. These factors all seem to suggest the potential of these transgenic lines exhibiting signs of early cardiac failure and support the data on our early-unexplained deaths.

However, the data set is not large enough to be conclusive and needs to be further substantiated before any claims can be made.

MEND IN ISOLATED TRANSGENIC CARDIOMYOCYTES

After the establishment of three breeding lines based on positive tail-snip PCR genotyping for pHluorin and cardiac fluorescence localization to the sarcolemma, we set out to determine if MEND can be monitored in the isolated primary cardiomyocytes using our established pHluorin protocols. Figure 3.4 shows a heterozygote transgenic with evenly distributed sacrolemmal surface labeling of NCX-pHl. Clear labeling of cardiac t-tubes is present throughout the experiment indicating that while t-tubule remodeling may occur, changes do not affect their overall superstructure. Similar to experiments performed in Appendix 1 on the HEK-NCX-pHl fibroblast and wildtype cardiomyocytes, transgenic primary cardiomyocytes were isolated and simultaneously monitored using whole-cell patch clamp electrophysiology and confocal imaging with excitation at 488nm and emission 500-580nm. Solutions were similar to those used in wildtype cardiac electrophysiology for appendix 1, with the exception that extracellular solutions were divided into three pH groups. A slightly alkalinized solution of pH 8 was utilized for maximal extracellular fluorescence while pH 6 was used for maximal quenching of the extracellularly expressed pHluorin probe. A neutral solution was used to activate calcium transients. As the experiment begins, capacitance holds steady at 200 pF while shifting from high to low pH caused 52% of the fluorescence signal to be quenched. While this indicates a fairly high basal amount of intracellular exchanger, the surface fraction signal is still large enough to easily monitor trafficking. Subsequent calcium transients induced very large currents, as to be expected with an overexpressing model, followed by rapid loss of nearly 50% of the capacitance value. MEND was not reversible. After stabilization, extracellular pH was shifted again with maximal

fluorescence intensity unchanged, but low pH quench was reduced to only 24% of the overall fluorescence. This loss of quenchable pHluorin indicates 46% of surface NCX trafficked with MEND, as it is no longer exposed to changes in extracellular pH. Like in fibroblast experiments, whole-cell patched cells did not acidify upon internalization and surface fraction lost highly correlates to the amount of capacitance lost. Experiments were repeated on multiple transgenic lines with an n=4 of each line tested.

ACIDIFICATION IN UNPATCHED CELLS

One phenomenon noted throughout the course of experiments was that fluorescence intensity of all three transgenic lines diminished over several hours when isolated cardiomyocytes were stored in physiological buffer (pH 7.4). However, individual cells that were patched and imaged as described above had little shift in maximal fluorescence over the course of the experiments. Is it possible that unpatched cardiomyocytes may internalize vesicles differently then when patched? Could those vesicles traffic into acidified compartments and lead to the observation of a time-dependent reduction in fluorescence? To answer these questions I established a series of experiments with patched and unpatched cells in a constant extracellular physiological buffer (pH 7.4). In this manner, differences in the intracellular acidification of pHluorin containing compartments could be visualized through application of agents that do not alter extracellular pH but alkalize the inside. If pHluorin was inside and acidified, fluorescence intensity would increase. Patched cells were treated with Bafilomycin A, a V-ATPase inhibitor that prevents acidification of vesicles (Williamson-"Fuqit" et al., 2010; Yoshimori et al., 1991). Like in fibroblasts, treatment had no significance in overall fluorescence; it is possible that diffusion properties up the pipette and the addition of 15 mM intracellular Hepes buffere used in our experimental conditions could be masking an effect. Therefore application of 500 nM Bafilomycin A to unpatched cells

was monitored for changes. Treatment caused a modest but not significant increase in overall fluorescence in all three transgenic lines. The lack of significance stems from a wide variability in the response of cells with some cells having virtually no fluorescence response and others showed regional increases in fluorescence of up to 40%. Alternatively, application of weak base NH_4Cl allows transmembrane diffusion of NH_3 and alkalization of intracellular compartments regardless of V-ATPase activity. Results of NH_4Cl showed larger increases in intensity when compared to Bafilomycin A within all transgenic line, but with a high degree of variability from cell to cell preventing any statistical differences to arise from patched to unpatched cardiomyocytes. It is possible that multiple mechanisms may be at work here and use of NH_4Cl makes a better candidate for monitoring of intracellular NCX-pHluorin as it does not depend on the presence and activity of the V-ATPase.

SPONTANEOUS INTERNALIZATION

During the course of these experiments several observations were made that managed to follow this variability and changes in fluorescence intensity within the same cell. Figure 3.5 shows a homozygote cardiomyocytes undergoing spontaneous MEND. Cells were imaged in our standard cardiac isolation buffer with 200 uM calcium and adjusted to pH 7.8 to enhance extracellular fluorescence. During confocal imaging, the cell started to spontaneously contract due to intracellular calcium activated calcium release cycles. Over the course of 20 minutes, the cell lost nearly 60% of its fluorescence intensity. This suggests that vesicles internalized were acidified in this particular circumstance. This fluorescence loss was reversed through application of the membrane permeable weak base NH_4Cl (20mM), with t-tubule morphology alterations and large fluorescent punctae visualized. This would indicate that large membrane shifts can occur

in the unpatched myocyte upon isolation and that these MEND like events traffic into normal degradation and lysosomal pathways.

We have demonstrated that spontaneous internalization can occur in the cardiomyocytes with vesicles following an acidic pathway, as occurs during degradation (Yoshimori et al., 1991). Alternatively, MEND transpires in some myocytes only after large calcium transients on patched cells and without significant acidification of intracellular compartments. Unlike cultured fibroblasts, there is no need for exogenous MEND facilitating factors like polyamine or PIP_2. All this suggests that the cardiomyocyte membrane is unique and may contain factors that favor the massive rearrangement of lipids through multiple mechanisms. There is abundant literature demonstrating cardiac membrane has the ability to rapidly move membrane through the formation of large spherical lipid blebs that spontaneously appear attached to the sarcolemma (Hilgemann, 1989; Hilgemann, 1996; Hilgemann et al., 1991; Hilgemann and Lu, 1998). The variability and dynamic nature of the cardiac membrane suggests that the cardiac sarcolemma is primed for dramatic changes that differentiate it from most cells and warrant further analysis.

3.3 – MEND IN THE INTACT HEART

It is evident that large-scale changes can occur in the sarcolemma of isolated cardiomyocytes and we can observe these changes through trafficking of NCX in our transgenic models. However, these findings do not determine if this is a product of the isolation of individual cardiomyocytes, or a true physiological response to calcium. While t-tubule remodeling after isolation is an important finding that should be noted when trying to draw physiological data from research on isolated cardiac cells, our goal is

to establish the role of MEND in a pathophysiological system. Methods for monitoring NCX trafficking in the intact heart were established and combined with physiological approaches to and induce MEND.

A WHOLE-HEARTED EFFORT

Transgenic hearts were quickly isolated and perfused using our Langendorff apparatus as detailed in our cardiomyocyte isolation protocols. Instead of subsequent enzyme treatment with collagenase, these hearts were transported to either epifluorescence or confocal microscopes for surface monitoring of fluorescence. Tissue integrity was maintained as well as solution flow and temperature. All experimental solutions were perfused throughout the heart in efforts to try and induce exaggerated calcium transients and facilitate monitoring of intact cardiac MEND.

There are many hurdles to overcome when approaching intact cardiac fluorescence methods. 1.) During confocal imaging, visualization of nuclei, t-tubes and enhanced labeling at cardiac gap junctions was clear. However, contraction of cardiac tissue made it impossible to follow individual cells on the surface of the heart throughout the course of an experiment. Treatment with contractile inhibitors, Blebbistatin, BDM, and Cytochalasin D all slowed contractions, but did not block to the point where visualization was stable. 2.) During epifluorescence, much of the data and detail of localized trafficking within a single cell is lost and gross fluorescence is obtained only in the outer few cells within the cardiac ectoderm. 3.) In our transgenic model, perfusion of intact heart must be very consistent throughout. The intact cardiac muscle produces significant acid secretion during metabolism. If perfusion is compromised, even regionally, increases in acid production create an artificial loss of pHluorin expression.

This can be only partially compensated by increasing the amount of buffer in the extracellular solution.

While TX100 is small enough to pass through the capillary wall in Langendorff perfusion protocols, the ability for it to induce MEND was not consistently observed. Two possible explanations for the lack of amphipath MEND could arise. 1) TX100 is likely binding to the epithelial wall of the vasculature in the heart. 2) The rate in which TX100 binds to the surface of the cell could influence its ability to induce phase coalescence and MEND. TX100 binding to the epithelium of the capillaries could induced MEND and disrupt permissive nature of this barrier. Perfusion could be come occluded and sufficient delivery of amphipath throughout the heart would be compromised. In epifluorescent whole heart experiments, it was routinely observed that the *rates* of fluorescence shift, when pH was used to determine surface fraction, were decreased dramatically after exposure to TX100 even though the overall intensity shift did not significantly change. This is explained through decreases in perfusion throughout the heart and subsequent slower diffusion of pH changes to the surface of the cardiomyocytes. In addition, small regions throughout the ventricle became dark and resistant to perfusion shifts. This is likely not due to internalization of NCX, but rather the loss of perfusion in those regions resulting in metabolic acidosis and artifact. Even if capillary structure was maintained, TX100 diffusion from capillary to cardiomyocyte would be slower than when switching bath solutions around an isolated cell. If the amphipath slowly binds to the surface and flips in at a faster rate to the inside of the cell, accumulation of amphipath would not occur in the outer monolayer preventing coalescence and subsequent MEND.

It became evident that perfusion was extremely important when utilizing the pHluorin probe to image intact hearts. During contraction, the heart is highly metabolic

and extracellular acidification would occur naturally if proper buffers were not in place to prevent this from occurring. This was exacerbated by the role of NH_4Cl. As NH_3 travels through the membrane, it leaves behind HCl and acidification of the extracellular environment occurs. In isolated cells, buffers and fast solution flow would easily prevent HCl from lowering the extracellular pH to any significant extent. However, it was necessary to raise the physiological buffer Hepes to 55 mM in our extracellular solutions in order to minimize this effect.

After numerous experiments exploring the potential of oxidative stress in inducing membrane shifts, the most significant protocol was simple application of the catecholamine, Isoproterenol. Isoproterenol is a powerful β-agonist that causes inotropic responses in the heart. It increases contractile force and rate through increases in cytosolic calcium. Figure 3.6 is an example of our intact heart experiments where MEND was evident through elevation of cytosolic calcium. The heart was perfused with oxygenated solution containing high Hepes buffer (55 mM) and low sodium in an effort to reduce the rate NCX would actively extrude intracellular calcium for sodium. Over 30 minutes, the heart maintained consistent fluorescence and could be repeatedly switched to an similarly buffered solution set to pH 6.6. Each fluorescence shift indicated over 65% of the membrane could be quenched at low pH and then recover to maximal values. Isoproterenol was applied (500nM) for 10 minutes. During this time maximal fluorescence did not drop, but the fluorescence shift was reduced by over 35% indicating surface fraction loss into non-acidified compartments.

Confocal experiments using this protocol revealed beautiful images of cellular morphology, contraction even in the presence of 15 uM Blebbistatin, and the appearance of punctae near the perinuclear region. In the cardiomyocyte this region is very compact ands included golgi, ER, and lysosomal compartments. These punctate regions could

reveal trafficking of NCX from the surface, or novel synthesis of protein and will require additional work to isolate these regions within the cardiomyocyte. Unfortunately, high-resolution confocal images are difficult to maintain for significant periods as contraction and movement prevent visualization of the same myocytes throughout the experiment. Additionally, the cardiac tissue must be placed very close to the glass coverslip and during isoproterenol the cardiac tissue will hyper-contract removing the heart away from the surface forcing constant rearrangement of the whole apparatus. These experiments are very exciting, and recently work repeating such protocols using 2-photon laser confocal imaging will allow deeper penetration and perhaps more stable experiments. Until then, alternatives to exploring MEND within intact cardiac tissue were developed

VENTRICULAR STRIPS

A newer method for monitoring cardiac tissue has been established to try and offset these complications. As opposed to relying on the cardiac vasculature for perfusion, excision of a right ventricular strip allows for superfusion of oxygenated solution to the cells of interest. In addition, this method significantly reduces contraction artifact and allows for stable confocal imaging of large tissue sections sufficiently separated from the bottom of the dish to allow for fast solution switches yet close enough for monitoring of the individual cell.

Using these methods, preliminary data suggests isoproterenol treatment may indeed drive internalization of membrane through its inotropic effects on the heart. Fluorescence then recovers over the course of several hours. However, repeated numbers of experiments are too low for evaluation. Furthermore, it has been observed that this effect may be variable depending on what time of day the cardiac tissue is excised. This difference in surface expression between littermates may well be explained by the

phenomena of differential diurnal expression of NCX1.1 (Shen et al., 2007). While no mechanism has been established for this phenomenon, it is clear that the surface fraction of NCX increases significantly towards the end of the dark or active phase for mice. In order to objectify the data properly the lab is now entraining the mice to detect diurnal changes in membrane internalization through our transgenic optical measurements. Once this data set is complete, refined protocols should help determine if catecholamine is indeed impact the surface fraction of NCX through endocytosis within the intact heart.

Using superfusion, we are able to bypass the molecular size limitation created by perfusion from within the capillary walls. This allows us to examine the effect of enzymes that were too large to perfuse in Langendorff hanging heart experiments. Sphingomyelinase is one such enzyme that is too large to pass through the epithelial barrier. Initial evidence suggests a faster form of MEND occurring within minutes of application. This loss of fluorescence shift is quickly recovered after treatment suggesting that the cardiac membrane has the ability to quickly remodel its membrane environment. Within 5 minutes overall fluorescence drops suggesting internalization into acidified compartments. When extracellular solution is switched from high pH to low pH fluorescence loss was 25% lower than repeated shifts prior to enzyme application. Once the enzyme was removed overall fluorescence returns to original levels within several minutes implicating the return of the acidified vesicles back to the surface where the pHluorin probe is exposed to the higher extracellular pH and increases in fluorescence intensity.

Similar and consistent results of this manner are also obtained through application of TX100. While not successful in whole-heart experiments, the artifacts of capillary constriction and diffusion limitations are not as prevalent in ventricular strips. Since extracellular solution is directly applied to the surface of the strip we are

monitoring we are able to maintain consistent exposure and buffer to the quantifiable region of interest. Like Sphingomyelinase, TX100 causes a loss in overall fluorescence that is quickly recovered. Drops in the amount of fluorescence shift during TX100 treatment also indicate an increase in internalized NCX. Like similarities between these protocols in fibroblast experiment, the responses obtained from TX100 exposure are very similar to Sphingomyelinase treatment in the ventricular strip further implicating this as a real MEND response within cardiac tissue. The difference here is that the membrane appears to recycle rapidly and the fluorescence shifts rarely exceed 30% of overall signal. If intact cardiac tissue does aggressively recycle membrane this could explain why it is difficult to monitor for loss of NCX using high calcium protocols. The rate of membrane insertion could mask any changes in the rate of endocytosis. However, these protocols are still in the design phase but do suggest promise for imaging MEND and surface trafficking in the intact heart.

40 total deaths					
14 Known Male Deaths			78.35714286	Avg Male lifespan	
18 Known Female Deaths			113.5263158	Avg Female Lifespan	
102.0465116	Average Life Span				
41.46711462	st. dev				
6.323675695	error				
	total	male	female	282 tot/m/f	297tot/m/f
0-30 days	0	0	0	0 / 0 / 0	0 / 0 / 0
31-60 days	5	3	1	4 / 3 / 0	1 / 0 / 1
61-90 days	12	6	4	4 / 2 / 2	8 / 4 / 2
91-120 days	12	4	6	3 / 2 / 0	8 / 1 / 6
121-150 days	6	1	3	3 / 1 / 1	2 / 0 / 2
151-180 days	7	0	4	7 / 0 / 4	0 / 0 / 0
>180 days	1	0	1	0 / 0 / 0	1 / 0 / 1
282 death count	297 death count	(non het)	282 lifespan	297 lifespan	
21	20	Total			
8	5	Male	74.25	87.42857143	Avg Male lifespan
7	12	Female	115.8888889	103.3333333	Avg Female lfspan

Table 3 Six-month analysis of unexplained deaths in transgenic lines. Transgenic Line 282 and 297 over-expressing NCX-pHl were observed to have higher death rates within the first 6 months of life. This table contains descriptions, timelines, and sex of all unexplained deaths during a 6-month retroactive study period. Transgenic line 292 and wild type had no exceptional increase in death rates during the same time period.

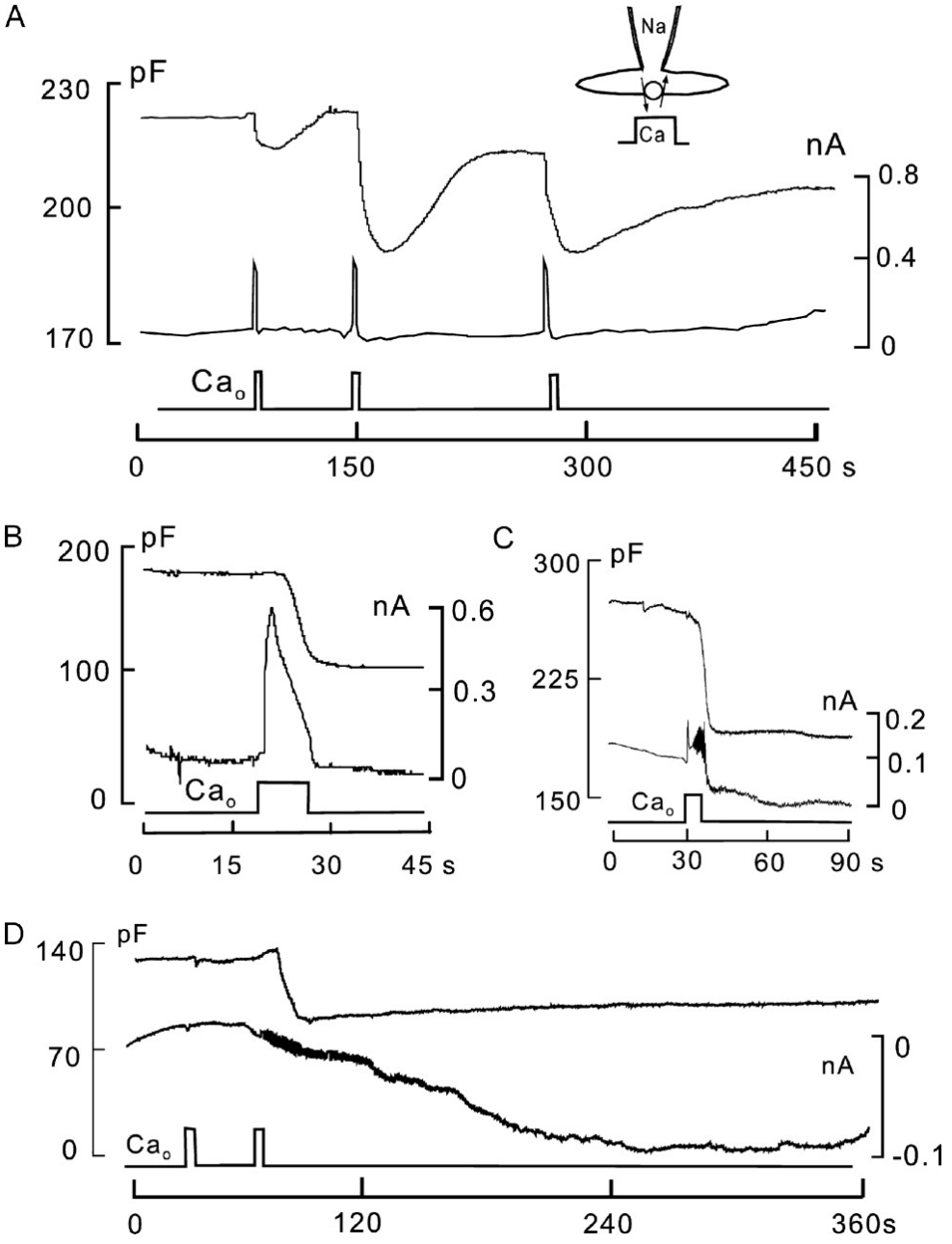

Fig 3.1 Calcium Activated MEND in Isolated Cardiomyocytes. A) Rat cardiomyocytes undergo repeated MEND through reverse activation of endogenous NCX. Calcium Transients were very brief followed by membrane recovery. (All solutions contained 6 mM ATP) B-D) Mouse cardiomyocytes also undergo large calcium induced MEND responses. D) Mouse myocytes undergo MEND through calcium activated spontaneous calcium release. Very small calcium transients trigger contractile activity as seen in the current trace. Eventually the spontaneous calcium release is enough to trigger MEND (Lariccia et al., 2011).

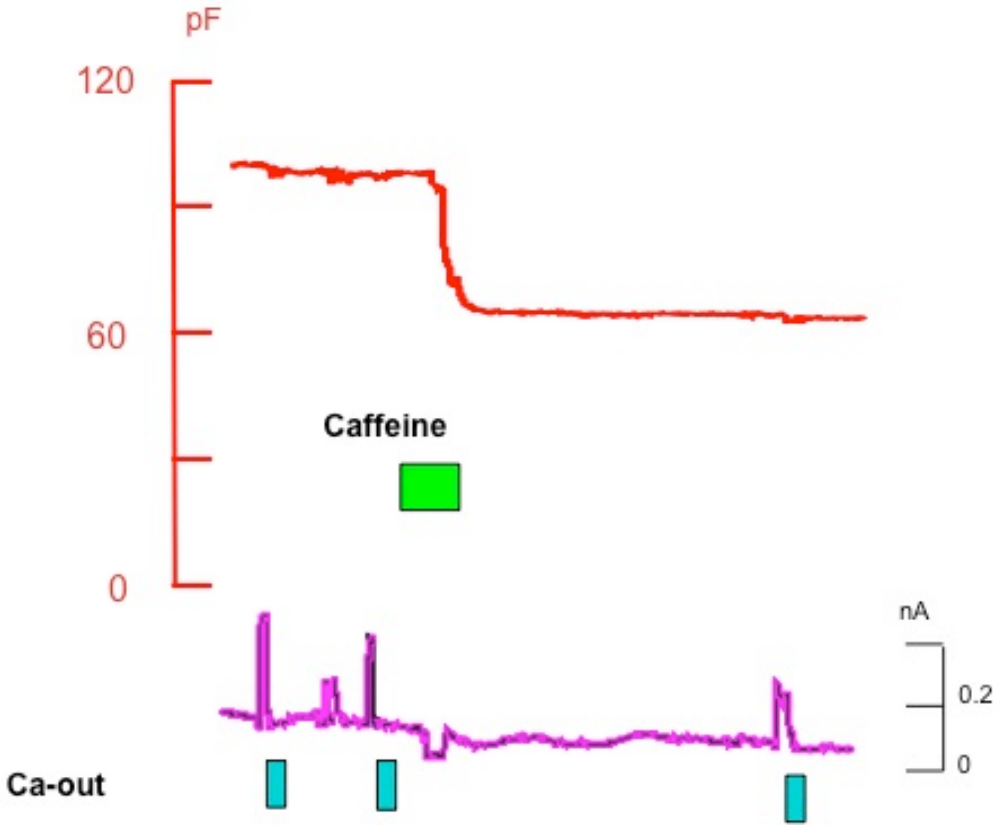

Fig 3.2 Caffeine Induced MEND in Cardiomyocytes. Wildtype isolated murine cardiomyocytes can undergo MEND in response to 5 mM caffeine. Cells were briefly loaded with calcium through small transients induced by reverse activation of NCX. MEND did not occur in response to NCX transients. Subsequently, caffeine was applied for 10 sec releasing calcium from intracellular stores. Capacitance dropped nearly 40% indicating intracellular calcium release may be sufficient to induce MEND. Experiment displayed is work performed by Dr. Donald Hilgemann

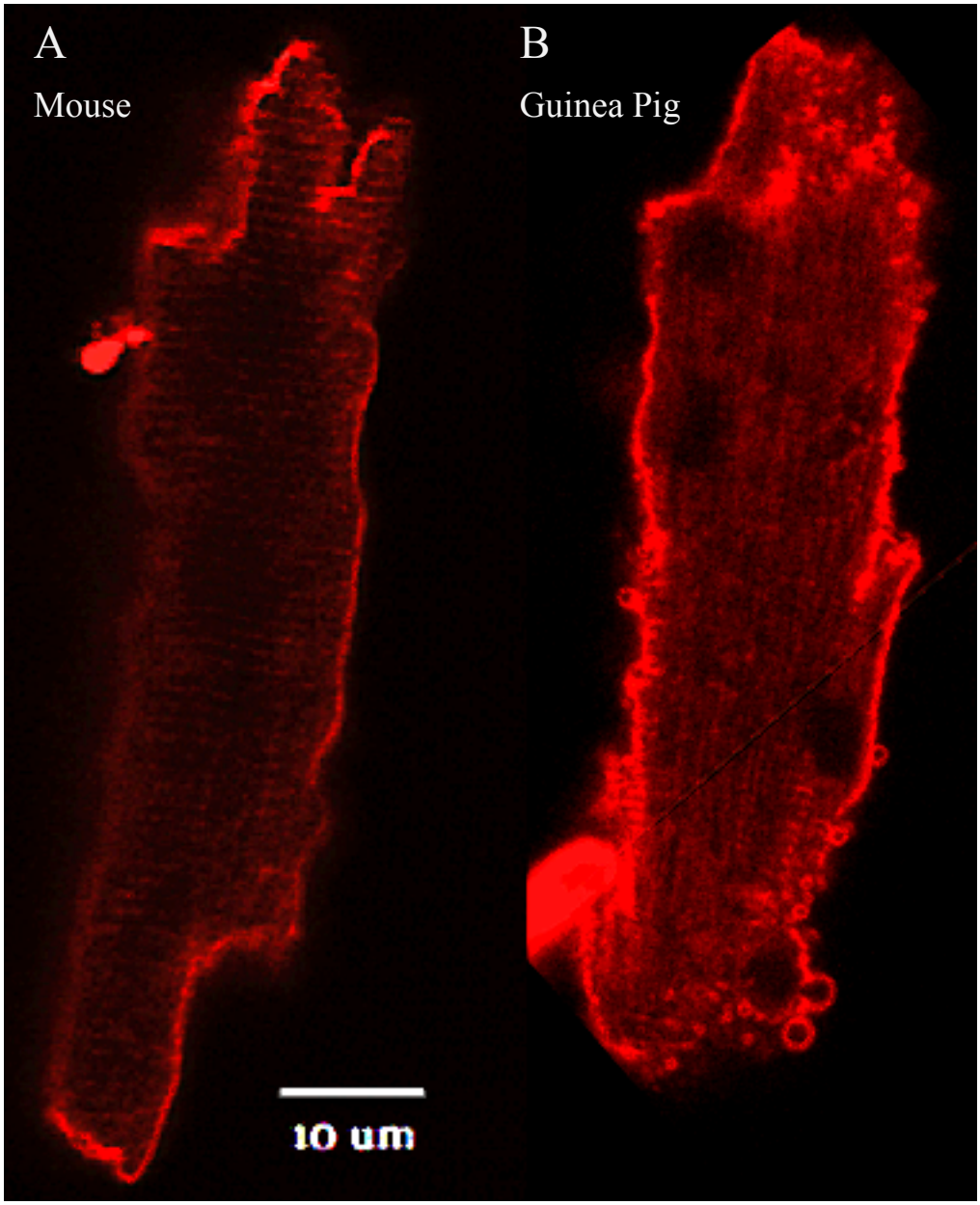

Fig 3.3 Cardiomyocyte membrane labeling across species. A) Murine cardiomyocytes freshly isolated were incubated at RT for 10 minutes in 80 uM di-4-ANEPPS and imaged at 60x using 488 nm ex. And 500-580 nm em. B). Guinea Pig cardiomyocytes imaged using the same protocol. Blebbistatin (10 uM) was used in both treatments to reduce contractility. Note the appearance of t-tubule labeling in the murine myocyte with moderate outer sarcolemma labeling. In the guinea pig there is extensive labeling near the outer sarcolemma, the appearance of small membrane blebs and an near absence of deep t-tubule labeling. These feature indicate that the guinea pig myocyte is undergoing extensive membrane remodeling during the isolation process. Photo contrast and threshold uniformly modified with Fiji to enhance image for print.

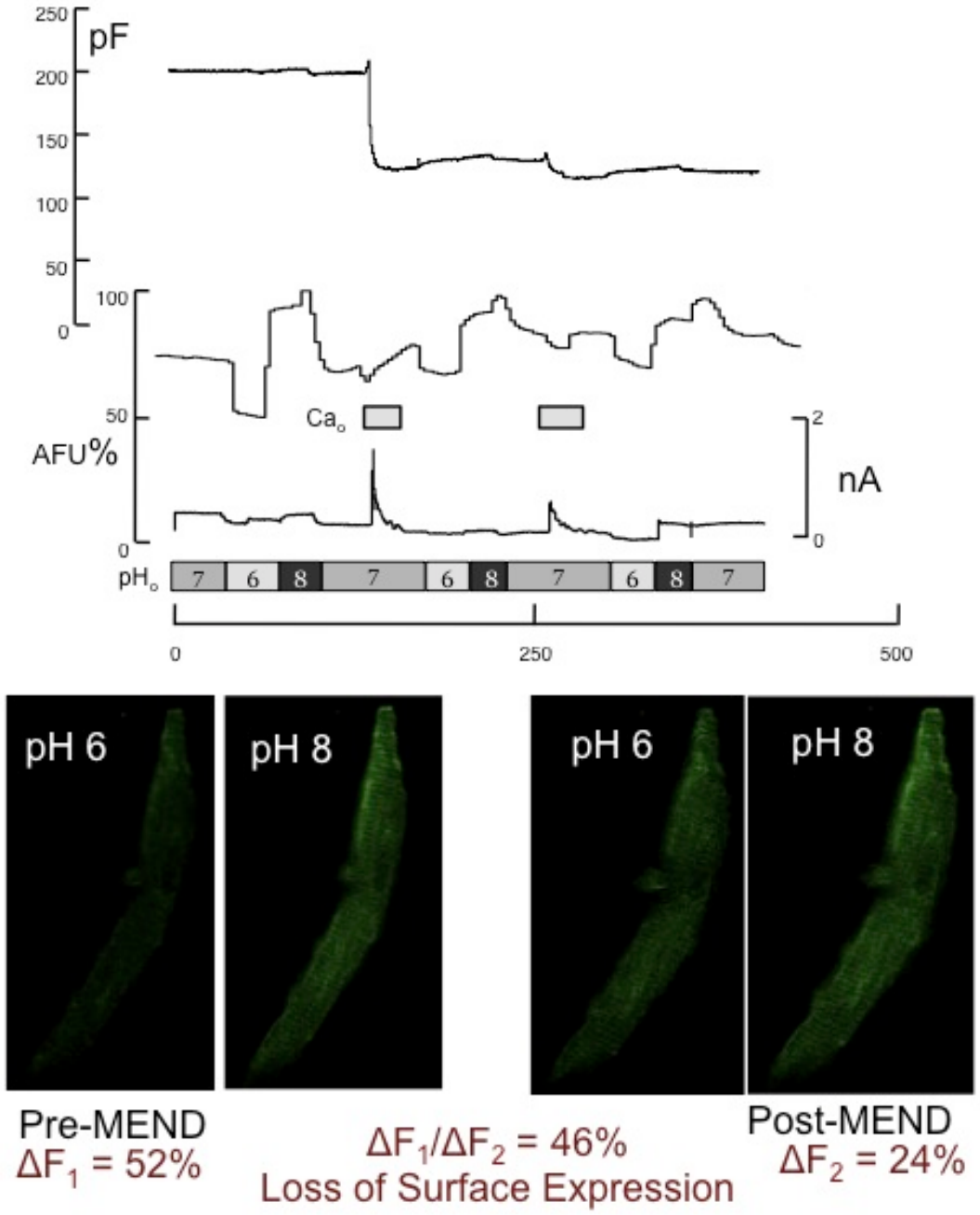

Fig 3.4 Transgenic NCX-pHl cardiomyocyte MEND and NCX Internalization Expression of NCX-pHl in heterozygote transgenic isolated cardiomyocytes shows uniform expression throughout the sarcolemma and t-tubule structures. Confocal images demonstrate 52% of the fluorescence is quenched at low pH. (ΔF_1) Simultaneous whole cell-patch clamp monitoring capacitance (pF) and current (nA) was performed with standard solutions as outlined in Appendix 1. Calcium transients generated large current response (1.8 nA). Following the calcium transient, capacitance dropped nearly 50% indicating the cell under went MEND. Maximal fluorescence values did not change after MEND but the amount of fluorescence quenched at low extracellular pH was reduced to 24% (ΔF_2). Optically, the fraction of NCX-pHl internalized during is calculated at 46% correlating very strongly with the overall surface area lost during MEND.

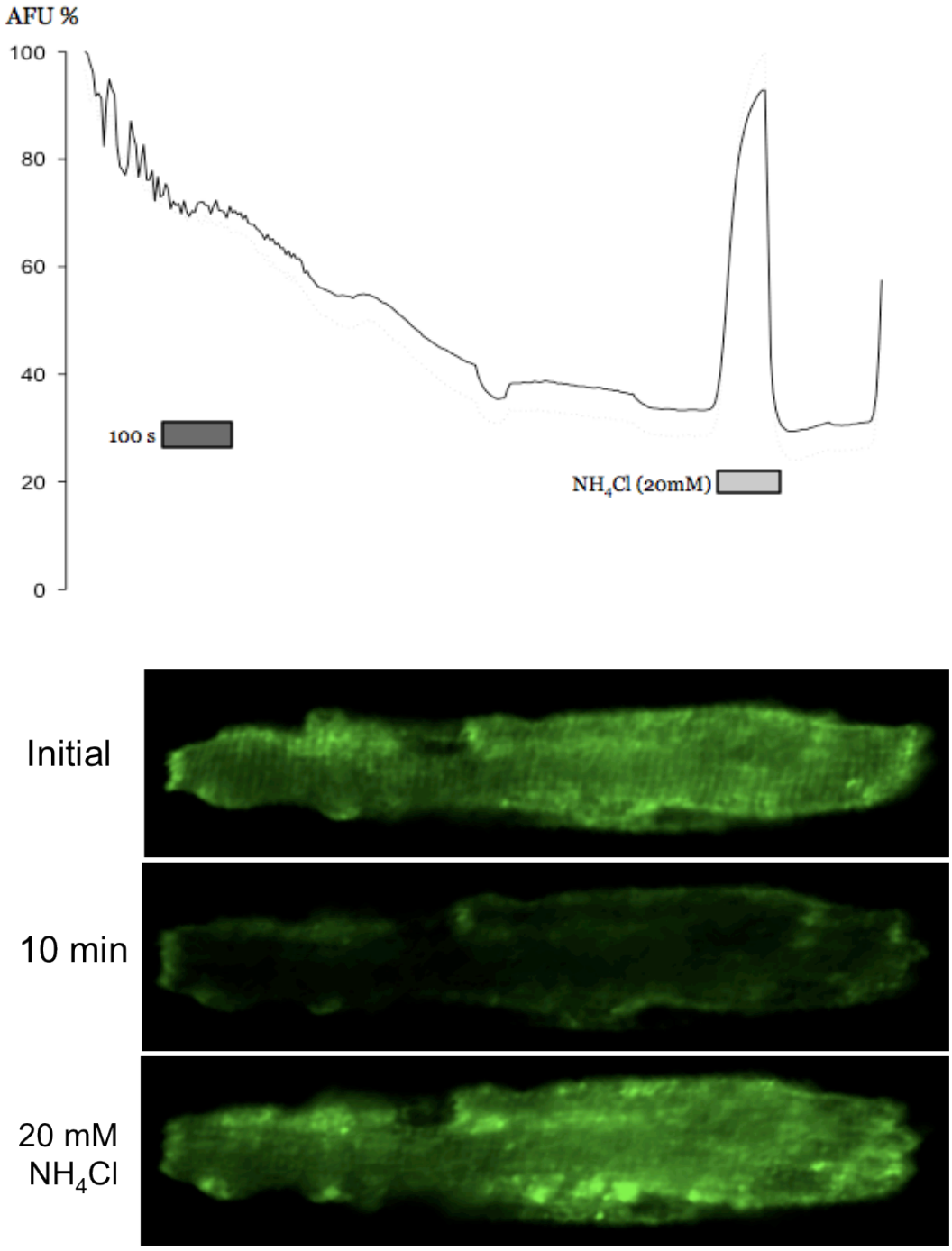

Fig 3.5 Spontaneous MEND in isolated Cardiomyocytes Freshly isolated myocytes observed using confocal microscopy to undergo spontaneous internalization of NCX-pHl. Cells were not patched and in our modified cardiomyocytes bath solution (140 mM NaCl, 15 Hepes, 15 Glucose, 4 KCl, 0.5 NaH_2PO_4, 2 $MgCl_2$, 200 uM $CaCl_2$ set to pH 7.8). Spontaneous calcium release triggered contraction and loss of fluorescence over 20 minutes. Application of 20 mM NH_4Cl caused intracellular alkalization and return of fluorescence to near initial values. However, while some t-tubule structure remains, large punctae of fluorescence were observed.

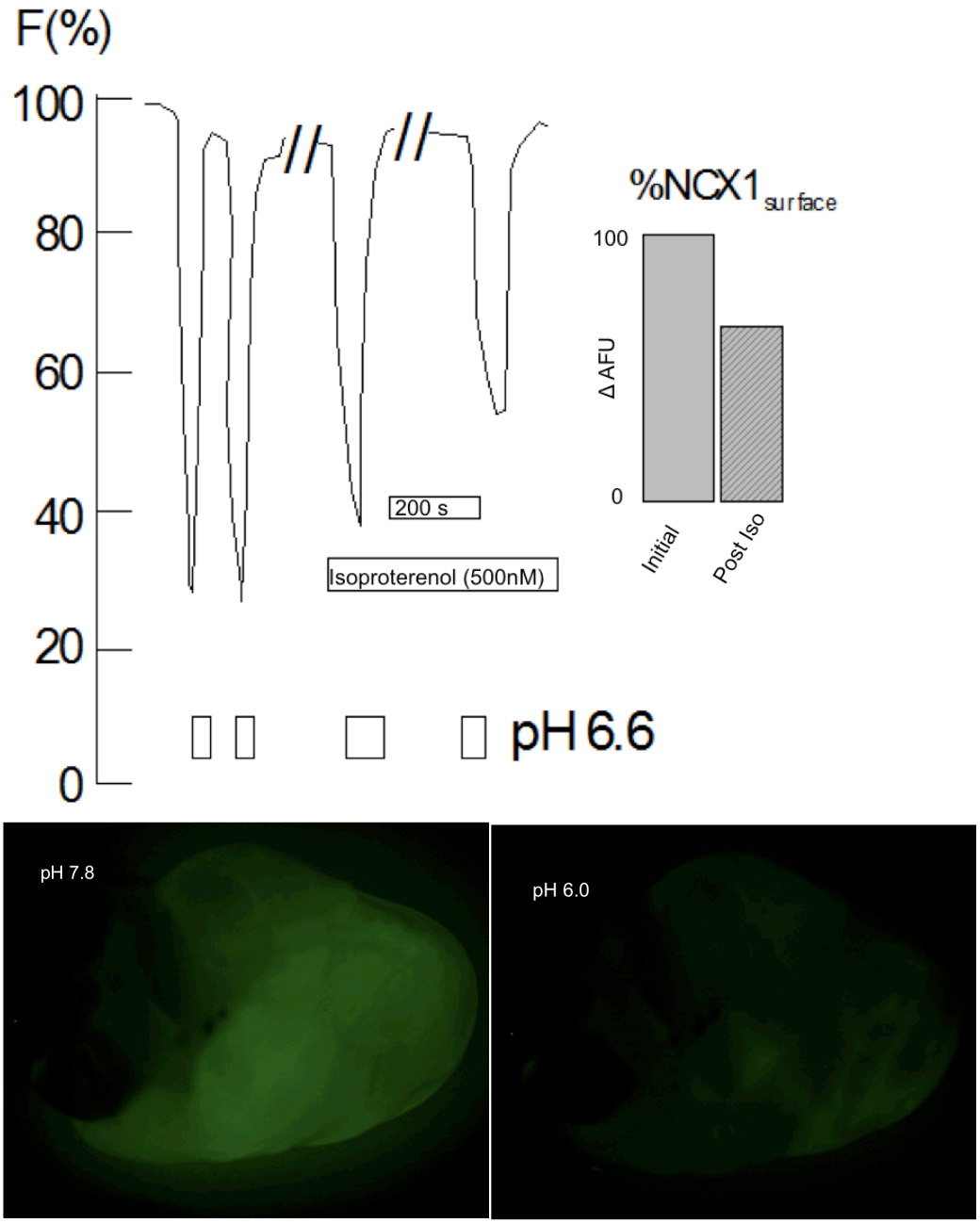

Fig 3.6 Epifluorescent Imaging of MEND in Intact Heart Intact heart was Langendorf perfused with modified cardiac solution containing 55 mM Hepes to stabilize pH and reduced NaCl to slow the rate in which calcium is extruded via NCX. Fluorescence shifts from pH 7.8 to pH 6.6 account for over 70% of the initial fluorescence. After 10 min of Isoproterenol treatment (500 nM) fluorescence shift is reduced to 45% of total fluorescence. This accounts for a relative loss of 30% of the surface fraction of NCX.

CHAPTER 4 – CONCLUSION

Massive endocytosis is a phenomenal example of the power of the lipid membrane. Much of the focus in biological research over the past 20 years has been directed towards understanding the roles genes and proteins play in in the great mystery of life. The plasma membrane has been pushed to the back burner and thought of as a simple barrier that surrounds the cell and holds proteins in place to do their requisite jobs. But for all the potential enzymes and proteins the cell produces there are literally hundreds of lipids. The diversity and specialization of these lipids is rigorously maintained by the cell at great cost. There is an entire field of unexplored science that begs the questions: Why has life evolved to contain such a complicated lipidic environment? What is the purpose and power of the lipid? It is likely these answers surround the fact that the origins of membrane regulation required much of the work to be performed by the lipids themselves. Life evolved to maintain these lipids in such a way that the membrane is always at the edge of phase separating. The ability for small changes within the membrane to allow coalescence of these phases and drive internalization is a by product of the need for cells to react to changes in their environment by bringing in new material or protecting itself from damage. The function of proteins like clathrin and caveolin is to facilitate the lipid environment and allow for greater specificity or targeting of internalized membrane. All of these examples are purely speculation, however the power and potential of the lipidic forces behind MEND are clear and the requirement are as follows.

MEND is a non-canonical form of endocytosis independent from any known adapters. MEND does not require complex rearrangements of the cytoskeleton. While factors like calcium and polyamine contribute to MEND, endocytosis can occur solely through changes in lipid environment. Cleavage of sphingomyelin, manipulation of cholesterol and accumulation of lipid PIP_2 all allow for MEND through changes in their lipid environment. Coalescence of membrane phases contributes to MEND. Application of amphipathic agents like TX100, NP-40 and SDS cause phase separation forcing the *Ld* membrane environment to expand and selectively push the *Lo* phase inward, eventually leading to endocytosis. Selective labeling indicates that the majority of compounds remain in the disordered phase but some functional sorting may exist. Proteins like NCX appear to functionally traffic with MEND. But in addition to any protein sorting that takes place with MEND, there is also evidence that MEND can signal through the lipid bilayer and selectively aggregate intracellular signaling lipids like PIP_2.

4.1 MEND AS A RESEARCH TOOL

LIPID SELECTIVITY

Figure 4.1 shows an example of amphipathic MEND signaling across the bilayer and causing aggregation of PIP_2 into vesicles are internalized in MEND. This would be the first evidence of significant and selective sorting of a compound into the *Lo* phase that is internalized. BHK fibroblasts were co-transfected with PH-GFP, a PIP_2 binding fluorescent peptide, and dr-VSP, a voltage sensitive PIP_2 phosphatase that cleaves PIP_2 at +100mV membrane potentials. Cells were whole-cell patched and imaged through confocal microscopy. Typically, our membrane potential is held fixed at 0 mV and the dr-VSP is inactive. PIP_2 is imaged through the PIP_2 pleckstrin homology domain, PH-GFP, and reveals a fluorescent rim at the surface plasma membrane where PIP_2 is

enriched. By manually increasing the potential to 100 mV activation of the phosphatase cleaves PIP_2 into PIP releasing the PH domain into the cytosol. This is observed as a rapid loss of fluorescence at the edge and an even distribution of cytosolic fluorescence. When membrane potential is returned to 0 mV, the cell rapidly re-phosphorylates PIP into PIP_2 and the fluorescence returns to the plasma membrane. When amphipath MEND causes a 50% reduction in cellular surface area, the 100 mV pulse no longer causes the fluorescence to shift to the cytosol. This would indicate that PIP_2 is highly enriched in the vesicles that have internalized and no longer sensitive to membrane potential. This should come as no surprise as there have been reports that PIP_2 is enriched in detergent resistant domains and localized with specialized "raft" markers(van Rheenen et al., 2005). The one concern for this experiment is the inability to distinguish whether or not it was PIP_2 or the phosphatase, or both that was internalized during MEND. Experiments using FRAP, fluorescence recovery after photobleaching, could be useful, as well as looking for the charge movement of the phosphatase activity before and after MEND. Regardless of the specificity, this experiment clearly demonstrates the potential selectivity of MEND.

PROTEIN SELECTIVITY

With the ability to selectively analyze movements of specific endogenous proteins and lipids both optically and electrically, the potential of MEND as a new tool in membrane research is revealed. Determination of which proteins associate with disordered or ordered membrane could yield interesting relationships in cell signaling and help explain fundamental unknowns regarding the relationships between lipids and proteins. Selecting which lipids best associate with function could help reveal insights into structure determination and even potential novel applications that can alter protein function through modulation of related lipids. On going work in the Hilgemann lab will

focus on taking channels such as the voltage sensitive inward-rectifying potassium channel, $K_{ir,}$ and determine localization within either membrane phase. There is strong evidence that lipid signaling alters functions of potassium channels with dramatic shifts in function following SMase treatment {Bock, 2003 #1108;Ramu, 2006 #1109}. Perhaps novel forms of lipid signaling could arise from the knowledge of how proteins are functionally sorted and what lipids have local interactions.

PROTEIN COMMUNICATION

One question that arises when dealing with the complexity of the plasma membrane and MEND is the potential involvement of protein in the recruitment lipids and phase separation. While it is clear that MEND occurs without involvement of known endocytic adapters, there could still be a role of resident membrane proteins in the promotion of coalesced domains. Evidence supporting an unknown function of proteins arises from an experiment performed to visualize protein internalization during MEND. BHK-NCX fibroblast cells were treated with 5/6-carboxyfluorescein succinimidyl ester. This fluorescent compound reacts with lysine at high pH covalently binding to any exposed residues. The compound remains bound to the amino acid when pH is returned to physiological levels. The compound is not cell permeable and when reacted to cells in culture, massive binding to the outer plasmalemma is easily observed in confocal imaging. Cells maintain their ruffled appearance and can be patched using our typical whole-cell electrophysiological methods. The original intent was to see if we could visualize proteins during MEND and follow the progression and trafficking patterns after MEND. Interestingly, this protocol completely blocked all attempts at calcium and amphipath induced MEND. In this manner, the non-specific binding to all lysine residues could have altered membrane resident proteins that are involved in MEND. Perhaps, there is an unknown role for proteins in MEND. Alternatively, the covalently

attached compound may simply by preventing proteins from packing together as might be required during phase coalescence. This in ability for proteins to sort into their requisite lipid phases prevents the lipids themselves from forming large enough domains to undergo MEND. Regardless of the cause, this apparent communication between lipid and protein stress the important of the power of lipidic forces and the role of MEND in physiology.

4.2 TRANSLATIONAL APPROACHED TO MEND

Studies on membrane movement within intact cardiac tissue have strong implications toward clinical development. Cardiac disease is the number one cause of death in the United States, is a large strain on the already pinched healthcare system and costs billions of dollars each year. While research has revealed some new ways to treat or prevent cardiac failure, efforts to elucidate a mechanism of how some cardiac tissues can survive the stresses of cardiac disease while other regions undergo massive apoptotic events leading to cardiac failure. Focus on the sarcolemma and the powers of lipids, other than serum cholesterol levels, has been downplayed even with mounting evidence of their importance. Many of the hallmarks of cardiac disease indeed exhibit commonalities with triggers of massive endocytosis. Changes in cholesterol, augmentation of t-tubule morphology, exaggerated calcium transients, PIP_2 activiation, SMase activation and production of endogenous amphipathic lysolipids have all been observed in cardiac disease models (Cogolludo et al., 2009; Gwathmey et al., 1987; Karliner and Brown, 2009; Mancuso et al., 2003). What is not known is the role membrane movement is playing in cardiac disease. Is membrane internalization cardioprotective? MEND may allow for rapid internalization of surface transporters during ischemic events such as theorized in the cellular wound response. These internalized transporters would then protect the cell by maintaining an environment in

which calcium levels stayed low. When extracellular conditions improved, the cell could then reinsert this membrane to allow for optimal function post-ischemia. On the other hand, MEND may be a result of cardiac membrane stress leading to increased apoptosis. In this regard, efforts to determine ways to block membrane coalescence and MEND may improve cardiac function during post-ischemia and reperfusion of the tissue. As described earlier, there are ways to block MEND exogenously, however it is necessary to further specify the mechanisms and functions of protein involvement before cardiac specific treatments could arise.

Additionally, our lab has observed diurnal shifts in surface expression of NCX in mice. If indeed changes in NCX are related to circadian events, this might explain how instances of cardiac failure also appear to be circadian-dependent {Huikuri, 1992 #1110}. The use of our transgenic model that allows for trafficking of NCX in circadian studies could provide insight into how and why this phenomena is occurring. Improvements in live-animal optical measurements have made it possible to image fluorescence of transgenic organs in the live animal. An exploration of daily changes in the animal surface expression of NCX would be invaluable to cardiac researchers. This technique could also be applied to cardiac failure models such as aortic banding and hypertrophy. A time-course of surface fraction of critical membrane transporters throughout the course of increasing cardiac disease could reveal levels of detail in the development of cardiac failure that have not been observed.

In a more general sense, MEND could have implications in many forms of clinical research. In our model, coalescence of similar phases is a root cause of endocytosis and this can be triggered from the outside of the cell and not through manipulation of intracellular adapters like caveolin and clathrin. Amphipathic compounds that trigger MEND can be modified to sequester non-hydrophobic drugs for

delivery into cells that normally would have been blocked by the plasma membrane. One of the difficulties in drug design is delivery. A screened compound intended to treat clinical pathologies may be found to have wonderful *in-vitro* properties, however even in cell culture this compound would have to be modified dramatically to traverse the cells lipid bilayer. Attempts to bypass this through binding to antibody like compounds that are targeted for clathrin mediated endocytic pathways have not yielded much success. Perhaps the best approach is to try and use the power of lipids to induce internalization of materials we would want into the cytosolic environment.

Viruses like HIV sometimes utilize secondary non-canonical forms of endocytosis (Vidricaire and Tremblay, 2007). This makes designing treatments difficult, as avenues used to block traditional viral binding and internalization would only partially block disease transmission. These viruses have been theorized to gain access to the cell through raft aggregation and eventual endocytosis. Phase coalescence could be crucial for inward curvature of the membrane and internalization. In the case of HIV, this secondary form of HIV infection typically occurs during transmission across the placenta. In this manner, HIV transmission could be blocked from mother to child, *in-utero*, through compounds that reduce the ability for membranes to phase aggregate within the placenta.

On the other side of the spectrum would be determination of translational approaches to increase the likelihood of MEND. A prime example would be through treatment of cancer. Cancer cells constantly shed membrane, produce higher polyamine levels, and activate pathways that stimulate ceramide such as sphingomyelinase activation. Edelfosine and tamoxifen are powerful anti-cancer drugs that we demonstrated to induce MEND on fibroblasts and cancer cell lines. While the mechanism of action of these drugs goes beyond membrane perturbation, there is evidence to support

new cancer therapies may well be acting on the membrane to induce aggregation and lipid signaling toward apoptotic pathways {van der Luit, 2007 #1119}. If cancer cells are primed for MEND processes, treatments, both surgical and therapeutic, could be designed to gently push the membrane towards phase separation while managing to have minimal effects of non-tumorigenic cells. This approach not unlike the basis of chemotherapies could open up new targets for anti-cancer drugs. Screens could be developed where specific tumors are grown in culture surrounded by non-cancerous tissue. Application of MEND inducing compounds could be applied at varying concentrations while measurements of membrane uptake are observed. If the level of membrane uptake is significantly higher in the tumor plaques than the surrounding tissues, a potential new hit would have been found.

Since the power of lipids affects every cell in our bodies, the potential output for understanding the dynamics of how lipids control uptake and communicate with their resident proteins is boundless. Neurodegeneration has been linked to accumulation of protein aggregates that pass through the neuronal plasma membrane through non-canonical means. Here they can disrupt ion transporter function and lead to cellular death through apparently divergent mechanisms {Dante, 2006 #1137;Mark, 1995 #1138}. If transport of these plaques through the membrane occurs through the use of phase coalescence, the knowledge of different techniques that alter the ability for this to occur could lead to new treatments and therapies for countless conditions. For years, the focus of therapeutic design has been to target the proteins or genes involved in the mechanism of disease causality. The time to shift gears and realize the power of lipidic forces and their influence on proteins, the cellular environment, life and disease has come. Now we must understand these powers, control them, and use them wisely for the betterment of clinical and academic advances.

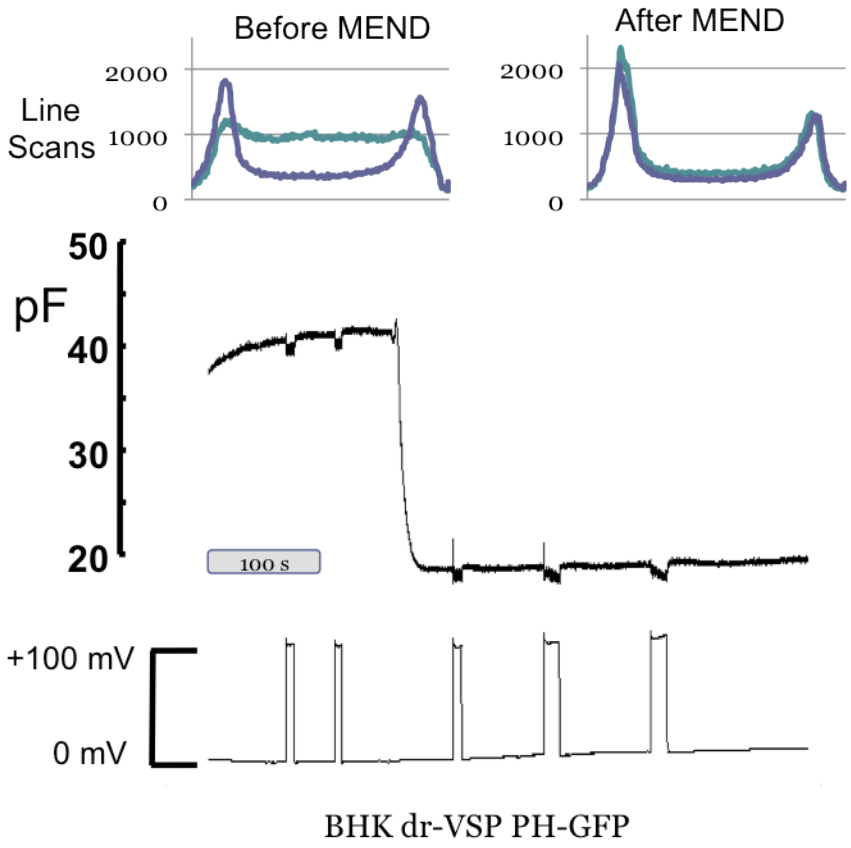

Fig 4.1 Lipid Selectivity in MEND BHK fibroblasts were transfected with PH-GFP, a PIP_2 binding fluorescent peptide, and dr-VSP, a voltage sensitive PIP_2 phosphatase that cleaves PIP_2 at 100mV membrane potentials. Cells were whole-cell patched and imaged through confocal microscopy. Line Scans were taken before activation of the phosphatase (purple) and during (blue). Loss of edge fluorescence as seen before MEND indicates PIP_2 was present at the surface of the cell. After 150 uM treatment of TX100, MEND causes a 50% loss in capacitance, but phosphatase activation no longer cleaves PIP_2. One explanation is that PIP_2 has been highly selected for internalization during MEND and is trapped in vesicles near the surface of the cell, thus no longer sensitive to changes in membrane potential.

APPENDIX –

The subsequent Appendix is a republication of the treatise on MEND as appears in the January and February 2011 issues of the *Journal of General Physiology*. The following includes the manuscript and figures included within the published journal. For supplemental data and videos please visit http://jgp.rupress.org/

APPENDIX 1:

Massive Calcium-Activated Endocytosis Without Involvement of Classical Endocytic Proteins

by

Vincenzo Lariccia, Michael Fine, Simona Magi, Mei-Jung Lin,
Alp Yaradanakul, Marc C. Llaguno, and Donald W. Hilgemann

Department of Physiology
University of Texas Southwestern Medical Center at Dallas
5323 Harry Hines Blvd.
Dallas, Texas 75390-9040 USA

Address correspondence to:

Donald W. Hilgemann
University of Texas Southwestern Medical Center at Dallas
5323 Harry Hines Blvd.
Dallas, Texas 75390-9040 USA

Email: donald.hilgemann@utsouthwestern.edu
Tel: 214-645-6031
Fax: 214-645-6049

Running Title:

Ca^{2+}-Activated Massive Endocytosis

Abbreviations. adapter protein 2, AP2; adenylyl imidodiphosphate, AMP-PNP; adenosine 5′-[γ-thio]triphosphate, ATPγS; bromoenol lactone, BEL; β-methylcyclodextrin, BMCD; cardiac Na/Ca exchanger, NCX1; membrane capacitance, C_m; cyclosporinA, CsA; diaminobenzidine, DAB; ethylenediamine, EDA; guanosine 5′-[γ-thio]triphosphate, GTPγS; horseradish peroxidase, HRP; hydroxypropyl-β-cyclodextrin, HPCD; massive endocytosis, MEND; nitrilotriacetic acid, NTA; phosphatidylinositiol-bis 4,5-phosphate, PIP_2; sphingomyelinase, SMase

Abstract

We describe rapid massive endocytosis (MEND) of >50% of the plasmalemma in BHK and HEK293 cells in response to large Ca transients. Constitutively expressed Na/Ca exchangers (NCX1) are used to generate Ca transients, while capacitance (C_m) recording and a membrane tracer dye, FM 4-64, are used to monitor endocytosis. With high cytoplasmic ATP (>5 mM), Ca influx causes exocytosis followed by MEND. Without ATP, Ca transients cause only exocytosis. MEND can then be initiated by pipette perfusion of ATP, and multiple results indicate that ATP acts via PIP_2 synthesis: PIP_2 substitutes for ATP to induce MEND. ATP-activated MEND is blocked an inositol 5-phosphatase (IPP5c), and it is blocked by GTPγS. Block by GTPγS is overcome by the phospholipase C (PLC) inhibitor, U73122, and PIP_2 induces MEND in the presence of GTPγS. MEND can occur in the absence of ATP and PIP_2 when cytoplasmic free Ca is clamped to 10 μM or more by Ca-buffered solutions. ATP-independent MEND occurs within seconds during Ca transients when cytoplasmic solutions contain polyamines (e.g. spermidine) or the membrane is enriched in cholesterol. While PIP_2 and cholesterol can induce MEND minutes after Ca transients have subsided, polyamines must be present during Ca transients. MEND can reverse over minutes in an ATP-dependent fashion. It is blocked by brief β-methylcyclodextrin (BMCD) treatments, and tests for involvement of clathrin, dynamins, calcineurin, and actin cytoskeleton were negative. Therefore, we turned to the roles of lipids. Bacterial sphingomyelinases (SMase) cause similar MEND responses within seconds, suggesting that ceramide may be important. However, reagents that inhibit SMases do not block Ca-activated MEND. MEND is abolished by the alkylating PLA2 inhibitor, bromoenol lactone (BEL), while exocytosis remains robust, and Ca influx causes MEND in cardiac myocytes without preceding exocytosis. Thus, exocytosis is not prerequisite for MEND. From these results and two companion studies, we suggest that Ca promotes formation of membrane domains that spontaneously vesiculate to the cytoplasmic side.

Introduction

Experiments demonstrating that Ca influx triggers exocytosis of neurotransmitters are a cornerstone of modern physiology (Katz, 1996). Recently, the regulatory roles of Ca in endocytic responses, occurring subsequent to exocytosis, have gained attention. One common observation is that progressively larger Ca transients trigger progressively larger

endocytic responses, resulting in 'excessive' endocytosis, such that cell area decreases below basal levels (Engisch and Nowycky, 1998; Smith and Neher, 1997; Thomas et al., 1994). In melanotrophs, 25% of the cell surface can be internalized in a few seconds after release of caged Ca (Thomas et al., 1994). These responses occur in the absence of cytoplasmic potassium, a condition in which clathrin-dependent endocytosis is blocked (Ivanov, 2008) by disruption of AP2 complexes (Altankov and Grinnell, 1995). Furthermore, the vesicles generated can be larger than expected for clathrin-mediated endocytosis (Thomas et al., 1994). In synapses, endocytic mechanisms that appear to be related to 'excessive' endocytosis become dominant as synaptic activity increases. Dubbed 'bulk endocytosis', this form of scaffold-independent endocytosis is evidently controlled and/or driven by dynamins (Clayton and Cousin, 2009). That Ca influx through Ca channels can trigger endocytosis is also well established in non-excitable cells, such as oocytes (Vogel et al., 1999). A general biological response involving Ca-activated endocytosis is the response of cells to membrane ruptures or 'wounding' (Idone et al., 2008). In brief, punctures of the cell surface flood cells with Ca, and such membrane wounds are closed by fusion of internal membranes with the cell surface, followed by removal of 'lesion' membrane by endocytosis (Idone et al., 2008) to non-acidified membrane compartments (Cocucci et al., 2004).

Calmodulin and Ca/calmodulin-dependent phosphatases have been suggested repeatedly to play crucial roles in the actions of Ca to promote endocytosis in secretory cells (Artalejo et al., 1996; Chan and Smith, 2001; Engisch and Nowycky, 1998; Marks and McMahon, 1998; Wu et al., 2009). Inhibition by specific inhibitors of calcineurin (Engisch and Nowycky, 1998; Marks and McMahon, 1998) provides clear evidence for a role of this phosphatase, a role that may reflect regulation of dynamin I by its dephosphorylation (Smillie and Cousin, 2005). However, other reagents used to implicate calmodulin are less specific. Cationic peptides used to 'block calmodulin' (Wu et al., 2009) bind PIP_2 with high affinity (de Haro et al., 2004), and the use of calmodulin antibodies to define calmodulin-dependent processes (Artalejo et al., 1996) has not yet been demonstrated to be reliable or specific.

We describe here efforts over several years to understand how large Ca transients cause massive endocytic responses (MEND) in BHK fibroblasts, HEK293 cells, and cardiac myocytes. During these studies, it became apparent that Ca promotes MEND by long-

term effects that can accumulate over multiple Ca transients, as well as by short-term mechanisms that require the immediate presence of cytoplasmic Ca. To our surprise, we were not able to implicate any classical endocytic protein in MEND, including clathrin, dynamins, and actin cytoskeleton, while it became increasingly clear that the membrane itself (e.g. its cholesterol content) strongly influences MEND. Thus, we were forced to consider how mechanisms inherent to the membrane itself might be important.

From several possibilities, ceramide metabolism appeared of interest. Bacterial sphingomyelinases (SMases), which generate ceramide from sphingomyelin, cause large endocytic responses in ATP-depleted macrophages and fibroblasts (Zha et al., 1998) and cause giant liposomes to bud vesicles to the membrane side opposite to which they are applied (Holopainen et al., 2000). This type of endocytosis reflects formation of ceramide domains that develop high inward curvature and undergo spontaneous budding and fission (Goni and Alonso, 2009; Staneva et al., 2009). As described here, exogenous SMases can indeed cause MEND within seconds. However, Ca-activated MEND is not caused by the exocytosis of SMases and ceramides, as suggested in a study published since this article was first submitted (Tam et al., 2010). Rather, MEND can be dissociated from exocytosis by pharmacological means, and MEND occurs in some cell types without detectable exocytosis. Furthermore, MEND is not blocked by cell treatments that are described to disrupt acid SMase activities. We suggest that Ca-activated MEND may rather reflect the coalescence of previously existing lipid domains followed by their spontaneous budding and fission to the cytoplasmic side.

As orientation to our presentation of Results, we describe first electrical and optical data demonstrating that MEND represents endocytosis rather than membrane shedding and that membrane proteins are internalized. Equivalent results are presented as Supporting Data for two other MEND protocols. Second, we describe the existence of two different forms of Ca-activated MEND. Third, we describe five different protocols that induce Ca-dependent MEND followed by salient observations made with each protocol. Fourth, we describe MEND responses induced by bacterial SMases and evidence that the exocytosis of SMases does not mediate Ca-activated MEND. Finally, we describe Ca-activated MEND that occurs in cardiac myocytes without preceding exocytosis.

Materials and Methods

Cell Culture, NCX1-pHluorin fusion, and myocytes. BHK cells expressing NCX1.1 (Linck et al., 1998) were maintained as described (Yaradanakul et al., 2007). T-REx-293 cells (Invitrogen, Carlsbad, CA) were stably transfected with pcDNA3.1 (+) to express an NCX1.1 fusion with a pH-sensitive green protein, pHluorin (Miesenbock et al., 1998), near the NCX1 glycosylation site (Hryshko et al., 1993). Cells were grown in DMEM (Mediatech, Manassas, VA) with 10% (w/v) fetal bovine serum (FBS), 2 mM L-glutamine, 100 U/ml penicillin, and 100 µg/ml streptomycin. T-REx-293 cells were selected with G418, Zeocin, and Blasticidine, and transfections were with Lipofectamine 2000 (Invitrogen, Carlsbad, CA). Cells were harvested at 80-90% confluency with trypsin (0.25%). Cardiac myocytes were isolated as described (Yaradanakul et al., 2007) and employed within 3 h.

Generation of the NCX1-pHluorin fusion near the NCX1 glycosylation site. The pcDNA3.1 (+) NCX1.1 (GeneBank #L06438) plasmid (Dr. J.P. Reeves, UMDNJ, Newark) was mutagenized using a QuickChange Site-Directed Mutagenesis kit (Stratagen, Cat#200518) to include a novel *ClaI* restriction site near to the glycosylation site using the primers 5'-GCT CTC TTG TTT TCC CAT ATC GAT GTG GAC CAT ATA AGT GC-3' and 5'-GCA CTT ATA TGG TCC ACA TCG ATA TGG GAA AAC AAG AGA GC-3'. pHluorin cDNA flanked with *ClaI* restriction sites was generated by PCR from a Vamp2-pHluorin plasmid (Dr. R.H. Edwards, UCSF, San Francisco) and the following oligonucleotide primers: 5' ATC GAT AGC GGC GGA AGC GG-3' and 5' ATC GAT TCC GCC GGT TTT GTA TAG TTC ATC C-3'. The *ClaI*-pHluorin-*ClaI* cDNA PCR product was then cloned into the modified pcDNA3.1 (+) NCX1.1 plasmid at its new *ClaI* site to create the final pcDNA3.1-NCX1.1-pHluorin. Stable cells were screened and selected according to the supplier's protocols.

Cell preparation and selection, patch clamp, C_m recording and imaging. All BHK and T-REx-293 cells were removed from dishes by trypsin and allowed to recover in suspension for 20 min before experiments. In general, relatively large cells were selected for experiments because results were less variable from cell to cell, and our methods to perfuse pipettes are more facile because larger pipettes can be used with larger cells.

Patch clamp with *on-line* recording of cell electrical parameters and pipette perfusion was performed as described (Wang and Hilgemann, 2008; Yaradanakul et al., 2007). Temperature was 35-37°C and input resistances were 2-8 MΩ. Unless stated otherwise, square wave voltage perturbation (20 mV, 0.2-1 kHz) was employed for C_m measurements. During patch clamp recording without imaging, solution switches were made by rapidly moving the microscope platform *by hand* so that the cell being monitored was placed directly in front of the solution outlet of interest. The height of solution reservoirs was adjusted to generate flow speeds of at least 2 mm per s in the center of solutions streams. Currents that respond immediately to solution changes typically came to >80% of steady state within 100 to 150 ms upon changing solutions. The apparent cell resistances were 0.05-3 GΩ. BHK cells usually had lower resistances than T-REx-293 cells. In our experience, this 'resting' resistance reflects mostly the seal/leak pathway in BHK cells. Since the seal resistance pathway does not pass through the entire cell access resistance pathway (Lindau and Neher, 1988), it is impossible to calculate C_m changes accurately when conductance changes may reflect either seal or cell resistance changes. Nevertheless, it can be determined to what extent C_m changes may be misrepresented if *exclusively* seal or membrane resistance changes are occurring. On this basis, we have discarded all results in which conductance changes potentially affect C_m measurements.

For confocal imaging, a Nikon TE2000-U microscope (60x oil immersion 1.45 NA objective; Warner Instruments RC-26 recording chamber) was used with a 40 mW Spectra Physics 163-CO_2 laser operating at 488 nm and a 1.5 mW Melles Griot cylindrical HeNe Laser at 543 nm at 3% and 7% of maximum capacity for pHluorin and FM 4-64 recordings, respectively. Resolution was set to 256x256, yielding <1 second exposure times with a pinhole of 100 μm. Bleaching of fluorophores was negligible during experiments.

Solutions and Materials. Solutions employed minimized all currents other than NCX1 current. Free Mg of all cytoplasmic solutions was 0.4 mM. Standard Extracellular Solution contained in mM: 120 LiOH, 4 $MgCl_2$ or 2 $MgCl_2$ + 2 $CaCl_2$, 20 TEA-OH, 10 HEPES, 0.5 EGTA, pH 7.0 with aspartate. The Standard Cytoplasmic Solution contained in mM: 80 LiOH, 20 TEAOH, 15 HEPES, 40 NaOH, 0.5 $MgCl_2$, 0.5 EGTA, 0.25 $CaCl_2$, set to pH 7.0 with aspartate. Unless indicated otherwise, 0.2 mM GTP was employed in

nucleotide containing solutions. A Modified Cytoplasmic Solution used in myocyte recordings and selected recordings in two companion papers (Fine et al., 2011; Hilgemann and Fine, 2011) contained in mM: 60 KOH, 50 NaOH, 15 TEAOH, 15 HEPES, 0.5 $MgCl_2$, 1.0 EGTA, 0.2 $CaCl_2$, set to pH 7.0 with aspartate. For pipette perfusion experiments in Figs. 4C and 4D, NaOH was replaced in the cytoplasmic solutions by CsOH. For experiments with spermidine reported in Fig. 8D, TEA-OH was replaced in standard solutions by 15 LiOH and 5 CsOH, and aspartate was replaced by MES, as removal of all amines except spermidine improved reliability of the protocol. By contrast, the unnatural polyamine, ethylenediamine (EDA), was maximally effective with the Standard Cytoplasmic Solution.

All chemicals were the highest grade available from SIGMA, unless indicated otherwise. Recombinant K44A dynamin 2 was a gift of Dr. Joseph Albanesi (UTSouthwestern, Dallas). Commercial *Bacillus cereus* SMase was from SIGMA. As this preparation is not pure, the concentrations employed are given as Units per ml. Purified *Bacillus cereus* SMase was a generous gift of Dr. Jun Sakurai (Tokushima Bunri University, Tokushima Tokyo University). Recombinant bacterial sphingomyelinase was a generous gift of Dr. Zhe Lu (U. Penn, Philadelphia).

Preparation of hydroxypropyl-β-cyclodextrin (HPCD)-cholesterol complexes. 20 mM HPCD was dissolved in standard extracellular solution, 25% ethanol was added, and the solution was heated under stirring to 70˚C. Cholesterol was added slowly while stirring vigorously in 25 µL aliquots from a 40 mM stock solution to give a final concentration of 0.8 mM. The solution was stirred further, applying heat that induced just detectable boiling, until volume was reduced to 90% of the original volume without ethanol. Finally, volume was readjusted with distilled water to the original volume, and the solution was passed through a 0.2 micron filter.

Data Analysis and Statistics. Experiments were performed in pair-wise fashion for each manipulation and its control with each cell batch. Unless indicated otherwise, error bars in figures give the standard errors for 5 or more observations, usually 7 or more. To simplify figures, 'control' results from multiple sets of experiments were pooled when mean results from the different sets were not statistically different. Significance of results was determined by Student's t-test. Outliers were eliminated using 2 standard deviations

from the mean as criterion. In several figures, a representative experimental record is given together with normalized data points for a data set. To do so, C_m records were normalized to C_m at a specified time point within each experiment, and then the normalized C_m data points were scaled to C_m at the specified time point in the experiment.

Characteristics of NCX1-mediated Ca Transients and C_m changes. Figures 1 and 2 demonstrate our methods to monitor the electrical properties of cells simultaneously with optical recording of fluorescent probes and manipulation of solutions on both membrane sides. Fig. 1 illustrates recording of cell capacitance (C_m, measured in picofarads, pF), membrane currents (I_m) and cellular fluorescence (F) of a Ca indicator by confocal imaging, simultaneously with pipette perfusion to manipulate and/or control the cytoplasmic contents of cells (Yaradanakul et al., 2008). Here, and in most figures, we employ BHK cells constitutively expressing cardiac Na/Ca exchangers (NCX1) that can be used to evoke large Ca transients when Ca is applied to the extracellular membrane surface. Patch clamp is established with Ca-free extracellular solution, and cells are positioned in a temperature-controlled solution stream. Then, outward NCX1 current (i.e. Ca influx; see 'I_m' record) is activated by applying 2 mM extracellular Ca for 5 s with high (40 mM) cytoplasmic Na and low (0.5 mM) cytoplasmic EGTA. In this case, a low affinity Ca indicator, Fluo-5N (3 μM; K_d = 90 μM; (Takahashi et al., 1999)), was included in pipette solutions to allow estimation of free Ca changes. The initial pipette solution contains 0.5 mM EGTA with 0.25 mM Ca (i.e., 0.4 μM free Ca) and 2 mM ATP. When 2 mM Ca is applied, current rises rapidly to a peak of 120 pA, decays partially during the application of Ca, and then decays to baseline within 2 s when Ca is being removed. C_m increases by about 50% during the Ca transient, as vesicles fuse to the cell surface (Yaradanakul et al., 2008). Peak fluorescence occurs at 3 s. Fluorescence begins to decay before removal of Ca and then decays completely within a few seconds after NCX1 current decays. Upon perfusion of the pipette tip with solution containing 0.5 mM free Ca (i.e. with 1 mM total Ca in the 0.5 mM EGTA-containing Standard Solution), fluorescence rises toward a steady "maximal" level over a time course of about 1 min. Since the great majority of Ca is bound as Ca enters the cell (Yaradanakul et al., 2008), this time course is many times longer than exchange of ions that are not buffered by cell constituents (e.g. potassium). During Ca perfusion, C_m approximately doubles with respect to the pre-perfusion level with a delay to the Ca signal, demonstrating the

existence of a large membrane reservoir in these cells. As apparent at the end these records, the increase of C_m during Ca perfusion was followed by a decline. This decline is described in more detail in Figs. 4C and D, whereby the decline is larger and occurs more rapidly using highly Ca-buffered pipette solutions. Peak fluorescence during the Ca transient reaches 57% of the maximal fluorescence of dye saturated with 0.5 mM free Ca. Assuming a K_d of 90 μM for the Fluo3 dye, the peak free Ca occurring during the Ca transient is 157 μM Thus, these protocols generate Ca transients that exceed normal Ca signaling in cells, except as may occur, for example, during 'cell wounding' .

Online Supplemental Material. Complete video recordings of the experiments presented in Fig. 2A and 2B are provided as Online Supplemental Material. Also, a video record of the myocyte experiment presented in Fig. 11D is provided. In addition, the following experimental data is provided: Optical measurements of membrane and NCX1 internalization during Ca/polyamine- and SMase-induced MEND (Figs. S1 and S2), control experiments for FM 4-64 and NCX1-pHluorin experiments demonstrating repeatability of protocols without MEND (Fig. S3), experiments demonstrating that MEND results in a loss of inward exchange current (Fig. S4), description of polyamine/Ca induced MEND in a cell population (Fig. S5), internalization of NCX1 in response to SMase treatment in cover slip-attached cells (Fig. S6), analysis of the ATP dependence of ATP-dependent MEND (Fig. S7), evidence that BMCD-induced reductions of membrane area (i.e. Cm) result mostly from extraction of cholesterol and phospholipids, rather than endocytosis (Figs. S8 and S9), activation of MEND by multiple SMases, but not by other phospholipases (Fig. S10), experiments demonstrating the long-lived nature of MEND facilitation by Ca (Fig. S11), and description of large capacitance steps often observed during MEND when induced by pipette perfusion of PIP_2 (Fig. S12).

Results.

Measurement of membrane and NCX1 internalization. To facilitate and abbreviate the subsequent presentation and descriptions of MEND, we describe first our methods to monitor the internalization of membrane *per se* and of cardiac Na/Ca exchangers using one of the MEND protocols described subsequently. Equivalent data is presented in Supporting Figs. S1 and S2 for two other MEND protocols. Full length videos of the experiments shown in Fig. 2 are available as Supporting Data. In each case, the

magnitudes of MEND determined by capacitance recording are verified by optical measurements of FM 4-64 dye uptake into vesicles below the cell surface, and nearly equivalent fractions of Na/Ca exchangers are internalized. In the protocol described in Fig. 2, a large Ca transient is induced by activation of reverse Na/Ca exchange in the absence of ATP, and MEND is subsequently activated by pipette perfusion of ATP (2 mM) into the cell. Results for the membrane tracer dye, FM 4-64, employ BHK cells, and results for NCX1 employ the T-REx-293 cell line expressing the pHluorin-NCX1 fusion protein described above.

As illustrated in Fig. 2A, FM 4-64 binds and unbinds rapidly from BHK cells when applied and removed, thereby defining fluorescence contributed by dye in the outer plasmalemma monolayer. In Supporting Data Fig. S3, we show that, even after prolonged incubation without activating Ca influx, FM 4-64 dissociates nearly completely from BHK cells within seconds. As indicated in Fig. 2A, application of Ca for 10 s causes substantial exocytosis. During exocytosis, FM fluorescence increases by 140%, while C_m increases by only 59%. Thereafter, fluorescence declines by 73% when dye is washed off, and the presence of a residual fluorescence rim indicates that significant endocytosis occurred during fusion. In all experiments with large exocytic responses, the magnitude of FM fluorescence that washed off within a few seconds was markedly increased, and reapplication of FM dye then caused a clearly detectable capacitive signal. This capacitive signal is described in more detail in Supporting Data to a companion article (Hilgemann and Fine, 2011). Quantitatively, the fluorescence signal corresponding to rapid FM dye binding-unbinding increased on-average 30% more than expected from C_m changes during membrane fusion. Thus, FM dye binds more avidly to the cell surface after a large Ca transient.

During MEND in Fig. 2A, FM fluorescence grows by 15% over 2 min. Thereafter, FM fluorescence decreases by only 35% upon washout of dye, and the response to applying and removing dye is then reduced by 60% in comparison to the rapid response before MEND. The FM signal that does not wash off amounts to 60% of the rapid response before MEND. Thus, the optical signals are closely consistent with the 65% decline of C_m reflecting an endocytic response, rather than membrane shedding. After the final dye washout, the retained fluorescence (see inset) reveals many large vacuoles up to 2.5 μm in diameter. These vacuoles presumably form by fusion of small vesicles, subsequent to

their endocytosis, as we do not routinely observe in this protocol capacitance steps that would account for vacuoles being generated in single endocytic steps. We note that formation of vacuoles during MEND was a variable observation, and that in a majority of cases the vesicles in the retained fluorescence rim were too small to accurately determine their size optically.

Internalization of NCX1 transporters during MEND is documented in Fig. 2B using the extracellular NCX1 fusion with the pH-sensitive green fluorescent protein, pHluorin(Miesenbock et al., 1998), constitutively expressed in T-REx-293 cells. As evident from the electrical records, C_m responses in T-REx-293 cells were very similar to those of BHK cells. In these experiments, fluorescence corresponding to NCX1 on the cell surface was rapidly determined by switching extracellular solutions from pH 7 to 6 to 8. At pH 6, fluorescence of pHluorin is negligible, and the jump on switching from pH 6 to 8 defines fluorescence from NCX1 at the cell surface. After one Ca influx episode and perfusion of ATP, C_m declines by >50% from its peak value, and the fluorescence jump from pH 6 to pH 8 decreases by 36%. Thus, only about 36% of exchangers are internalized when approximately 50% of the plasmalemma is internalized. Analysis of inward NCX1 currents, shown in Supporting Data Fig. S4, quantitatively supports the conclusion that NCX1 is not preferentially internalized during MEND. Since fluorescence is increased at pH 6, after C_m has decreased, and fluorescence at pH 8 is decreased, NCX1 must enter an intracellular membrane compartment that does not acidify quickly.

In the further presentation of Results, we assume that the C_m changes described reflect changes of cell surface area as a result of exocytic and endocytic responses with minimal membrane shedding. Besides the optical measurements presented above, which support this interpretation, Supporting Data Figs. S1 and S2 provide similar evidence for two other MEND protocols.

Two forms of Ca-activated MEND and membrane cycling in BHK cells under control of a polyamine switch. Figures 3A and 3B describe two different Ca-activated MEND responses that occur in BHK cells, one that is highly ATP/PIP_2-dependent and one that has no requirement for either ATP or PIP_2. As described in a previous study (Yaradanakul et al., 2008), Ca influx in BHK cells causes exocytic responses that are

compensated by approximately equal endocytic responses when cytoplasmic solutions contain 2 mM ATP. As shown in Fig 3A, much larger, 'excessive' endocytic responses occur when higher, more physiological ATP concentrations are employed. With 8 mM ATP, as shown in Fig. 3A, C_m increases in a few seconds by about 20% during Ca influx and remains stable as long as Ca influx continues. When Ca influx is terminated, C_m remains stable for 10 to 20 seconds and then falls over 2 min by nearly 50% from its peak value. As shown in the remainder of the record, these responses can be repeated multiple times with exo- and endocytosis amounting to 50% of the cell surface. We note that these exocytic decrease only partially with extended exposure to ATP-free solutions (Yaradanakul et al., 2008).

Polyamines (i.e. putrescine, spermidine and spermine) are ubiquitously present in eukaryotic cells at high concentrations. The free concentration of spermidine, which has gained much recent interest as a promoter of longevity (Kaeberlein, 2009), is in the range of several hundred micromolar (Igarashi and Kashiwagi, 2000). Relevant to this study, polyamines modulate the function of lipid kinases (Coburn et al., 2002), the cytoskeleton (Grant and Oriol-Audit, 1985) and the membrane itself (Schuber et al., 1983). As described in Fig. 3B, the presence of 1 mM spermidine in the cytoplasmic solution causes a drastic change of the membrane cycling pattern. Ca influx initially still activates exocytic responses, but exocytosis is rapidly overcome by endocytic responses that decrease C_m by large fractions of total C_m. As illustrated in Fig. 3B, C_m can recover completely after an endocytic response, and the endocytic responses become larger at subsequent Ca influx episodes. After multiple cycles of endo- and exocytosis, one-half of cell area is lost in a few seconds during relatively small exchange currents, and C_m recovers over a time course of several minutes. As described later, these endocytic responses do not require ATP, while recovery from endocytosis (i.e. exocytosis) is strongly dependent on ATP in cytoplasmic solutions under these conditions. We note that recovery of C_m without ATP was occasionally observed when MEND was initiated less than 60 s after opening a cell and when GTPγS was included in cytoplasmic solutions.

Five different experimental protocols to study Ca-activated MEND.

Figure 4 describes five protocols to induce MEND responses of similar magnitude but different characteristics. Salient features of these responses are noted here, and details are then presented in Figs. 4 to 7.

1. Ca influx with high cytoplasmic ATP. Figure 4A presents the complete electrical parameters of a cell during MEND activated by Ca influx in the presence of high ATP, as in Fig. 3A. With 8 mM cytoplasmic ATP, Ca influx by NCX1 for 10 s causes an exocytic response, followed by an 'excessive' endocytic response over 1 min with C_m reduced to 50% below baseline. Membrane conductance (G_m) increases transiently during Ca influx, membrane fusion, and the decline of C_m. The increase of G_m during endocytosis occurs with no change of membrane current (I_m) or access resistance (R_a) and is consistent with the formation of plasmalemma-attached vesicles with low-conductance pathways to the extracellular medium, dubbed 'fission pores' (Rosenboom and Lindau, 1994). For comparison, a C_m record from a cell without ATP (dotted record) is also shown, similar to >100 recordings. While exocytic responses are similar to control records (~60% increase of C_m), the decline of C_m is small or absent. As indicated in Fig. 4A, we estimate that the half-maximal ATP concentration is about 4 mM to support this type of delayed Ca-activated MEND.

2. ATP perfusion after a Ca transient. The second protocol, described in Fig. 4B, is the same as employed in Fig. 2. Experiments are initiated without nucleotides in the cytoplasmic solution, Ca-containing extracellular solution is then applied for 2 to 4 s to enable reverse Na/Ca exchange, and after a delay of 20 s to 2 minutes nucleotides are introduced into the cytoplasm by pipette perfusion. In this example, 2 mM ATP and 0.2 mM GTP were employed, and the ensuing MEND amounts to >50% of C_m during the plateau that occurs after Ca influx. C_m begins to recover during this 300 s observation period. Ca transients evoked by reverse exchange current can cause C_m to recover above previous peak values in seconds, reflecting a nearly 3-fold increase of cell area. An ATP concentration of 0.5 mM was adequate to cause maximal MEND responses in this protocol. However, as described in Supporting Data Fig. 7, the *rate* of MEND development increases almost linearly with ATP concentration up to 5 mM. Supporting Data Fig. S11 documents that MEND can be initiated several minutes after the Ca transient, indicating that the effect of Ca to promote MEND is long-lived.

3. Pipette perfusion of Ca-buffered solutions. Since Na/Ca exchangers inactivate, cytoplasmic Ca transients caused by reverse exchange current are transient. Therefore, in a third protocol described in Fig. 4C, Ca-buffered solutions were perfused into cells by

pipette perfusion to maintain a high free cytoplasmic Ca concentration. As evident in Fig. 1, high free cytoplasmic Ca can cause an apparent endocytic response over times of 2 to 3 minutes. Fig. 4C shows the more rapid response that occurs when cytoplasmic solutions are heavily buffered to 200 μM free Ca with nitrilotriacetic acid (NTA, 10 mM + 3.5 mM Ca), and the cytoplasmic solution contains 40 mM Cs instead of 40 mM Na. With 0.5 mM ATP, C_m rose on average by 15% within 30 s upon perfusion of Ca and then declined by >40% over 20 to 80 s. The average fall was 35±3% for 8 experiments. Fig. 4D shows composite results for a series of experiments employing 5 Ca concentrations (n=4-8 for each group) in the presence of Cs. Fitting the data to a sum of two opposing rectangular hyperbolae, the half-maximal C_m decline occurs at 9 μM free Ca (solid line). When all data points are fitted to a single hyperbola (gray line), the half-maximum is 26 μM. These characteristics were nearly unchanged when cytoplasmic solutions contained no ATP and a non-hydrolysable ATP analogue (AMP-PNP, 2 mM), or when they contained no ATP and apyrase (3.5 U / ml) to hydrolyze residual nucleotides. Thus, sustained high cytoplasmic Ca can support a form of MEND that is distinct from ATP-dependent MEND. As described next, polyamines also promote an ATP-independent MEND.

4. Polyamine/Ca-activated MEND. The fourth protocol, described in Fig. 4E, is to activate Ca influx by NCX1 in the presence of cytoplasmic spermidine (1 mM), as in Fig. 3B. In Fig. 4E, the cytoplasmic solution contains no ATP or GTP, but a profound endocytic response begins within 1 to 3 s after the initial rise of C_m caused by exocytosis. These MEND responses often exceed 50% of the cell surface in 3 s. We note that MEND responses at a first Ca transient were sometimes small, or even absent, but a second Ca transient usually evoked a rapid MEND. As indicated by a dotted line, MEND responses in this protocol terminated rapidly upon termination of Ca influx and could be reinitiated by re-activating Ca influx. Thus, MEND in this protocol has an immediate requirement for cytoplasmic Ca.

5. Ca influx after plasmalemma enrichment with cholesterol. Clathrin-independent endocytic processes are often inhibited by cholesterol extraction with β-cyclodextrins (Sandvig et al., 2008). As described subsequently, the use of β-cyclodextrins to deplete and enrich membrane cholesterol results in profound inhibition and stimulation of MEND. However, β-cyclodextrins, especially β-methylcyclodextrin, can cause

substantial decreases of C_m that do not reflect endocytosis (see Supporting Data Figs. S8 and S9). Therefore, we developed another approach to enrich the surface membrane with cholesterol. Using giant excised membrane patches, we previously coated patch pipette tips with inert hydrocarbon mixtures containing lipids of interest and found that some phospholipids incorporated well into the plasmalemma (Hilgemann and Collins, 1992). As a similar approach for cholesterol, we dissolved 100 mg/ml cholesterol in light mineral oil containing 10% ethanol at 60˚C. Pipette tips with thick walls (>5 μm at the pipette opening) were then dipped into this mixture before back-filling. The coating did not hinder giga-seal formation or cell opening, it remained adherent during experiments, and recordings without cholesterol (i.e. after coating with the mineral oil/10% ethanol mix) were indistinguishable from recordings with tips without coating.

As shown in Fig. 4F, using cholesterol-coated pipettes and no spermidine, Ca influx by NCX1 activated MEND within a few seconds in the absence of cytoplasmic ATP and spermidine. As evident in the record, endocytic responses were then often so fast that exocytic responses were not evident. On average (>10 observations), MEND in the absence of ATP and polyamines amounted to >50% of the initial C_m of cells.

Detailed studies of Ca-activated MEND subtypes. Figures 5 to 8 describe basic properties of the MEND subtypes, and Supporting Data provides the following additional relevant information: Optical measurements of MEND for multiple protocols (Figs. S1 and S2) with control measurements (Fig. S3). Documentation that inward Na/Ca exchange currents are down-regulated by ATP-dependent MEND (Fig. S4). An ultrastructural study of MEND using a protocol to induce MEND in cell populations (Fig. S5): In brief, a polyamine that can cross cell membranes, EDA, enables MEND in response to Ca influx, as verified by uptake of horseradish peroxidase (HRP) into vesicles and vacuoles below the cell surface. Demonstration that Na/Ca exchangers are internalized in response to SMase treatment of cells growing on cover slips (Fig. S6). Further electrophysiological studies of MEND (Figs. S4, S7, and S10-12): From several phospholipase types tested, only SMases cause MEND, and PLC activation via overexpressed M1 receptors neither causes nor inhibits Ca/polyamine-dependent MEND. The nucleotide-dependence of ATP-dependent MEND. Substantial reductions of C_m induced by BMCD without internalization of Na/Ca exchangers.

Activation of MEND by ATP reflects generation of PIP_2. Figure 5 presents evidence that ATP promotes MEND via the generation of PIP_2. As shown in Fig. 5A, ATP-dependent MEND is completely blocked by a high cytoplasmic concentration (0.5 mM) of the nonhydrolysable GTP analogue, GTPγS. This blockade might reflect the function of many different G proteins, including dynamins. However, as shown in Fig. 5B, the blockade is fully relieved by including the phospholipase C (PLC) inhibitor, U73122 (10 μM), in the pipette solution. This reagent, while not specific, powerfully blocks PIP_2 cleavage by PLC's that can be activated by receptor-mediated (Horowitz et al., 2005) and GTPγS-mediated activation of Gq (Camps et al., 1990; Chidiac et al., 1999).

To test whether PIP_2 synthesis indeed underlies the activation of MEND by PIP_2, we first examined the effects of pipette perfusion of PIP_2 into cells in >50 experiments. Under the usual initial conditions of experiments, PIP_2 caused 5 to 20% declines of C_m (Yaradanakul et al., 2007). Much larger responses were obtained when PIP_2 was perfused into cells after a Ca influx episode with nucleotide-free cytoplasmic solutions. Fig. 5D shows the composite data for PIP_2 perfusion after one Ca influx episode without ATP. The average C_m decrease was 43 ± 8% . As shown in Fig. 5C, PIP_2 was also highly effective in the presence of GTPγS (0.5 mM) to block dynamin cycling. In this example, the initial cytoplasmic solution contained, as usual, 0.5 mM EGTA and 0.25 mM Ca. PIP_2 (50 μM) was then perfused into the pipette in Ca-free Standard Solution (3 mM EGTA and no Ca) to block Ca-dependent PLC cleavage of PIP_2. The endocytic response amounts to 65% of peak C_m. An example without GTPγS is provided in Supporting Data Fig. S12.

To determine more directly if PIP_2 plays a role in ATP-activated MEND, we tested whether ATP could be effective in cells perfused with a recombinant phosphoinositol 5-phosphatase, IPP5c (0.1 mg/ml)(Chi et al., 2004). Results are summarized in Fig. 5E. Using cells that were pre-perfused with cytoplasmic solutions with or without IPP5c, Ca influx by NCX1 was activated for 8 s, and ATP (2 mM) was introduced after a delay of 20 s. After ATP, C_m decreased on average 37% in control cells, but only 9% in cells with IPP5c. As described previously (Yaradanakul et al., 2007), peak outward NCX1 currents were nearly unaffected by PIP_2 depletion, although steady state NCX1 current is PIP_2 sensitive. Together, the experiments described in Fig. 5 make a strong case that

generation of PIP_2 is crucial for ATP to induce MEND. Additionally, it is established that both Ca transients and ATP depletion facilitate PIP_2-induced MEND.

Three features of polyamine/Ca-activated MEND. Figure 6 illustrates three characteristics of polyamine-dependent MEND. The experiments described employ nucleotide-free solutions, but we these same features were also routinely observed with ATP. As documented both here and in a companion article (Hilgemann and Fine, 2011; Hilgemann and Fine, xxxx), MEND can be triggered by many different means after a Ca influx episode. Triggers include perfusion of ATP or PIP_2, cholesterol enrichment, and a second Ca influx episode. However, as shown in Fig. 6A, polyamines must be present during the Ca transient to promote MEND. Perfusion of 1 mM spermidine into a BHK cell 30 s after inducing a Ca transient, associated with a 40% increase of C_m, causes no MEND (4 similar observations).

The second feature highlighted is that Ca-activated MEND can facilitate strongly from one Ca transient to the next. Using 1 mM cytoplasmic spermidine, Fig. 6B shows a common observation that MEND is very small at the first Ca influx episode, while a large MEND response occurs at the 2^{nd} and/or 3^{rd} Ca influx episode. Thus, some process set in motion by the first Ca transient enables MEND at a second Ca transient: Ca clearly has long-term and short-term effects. We note also the complete absence of recovery of C_m after MEND in this record without ATP or GTP. Under these conditions, recovery of C_m was invariably negligible when MEND occurred more than 100 s after opening cells (>50 observations).

The third notable feature of polyamine/Ca-activated MEND, shown in Figs. 6C and 6D, is its insensitivity to high concentrations of GTPγS (0.5 mM), similar to MEND induced by PIP_2 perfusion. In this set of experiments, we employed the unnatural polyamine, EDA (2 mM), because occurrence of MEND at the first Ca influx episode was more reliable than with spermidine. Since EDA can cross membranes, we employ it on both membrane sides. As shown in Figs. 6C and 6D, the average MEND amounted to 24% of C_m during a single Ca influx episode without GTPγS versus 32% with GTPγS. Thus, neither G protein cycling nor PIP_2 are required for the occurrence of polyamine/Ca-activated MEND.

Cholesterol can activate MEND long after Ca transients subside. As described in Fig. 4F, a direct method to apply lipids to cells suggests that cholesterol enrichment strongly promotes Ca-activated MEND with no ATP requirement. Fig. 7 extends those results to cholesterol enrichment with β-cyclodextrin-cholesterol complexes. To do so, we employed HPCD, which extracts phospholipids less potently than the β-methyl form (Ohtani et al., 1989), and therefore is less membrane-disruptive. For results in Fig. 7, ATP-, GTP-, and polyamine-free cytoplasmic solutions were employed. As shown in Fig. 7A, exposure of a cell to 10 mM HPCD causes only a small reduction of C_m over 5 min, whereas BMCD often caused decreases of >20% (see also Supporting Data Figs. 8 and 9). After the HPCD treatment, exchange currents and exocytic responses induced by Ca influx are of normal magnitudes for these cells. In contrast to results for free HPCD, Fig. 7B demonstrates that 10 mM HPCD loaded with 0.8 mM cholesterol causes a small (~10%) increase of C_m over 5 minutes (8 similar observations). Thereafter, activation of outward NCX1 current generates large, rapid MEND responses within seconds with almost no exocytic phase. As shown in Fig. 7C, cholesterol-HPCD complexes evoke large MEND responses (67 ± 9%, n=7) when applied *after* large Ca transients have primed the membrane for MEND. HPCD complexes themselves caused a smaller, significant decrease (25 ± 5%, n=6), which is described in Supporting Data Fig. S2 of a companion article (Hilgemann and Fine, xxxx)

Summary of Ca-activated MEND characteristics. Figure 8 summarizes extensive experiments suggesting that classical endocytic proteins are not involved in any of the MEND responses described in this article. In all cases, C_m at the end of the indicated MEND protocol is normalized to peak C_m , whether the peak occurred during or immediately after activation of Ca influx. Group A presents results for Ca-activated MEND in the presence of high (8 mM) ATP, as in Fig. 3A. MEND was negligible without ATP and amounted on average to only 10% of C_m with 2 mM ATP. A high concentration (5 μM) of the calcineurin inhibitor, FK506, did not alter these responses, while β-methylcyclodextrin (BMCD, 12 mM for 2 min) effectively blocked the decline of C_m. Fig. 8B shows composite C_m results for pipette perfusion of solutions with 0.2 mM free Ca to induce MEND, as in Fig. 4C, in the presence of 40 mM Cs. MEND was equally large when ATP (2 mM) was omitted and cytoplasmic solutions contained non-hydrolysable ATP (AMP-PNP, 2 mM) or apyrase (3.5 U / ml) to hydrolyze residual nucleotides.

Figure 8C shows composite C_m results for pipette perfusion of ATP to induce MEND, as in Fig. 2 and Fig. 4B. The average response for perfusion of 2 mM ATP was a 50% decline of C_m. Perfusion of ATP had no effect if the Ca transient was omitted in the protocol. An amphiphysin sequence, INFFEDNFVPEI (37 μM), which binds AP2 with high affinity (K_d, 2.5 μM) and blocks coat assembly (Gallop et al., 2006), was without effect when included in cytoplasmic solutions. Pipette perfusion of dominant-negative K44A dynamin 2 (0.5 μM) for 5 min did not affect the subsequent response to perfusing ATP. Similar to results with continuous ATP, shown in Fig. 5A, the non-hydrolysable GTP analogue, GTPγS (0.2 mM), blocks MEND in this protocol. Deletion of GTP from cytoplasmic solutions also can substantially blunt these MEND responses, perhaps because G-proteins such as ARF regulate PIP_2 synthesis (Brown et al., 2001). F-actin disruption with latrunculin A (1 μM) in the pipette solution, which results in blatant membrane blebbing, did not block MEND. And finally, the ATP analogue, ATPγS (0.5 mM), did not substitute for ATP in activating MEND, verifying that conventional protein kinases do not mediate the activation of MEND by ATP.

Figure 8D shows composite C_m results for Ca-activated MEND in the presence of 1 mM spermidine, as in Fig. 3B, evaluating MEND after one Ca influx episode of 20 s duration. Omission of ATP and inclusion of AMP-PNP (2 mM) did not significantly change the MEND response. As described above, EDA (2 mM) can substitute for spermidine to promote MEND, while pentalysine (Lys5) cannot. Inclusion of 0.5 mM GTPγS resulted in a partial inhibition of the MEND response to one Ca transient, as verified by two sets of experiments with 7 and 8 observations in the presence of GTPγS. For three reasons, we conclude that GTPγS specifically increases the variability of MEND occurrence with spermidine at a first Ca transient, noted in connection with Fig. 6B: First, GTPγS does not blunt MEND in the presence of EDA (Fig. 6D). Second, individual MEND responses in the presence of GTPγS amounted to more than 60% of the cell surface. And third, as described next, MEND responses at a 2nd Ca transient brought C_m closer to the 'control' MEND values.

Fig. 8E describes further experiments using two Ca influx episodes of 15 s separated by 2 min to induce MEND. All agents tested were added to pipette solutions. Cytoskeleton modifiers (latrunculinA, 3 μM; phalloidin, 10 μM; and colchicine, (30 μM) were

without a significant effect, as were cyclosporine (CsA, 5 μM), FK506 (10 μM), calmidazolium (CALMZ, 12 μM), overexpression of dominant-negative K44A dynamin 2 with GFP to identify transfected cells, the dynamin inhibitor, dynasore (200 μM) (Newton et al., 2006), and an unmyristylated dynamin inhibitor peptide (DynPep, Tocris Bioscience, #1774; 50 μM). As noted above, MEND was less affected by GTPγS (0.5 mM) using two Ca influx episodes than with 1 episode. We tested for a role of Ca-activated transglutaminases because polyaminylation was suggested earlier to play a role in endocytosis (Davies et al., 1980). Inhibitors of transglutaminases (e.g. dansylcadaverine (Davies et al., 1980) and Z-DON-Val-Pro-Leu-OMe; Zedira, Darmstadt) and amino oxidases (aminoguanidine, AG; 1 mM) (Brunton et al., 1991) had small inhibitory effects, equivalent to GTPγS.

We turn now to the membrane itself. As noted in the Introduction, a role for SMases and ceramide generated by SMases appeared attractive, since exocytic events might bring both SMases and ceramide into the extracellular membrane surface. Figs. 9 to 11 document the potential of SMases to generate MEND, as well as arguments against a major role for SMases and ceramide in Ca-activated MEND.

MEND induced by extracellular SMases.

Figure 9 describes MEND induced within seconds in BHK cells by extracellular application of SMase from *Bacillus cereus*. Results in panels A and C are with the commercial preparation (Sigma, 1U/ml), and results in panel B are with a purified enzyme (Ago et al., 2006). Although the commercial preparation contains additional enzymatic activities (Ramu et al., 2007), results for the two preparations were indistinguishable. Further, we demonstrate in Supporting Fig. S10 that recombinant bacterial SMase from *Bacillus anthrax* is similarly effective to induce MEND.

Bacillus cereus SMase requires Ca (or manganese) to adsorb to the surface of cells(Tomita et al., 1983). Therefore, solutions with 0.5 mM free extracellular Ca (0.5 mM EGTA with 1.0 mM added Ca) were employed. When using cells that expressed cardiac NCX1, we used Na-free, Li-based cytosolic solutions to avoid Ca influx. Fig. 9A shows records of cell electrical parameters determined by square wave voltage perturbation. In this experiment, the cytoplasmic solution contained no ATP or GTP to mimic ATP-depleted conditions of the previous cellular study (Zha et al., 1998). As

shown first, application and removal of Ca (2 mM) have no effect under these Na-free conditions. Upon applying SMase, together with Ca, C_m (46 pF) begins to decrease within a few seconds, achieves a maximal rate of decline of >12% per second, and stabilizes at about one-half of the initial value. A small, transient rise of cell conductance mirrors the rate of change of C_m (dC_m/dt), while membrane current (I_m) and access resistance (R_a) do not change.

Since sphingomyelin is present mostly in the outer plasmalemma monolayer, we tested whether SMase has any effect from the cytoplasmic side. Representative for 5 similar experiments, Fig. 9B shows that perfusion of purified SMase (5 μg/ml) into the cytoplasm of BHK cells in the presence of 5 μM free Ca (5 mM EGTA with 4.5 mM Ca) caused at most a 12% decrease of C_m over 4 min, while application of the same enzyme concentration to the outside causes a MEND response amounting to 65% of the cell surface in a few seconds.

Figure 9C shows one C_m record of SMase-induced MEND with high ATP and GTP concentrations (8 and 0.2 mM, respectively) and one without nucleotides, whereby C_m is normalized to its value at the start of the experiments. Composite results for 4 and 5 observations, respectively, are given as data points with error bars. In the presence of ATP, C_m recovered for the most part over several minutes after MEND, while there was no recovery in the absence of ATP. Membrane internalized with SMase treatment was found previously to recycle back to the cell surface by following transferrin receptor trafficking (Zha et al., 1998). Using the optical approaches described in Methods, Supporting Data Fig. S2 shows that SMase-induced MEND internalizes membrane and Na/Ca exchangers in equivalent fractional amounts.

Failure to confirm a role for secreted acid sphingomyelinase in Ca-activated MEND.

In the recent article by Tam et al. (Tam et al., 2010), a role for acid SMases in Ca-activated endocytosis was supported by multiple experimental approaches. We describe here equivalent experiments with BHK cells using chemical probes that provided arguments for SMase involvement in endocytosis. Our results for both probes are inconsistent with the involvement of secreted SMases in MEND.

Desipramine treatments do not block MEND. The amphipathic drug, desipramine, is considered to be a powerful reagent to displace acid SMases from membranes and over time to promote its degradation (Tam et al., 2010). In the study of Tam et al, cells were treated with 50 μM desipramine for 1 h. Thereafter, endocytosis in response to cell wounding appears to be blocked because FM dye uptake in the protocol employed is blocked. Using equivalent desipramine treatments, we do not find significant inhibition of MEND responses in our protocols. To ensure that desipramine treatment was adequate, we incubated BHK cells with 100 μM desipramine for 1 h prior to removing them from dishes, and thereafter we incubated cells again for 1 h at 37 C˚ with 100 μM desipramine in the absence of serum. In some experiments, we also added 100 μM desipramine to both cytoplasmic and extracellular solutions to promote the loss of SMase activities. As described in Fig. 10A, MEND responses to Ca influx in the presence of high ATP (8 mM, as in Fig. 3A) were entirely normal, amounting to more than 50% of the cell surface on average (n=7). As described in Fig. 10B, MEND responses to Ca influx in the presence of 1 mM spermidine (i.e. as in Fig. 3B) were entirely normal, amounting to loss of approximately 50% of the cell surface on average (n=7) within a few seconds.

MEND and Ca-activated exocytosis can occur independently. A second argument of Tam et al. for a role of secreted SMase in endocytic responses, subsequent to cell wounding, is that endocytosis was blocked when exocytosis was blocked, thereby establishing a causal relationship. As a means to block exocytosis, cells were treated with a high concentration (50 μM) of the alkylating 'active site' reagent, bromoenol lactone (BEL) that was suggested to block exocytosis. As described in Fig. 10C, we find that the equivalent BEL treatments of BHK cells indeed fully block endocytic responses, subsequent to Ca influx. However, we find that exocytic responses continue robustly with multiple Ca influx cycles, resulting in a doubling of membrane area in response to multiple Ca transients. We note that the conditions of experiments presented in Fig. 10C are otherwise identical to those employed in Fig. 10A (i.e. with 8 mM cytoplasmic ATP). Similarly, as described in Fig. 10D, we find that exocytic responses continue robustly in the equivalent protocols with 1 mM cytoplasmic spermidine and no ATP. Over several cycles of Ca influx, exocytosis results in a full doubling membrane area while endocytosis is entirely blocked. Thus, the reagents employed by Tam et al. provide no evidence in our hands for the hypothesis that acid SMase might be involved in Ca activated MEND responses.

MEND occurs in cardiac myocytes without exocytosis and can be initiated by spontaneous Ca release. Further relevant to the conclusions of Tam and colleagues, we describe in Fig. 11 that MEND occurs in cardiac myocytes without preceding exocytosis. Since BHK and HEK293 cells are highly proliferative and do not exhibit global Ca transients, we tested for the existence of MEND in adult murine and rat cardiac myocytes, using native NCX1 to generate Ca influx and to initiate cycles of spontaneous Ca release. Indeed, outward NCX1 currents (0.2 to 0.5 nA peaks) caused large declines of C_m in both murine and rat myocytes. Experiments described in Fig. 11 employ the Modified Standard Solution, described in Methods, with 6 mM ATP (Lariccia, xxxx) and no polyamines. Fig. 11A shows an example from a rat myocyte. Activation of reverse exchange current for just 2 seconds initiates a reversible endocytic response. C_m declines rapidly during Ca influx and then more slowly as spontaneous contractile activity initiated by Ca influx declines. We stress the time course of MEND in relation to the second and third Ca influx episodes: MEND clearly continues after Ca influx is terminated, suggesting that internal Ca release can drive MEND. Typical for all myocytes studied, C_m recovers progressively more slowly after each MEND response.

Since myocytes contract vigorously in this protocol, we tested the possibility that contraction might cause T-tubules to be physically pinched off by contractile activity. To do so, we employed high concentrations of the myosin 2 inhibitor, blebbistatin (17 μM), in both cytoplasmic and extracellular solutions to block contraction(Farman et al., 2008). In >20 observations, MEND remained robust when contraction was abolished in both rat and murine myocytes. As shown in Fig. 11B for a murine myocyte, activation of exchange current for 10 s resulted in C_m declines of >25% after a 2 to 3 s delay with no preceding exocytic response. Thus, it is unlikely that MEND is caused by contractile activity or by the exocytosis of ceramide/SMase-rich membrane.

Depending on myocyte batch and time after isolation, exchange currents can very small or negligible in murine myocytes. Figs. 11C and 11D illustrate that in such myocytes the application of extracellular Ca initiated cycles of spontaneous Ca release and contraction that were accompanied by MEND, which occurred after termination of Ca influx. Spontaneous activity in these myocytes can be followed electrophysiologically via transient current changes that occur synchronously with contraction. In Fig. 11C,

spontaneous activity occurs during application of Ca and terminates synchronously with MEND after Ca influx is deactivated. In Fig. 11D, Ca was applied twice for just 3 s. On the first Ca application, a single cycle of Ca release was evoked. The second application of Ca, however, caused a prolonged train of Ca release cycles. MEND both begins and terminates after the removal of extracellular Ca, demonstrating that MEND can be initiated by internal Ca release in myocytes. A bright field optical record of this experiment, provided as Supporting Video 3, documents that MEND is occurring with modest contractile activity that does not cause prolonged myocyte shortening.

Discussion

Large Ca transients promote large endocytic responses in BHK cells enriched in ATP, polyamines, or cholesterol. As summarized in cartoon form in Fig. 12, the underlying mechanisms appear to be 'non-canonical'. Ca acts via multiple calmodulin-independent mechanisms, while ATP acts via generation of PIP_2 without classical adapters or dynamins. Membrane recycling can occur in two different ways. Ca influx can cause ATP-independent membrane fusion followed by ATP-dependent endocytosis (Fig. 3A), or Ca influx can cause ATP-independent endocytosis followed by ATP-dependent vesicle recycling to the cell surface (Fig. 3B). Thus, these protocols should facilitate analysis of multiple partial reactions of membrane recycling. We discuss first the relevance of Ca-activated MEND described here to previous work and then the mechanisms by which Ca promotes MEND, bringing results from companion articles (Fine et al., xxxx; Hilgemann and Fine, xxxx) to bear on this study. Finally, we discuss how Ca-activated MEND may be promoted by PIP_2, polyamines and cholesterol.

The physiological relevance of Ca-activated MEND. Ca transients used to trigger MEND in this study usually exceed 100 μM free Ca (Fig. 1). Thus, the results are clearly relevant to cell wounds that flood cells with Ca (Idone et al., 2008). As noted in the Introduction, such wounds are closed by fusion of internal membranes to the cell surface, followed by endocytosis of plasmalemma into compartments that do not acidify (Cocucci et al., 2004). Besides having relatively high Ca requirements, similar to cell wound-induced endocytosis, the vesicles formed during MEND also do not readily acidify upon internalization (Figs. 2B and S1B).

The relevance of Ca-activated MEND to other physiological endocytic mechanisms studied previously is less secure. MEND can clearly be triggered by smaller Ca transients when multiple Ca transients occur (e.g. Fig. 3B). In myocytes, MEND can be induced by cycles of spontaneous Ca release initiated by 'trigger' amounts of Ca influx (Fig. 11A). Thus, it is established that physiological Ca signals can initiate MEND. When cytoplasmic free Ca is clamped by Ca buffers, MEND develops over the free Ca range of 10 to 35 μM (Fig. 4D). With the exception of skeletal muscle, this represents a range that may occur locally at Ca influx and release sites, but not globally (Clapham, 2007). 'Excessive endocytosis' in secretory cells (Engisch and Nowycky, 1998; Smith and Neher, 1997; Thomas et al., 1994) and 'bulk endocytosis' in synapses (Cousin, 2009) are both clathrin-independent, consistent with a mechanistic relationship to Ca-activated MEND described here. However, dynamin I is implicated to trigger and/or drive bulk endocytosis (Clayton et al., 2009), whereas dynamins appear to play no role in MEND. Recent *knock-out* studies in mice show that dynamin-1 (Ferguson et al., 2007) and AP2 (Kim and Ryan, 2009) are in fact not required for basal neuronal function (i.e. membrane cycling). Possibly therefore, mechanisms related to MEND maintain basal membrane recycling in those animal models. In this context, MEND might represent a core endocytic mechanism that becomes exploited, modified and/or regulated by dynamins and other classical endocytic proteins.

Recently, fast Ca-activated, clathrin/dynamin-independent endocytosis has been described in astrocytes (Jiang and Chen, 2009), reminiscent of Ca-activated MEND. In skeletal muscle, intense activity promotes the reversible formation of vacuoles from transverse tubules (Lannergren et al., 2002), and the MEND responses described here in cardiac myocytes (Fig. 11) may be related. Ca-activated MEND could play many roles in cardiac myocytes. In pathological circumstances, the removal of Na/Ca exchangers from the plasma membrane would protect from Ca overload (Shen et al., 2007).

Toward a mechanistic understanding of MEND. Our initial goal was to determine which classical endocytic proteins control and/or drive Ca-activated MEND. However, no positive outcomes emerged. Addressing first clathrin, it has to our knowledge never been questioned that clathrin-dependent endocytic processes require cytoplasmic potassium, and our experiments all employ potassium-free solutions. Second, in the case

of ATP-dependent MEND, a clathrin-binding domain of amphiphysin at a high concentration had no disrupting effect (Fig. 8C). Third, the formation and fission of large vesicles (Fig. S12) is not consistent with clathrin involvement, and rapid formation of vacuoles (Fig. 2A) seems questionable for clathrin-dependent endocytosis. In protocols that induce MEND under ATP-free conditions, PIP_2 will be depleted by lipid phosphatases (Falkenburger et al., 2010; Hilgemann, 2007). If not immediately depleted, Ca transients will rapidly deplete PIP_2 by PLC activation (Yaradanakul et al., 2007). However, MEND still occurs, often at a second or third Ca transient (e.g. Fig. 6B), as well as in the presence of a high GTPγS concentration (Figs. 5B, 5D, and 6D). Thus, polyamine-dependent MEND clearly does not require PIP_2 and might even be inhibited by PIP_2. Therewith, a role for adapters and G proteins that employ PH domains is eliminated.

In no protocol did dynamin-inhibitory peptides or dominant negative dynamins effectively block MEND (Fig. 8). Dynamin cycling requires GTP hydrolysis (Song et al., 2004). However, GTPγS at high concentrations does not block ATP-dependent MEND when PLC's are simultaneously inhibited and thereby PIP_2 hydrolysis is blocked (Fig. 5B). GTPγS does not block PIP_2-activated MEND in the presence of Ca chelators (Fig. 5D), and it does not block polyamine-dependent MEND effectively (Figs. 6D, 8D and 8E). Furthermore, reagents that inhibit calmodulin-dependent processes and disrupt actin cytoskeleton had no clear effect on MEND (Fig. 8). In summary, we have uncovered no evidence that Ca-activated MEND in BHK and HEK293 cells involves adapters, dynamins or actin cytoskeleton.

The mechanisms of Ca action in MEND. Ca-activated MEND is strongly dependent on physical properties of the membrane itself. It is blocked by brief β-cyclodextrin treatments (Fig. 8A). It is drastically promoted by cholesterol enrichment by either a direct method (Fig. 4F) or by cholesterol-HPCD complexes (Fig. 7). Exocytosis is then overwhelmed by MEND with >50% of the cell surface internalized within a few seconds.

Several observations suggest that exocytosis is not a prerequisite for the occurrence of MEND. First, MEND responses in the presence of spermidine or after cholesterol enrichment are extremely fast and large, and they can occur with almost no preceding exocytic phase. Second, spermidine-dependent MEND facilitates from one Ca transient

to the next, so that exocytic responses nearly exhaust the supply of vesicles before MEND occurs. Third, fast Ca-activated MEND occurs in ventricular cardiac myocytes that do not display Ca-activated exocytic responses (Fig. 11).

Ca appears to act by both long-term and immediate mechanisms. Regarding the long-term effect, our central observation is that large Ca transients facilitate subsequent MEND responses for several minutes after Ca transients subside. Triggers for a subsequent MEND response include a rise of cytoplasmic PIP_2 (Figs. 5C and 5D), a second Ca transient (Fig. 6B), membrane enrichment with cholesterol (Fig. 7C), and the extracellular application of certain detergents (Hilgemann and Fine, xxxx). Given that rather low concentrations of nonionic detergents cause MEND that is similar to Ca-activated MEND (Fine et al., xxxx), the long-term effect of Ca may be the generation of MEND-promoting lipids. Ca-binding proteins of an unknown identity, dubbed 'scramblases', facilitate movement of lipids between monolayers in all eukaryotic cells when free Ca rises into the range of tens of micromolar (Bevers and Williamson, 2010). Thus, the immediate effect of Ca could be to promote translocation of a MEND-promoting lipid from the cytoplasmic to the extracellular monolayer, independent of membrane fusion-derived lipids.

An alternative hypothesis arises from the fact that Ca-activated MEND internalizes primarily membrane with a high content of liquid-ordered (*Lo*) membrane (Hilgemann and Fine, xxxx). According to one theoretical model, nano- to microscopic membrane buckling can cause coalescence of extracellular *Lo* domains into buds (Minami and Yamada, 2007). In this context, Ca might act primarily through transmembrane or membrane-binding proteins that upon binding Ca induce the formation of membrane 'caps' and 'valleys', followed by domain coalescence, budding and vesiculation.

Failure to implicate ceramide or phospholipases in Ca-activated MEND. Phospholipases provide a plethora of mechanisms that might generate MEND-promoting lipids. We find up to now that PLC's and PLA2's do not promote endocytic responses, while extracellularly applied bacterial SMases are very effective (Fig. 9 and Supporting Data Figs. S2 and S10), consistent with a previous report for ATP-depleted fibroblasts (Zha et al., 1998). The generation of ceramide is relevant because large Ca transients (Babiychuk et al., 2008) and metabolic stress (Pavoine and Pecker, 2009) can both

promote sphingomyelin breakdown. In giant liposomes, ceramide generated by SMases coalesces into domains that rapidly vesiculate to the opposite membrane side (Bollinger et al., 2005). Thus, accumulation of ceramide during ATP depletion (Fig. 3) and over multiple Ca transient cycles (Figs. 9 and 10) might facilitate MEND.

Nevertheless, using the same interventions that Tam and colleagues employed with positive outcomes (Tam, 2010), we find no support for SMase and/or ceramide involvement in Ca-activated MEND. In this regard, it is not certain that the assays used by Tam and colleagues monitor the same exo- and endocytic responses occurring in our experiments. Ca-activated exocytosis is not blocked by tetanus toxin light chain in the cells employed by us (Wang and Hilgemann, 2008), although tetanus toxins blocks membrane resealing after cell wounding in 3T3 cells (Togo et al., 1999) and in sea urchin eggs and embryos (Bi et al., 1995). On the one hand, exocytosis in our experiments may be mechanistically different from exocytosis during cell wound responses. On the other hand, different sensitivities to tetanus toxins may reflect differences in the SNARE's expressed in different cell types (Wang and Hilgemann, 2008). Neither ATP-dependent nor polyamine-dependent MEND is suppressed by prolonged exposure to high concentrations of desipramine and/or its acute application on both membrane sides (Fig. 10), suggested to suppress acid SMase activities (Tam, 2010). The reagent employed by Tam and colleagues to block exocytosis, BEL, does not do so in our protocols (Fig. 10C and D). Rather, it powerfully blocks endocytosis while allowing Ca-activated exocytosis to occur unabated. Unusually, exocytosis continues for prolonged periods after Ca influx is terminated (Figs. 10C and 10D). This may reflect an unbridling of the exocytic mechanism, but alternatively a very effective blockade of endocytosis may reveal 'hidden', opposing exocytic events. Clearly, the hypothesis of Tam and colleagues now requires support by other lines of evidence that Niemann-Pick type A mutations cause defects in endocytic pathways.

The blockade of both ATP- and polyamine-promoted MEND by BEL opens a new pathway to elucidate the molecular basis of Ca-activated MEND. The iPLA2's that BEL inhibits most potently act as either mixed or selective PLA1/PLA2's (Cedars et al., 2009; Yan et al., 2005), whereby the generation of 2-arachidonoyl lysophophatidylcholine and its metabolites would be inhibited. From a companion study (Fine et al., xxxx), it is known that lysophospholipids can induce MEND, similar to detergents. A caveat is that

exogenous lysolipids dissociate rapidly from cell membranes, whereas the action of Ca to promote MEND is long-lived. We stress for now, therefore, that BEL may well be acting nonspecifically at the concentrations employed here, and that cysteines, serines and amines can all potentially be covalently modified.

The mechanisms by which PIP_2, polyamines, and cholesterol promote MEND. Given that classical endocytic proteins and actin cytoskeleton are not involved in MEND and that MEND internalizes selectively ordered membrane domains (Fine et al., xxxx; Hilgemann and Fine, xxxx), PIP_2, polyamines and cholesterol enrichment must all act in pathways that lead to domain coalescence, budding and fission.

PIP_2 synthesis is coupled to the organization of most endocytic processes described to date (Doherty and McMahon, 2009), and PIP_2 must be cleaved or dephosphorylated for fission to proceed in multiple cases, including actin-dependent endocytosis in yeast (Stefan et al., 2002) and phagocytosis in macrophages (Botelho et al., 2000). It has long been suggested that 'lipid rafts', which are enriched in sphingomyelin and cholesterol on the extracellular side, are enriched in PIP_2 on the cytoplasmic side (Liu et al., 1998). Although the biophysical basis for coupling across monolayers remains enigmatic, our data forces us to suggest that PIP_2 on the cytoplasmic side organizes the membrane for endocytosis by promoting the coalescence of membrane domains on the extracellular side. We can neither support nor contradict an involvement of membrane proteins at this time: PIP_2 might promote the association of PIP_2-binding proteins into complexes or promote conformational changes of membrane proteins that cause domain coalescence via membrane buckling. In either case, it will be of great interest to determine whether PIP_2 must be dephosphorylated before fission proceeds in delayed PIP_2-dependent MEND.

From the extracellular side, it is described in a companion article (Fine et al., xxxx) that certain amphipathic compounds (e.g. dodecylsulfate) promote a reorganization of membrane domains that predisposes them to internalize while blocking the final fission event until they are washed away. By a similar principle, PIP_2 on the cytoplasmic side might promote membrane reorganization that supports endocytosis but still hinder the final fission events, a hindrance that might be overcome by local activity of either phosphatases or dynamins. In this connection, we note that 'excessive' endocytosis in

chromaffin cells may be inhibited by PIP_2, since it is enhanced by over-expression of the inositol 5-phosphatase domain of synaptojanin 1 (Ira Milosevic (Yale), personal communication). Polyamine/Ca-activated MEND may be similar, because multiple Ca transients in ATP-depleted cells, which progressively deplete PIP_2 (Yaradanakul et al., 2007), cause progressively larger Ca/polyamine-activated MEND responses (Fig. 6B).

Spermidine overcomes the requirement for PIP_2 in Ca-activated MEND. Up to now, we have only been able to negate prominent candidate mechanisms in this effect (Fig. 8D). These include actin bundling, Ca-activated transglutaminases, and amino oxidases. Direct effects of Ca and polyamines on the membrane require further attention. Polyamines might promote anionic lipids, especially phosphatidylserine, to form domains that substitute for PIP_2-containing domains in promoting MEND. Both old and new studies provide a reminder that the Ca binding sites that activate MEND can potentially be anionic phospholipids: Micromolar polyamine concentrations greatly reduce Ca requirements for aggregation and fusion of vesicles containing acidic phospholipids and cholesterol (Schuber et al., 1983). In membranes containing zwitterionic lipids, PIP_2, and cholesterol, Ca at concentrations of 2 to 10 μM can cause the formation of PIP_2-rich domains (Levental et al., 2009). From many possible protein effectors, Ca/lipid-binding annexins are clearly attractive candidates as individual annexins have been shown to promote the formation of membrane domains (Chasserot-Golaz et al., 2005).

Cholesterol may facilitate both domain coalescence and membrane bending (Groves, 2007; Sarasij et al., 2007). The remarkable dependence of Ca-activated MEND on the membrane cholesterol content (Figs. 4F and 7) underscores that endocytosis may potentially regulate the cholesterol content of the membrane. In this connection, we note the probable explanation for one confusing experimental result related to cholesterol studies: Cyclodextrins used to extract cholesterol can cause substantial declines of membrane capacitance primarily by extracting membrane constituents, rather than by promoting endocytosis (see Supporting Figs. S10 and S11).

In summary, Ca promotes MEND by two mechanisms that do not appear to require clathrin, dynamins, or F-actin turnover. ATP promotes MEND by supporting the synthesis of PIP_2. Ca promotes polyamine-dependent MEND by one mechanism that requires the immediate presence of Ca and another mechanism that accumulates over

multiple Ca transients, separated by many seconds and even minutes. Calmodulin does not appear to be involved in either of these actions. Cholesterol content of the membrane is a strong determinant of the occurrence and extent of Ca-activated MEND.

Acknowledgements

We thank Jun Sakurai (Tokushima Bunri University, Tokushima Tokyo University) for purified B. cereus neutral sphingomyelinase, James H. Hurley (NIH, Bethesda) for recombinant IPP5c, Zhe Lu (U.Penn, Philadelphia) for recombinant anthrax sphingomyelinase, Sherry Sours-Brothers, Annamaria Assunta Nasti, Chengcheng Shen, and Jeremy Leitz (UTSouthwestern) for expert assistance and discussion, Harvey Mc Mahon (MRC, Cambridge) for the amphyphysin-based peptide, Joseph Albanesi (UTSouthwestern, Dallas) for dynamins, dynamin constructs and discussion, and Kenneth Philipson and Debora Nicoll (UCLA, Los Angeles) for advice, discussion, and NCX1 constructs. This work was supported by RO1-HL067942 and HL513223 to DWH.

Figure Legends

Figure 1. Measurement of C_m and cytoplasmic free Ca changes during activation of outward NCX1 currents in a BHK cell. The pipette solution contains 0.5 mM EGTA and 0.25 mM Ca (i.e. 0.4 μM free Ca), 2 mM ATP, no GTP, and 3 μM Fluo 5N (K_d, 90 μM). When 2 mM Ca is applied for 6 s, current rises to a peak of 120 pA and decays partially during the Ca application. C_m rises by about 50% during this time. Peak fluorescence occurs at 5 s and decays toward baseline with a time constant of about 4 s after deactivation of current. Upon perfusing the pipette tip with 0.5 mM additional Ca, fluorescence rises to a steady "maximal" level in a nearly linear fashion over 1 min, while C_m approximately doubles and then begins to decline, as described in more detail in Figs. 4C and D.

Figure 2. Internalization of membrane and NCX1 exchangers during Ca-promoted MEND with activation by ATP perfusion **(A)** Uptake of FM 4-64 dye (8 μM) in a BHK cell subjected to a Ca transient in the absence of ATP followed by cytoplasmic perfusion of ATP (2 mM). As indicated below the C_m record, the cell was maintained in Standard Solutions without ATP or GTP for 3 min. Outward NCX1 current was activated with 2 mM extracellular Ca for 10 s, and ~2 min later 2 mM ATP and 0.2 mM GTP were perfused into the cell. During the experiment, FM dye was applied and removed multiple

times to monitor dye binding to the outer cell surface versus dye that had been internalized. After the Ca-activated exocytic response, surface fluorescence is increased 34% more than expected from the increase of C_m. Thereafter, introduction of nucleotides causes a 65% decrease of C_m, and the 'washable' fluorescence decreases by 60% with a corresponding increase of 'un-washable' fluorescence. Dye that is trapped in vesicles and vacuoles form a clear rim close to the cell surface (see inset and Supplementary Video 1; calibration bar, 10 μm). **(B)** Internalization of NCX1-pHluorin fusion protein during MEND in a T-REx-293 cell. Using the same ATP-perfusion protocol as in 'A', fluorescence originating from NCX1 at the cell surface was defined by rapid pH jumps from 6 to 8. Subsequent to the decline of C_m by about 45%, the NCX1 fluorescence at the cell surface is decreased by >30%. This internalized pH insensitive florescence corresponds to the percent of NCX1 exchangers internalized during MEND as internalized membrane does not enter acidified compartments.

Figure 3. Two types of Ca-activated MEND responses in BHK cells, resulting in membrane recycling by different mechanisms. **(A)** Using Standard Cytoplasmic Solution with 8 mM ATP and 0.2 mM GTP, activation of Ca influx by NCX1 for 20 s causes an immediate exocytic response followed by a delayed MEND response that amounts to more than 50% of the cell surface over 2 min. Cycles of large exocytic responses followed by MEND can then be repeated multiple times in the same cell. **(B)** Using the same cytoplasmic solution as in 'A' with an additional 1 mM spermidine, large endocytic responses are initiated during Ca transients, rather than after Ca transients, as in 'A'. Over the course of multiple Ca influx episodes, recovery from MEND becomes more pronounced, and MEND responses amounting to more than 50% of the cell surface can be repeated multiple times with recovery taking place over several minutes.

Figure 4. Ca-activated MEND in five different protocols. Electrical parameters are monitored via 0.2 to 0.5 kHz/20 mV square wave voltage oscillations. **(A)** MEND with high cytoplasmic ATP (8 mM). From top to bottom, solid records give the calculated cell C_m in pF, conductance (G_m) in nS, membrane current (I_m) in pA, and access resistance (R_a) in MΩ. The dotted record is a representative C_m response of a cell when ATP is omitted from the pipette solution. **(B)** MEND incurred by perfusion of ATP into cells after nucleotide depletion and introduction of a Ca transient without nucleotides, as in Fig. 2. The ATP/GTP-free period was 3 min, NCX1 current was activated for 3 s, and 20 s later the pipette was perfused with solution containing 2 mM ATP and 0.2 mM GTP. **(C**

& D) MEND induced by perfusion of Ca-buffered pipette solutions. C_m responses were monitored during pipette perfusion of solutions buffered to free Ca concentrations of 5 to 200 μM. The experimental record illustrates MEND generated by perfusion of solution with 200 μM free Ca (10 mM NTA; 0.5 mM ATP + 0.1 mM GTP). The cytoplasmic solution contains 80 mM Li, 40 mM Cs, and no Na. As shown in the graph for experiments with 5 different free Ca concentrations, the half-maximal Ca concentration was 9 μM. Standard errors were less than 15%. **(E)** Ca-activated MEND in the presence of 1 mM cytoplasmic spermidine. MEND occurs within seconds *during* Ca influx via NCX1 and stops rather quickly when Ca influx is terminated. **(F)** Immediate, Ca-activated MEND response in a cholesterol-enriched BHK cell without spermidine. Patch pipettes were dipped in a hot (60˚C) mineral oil-cholesterol solution (150 mg cholesterol/1ml oil with 10% ethanol) before seal formation. Seals were highly stable, and MEND occurred very rapidly upon activating Ca influx with almost no detectable exocytic response.

Figure 5. PIP_2–dependence of ATP-activated MEND: PIP_2 mediates ATP-dependent MEND and induces MEND without involvement of G protein cycling. Composite results are expressed as percent of peak C_m after Ca influx (n=7 to 15). **(A)** Ca-activated MEND with high (8 mM) ATP is blocked by cytoplasmic GTPγS (0.5 mM). **(B)** Blockade of ATP-dependent MEND by GTPγS, as in 'A', is relieved by inclusion of the PLC inhibitor, U73122 (10 μM), in the pipette solution. **(C)** Pipette perfusion of PIP_2 (50 μM) substitutes for ATP in the activation of MEND after a Ca transient. Bar graphs give normalized C_m in BHK cells before and after perfusion of PIP_2 (40 μM) for 4 min. Prior to PIP_2 perfusion, cells were perfused with ATP/GTP-free solution for 4 min, followed by NCX1-mediated Ca influx for 6 s. **(D)** The ability of PIP_2 to induce MEND is unaffected by GTPγS (0.5 mM) when PIP_2 is introduced in Ca-free solution (3 mM EGTA). **(E)** PIP_2 is required for nucleotide reperfusion-induced MEND. Average C_m responses in BHK-NCX1 cells perfused with ATP/GTP-free solution for 4 min, followed by NCX1- mediated Ca influx for 6 s, and then perfusion of ATP (2 mM) for 3 min. Inclusion of 0.1 mg/ml IPP5c in cytoplasmic solutions reduced ATP-activated MEND by >80%.

Figure 6. Salient features of polyamine/Ca-activated MEND using *nucleotide-free* Standard Cytoplasmic Solutions. **(A)** In contrast to other MEND-promoting agents, spermidine does not cause MEND after a Ca transient has occurred; it must be present in the cytoplasm during the Ca transient. **(B)** Ca-activated MEND with spermidine is often small at the first Ca influx episode but large and rapid at a second Ca transient. Thus, MEND undergoes long-term facilitation by a mechanism that does not involve phosphorylation. **(C)** The occurrence of MEND at the first Ca influx episode is more reliable using EDA (2 mM) as polyamine in both intra- and extracellular solutions (n=6). **(D)** Whereas GTPγS (0.5 mM) blocks ATP-dependent MEND (Fig. 5A), EDA/Ca-activated MEND is unaffected (n=7). Results in 'C' and 'D' are paired experiments from one batch of BHK cells.

Figure 7. Cholesterol enrichment enables fast Ca-activated MEND without polyamines. All results employ BHK cells with ATP-, GTP-, and polyamine-free cytoplasmic solution. Composite C_m changes from multiple experiments (n= 4-6) are plotted by normalizing C_m after an intervention (open squares with standard errors) to C_m values before the intervention (filled squares). **(A)** Treatment of BHK cells with HPCD (10 mM) for 5 min does not affect in an evident manner NCX1 currents or membrane fusion responses evoked by outward NCX1 current. C_m decreases by <10% during HPCD treatment. **(B)** Treatment of BHK cells with cholesterol-loaded HPCD for 5 min causes an average increase of C_m of 12%. Thereafter, activation of outward NCX1 current causes an average 36% fall of C_m within 5 s, often with no evident preceding membrane fusion response. **(C)** Calcium transients force cells into a MEND-permissive state for many minutes. Although treatment of cells with HPCD complexes does not cause endocytic responses in control cells (see B), cholesterol enrichment causes profound MEND over 2 to 4 min when treatment is initialized after an NCX1-mediated Ca transient.

Figure 8. Composite results of experiments characterizing MEND in five protocols. Bar graphs represent the peak C_m occurring in an experiment, during or shortly after a Ca transient, in relation to C_m after the occurrence of MEND. Each data set reflects five or more observations. **(A)** MEND occurring with the indicated cytoplasmic ATP concentrations in response to a single Ca influx episode of 12 to 16 s. **(B)** MEND occurring upon pipette perfusion of an NTA-buffered solution with 0.2 mM free Ca. **(C)** MEND occurring upon pipette perfusion of ATP (2 mM) and GTP (0.2 mM) after cells were opened and maintained without nucleotides for 3 min and exposed to one Ca influx

episode for 2 s. **(D)** MEND occurring during a single Ca influx episode for 15 s in the presence of cytoplasmic spermidine (1 mM). **(E)** MEND occurring over two Ca influx episodes of 15 s duration, separated by 2 min, in the presence of cytoplasmic spermidine (1 mM). See text for complete details.

Figure 9. Activation of MEND by extracellular application of *Bacillus cereus* SMase (1 U/ml) in BHK fibroblasts with *Na-free* solutions. **(A)** BHK cell perfused for > 2 min with Na-, ATP- and GTP-free cytoplasmic solution. Application of Ca (1 mM) from outside has no effect on C_m, while application of Ca with SMase causes a 54% drop of C_m at a peak rate of 12% per second. Membrane current (I_m) shows no response, access resistance (R_a) increases by 10%, and membrane conductance increases transiently by 0.8 nS in parallel with the first derivative of C_m ($-dC_m/dt$). **(B)** Cytoplasmic application of SMases does not cause MEND. Perfusion of purified SMase into the cytoplasm of a BHK cell causes at most 12% decline of C_m at the same concentration that causes >50% decline of C_m from outside within seconds. **(C)** Reversal of SMase-induced MEND. SMase application as in 'A' caused on average a 53% fall of C_m within 15 s. With 6 mM ATP in the cytoplasmic solution (left panel), C_m recovered toward baseline by 60% over 5 min, while C_m did not recover in the absence of nucleotides did not reverse (rt. panel).

Figure 10. Desipramine treatment does not block MEND, while BEL treatment blocks MEND but not exocytosis. **(A)** ATP-dependent MEND in response to a Ca transient is unchanged by pretreatment of cells with 100 μM desipramine for 1h in serum-free media, followed by further incubation with 100 μM desipramine for 1h and execution of experiments with 100 μM desipramine in both cytoplasmic and extracellular solutions. **(B)** Similar treatment with desipramine fails to inhibit spermidine-dependent MEND in the absence of ATP. **(C)** Same solutions as Fig. 10A. BHK-NCX1 cells, which were pre-treated with 50 μM BEL for 1 hr in serum free media, show robust Ca-activated exocytosis with C_m doubling over three Ca influx episodes while endocytic responses are potently inhibited. **(D)** Same solutions as in Fig. 10B with BEL treatment as in Fig. 10C. BEL treatment does not block exocytic responses that occur in the absence of ATP and presence of cytoplasmic spermidine (1 mM). However, endocytic responses are completely suppressed.

Figure 11. MEND occurs in cardiac myocytes without preceding exocytic responses and can be induced by spontaneous cycles of Ca release. **(A)** Rat cardiac myocyte with

cytoplasmic ATP (6 mM), MEND develops rapidly during activation of NCX1 and continues for several seconds after terminating Ca influx as cells continued to contract spontaneously. MEND reversal in myocytes is labile, becoming substantially slower from one MEND cycle to the next. Reversal was negligible when MEND was allowed to proceed to a final loss of more than 30% of the cell surface. **(B-D)** Different patterns of MEND responses observed in murine cardiac myocytes. **(B)** Murine myocyte with contraction blocked by blebbistatin (17 μM). Na/Ca exchange current is relatively large, MEND begins with within 3 s of activating Ca influx, and MEND terminates when exchange current is deactivated . **(C)** Murine myocyte without blebbistatin. Brief activation of reverse exchange current promotes spontaneous cycles of Ca release, accompanied by transient current changes that are evident in the current record. MEND begins with no exocytic response and terminates spontaneously as spontaneous contractile activity terminates. **(D)** Murine myocyte without blebbistatin. Exchange current is negligibly small. Application of Ca activates spontaneous cycles of Ca release accompanied by transient current changes. MEND begins after extracellular Ca has been removed, during spontaneous contractile activity, and terminates spontaneously with no evident relationship to the termination of spontaneous activity. The bright field record of this experiment is provided as Supporting Video 3.

Figure 12. Ca-activated endocytosis involves three distinct processes. (1) Large Ca transients cause long-term changes of the outer plasmalemma monolayer that promote endocytosis (Hilgemann and Fine, xxxx). Possible mechanisms include the generation of lipids that promote growth of lipid domains (i.e. the coalescence of small domains to large domains) and/or the translocation of such lipids to the outer monolayer. (2) In synergy with spermidine, high cytoplasmic Ca causes inner monolayer changes that promote endocytosis. One possible mechanism is the coalescence of lipid domains by Ca- and lipid-binding proteins (e.g. annexins (Chasserot-Golaz et al., 2005)). (3) After membrane modification by Ca, the ATP-dependent synthesis of PIP_2 promotes MEND by Ca-independent mechanisms. Clustering of PIP_2 and PIP_2-binding proteins may promote trans-bilayer domain coupling and membrane buckling that in turn drives endocytosis.

Supporting Data.

The Supporting Data presents optical measurements of membrane and NCX1 internalization during Ca/polyamine- and SMase-induced MEND (Figs. S1 and S2), control experiments for FM 4-64 and NCX1-pHluorin experiments demonstrating repeatability of protocols without MEND (Fig. S3), experiments demonstrating that MEND results in a loss of inward exchange current (Fig. S4), description of polyamine/Ca induced MEND in a cell population (Fig. S5), internalization of NCX1 in response to SMase treatment in cover slip-attached cells (Fig. S6), analysis of the ATP dependence of ATP-dependent MEND (Fig. S7), evidence that BMCD- induced reductions of membrane area (i.e. Cm) result mostly from extraction of cholesterol and phospholipids, rather than endocytosis (Figs. S8 and S9), activation of MEND by multiple SMases, but not by other phospholipases (Fig. S10), experiments demonstrating the long-lived nature of MEND facilitation by Ca (Fig. S11), and description of large capacitance steps often observed during MEND when induced by pipette perfusion of PIP_2 (Fig. S12).

Figure S1. Internalization of membrane and NCX1 during polyamine-dependent MEND. Optical results are similar to those presented in Fig. 2. **(A)** Using a BHK cell with spermidine (1 mM) in the Standard Cytoplasmic Solution, activation of Ca influx by NCX1 causes a 24% MEND response during the Ca transient. FM 4-64 (8 uM) was applied and removed once before MEND. Then, dye was reapplied before exposure to Ca, and Ca was applied together with dye. Thereafter, FM fluorescence that cannot be washed out amounts to 21% of total dye labeling before washout. **(B)** Using a T-REx-293 cell expressing NCX1-pHluorin, cell fluorescence originating from NCX1 in the cell surface (defined by the rapid pH 6 to 8 jump) is decreased by 40% when Cm decreases by 30%.

Figure S2. Optical measurements of SMase induced MEND **(A)** Uptake of FM 4-64 in a BHK cell in response to SMase treatment. FM 4-64 dye (8 uM) was applied and washed twice, the first time without and the second time with purified SMase (5 ug/ml). Images from the time points indicated in the Cm record are normalized to the fluorescence in response to the first dye application. Dye uptake amounts to 45% of the initial dye staining that could be washed off. **(B)** Internalization of NCX1-pHluorin in a T-REx-293 cell. SMase treatment (1 U/ml commercial preparation) reduces the NCX1-pHluorin

fluorescence originating from the cell surface (i.e. the fluorescence jump upon switching extracellular solution from pH 6 to pH 8) by 47% in a response in which Cm declines by 58%.

Figure S3. Control experiments for FM 4-64 and NCX1-pHluorin fluorescence experiments. Same solutions and protocols as in Figure 2 of the article, but without activation of Ca influx. **(A)** FM 4-64 dye (10 uM) is applied and removed three times, and fluorescence is quantified in two ways. Continuous records show the fluorescence of the cell boundary, i.e. not including the central region of the cell. Note that residual fluorescence after wash-out continues to decline to nearly baseline over 120 s. In the micrographs, fluorescence of the entire cell is quantified by defining the background fluorescence before applying dye as '0%' and the maximal fluorescence upon first application of dye as '100%'. In contrast to the MEND experiments described in the article, the FM 4-64 fluorescence baseline remains stable. **(B)** NCX1-pHluorin fluorescence is quantified similarly to FM 4-64 fluorescence. For two prolonged sequences, fluorescence changes upon switching from pH 7 to 6 to 8 are stable, and bleaching of the NCX1-pHluorin construct is negligible over 500 s under the optical conditions of our experiments.

Figure S4. Loss of inward NCX1 currents in ATP-dependent MEND. *Inward NCX1 currents do not inactivate and are not subject to many regulatory influences that affect outward current. Therefore, inward currents may reflect rather accurately changes of NCX1 density in the plasmalemma.* Pipette perfusion is used to allow measurement of inward exchange current, then outward exchange current, and again inward exchange currents. At the beginning and end of the experiment, inward NCX1 currents are determined using a cytoplasmic solution buffered to 3 uM free Ca with 2 mM EGTA with no Na. The inward current was turned on and off by replacing 120 mM extracellular Li for 120 mM Na multiple times in the presence of ATP (2 mM) and GTP (0.2 mM). After examining inward current three times at the beginning of the experiment, cytoplasmic solution was switched to one containing 40 mM Na, no nucleotides and buffered to 0.3 uM free Ca with 0.5 mM EGTA. The outward current was activated briefly three times by applying and removing 2 mM extracellular Ca, accompanied by increases of Cm, as Ca influx activates fusion events. The increase of membrane area remained stable at the elevated level until reperfusion of the original cytoplasmic solution with ATP and GTP. After nucleotide replenishment and induction of MEND (see Cm

record), the inward current is almost abolished in this experiment with a 70% fall of Cm. As shown in the inset, inward exchange current was reduced on average by 34% (n=14; *, P<0.05), when Cm fell on average by 45%, consistent with optical records showing that the fraction of NCX1 removed from the cell surface is somewhat smaller than the fraction of total plasmalemma removed.

Figure S5. Analysis of polyamine-dependent MEND in an HEK293 cell population without voltage clamp. **(A)** Demonstration of fast Ca-activated MEND response of a BHK cell superfused with solution containing 2 mM of ethylenediamine (EDA). Cytoplasmic solution contains 2 mM ATP, 0.2 mM GTP and no polyamines. Spermidine and spermine were completely ineffective in supporting fast MEND in this protocol. This established membrane permeability of EDA is high enough to allow MEND from *extracellular* application of this polyamine when perfusion of cytosolic constituents is prohibited. **(B and C)** Ultrastructural and biochemical analysis of NCX1-expressing BHK cells in a protocol developed to induce MEND by polyamines and Ca in cell populations without patch clamp. **Solutions and Materials.** Three solutions were employed: *Solution 1:* 120 NaCl, 0.45 CaCl2, 0.5 EGTA, 2 MgCl2, 5 dextrose, 40 sucrose, 40 NaHCO3, 5 HEPES pH 7.0 with HCl. *Solution 2:* 120 LiCl, 0.45 CaCl2, 0.5 EGTA, 2 MgCl2, 5 dextrose, 40 sucrose, 40 NaHCO3, 5 HEPES pH 7.0 with HCl. *Solution 3:* 120 LiCl, 2 CaCl2, 0.5 EGTA, 2 MgCl2, 5 dextrose, 40 sucrose, 40 NaHCO3, 5 HEPES pH 7.0 with HCl. Reagents for ultrastructural studies were from Electron Microscopy Sciences. Peptide 19-31 was from Calbiochem. Other chemicals were the highest grade available from SIGMA. **Electron Microscopy.** Effect of EDA loading with HRP as Fluid Phase Marker. BHK-NCX1 cells were trypsinized, allowed to recover for 20 minutes in growth medium, and divided into 5 aliquots: control, Na-loaded cells with and without 1 mM EDA, Na and Ca-loaded cells with and without 1 mM EDA. Hereafter, any wash or solution change consists of a spin down at 200 *g* for 1 minute and resuspension. Control was kept in growth medium for 30 minutes, and resuspended in medium with 10 mg/mL HRP for 1 minute. These cells were then washed with medium and fixed in 2.5% glutaraldehyde in 0.1 M cacodylate buffer for 30 min. The four other aliquots were washed and kept in Na loading solution (solution 1). After 30 minutes, two of the aliquots (with and without EDA) were resuspended in the same solutions containing HRP for 1 minute, washed and fixed. The last two aliquots loaded with Na were washed with a Li-based solution *(solution* 2) for 2 minutes and resuspended in

solutions with 2 mM Ca (solution 3) and HRP for 1 minute. After a final wash, the cells were fixed. All the aliquots were washed with 175 mM Tris-Cl buffer twice. They were then resuspended in the same buffer containing 0.02% H_2O_2 and 0.1% diaminobenzidine (DAB) for 20 minutes. The cells were washed 3 times with buffer, enrobed in agarose, and prepared for TEM processing. **TEM Processing.** Agarose embedded cells were cut into 1 mm3 sized pieces and washed with cacodylate buffer. They were post-fixed in 1% OsO4 in cacodylate buffer for 1 hour and stained *en bloc* with 2% uranyl acetate for 1 hour. After rinsing with water, the cells were dehydrated in an ascending series of ethanol followed by infiltration with Embed812 and polymerization at 60o C overnight. Thin (70 to 80 nm) sections were cut with a Ultramicrotome Leica EM UC6 and mounted on 200 mesh copper grids. Sections were post-stained with 2% uranyl actetate for 15 minutes and lead citrate for 5 minutes. The cells were imaged in a FEI Tecnai G2 Spirit Biotwin TEM. **Determination of NCX1 Surface Fraction (F_{surf}).** Five groups of adherent cells were treated using the same protocols as HRP loaded cells, and the fraction of NCX1 at the cell surface was quantified via PEGylation as described (Shen et al., 2007). **(B)** Vacuoles loaded with HRP are indicated with arrowheads. Some vacuoles are clearly multilaminar. **(C)** The numbers are HRP-loaded vesicles and vacuoles are inversely proportional to the fraction of Na/Ca exchangers at the cell surface, determined by PEGylation.

Figure S6. Internalization of NCX1-pHluorin in T-REx-293 cells maintained on cover slips. Brief SMase treatment reduced the NCX1-pHluorin fluorescence originating from the cell surface by 24% (the fluorescence jump upon switching E.C. solution from pH 6 to pH 8). The medium employed was a phosphate-buffered physiological saline solution.

Figure S7. MEND induced in BHK cells by ATP perfusion subsequent to a 2 s Ca influx episode in the absence of ATP. **(A)** Experimental records for pipette perfusions of 0.5, 2 and 8 mM ATP. **(B)** ATP dependence of the magnitude of the complete MEND response. **(C)** ATP dependence of the maximal rate of decline of Cm during ATP perfusion. While the final magnitude of MEND is maximal already with 0.5 mM ATP, the rate of development of MEND increases almost linearly with ATP concentration.

Figure S8. Representative effects of BMCD on Cm in BHK cells. (A) Routine observation that relatively low concentrations (2 mM) of BMCD initiate with no delay a steady decrease of Cm that continues almost linearly for several minutes. This decline amounts to approximately 1% of the membrane per minute. The rate of decline increases

approximately linearly over the concentration range of 1 to 30 mM. **(B)** The rate of decline begins to saturate over time with BMCD concentrations in the range of 10 mM. Supporting Data Fig. S2 of a companion paper (Fine, xxxx) demonstrates that BMCD is equally effective when perfused into cells from the cytoplasmic side, and the effects from inside are approximately additive with effects from outside. Over several minutes, Cm can decrease by more than 50%.

Figure S9. BMCD does not cause internalization of NCX1-pHluorin fusion protein. **(A)** To evaluate whether BMCD causes Cm to decrease as a result of endocytosis or simple extraction of membrane components, we employed T-REx-293 cells expressing NCX1-pHluroin fusion protein to test whether NCX1 was internalized during BMCD application. As shown here, this is not the case. BMCD (35 mM) in this experiment causes a 35% decrease of Cm, while the fluorescence jump upon acidification of the extracellular surface, associated with NCX1, is nearly unchanged. Arrows denote the expected size of the fluorescence jump, if BMCD were causing endocytosis. **(B)** Composite results for four similar experiments. As indicated by the left two bars, Cm decreased on average by 25% during application of BMCD, while pH-sensitive NCX1 fluorescence decreased by just 10%. We note in connection with these experiments that FM dyes could not be used together with BMCD because BMCD binds these dyes with good affinity.

Figure S10. Selective activation of MEND by a SMase activity, but NOT by PLC's or PLA2's. **(A)** Activation MEND response by a recombinant bacterial SMase (BaSMase, 100 ug/ml), kindly provided by Dr. Zhe Lu (U. Penn, Philadelphia). The enzyme was cloned from *B. anthracis* and expressed in *E. coli,* as described (Ramu et al., 2007). BHK cells were employed with Na-free cytoplasmic solution containing 120 mM Li, 0.5 mM EGTA with 0.25 mM Ca, and no ATP, GTP, or spermidine. Standard extracellular solution was employed with free Ca adjusted to 0.1 mM (i.e. 0.5 mM EGTA and 0.6 mM Ca), as micromolar Ca concentrations promote bacterial SMase adsorption to cells (Tomita et al., 1983). The SMase caused an average 42% MEND response (n=4) within 90 s. **(B)** PIP2 depletion by GPCR-activated PLC's neither promotes nor blocks Ca-activated MEND in the presence of spermidine. Native PLC activity was activated in BHK cells overexpressing muscarinic M1 receptors, under conditions in which carbachol promotes within seconds cleavage of >90% of cellular PIP2 (Horowitz et al., 2005; Shen et al., 2007). The cytoplasmic solution contained 40 mM Na, 8 mM ATP, 0.2 mM GTP

and 1 mM spermidine. Carbachol (0.15 mM), applied for 15 s prior to activation of outward NCX1 current, does not promote MEND nor does it block subsequent Ca-activated MEND. **(C)** In contrast to *BaSMase,* PLA2 enzymes from bee venom (Cayman; 1 □g/ml) and from snake venom (Worthington; 10 ug/ml) caused slow increases of Cm at concentrations that eventually caused significant conductance increases and cell (or patch seal) disruption. Finally, a bacterial PLC (Chen et al., 2009), kindly provided by Dr. Mary F. Roberts (Boston College, Chestnut Hill, Massachusetts) caused no endocytic responses at a concentration expected to rapidly cleave GPI anchors from mammalian cells (Ikezawa, 1991).

Figure S11. The facilitating effect of Ca to promote ATP-dependent MEND is long-lived, and neither the A TP analogue, AMP-PNP, nor GTP can substitute for ATP in MEND. 'NTP'=NucleotideTriPhosphate. In this example experiment, reverse NCX1 current was activated in a BHK cell multiple times for 3 s, resulting in increases of Cm with each Ca influx episode. Thereafter, AMP-PNP (2 mM) was first perfused into the pipette. Then, GTP (0.2 mM) was perfused in the presence of AMP-PNP, and finally ATP (2 mM) was perfused into the pipette without the other nucleotides. Only ATP supports MEND. From data presented in Fig. 4A of the article, it is known that ATP depletion and replenishment causes MEND only if a Ca transient occurs in the ATP-free period. Thus, the effect of Ca to promote MEND is long-lived. We point out that the pipette perfusion experiments may be affected by the presence of ATP gradients.

From measurements of BHK cell metabolism (Neermann and Wagner, 1996; Cruz et al., 1999), BHK cells use about 45 nmol glucose per 106 cells per minute, with most glucose appearing as lactate, and about 6 nmol glutamine per 106 cells per minute in oxidative metabolism. Assuming that 2 ATP are generated per glucose and 1 ATP per glutamine, an average BHK cell hydrolyzes about 109 ATP per s. Diffusion through a 5 MOhm pipette tip containing 2 mM ATP, simulated as described (Kang et al., 2003) or estimated from Fick's law, will provide at most 109 ATP molecules per second. Thus, ATP-dependent processes may be limited by ATP supply when substrates are not provided.

Figure S12. MEND induced by perfusion of PIP_2 (40 uM) into a BHK cell after 3 min with ATP/GTP-free cytoplasmic solution. Cm decreases by >50% over 4 min, and NCX1-induced Ca transients subsequently restore Cm to pre-MEND values. During MEND, large (30-130 fF) Cm steps occur (see inset).

Figure 1

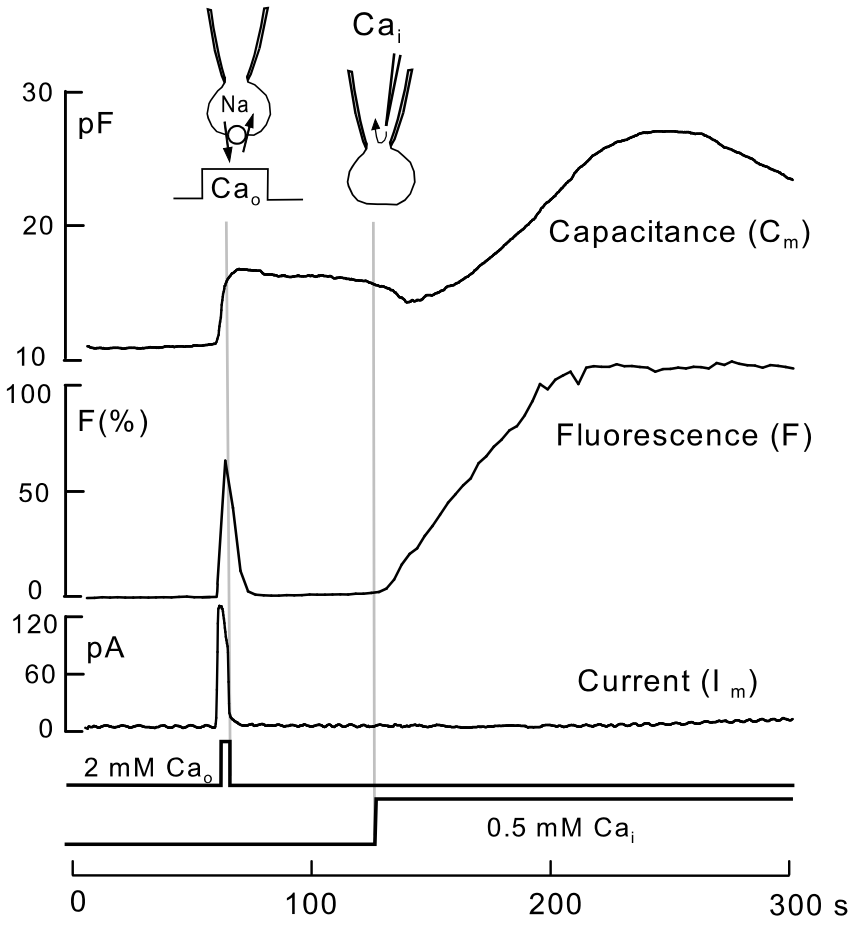
Ca$_i$
Na
Ca$_o$
30
pF
20
10
Capacitance (C$_m$)
100
F(%)
50
0
Fluorescence (F)
120
pA
60
0
Current (I $_m$)
2 mM Ca$_o$
0.5 mM Ca$_i$
0
100
200
300 s

Figure 2

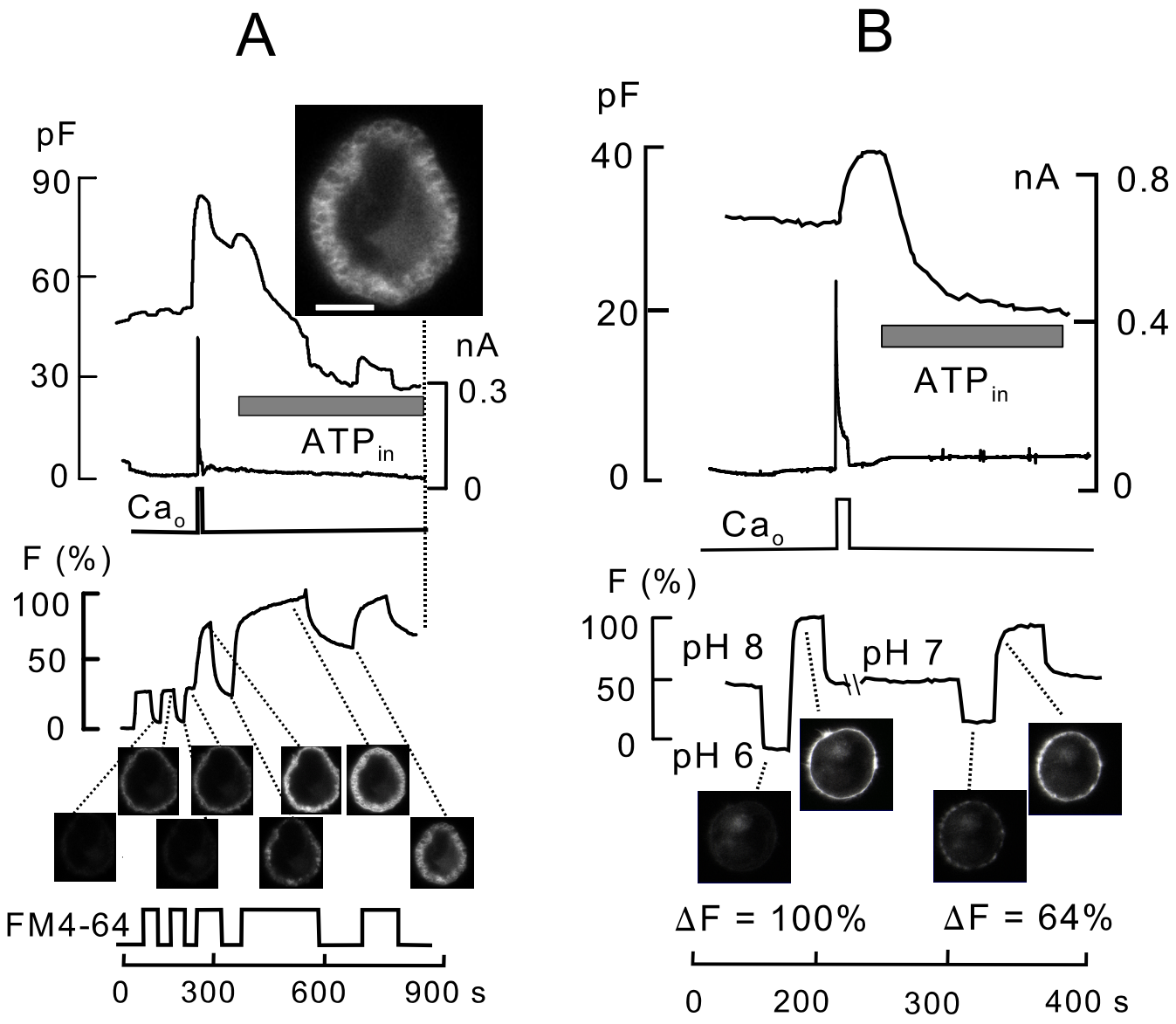
A
pF
90
60
30
0
nA
0.3
0
ATP in
Ca o
F (%)
100
50
0
FM4-64
0
300
600
900 s
B
pF
40
20
0
nA
0.8
0.4
0
ATP in
Ca o
F (%)
100
50
0
pH 8
pH 7
pH 6
ΔF = 100%
ΔF = 64%
0
200
300
400 s

Figure 3

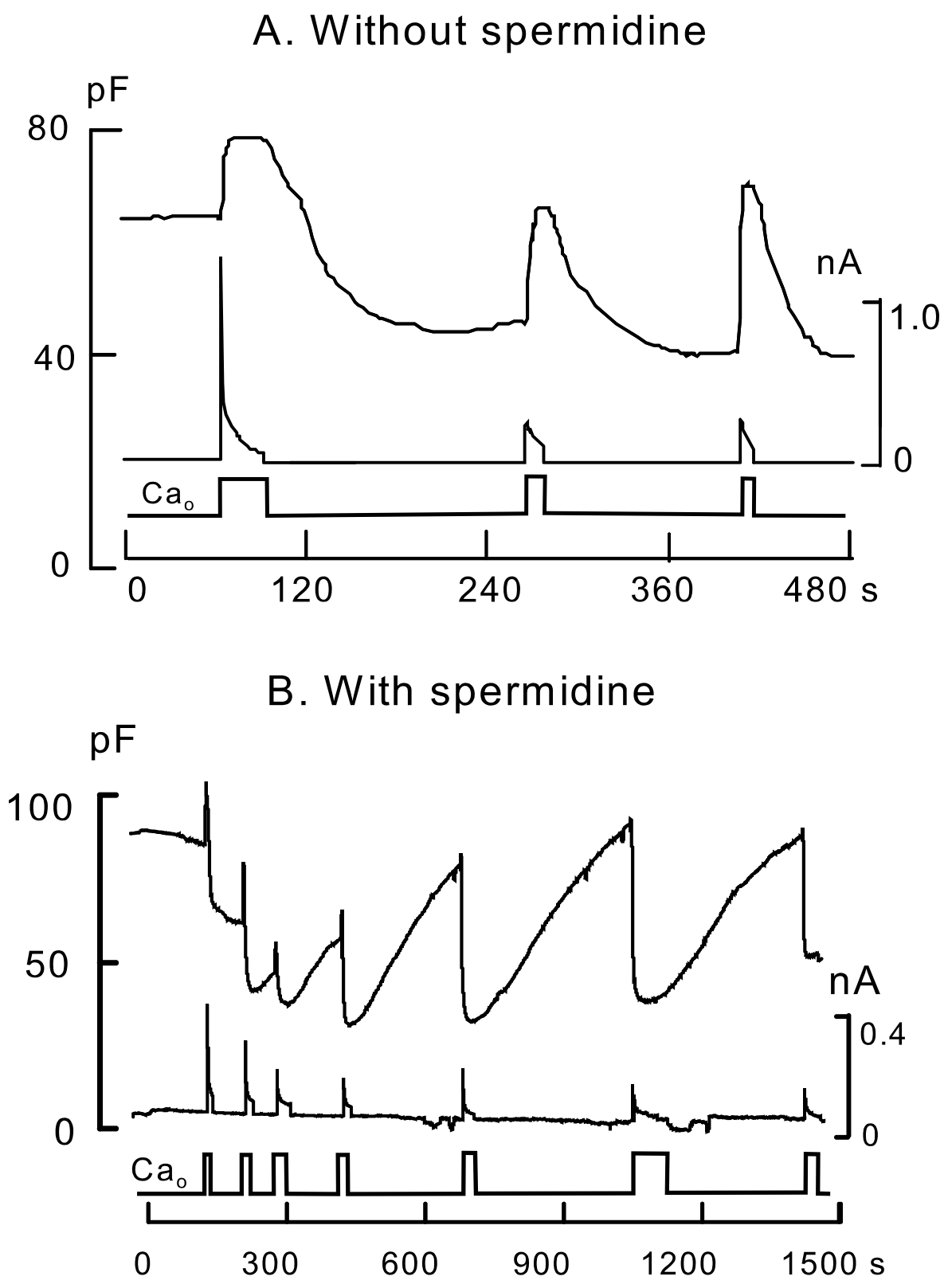
A. Without spermidine
pF
80
40
0
nA
1.0
0
Ca_o
0
120
240
360
480 s
B. With spermidine
pF
100
50
0
nA
0.4
0
Ca_o
0
300
600
900
1200
1500 s

Figure 4

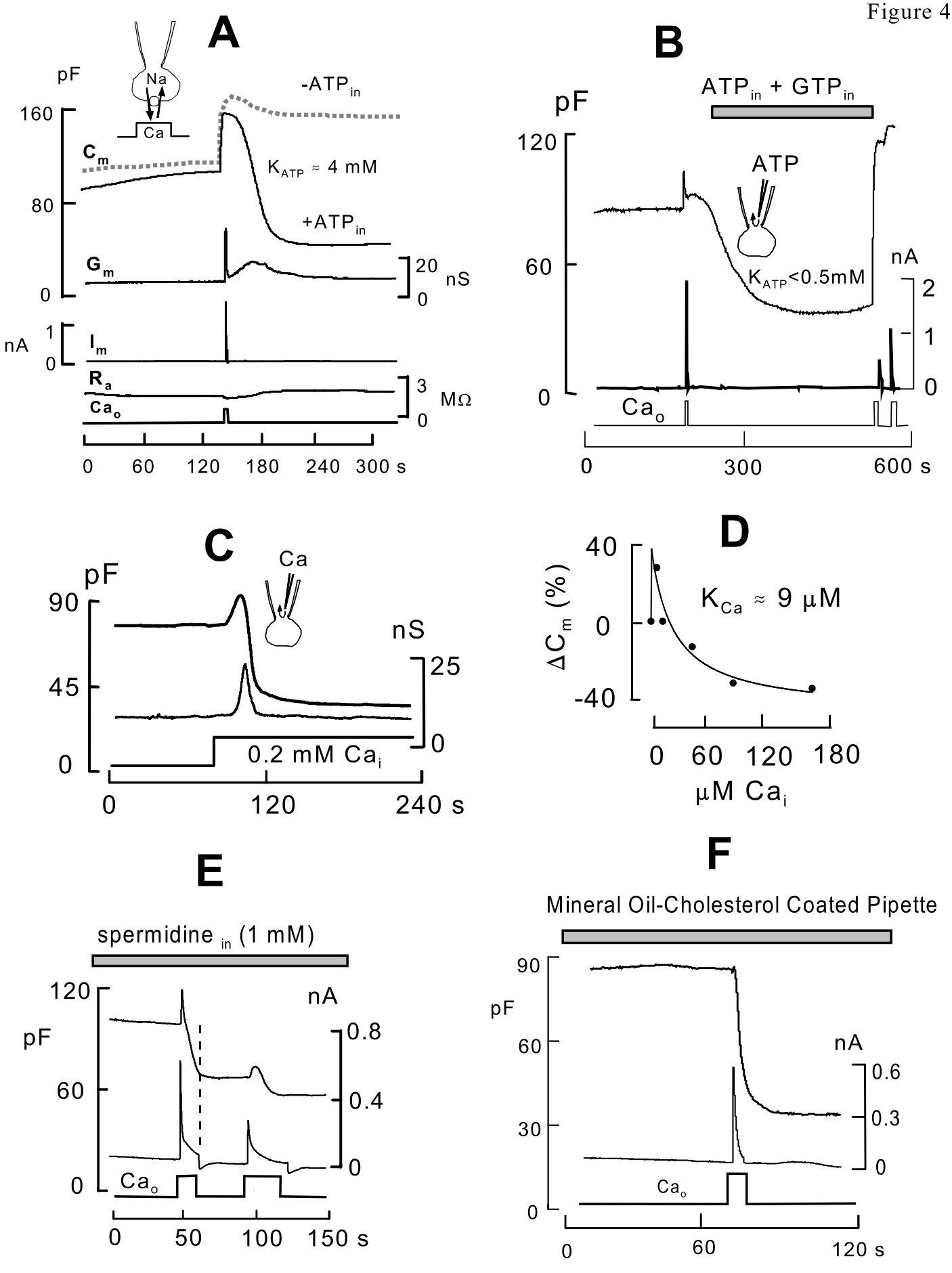
A
pF
Na
Ca
-ATP$_{in}$
160
C$_m$
K$_{ATP}$ ≈ 4 mM
80
+ATP$_{in}$
G$_m$
20
nS
0
nA
1
I$_m$
0
R$_a$
3
MΩ
Ca$_o$
0
0 60 120 180 240 300 s
B
ATP$_{in}$ + GTP$_{in}$
pF
120
ATP
60
K$_{ATP}$<0.5mM
nA
2
1
0
0
Ca$_o$
0 300 600 s
C
pF
Ca
90
nS
45
25
0
0.2 mM Ca$_i$
0 120 240 s
D
40
ΔC$_m$ (%)
0
K$_{Ca}$ ≈ 9 μM
-40
0 60 120 180
μM Ca$_i$
E
spermidine $_{in}$ (1 mM)
120
nA
pF
0.8
60
0.4
0
Ca$_o$
0 50 100 150 s
F
Mineral Oil-Cholesterol Coated Pipette
90
pF
nA
60
0.6
30
0.3
0
Ca$_o$
0 60 120 s

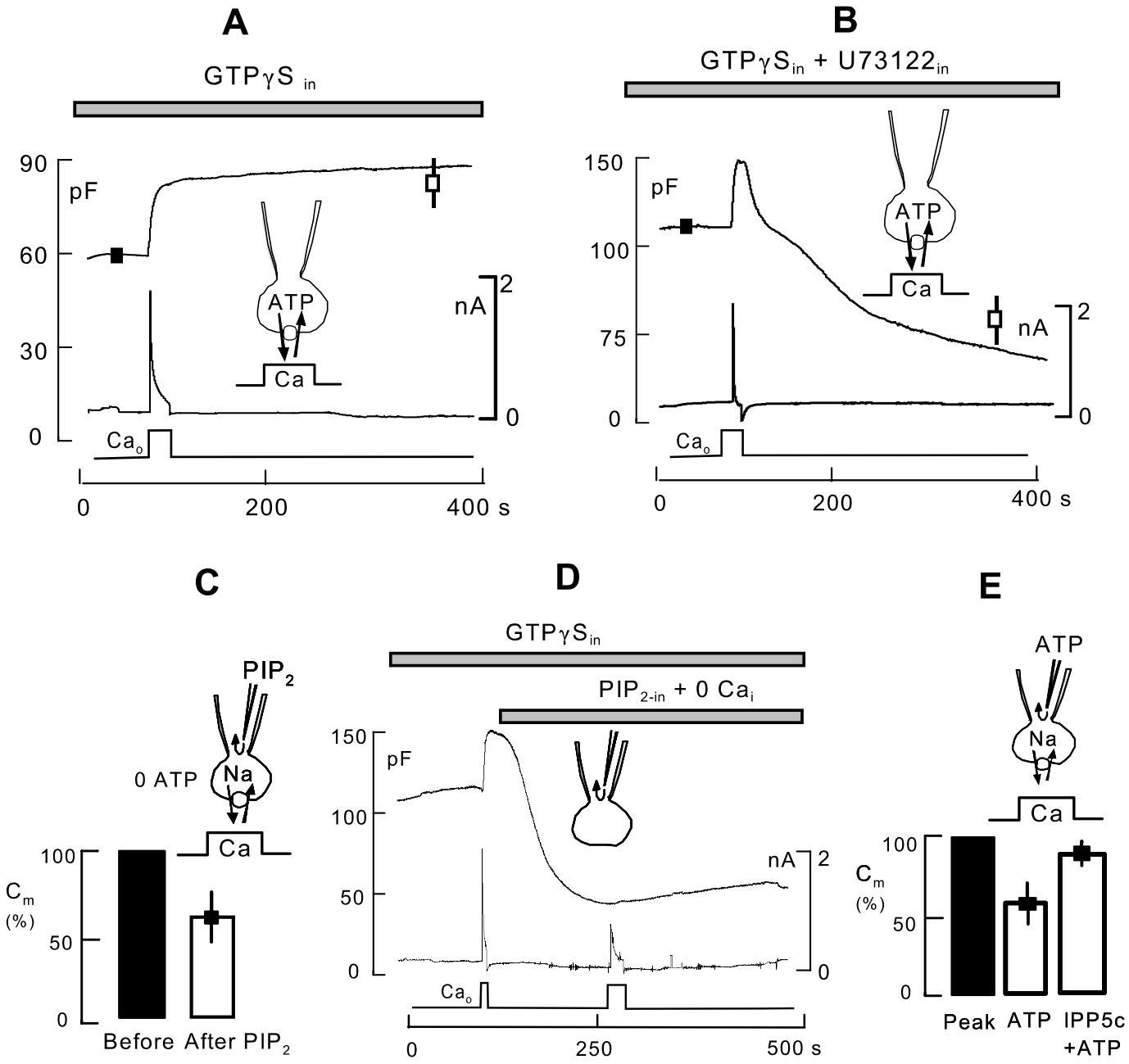
A
GTPγS in
90
60
30
0
pF
ATP
Ca
nA
2
0
Ca$_o$
0
200
400 s
B
GTPγS$_{in}$ + U73122$_{in}$
150
100
75
0
pF
ATP
Ca
nA
2
0
Ca$_o$
0
200
400 s
C
PIP$_2$
0 ATP
Na
Ca
100
50
0
C$_m$
(%)
Before
After PIP$_2$
D
GTPγS$_{in}$
PIP$_{2\text{-}in}$ + 0 Ca$_i$
150
100
50
0
pF
nA
2
0
Ca$_o$
0
250
500 s
E
ATP
Na
Ca
100
50
0
C$_m$
(%)
Peak
ATP
IPP5c
+ATP

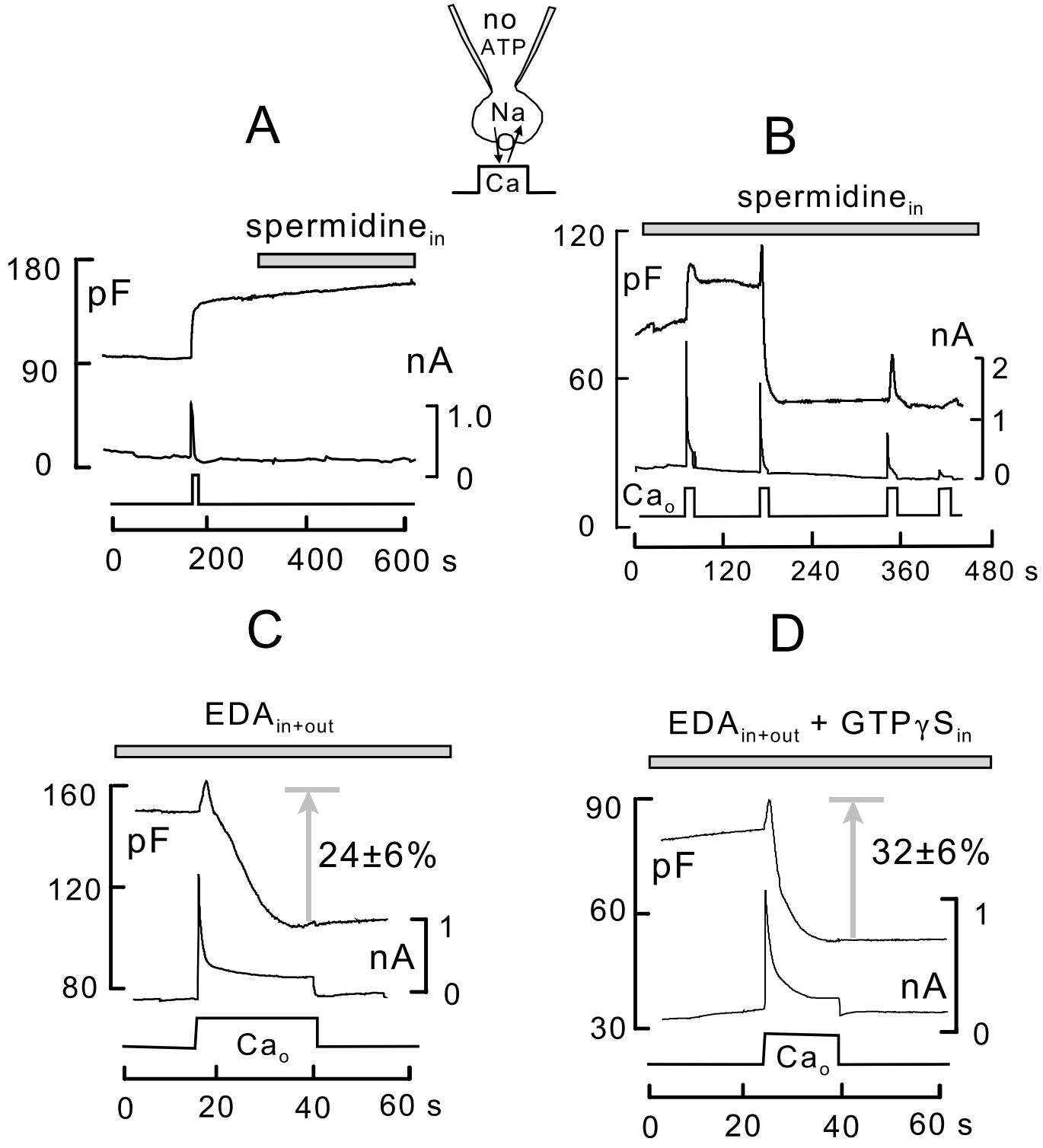
no
ATP
Na
Ca
A
spermidine$_{in}$
180
pF
90
0
nA
1.0
0
0
200
400
600 s
B
spermidine$_{in}$
120
pF
60
0
nA
2
1
0
Ca$_o$
0
120
240
360
480 s
C
EDA$_{in+out}$
160
pF
120
80
24±6%
nA
1
0
Ca$_o$
0
20
40
60 s
D
EDA$_{in+out}$ + GTPγS$_{in}$
90
pF
60
30
32±6%
nA
1
0
Ca$_o$
0
20
40
60 s

Figure 7

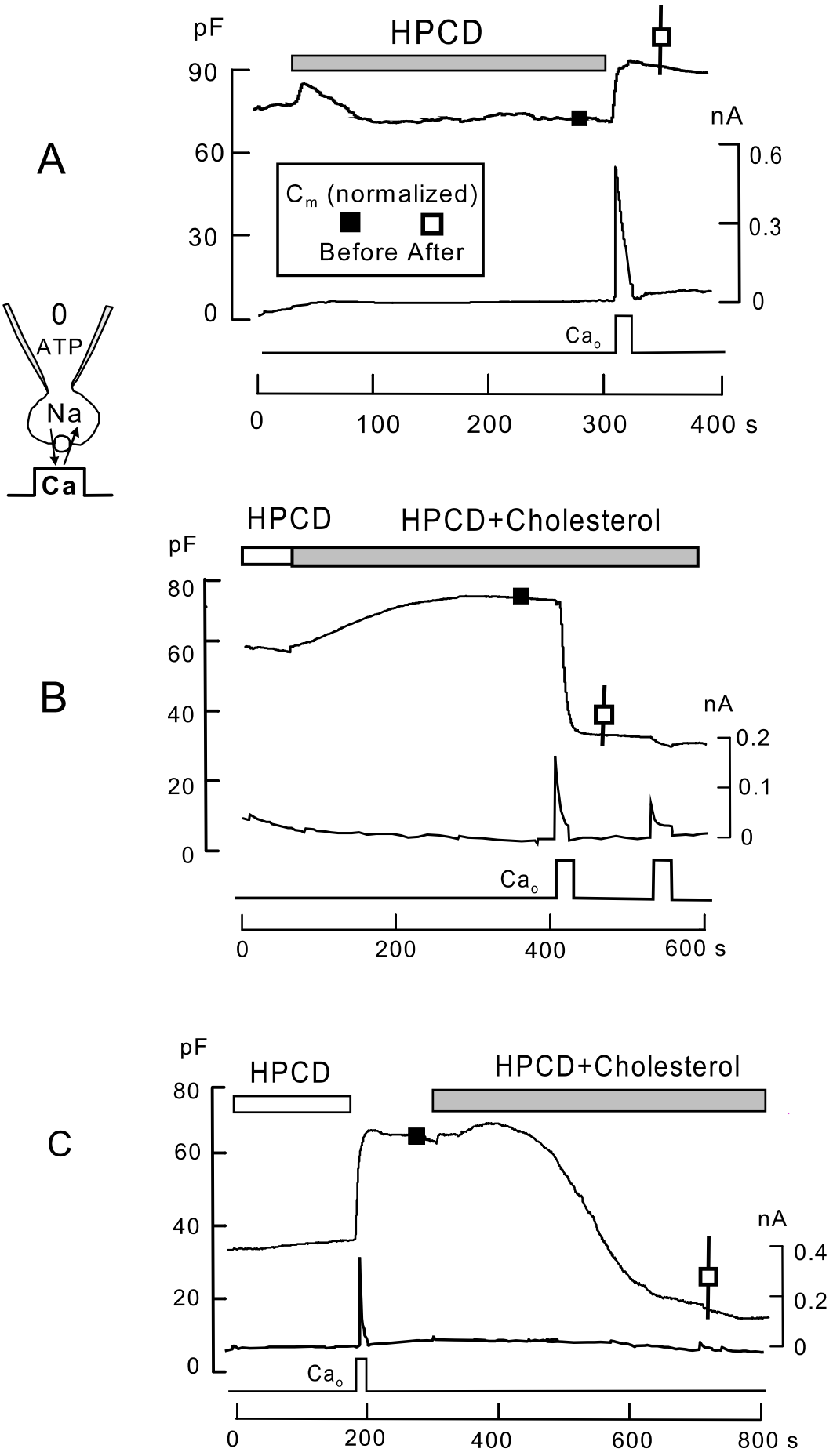
A
pF
HPCD
90
60
30
0
nA
0.6
0.3
0
C_m (normalized)
Before After
Ca_o
0
100
200
300
400 s
0
ATP
Na
Ca
B
HPCD
HPCD+Cholesterol
pF
80
60
40
20
0
nA
0.2
0.1
0
Ca_o
0
200
400
600 s
C
pF
HPCD
HPCD+Cholesterol
80
60
40
20
0
nA
0.4
0.2
0
Ca_o
0
200
400
600
800 s

Figure 8

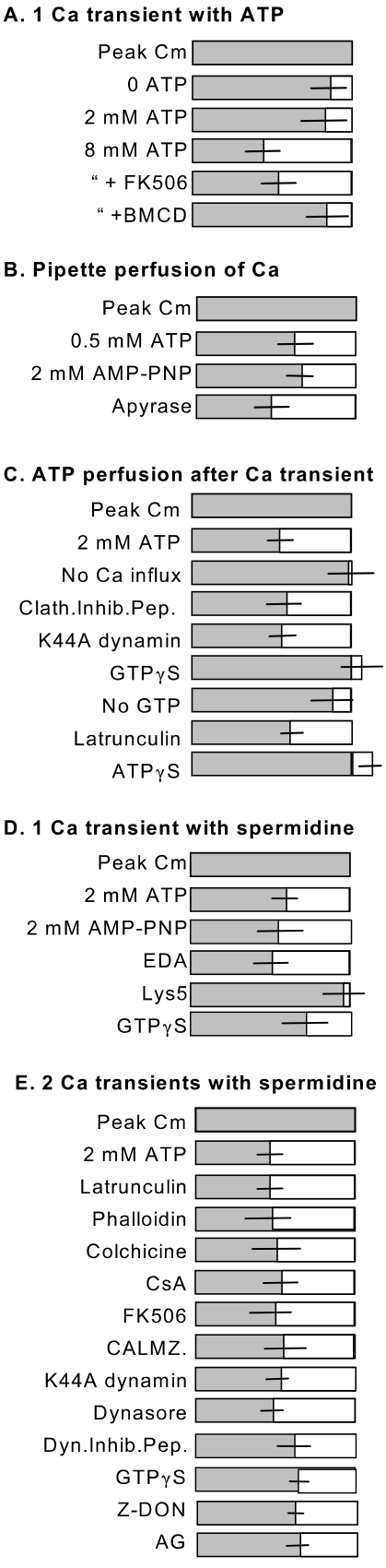
A. 1 Ca transient with ATP
Peak Cm
0 ATP
2 mM ATP
8 mM ATP
“ + FK506
“ +BMCD
B. Pipette perfusion of Ca
Peak Cm
0.5 mM ATP
2 mM AMP-PNP
Apyrase
C. ATP perfusion after Ca transient
Peak Cm
2 mM ATP
No Ca influx
Clath.Inhib.Pep.
K44A dynamin
GTPγS
No GTP
Latrunculin
ATPγS
D. 1 Ca transient with spermidine
Peak Cm
2 mM ATP
2 mM AMP-PNP
EDA
Lys5
GTPγS
E. 2 Ca transients with spermidine
Peak Cm
2 mM ATP
Latrunculin
Phalloidin
Colchicine
CsA
FK506
CALMZ.
K44A dynamin
Dynasore
Dyn.Inhib.Pep.
GTPγS
Z-DON
AG

Figure 9

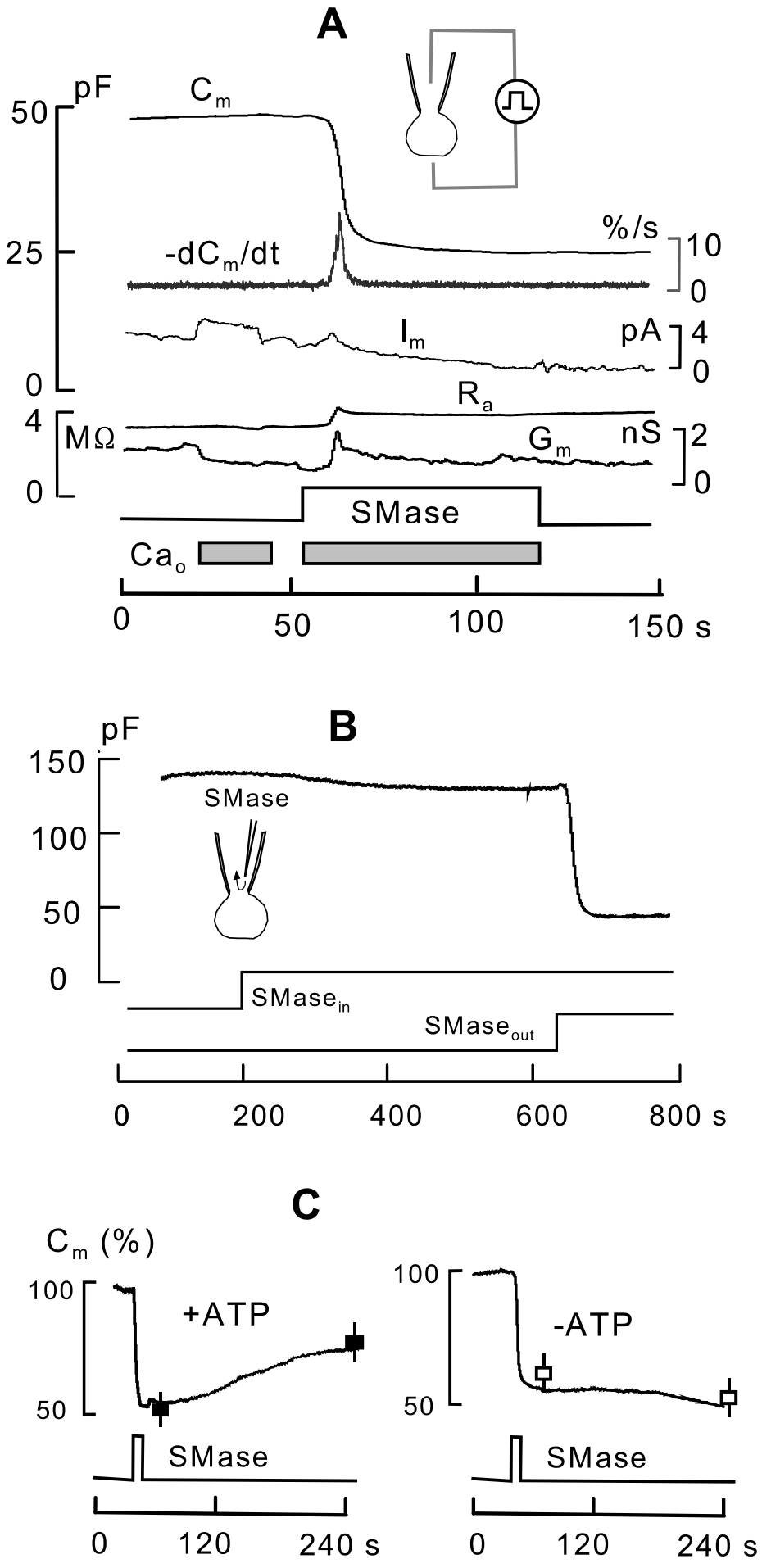
A
pF
50
25
0
C_m
$-dC_m/dt$
%/s
10
0
I_m
pA
4
0
R_a
4
MΩ
0
G_m
nS
2
0
SMase
Ca_o
0
50
100
150 s
B
pF
150
100
50
0
SMase
$SMase_{in}$
$SMase_{out}$
0
200
400
600
800 s
C
C_m (%)
100
50
+ATP
SMase
0
120
240 s
100
50
-ATP
SMase
0
120
240 s

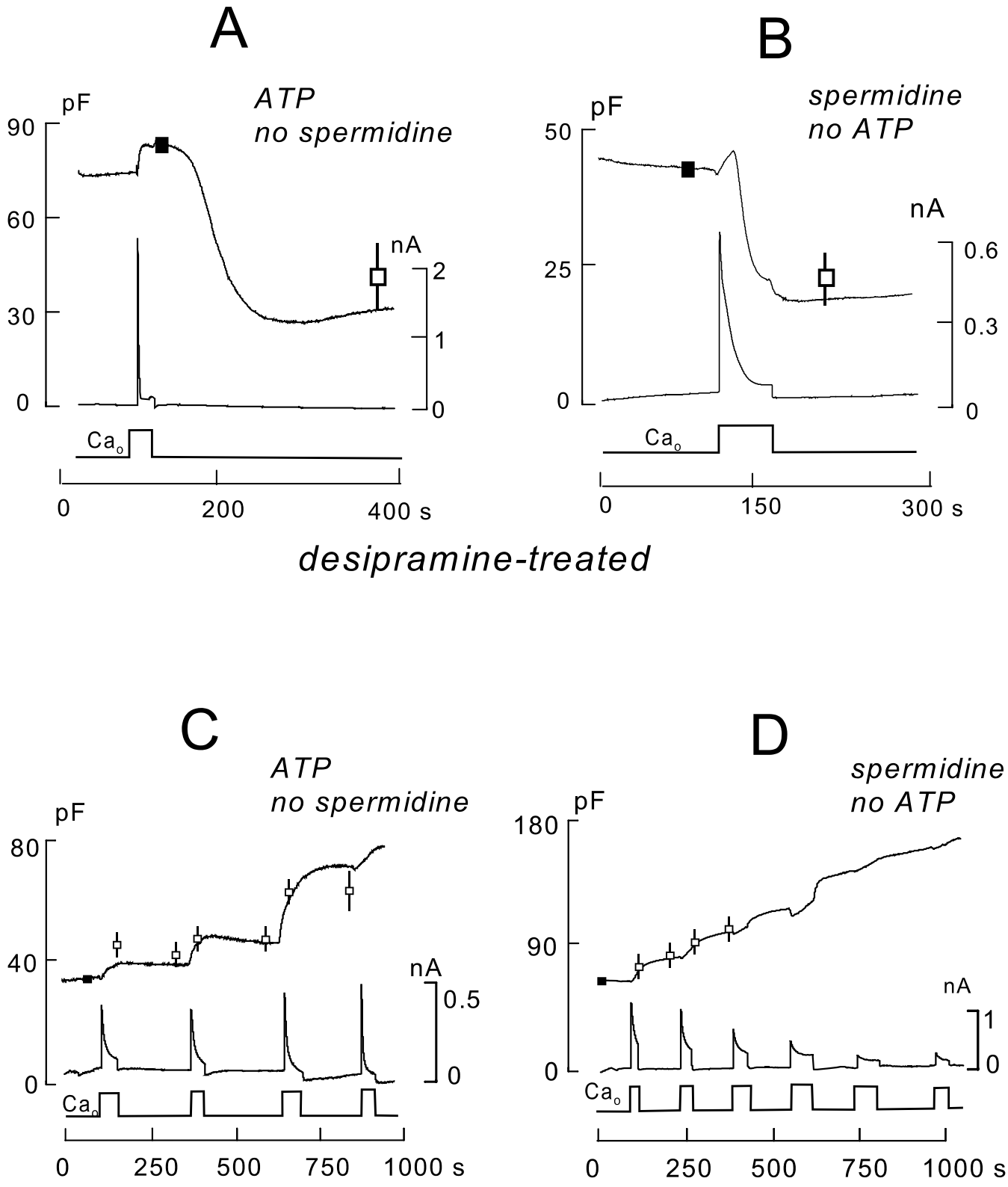
A
ATP
no spermidine
pF
90
60
30
0
nA
2
1
0
Ca$_o$
0
200
400 s
B
spermidine
no ATP
pF
50
25
0
nA
0.6
0.3
0
Ca$_o$
0
150
300 s
desipramine-treated
C
ATP
no spermidine
pF
80
40
0
nA
0.5
0
Ca$_o$
0
250
500
750
1000 s
D
spermidine
no ATP
pF
180
90
0
nA
1
0
Ca$_o$
0
250
500
750
1000 s
BEL-treated

Figure 11

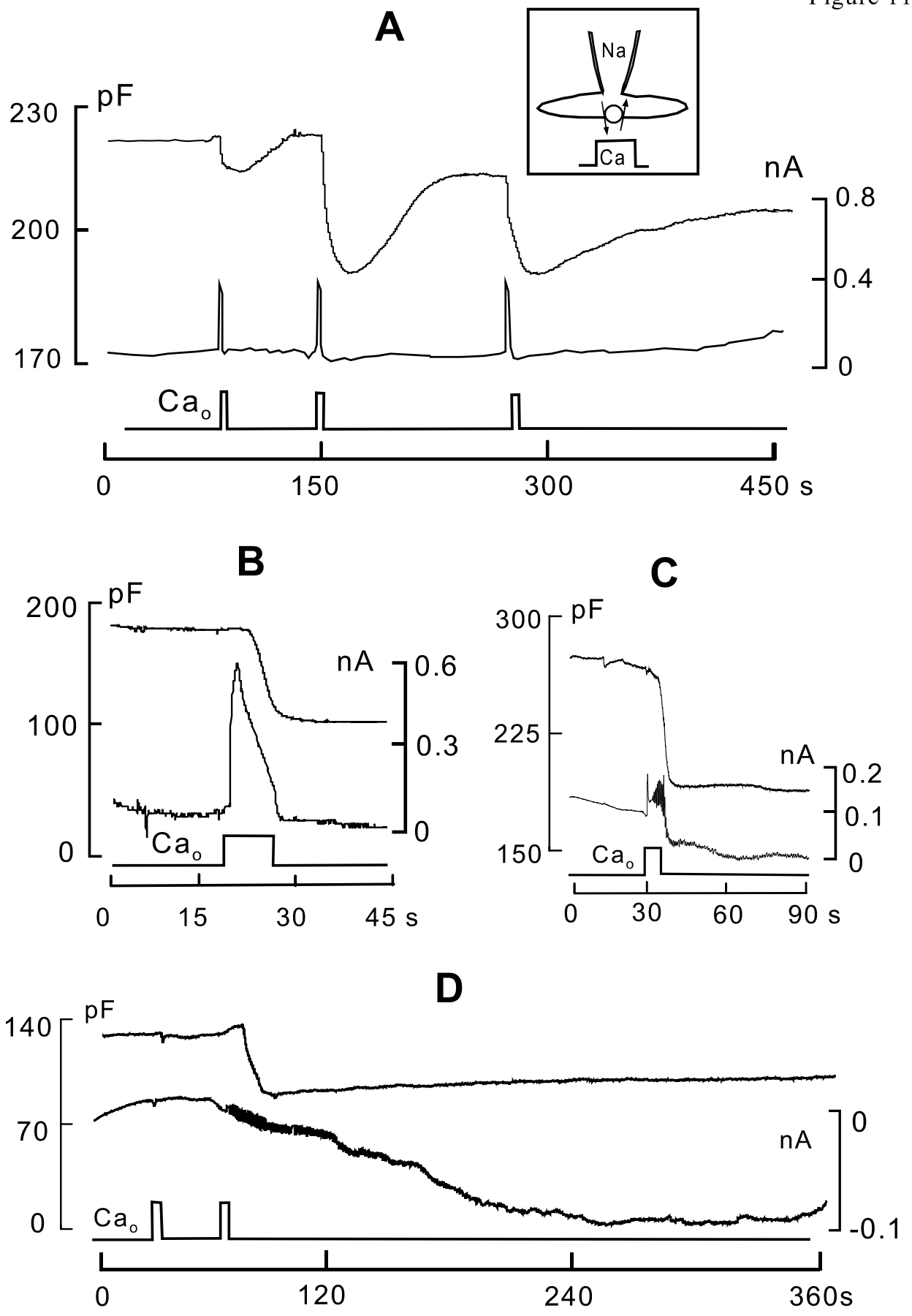
A
Na
Ca
pF
230
200
170
nA
0.8
0.4
0
Ca$_o$
0
150
300
450 s
B
pF
200
100
0
nA
0.6
0.3
0
Ca$_o$
0
15
30
45 s
C
pF
300
225
150
nA
0.2
0.1
0
Ca$_o$
0
30
60
90 s
D
pF
140
70
0
nA
0
-0.1
Ca$_o$
0
120
240
360s

Supporting Data Figures

Figure S1

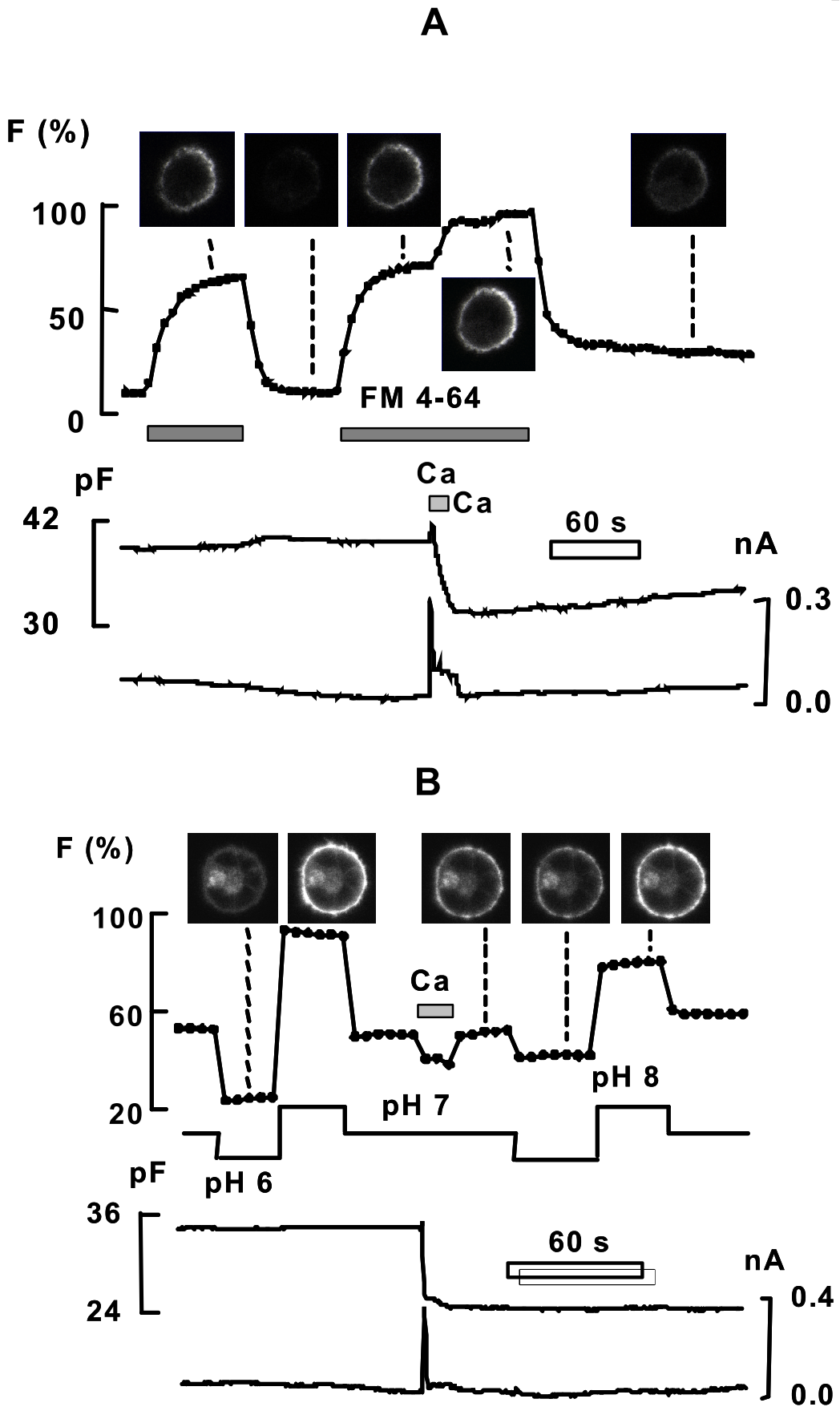
A
F (%)
100
50
0
FM 4-64
pF
42
30
Ca
Ca
60 s
nA
0.3
0.0
B
F (%)
100
60
20
Ca
pH 8
pH 7
pH 6
pF
36
24
60 s
nA
0.4
0.0

Figure S2

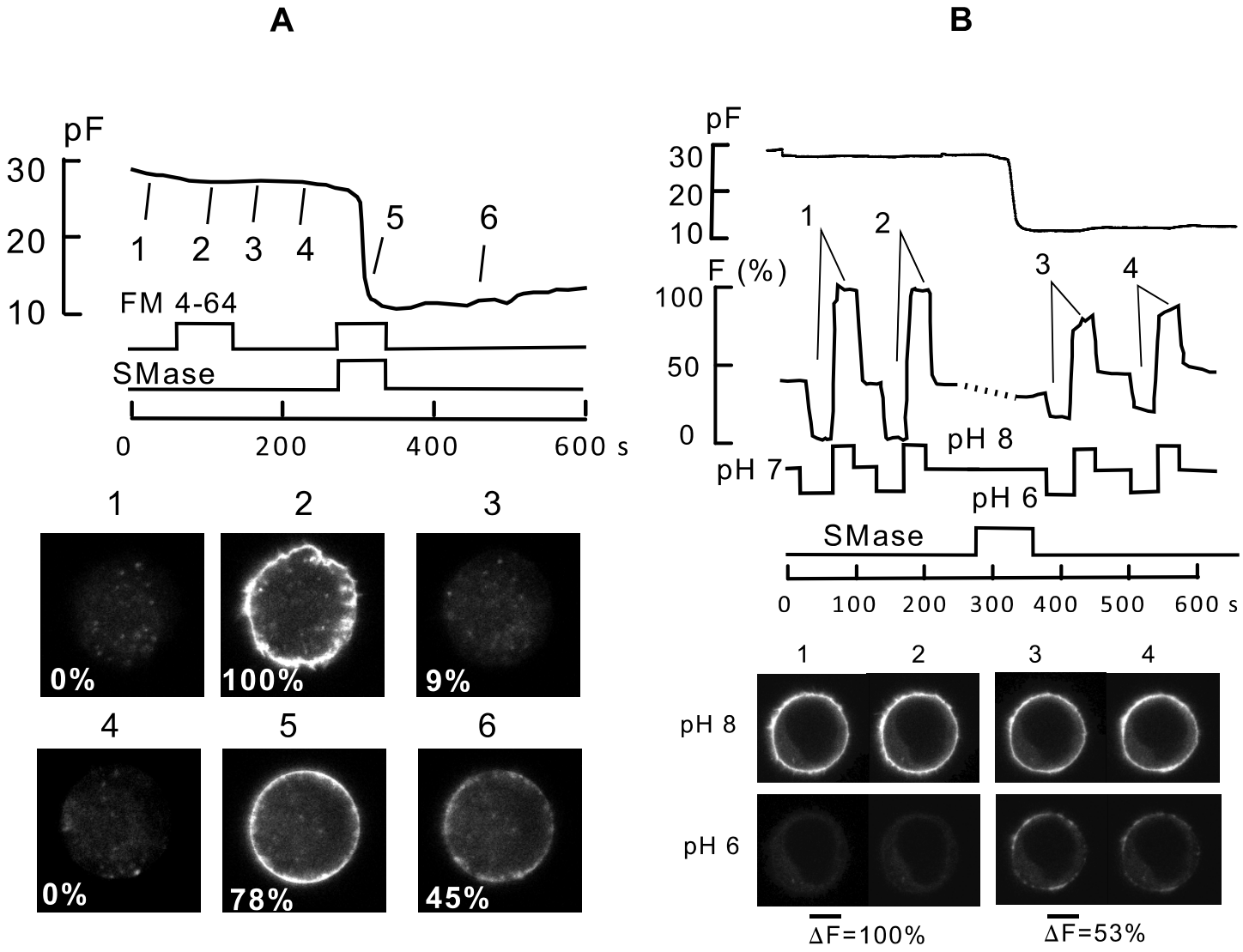
A
B
pF
30
20
10
1
2
3
4
5
6
FM 4-64
SMase
0
200
400
600 s
0%
100%
9%
0%
78%
45%
F (%)
100
50
0
pH 8
pH 7
pH 6
100
300
500
pH 8
pH 6
ΔF=100%
ΔF=53%

Figure S3

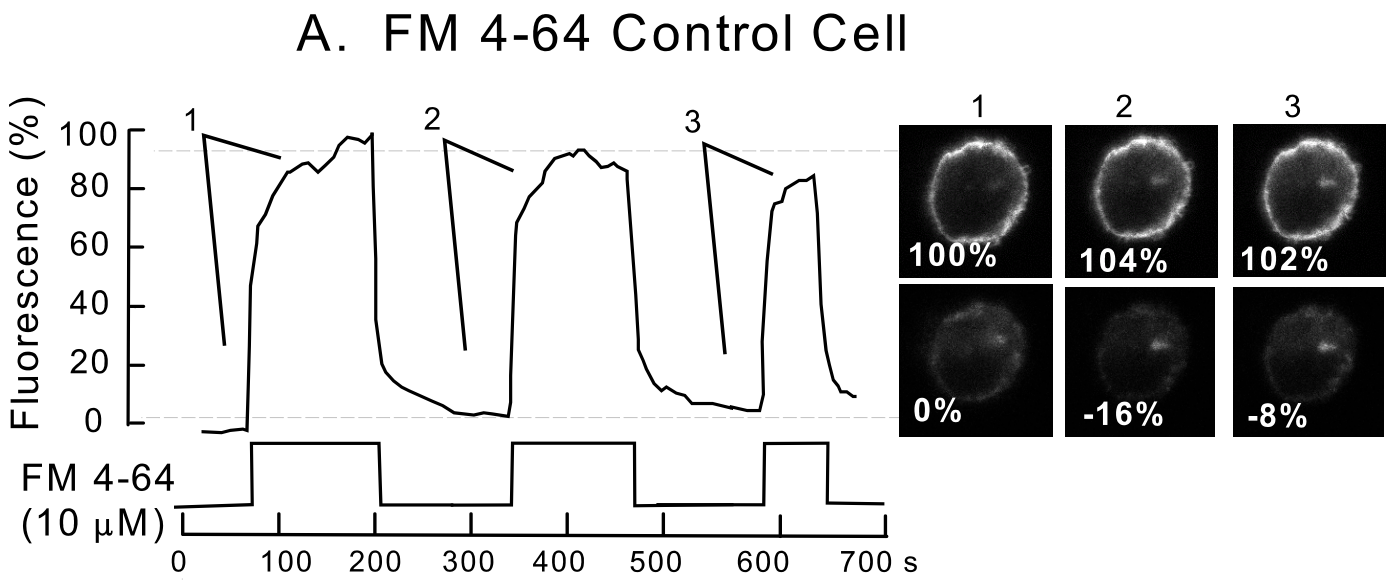
A. FM 4-64 Control Cell
Fluorescence (%)
100
80
60
40
20
0
1
2
3
FM 4-64
(10 μM)
0
100
200
300
400
500
600
700 s
1
2
3
100%
104%
102%
0%
-16%
-8%

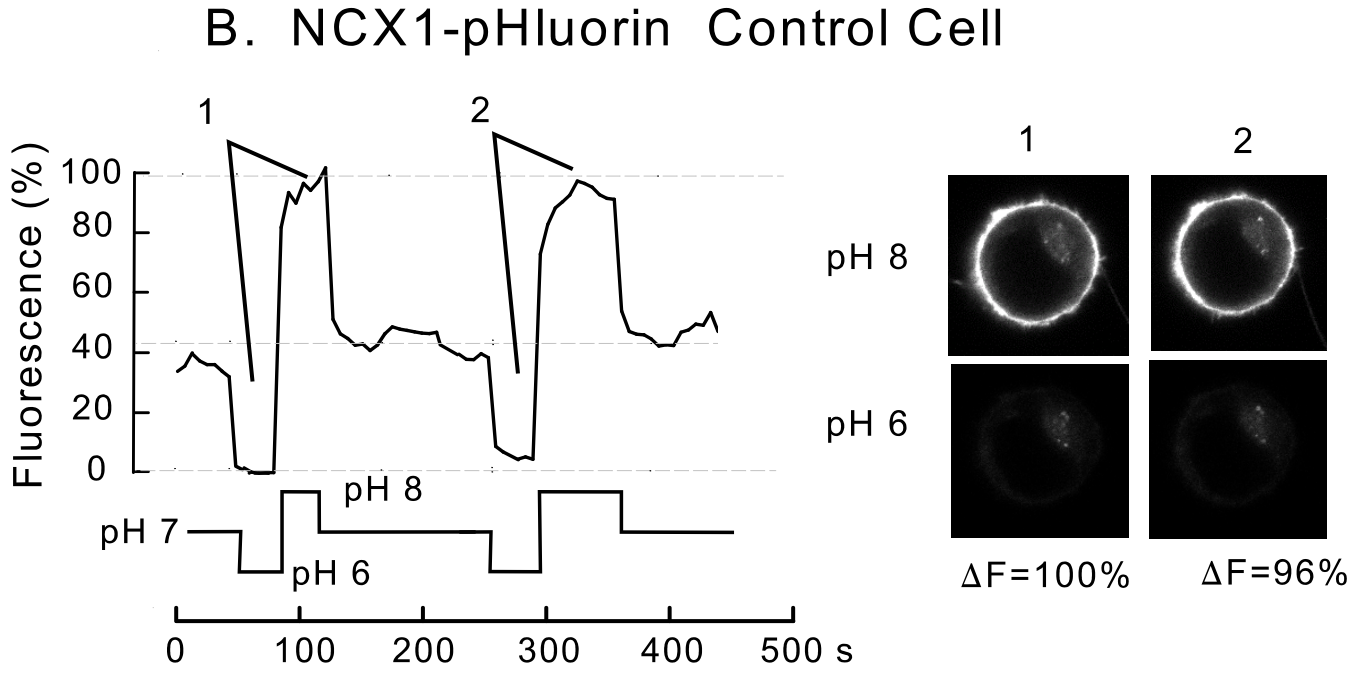
B. NCX1-pHluorin Control Cell
Fluorescence (%)
100
80
60
40
20
0
1
2
pH 8
pH 7
pH 6
0
100
200
300
400
500 s
1
2
pH 8
pH 6
ΔF=100%
ΔF=96%

Figure S4

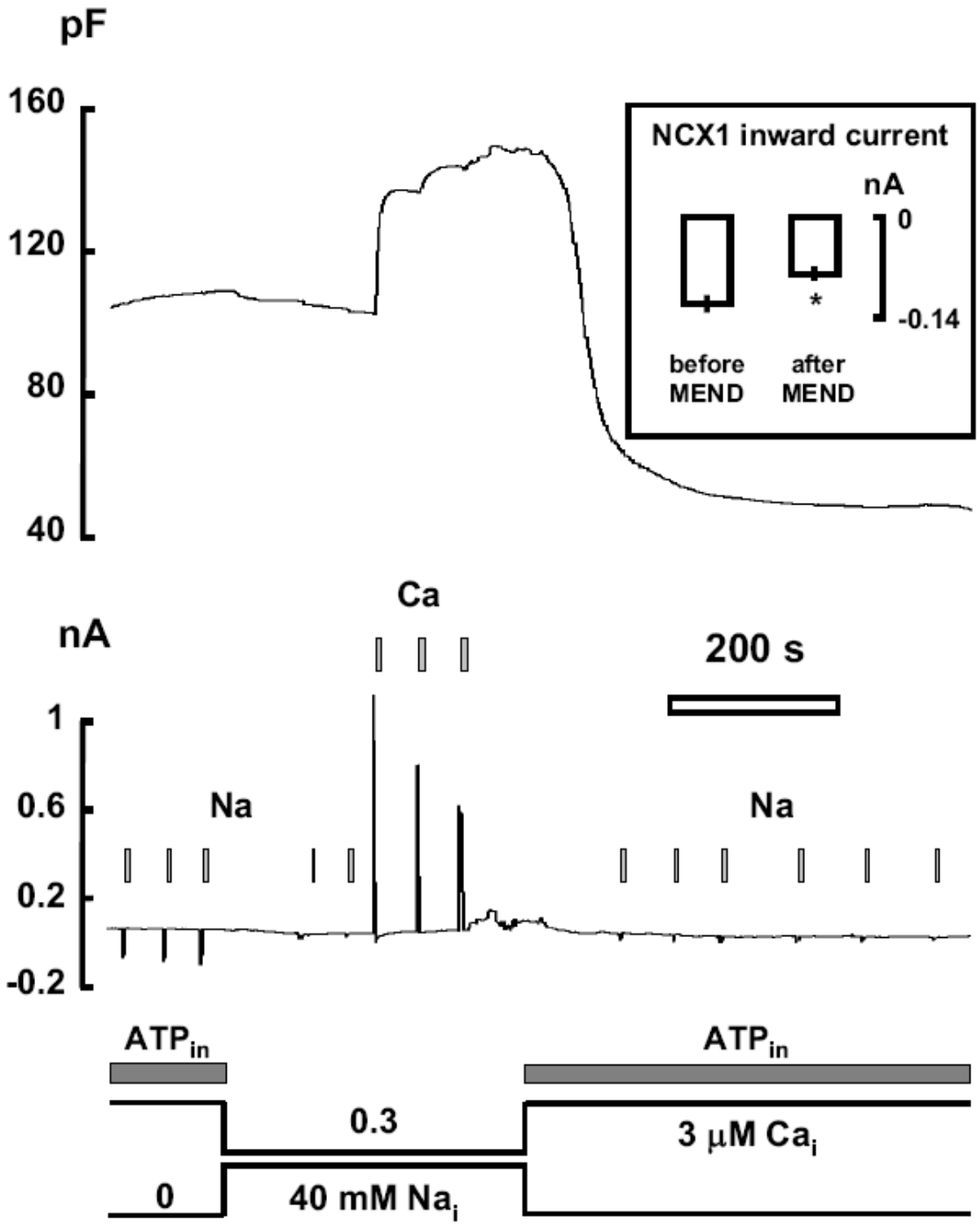
pF
160
120
80
40
NCX1 inward current
nA
0
-0.14
*
before MEND
after MEND
Ca
nA
200 s
1
0.6
0.2
-0.2
Na
Na
ATPin
ATPin
0.3
3 μM Cai
0
40 mM Nai

Figure S5

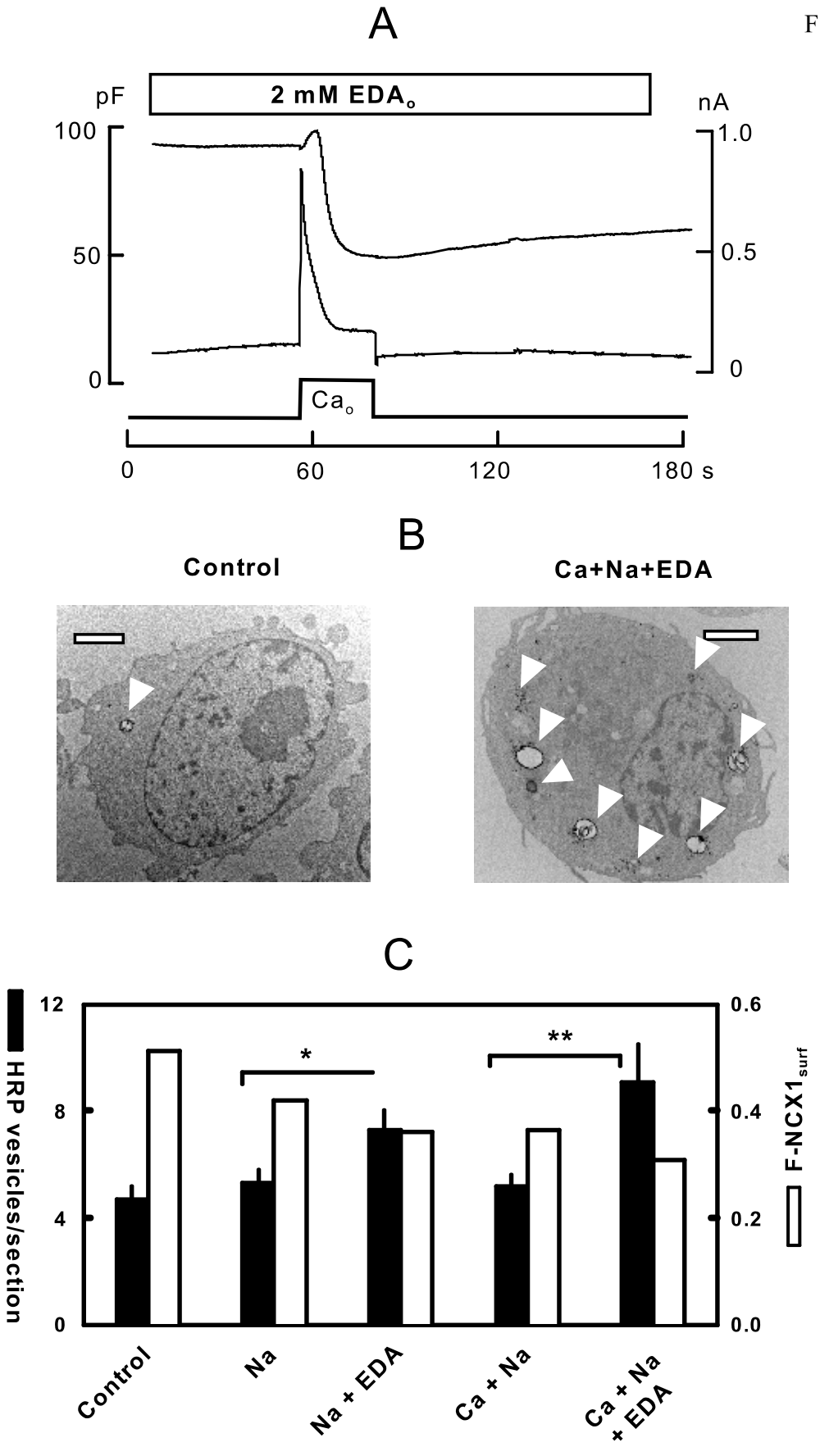
A
pF
2 mM EDA$_o$
nA
100
50
0
1.0
0.5
0
Ca$_o$
0
60
120
180 s
B
Control
Ca+Na+EDA
C
HRP vesicles/section
F-NCX1$_{surf}$
12
8
4
0
0.6
0.4
0.2
0.0
*
**
Control
Na
Na + EDA
Ca + Na
Ca + Na + EDA

Figure S6

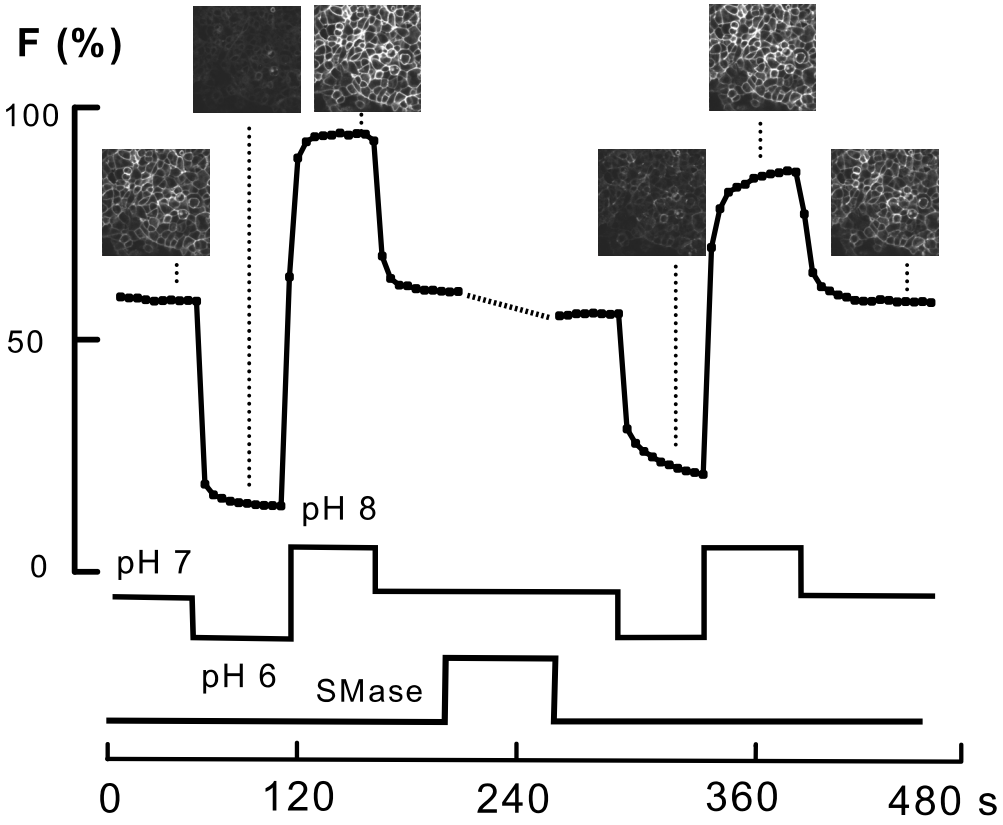

Figure S7

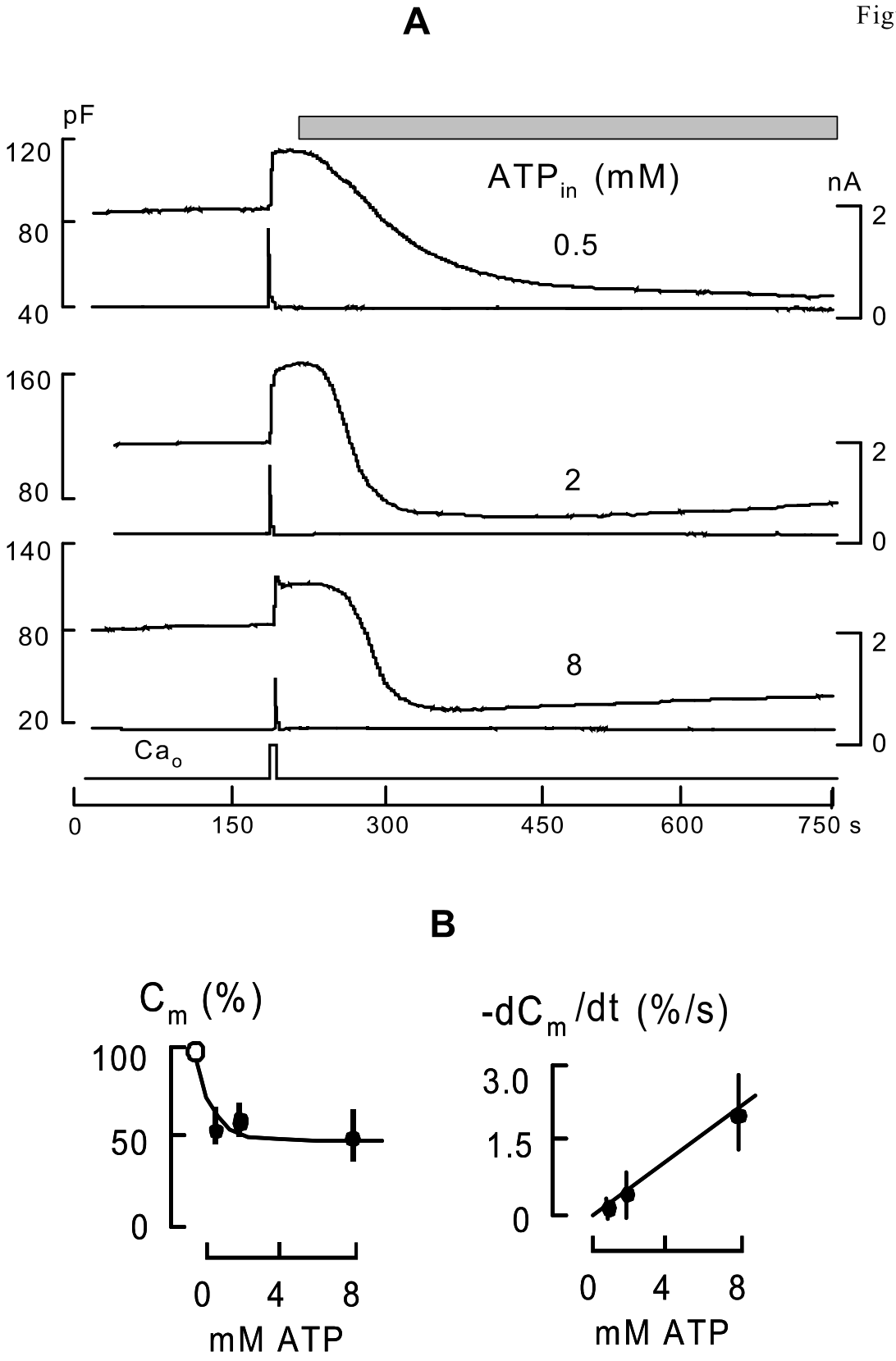
A
pF
120
80
40
ATP$_{in}$ (mM)
nA
0.5
2
0
160
80
2
2
0
140
80
20
8
2
0
Ca$_o$
0
150
300
450
600
750 s
B
C$_m$ (%)
100
50
0
0 4 8
mM ATP
-dC$_m$/dt (%/s)
3.0
1.5
0
0 4 8
mM ATP

Figure S8

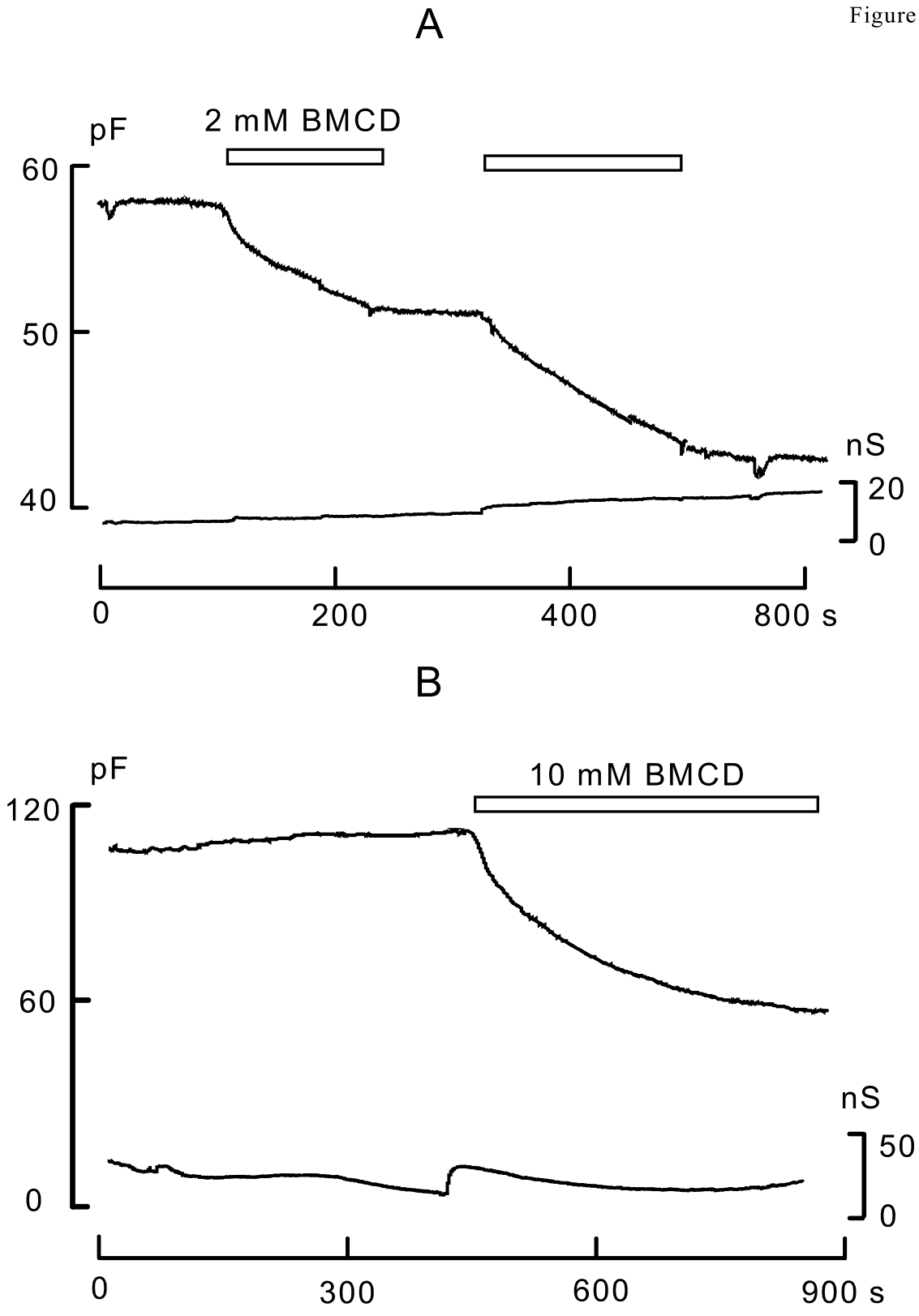
A
pF
2 mM BMCD
60
50
40
nS
20
0
0
200
400
800 s
B
pF
10 mM BMCD
120
60
0
nS
50
0
0
300
600
900 s

Figure S9

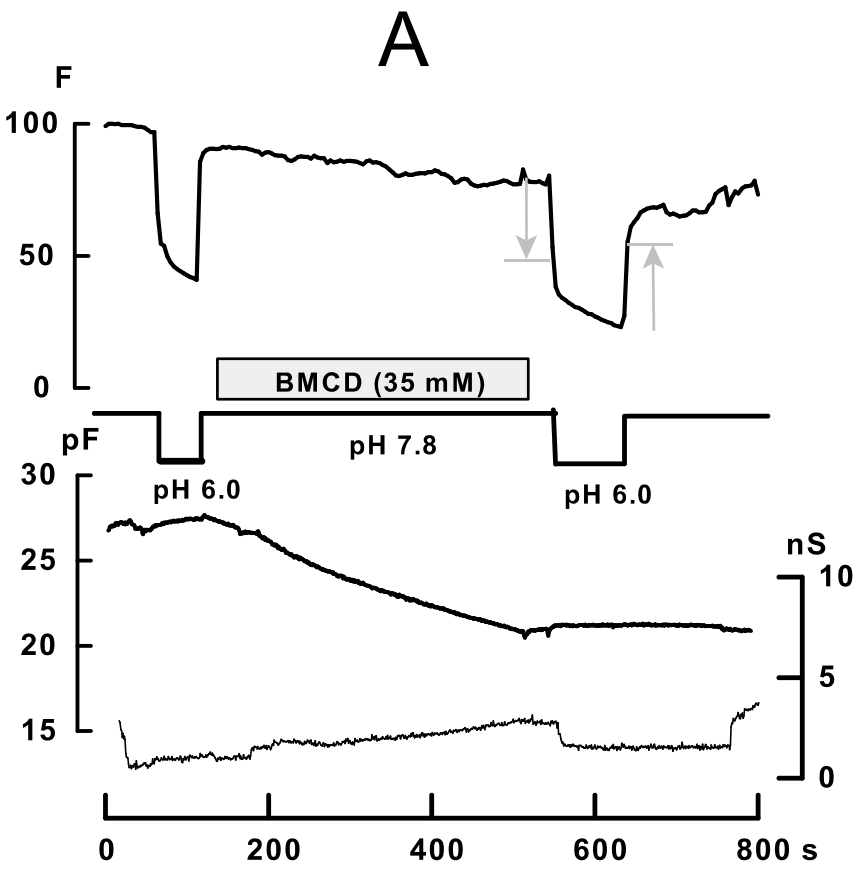
A
F
100
50
0
BMCD (35 mM)
pH 7.8
pF
30
25
20
15
pH 6.0
pH 6.0
nS
10
5
0
0
200
400
600
800 s

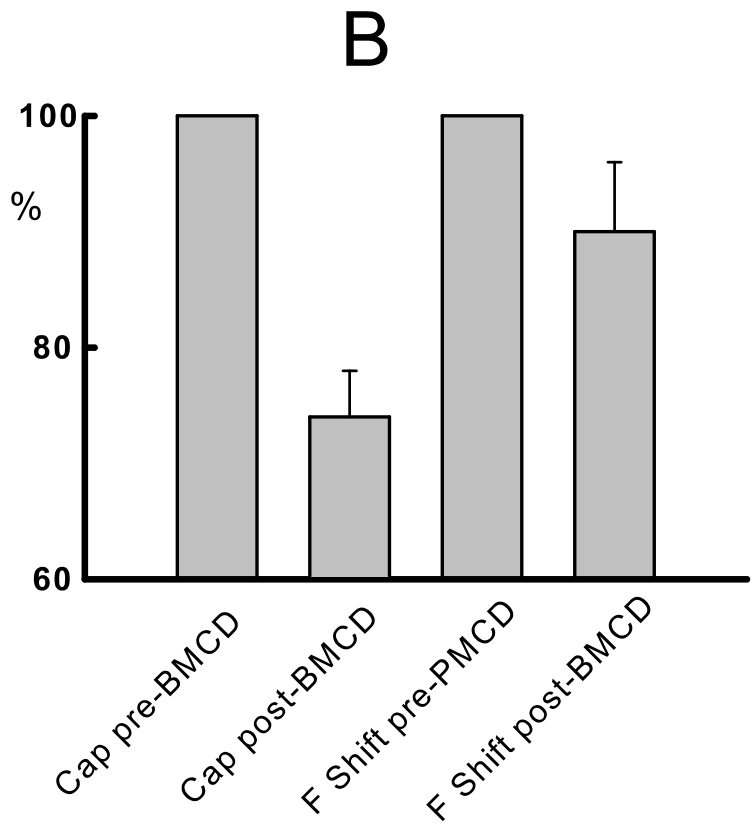
B
100
%
80
60
Cap pre-BMCD
Cap post-BMCD
F Shift pre-PMCD
F Shift post-BMCD

Figure S10

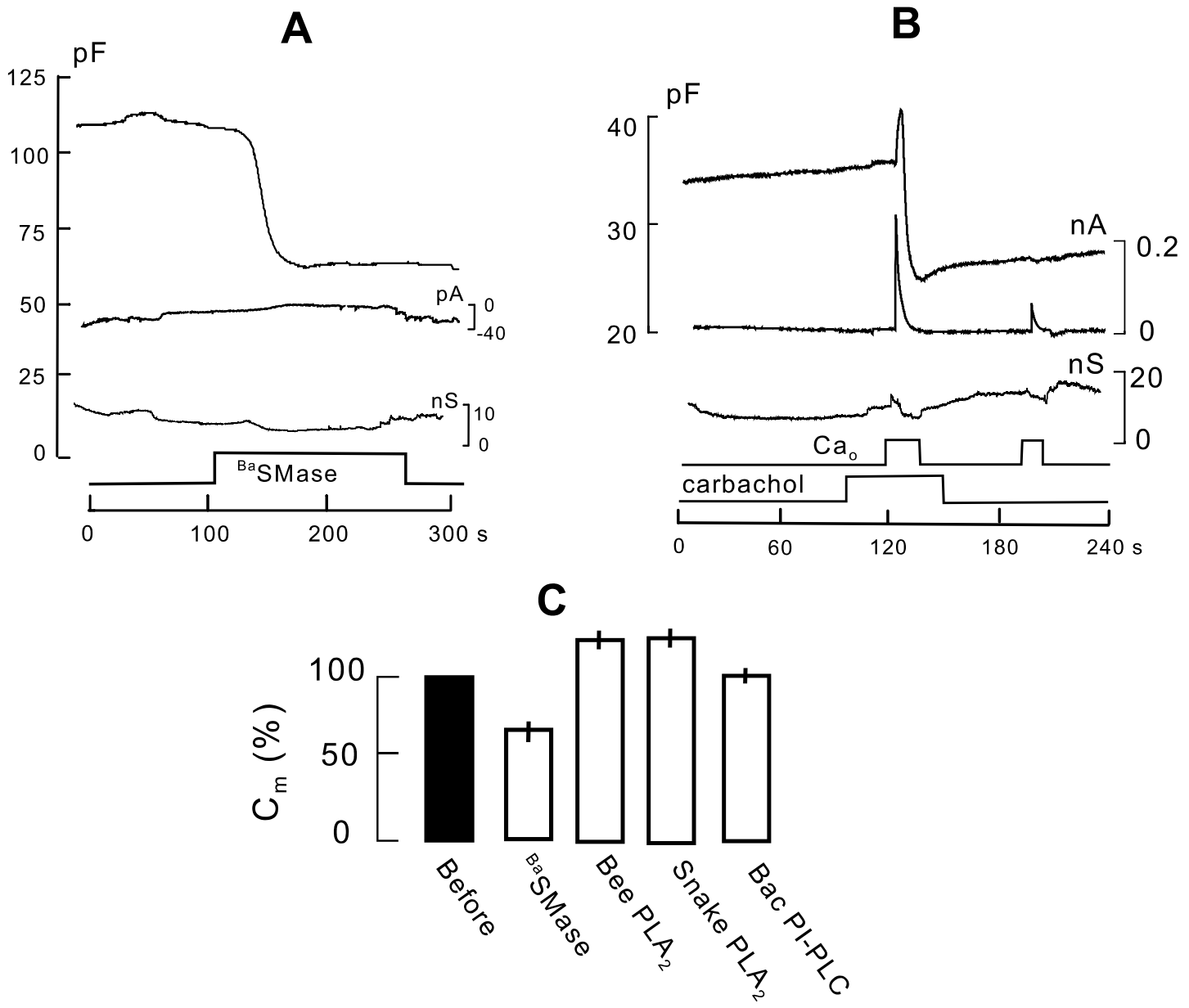
A
pF
125
100
75
50
25
0
pA
0
-40
nS
10
0
BaSMase
0
100
200
300 s
B
pF
40
30
20
nA
0.2
0
nS
20
0
Cao
carbachol
0
60
120
180
240 s
C
Cm (%)
100
50
0
Before
BaSMase
Bee PLA2
Snake PLA2
Bac PI-PLC

Figure S11

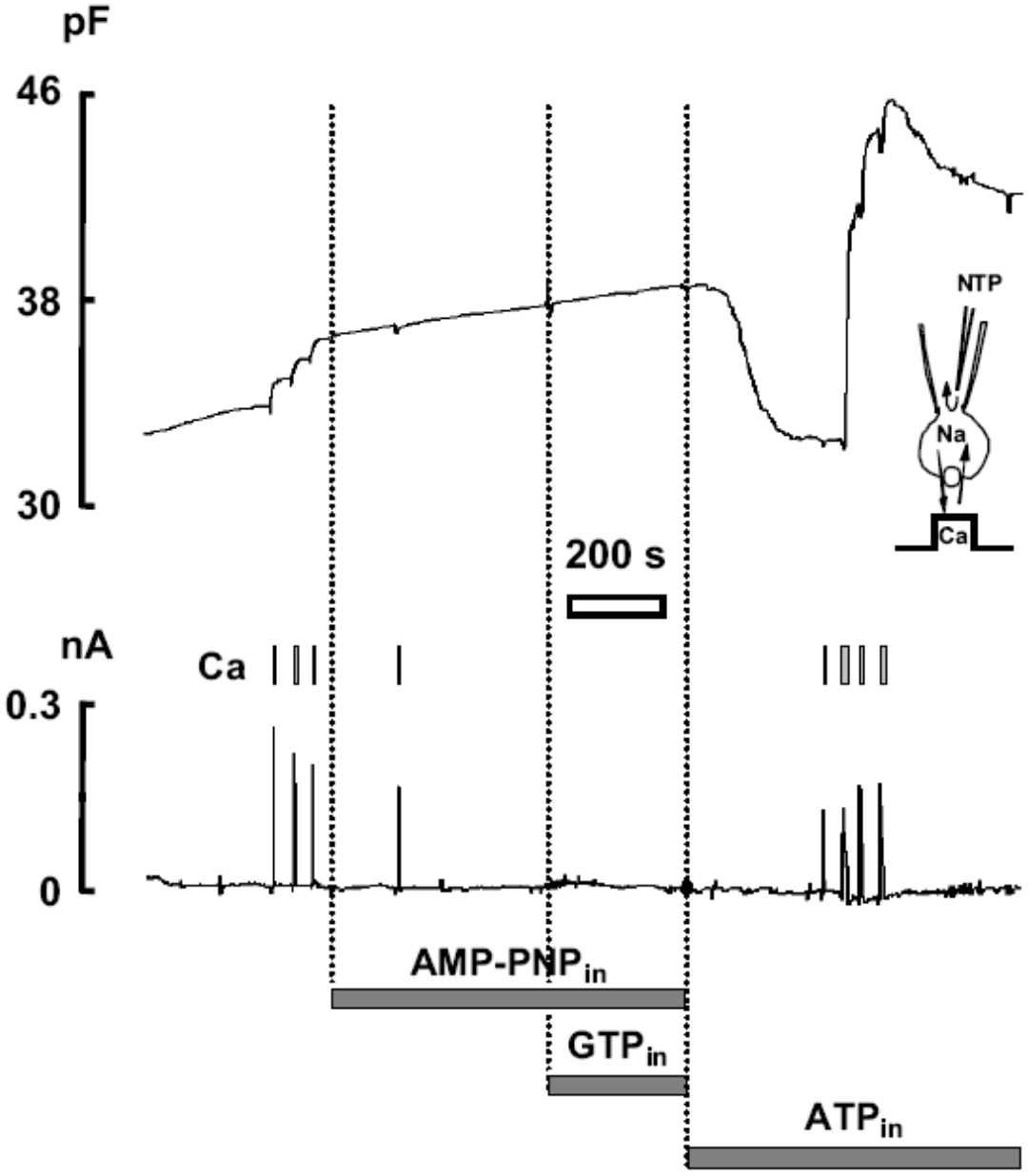

Figure S12

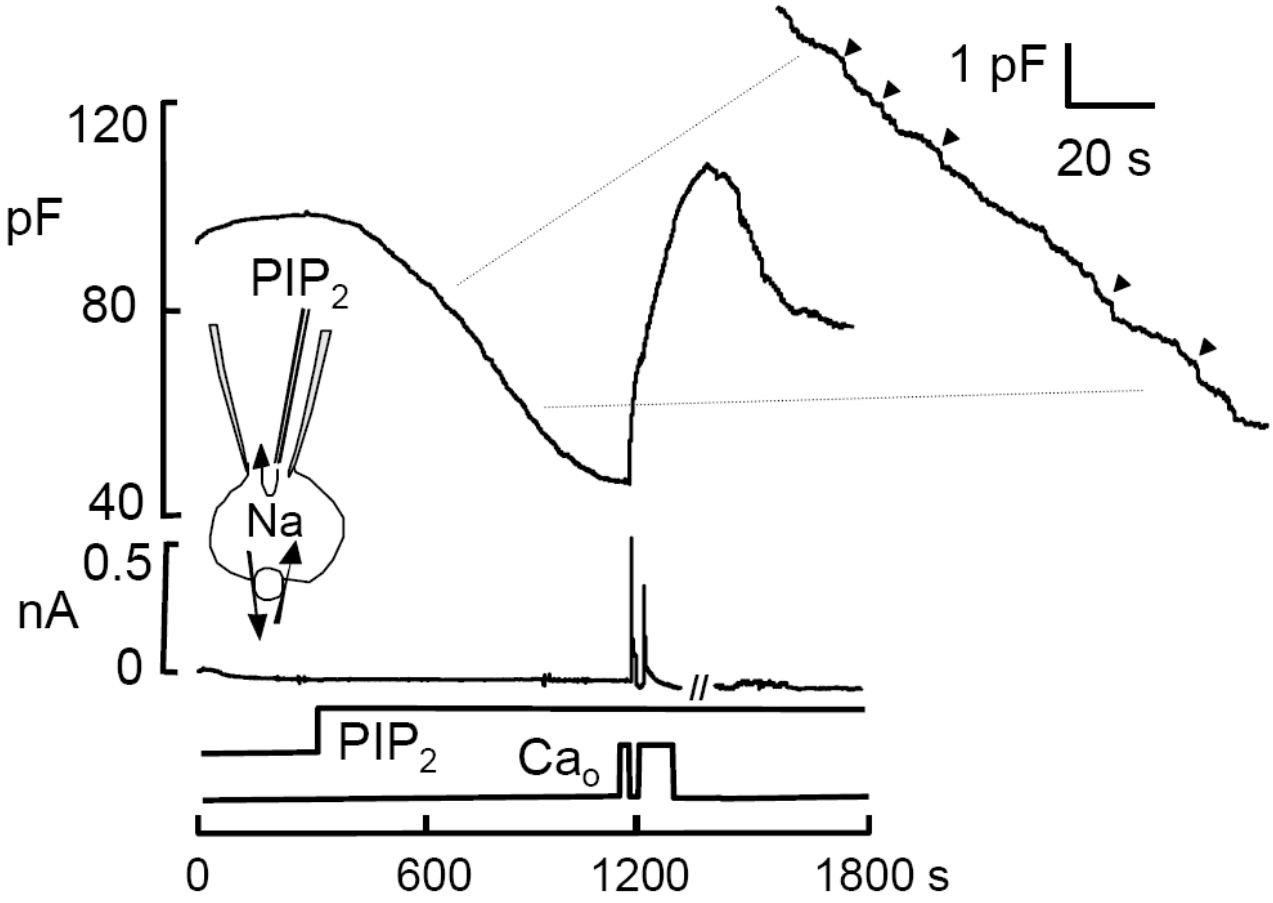

APPENDIX 2:

Massive Endocytosis Driven by Lipidic Forces Originating in the Outer Plasmalemmal Monolayer:

A New Approach to Membrane Recycling and Lipid Domains

by

Michael Fine, Marc C. Llaguno, Vincenzo Lariccia,
Mei-Jung Lin, Alp Yaradanakul, and Donald W. Hilgemann

Department of Physiology
University of Texas Southwestern Medical Center at Dallas
5323 Harry Hines Blvd.
Dallas, Texas 75390-9040 USA

Address correspondence to:

Donald W. Hilgemann
University of Texas Southwestern Medical Center at Dallas
5323 Harry Hines Blvd.
Dallas, Texas 75390-9040 USA

donald.hilgemann@utsouthwestern.edu
Tel. 214-645-6031
Fax. 214-645-6049

Running title: Amphipath-activated Massive Endocytosis.

Abbreviations. adenylyl imidodiphosphate, AMP-PNP; diaminobenzidine, DAB; dodecylglucoside, DDG; dodecylmaltoside, DDM; guanosine 5′-[γ-thio]triphosphate, GTPγS; hexamethyldisilazane, HMDS; hexyltriphenylphosphonium, C6TPP; horseradish peroxidase, HRP; lysophophatidylcholine, LPC; massive endocytosis, MEND; N-ethylmaleimide, NEM; tergitol, NP-40; phosphatidylinositiol-bis 4,5-phosphate, PIP_2; sodium dodecylsulfate, SDS; sphingomyelinase , SMase; tetradecyltrimethylammonium, TMA; Triton X-100, TX100; β-methylcyclodextrin, BMCD; hydroxypropyl-β-cyclodextrin, HPCD.

Abstract

The roles that lipids play in endocytosis are the subject of debate. Using electrical and imaging methods, we describe massive endocytosis (MEND) in BHK and HEK293 cells when the outer plasma membrane monolayer is perturbed by the nonionic detergents, Triton X-100 (TX100) and NP-40. Some alkane detergents, the amphipathic drugs, edelfosine and tamoxifen, and the phospholipase inhibitor, U73122, are also effective. Uptake of the membrane tracer, FM 4-64, into vesicles and loss of reversible FM 4-64 binding confirm that 40 to 75% of the cell surface is internalized. Ongoing MEND stops in 2 to 4 s when amphipaths are removed, and amphipaths are without effect from the cytoplasmic side. Thus, expansion of the outer monolayer is critical. As found for Ca-activated MEND, vesicles formed are less than 100 nm in diameter, membrane ruffles are lost, and β-cyclodextrin treatments are inhibitory. However, amphipath-activated MEND does not require Ca transients, ATP hydrolysis, G-protein cycling, dynamins, or actin cytoskeleton remodeling. With elevated cytoplasmic ATP (>5 mM) MEND can reverse completely and be repeated multiple times in BHK and HEK293 cells, but not cardiac myocytes. Reversal is blocked by N-ethylmaleimide (NEM) and a nitric oxide (NO) donor, nitroprusside. Constitutively expressed Na/Ca exchangers (NCX1) internalize roughly in proportion to surface membrane, while Na/K pump activities decrease over-proportionally. SDS and dodecylglucoside (DDG) do not cause MEND during their application, but MEND occurs rapidly when they are removed. As monitored capacitively, binding of these detergents decreases with MEND, whereas TX100 binding does not decrease. In summary, nonionic detergents can fractionate the plasma membrane *in vivo*, and vesicles formed connect immediately to physiological membrane trafficking mechanisms. We suggest that lateral and transbilayer inhomogeneities of the plasma membrane provide potential energies that, when unbridled by triggers, can drive endocytosis by lipidic forces.

Introduction

Numerous recent studies document the plasticity of endocytic processes in eukaryotic cells. Neurons, like yeast (Geli and Riezman, 1998), continue to carry out essential membrane cycling after disruption of classical players of 'scaffold-mediated' endocytosis. Beside clathrin deletion (Sato et al., 2009), deletion of adapter protein 2 (AP2) (Kim and Ryan, 2009) and multiple dynamins (Ferguson et al., 2007) follow a similar pattern. While it is possible that membrane internalization is then supported by non-classical

scaffolding proteins, an alternative explanation is that classical endocytic proteins function primarily to bring control and specificity to a core mechanism that continues to operate in their absence.

The existence, diversity and activity of clathrin-independent endocytic mechanisms in mammalian cells are abundantly documented (Doherty and McMahon, 2009; Donaldson et al., 2009; Ivanov, 2008; Mayor and Pagano, 2007). Multiple forms of clathrin-independent endocytosis depend on cholesterol and sphingomyelin's (Doherty and McMahon, 2009; Lajoie and Nabi, 2007; Mayor and Pagano, 2007; Romer et al., 2010; Sandvig et al., 2008). These dependencies may reflect at least in part the formation of domains in the outer monolayer by these membrane components (Lingwood and Simons, 2010; Rajendran and Simons, 2005). However, the mechanisms by which lipid domains, membrane proteins (e.g. integrins), and membrane-associated proteins interact to drive clathrin-independent endocytosis remain poorly established (Mayor and Pagano, 2007).

In this light, we have attempted over several years to develop new experimental models to study endocytic processes that do not rely on adapters. In a companion article (Lariccia, xxxx), we have described multiple forms of Ca-dependent endocytosis that seem to involve no classical endocytic protein. In a second companion article (Hilgemann and Fine, xxxx), these processes are demonstrated to rely on, and internalize, ordered membrane domains that do not bind well many electrogenic and fluorescent membrane probes. As an initial model of lipid-driven endocytosis in intact cells, we have demonstrated that generation of ceramide by bacterial sphingomyelinases (SMases) can drive more than one-half of the cell surface to internalize within seconds. While perhaps not a physiological mechanism, these experiments demonstrate a profound potential for lipidic forces, related to lipid domains, to drive endocytosis. Lipid domains, whenever they occur in membranes, will experience 'line-tension' to the surrounding membrane that tends to minimize their perimeters (Garcia-Saez et al., 2007; Vind-Kezunovic et al., 2008; Yanagisawa et al., 2007). Besides line tension, related to mismatch of lipid dimensions at a boundary, the shapes of phospholipids within domains, their tendency to tilt in a concerted manner, and asymmetries across monolayers will come into play in intact cells.

At the theoretical level, it is increasingly possible to simulate bilayer behaviors that are relevant to endocytosis. Relevant to the influence of detergents, small excess areas in a monolayer promote membrane 'buckling' that in turn causes coalescence of lipid domains with phase separations occurring between membrane 'caps' (Minami and Yamada, 2007; Yanagisawa et al., 2007). Further, it has been suggested from simulations that ordered membrane domains can develop chirality-dependent 'collective tilt', leading to spontaneous budding and fission of vesicles when domain diameters reach 50-100 nm (Sarasij et al., 2007). Even in clathrin-driven endocytosis, it has been suggested that phase separations of lipids may *drive* the final steps of fission (Liu et al., 2006). Clearly, there is now a great need to bridge insights from the theoretical, liposome, and cellular studies of domains in relation to endocytic processes in real cells.

Moving beyond biochemical membrane modifications, we describe in this study that common membrane perturbants, including multiple detergents and other amphipathic compounds (i.e. compounds with both hydrophilic and hydrophobic elements) , can drive massive endocytic processes that are even larger and faster than SMase-activated MEND. Modification of membrane structures and forces by low concentrations of detergents have been the subject of much careful biophysical analysis over several decades (Heerklotz, 2008). Besides affecting membrane tension, nonionic detergents, such as TX100, can cause domain formation in artificial membranes composed of complex phospholipid mixtures with detergent segregating to the fluid domains (Heerklotz et al., 2003). On the one hand, this outcome clearly shows that *lipid raft fractions* isolated in biochemical experiments can be generated artificially by the amphipaths used to isolate them. On the other hand, this outcome suggests that detergents can be used in much more subtle ways to probe complex biophysical behaviors of biological membranes. Most importantly with respect to this article, nonionic detergents can cause domain formation in complex giant lipid vesicles that is followed by budding and fission of small vesicles with a suggested involvement of line tension as a primary driving force (Hamada et al., 2007; Staneva et al., 2005).

Using cell capacitance (C_m) recording and optical methods to monitor changes of membrane area and conductance, we describe here the largest and fastest endocytic responses described in any cell type to date. These amphipath-activated MEND responses can reverse via ATP-dependent trafficking mechanisms that are inhibited by oxidizing

agents. However, their occurrence does not require nucleotides, Ca transients, an intact actin cytoskeleton, or the activity of dynamins. While triggered here by non-physiological perturbants, namely detergents, amphipath-activated MEND responses are strongly implicated to rely on preexisting membrane domains and asymmetries.

Methods

All methods and cell lines employed were as in a companion article, using the modified HEK293 cell line, T-REx-293 (Invitrogen, Carlsbad, CA), to express NCX1 (Lariccia, xxxx). NP-40 detergent was from CalBiochem. The fixable membrane tracer, FM 1-43FX, was from Invitrogen.

Solutions and Materials. Solutions employed minimized all currents other than NCX1 current. Free Mg of all cytoplasmic solutions was 0.4 mM. Standard Extracellular Solution contained in mM: 120 LiOH, 4 $MgCl_2$ or 2 $MgCl_2$ + 2 $CaCl_2$, 20 TEA-OH, 10 HEPES, 0.5 EGTA, pH 7.0 with aspartate. The Standard Cytoplasmic Solution contained in mM: 80 LiOH, 20 TEAOH, 15 HEPES, 40 NaOH, 0.5 $MgCl_2$, 0.5 EGTA, 0.25 $CaCl_2$, set to pH 7.0 with aspartate. Unless indicated otherwise, 0.2 mM GTP was employed in nucleotide containing solutions. Modified Cytoplasmic Solution contained in mM: 60 KOH, 50 NaOH, 15 TEAOH, 15 HEPES, 0.5 $MgCl_2$, 1.0 EGTA, 0.2 $CaCl_2$, set to pH 7.0 with aspartate. The LPC employed was isolated from bovine brain (SIGMA product #L1381) and is reported to contain predominantly palmitic, stearic and oleic acids.

Fluorescence Imaging of Fixed cells. Trypsinized HEK293 cells were allowed to attach to glass bottom dishes for 1 hour in growth medium. They were washed with extracellular solution, incubated with and without NP-40 (150 μM) in the presence of 10 μM FM 1-43FX for 1 minute, then washed again three times to remove excess dye, fixed with 2.5% glutaraldehyde in 0.1M cacodylate buffer for 20 minutes, and finally washed with buffer and treated with 50 mM glycine for 5 minutes to minimize background. Cells were imaged on an Olympus IX-90 microscope with a Coolsnap ES21 camera (Photometrics).

NP-40 experiments for SEM and TEM. Trypsinized HEK293 cells were allowed to attach on poly-L-lysine coated cover slips for 1 hour in growth medium. NP-40-treated and untreated groups were washed with extracellular solution prior to incubation with 10

mg/mL HRP with and without NP-40 (150 μM) for 1 minute. The cells were then washed and fixed with 2.5% glutaraldehyde in 0.1 M cacodylate buffer for 1 hour. After washing with 175 mM Tris-Cl buffer, the cells were incubated in 0.02% H_2O_2 and 0.1% diaminobenzidine (DAB) in buffer for 20 minutes. The cells were washed and placed in 1% OsO_4 for 30 minutes and washed with 0.1 M cacodylate buffer.

TEM. One set of cover slips for TEM imaging (control and NP-40 treated) was further placed in 2% uranyl acetate for 15 min. They were then dehydrated in an ascending ethanol series and infiltrated with Embed812. Cover slips were mounted on BEEM capsules and polymerized overnight at 60˚C. Separation of cover slips was done by plunging the capsules into liquid nitrogen. Thin (70 to 80 nm) sections were prepared using an Ultramicrotome Leica EM UC6 and mounted on 200 mesh copper grids. Sections were post-stained with 2% uranyl acetate for 15 minutes and lead citrate for 5 minutes. Cells were imaged in a FEI Tecnai G2 Spirit Biotwin TEM.

SEM. Samples for SEM were also dehydrated using ethanol followed by transition into pure hexamethyldisilazane (HMDS). Cells were air dried and immediately coated with a gold layer using a Cressington 108 sputter coater. Cover slips were mounted on Al stubs using conductive carbon tape and imaged with an FEI XL30 ESEM.

Online Supplemental Material. The following supporting data is provided *on-line*: Supporting Figs. S1 and S2 document that β-cyclodextrin treatments only partially block detergent-activated MEND, whereby BMCD treatment can itself cause large decreases of C_m from both membrane sides. Supporting Fig. S3 documents that benzyl alcohol, commonly employed as a 'membrane fluidizer', does not block, but rather promotes and accelerates TX100-activated MEND. Supporting Fig. S4 documents that dodecylmaltoside induces MEND by a pattern that is intermediate between TX100 and SDS. Supporting Fig. S5 documents that that C6TPP induces MEND by the SDS pattern, when employed in concentrations of 5 to 10 mM. Supporting Fig. S6 documents that amphipaths, which are effective MEND inducers in fibroblasts, are also effective in cardiac myocytes. Supporting Fig. S7 documents that MEND occurring on removal of SDS reverses quickly on reapplication of SDS. Finally, Supporting Fig. S8 documents that many detergents disrupt patch clamp experiments without inducing MEND.

Results

MEND induced by nonionic detergents. As outlined in the Introduction, low concentrations of nonionic detergents can cause phospholipid phase separations in complex artificial membranes (Heerklotz et al., 2003) that can in turn promote membrane vesiculation (Staneva et al., 2005). Figs. 1 and 2 present the effects of non-lytic concentrations of TX100 and NP-40 (<250 μM) in BHK cells. Fig. 1 shows the complete electrical parameters of a cell during extracellular application of TX100 (150 μM) for 15 s. C_m rises very briefly and then plummets by >50% with a maximal decline rate of 13% per second. Thus, the response is at least as large and fast as SMase-induced MEND described in a companion article (Lariccia, xxxx). The small rise of C_m that precedes the fall probably reflects expansion and thinning of the membrane by detergent insertion. Other cell electrical parameters are nearly unaffected by the detergent, and this was similar for the other amphipaths described subsequently.

The structurally related non-ionic detergent, NP-40, causes MEND responses that are indistinguishable from those of TX100 (>500 observations), and we have used these detergents interchangeably over the last 3 years. Fig. 2 describes MEND responses induced by these detergents in more detail. Fig. 2A shows averaged C_m data for four TX100 concentrations from which we determined, as indicated by gray lines, the average maximal rates of C_m decline in percent per second. The results are described in Fig. 2B by a power function ($k \cdot [TX100]^n$) with an exponent, n, of 3.8. Thus, detergents promote MEND precipitously at a critical concentration, which is less than the critical micelle concentration. Often, an adjustment of the detergent concentration by 10% caused or prevented MEND that involved >50% of the cell surface in a few seconds.

Responses to NP-40 are shown in Figs. 2C to 2E. The Standard Cytoplasmic Solution in Fig. 2C is without ATP or GTP. In Fig. 2D, it contains the non-hydrolysable ATP analogue, AMP-PNP (2 mM), with no ATP or GTP. Therewith, these results illustrate that detergent-activated MEND does not require nucleotide hydrolyzing enzymes. As illustrated in Fig. 2C, we attempted extensively to determine the size of vesicles formed during MEND via capacitance recording at high resolution, but C_m steps were not routinely observed. To optimize resolution of capacitance steps, we used relatively small cells at room temperature with sinusoidal voltage perturbation (Wang and Hilgemann, 2008). In brief, we occasionally observed clear steps of 15 to 50 fF, but this was not

routine. Fig. 2C shows an optimized record using 2 kHz sinusoidal voltage perturbation (R_a<2 MΩ). Five perturbation cycles were averaged per point displayed. There is a clear increase of RMS noise variance upon applying detergent, and noise variance decays in parallel with C_m. However, when exponential functions were subtracted from declining C_m signals, the residual signals still did not allow clear resolution of C_m steps to a resolution of about 10 fF (see inset). The ratio of signal variance to declining C_m was less than 0.2 fF, suggesting that vesicles are not more than 80 nm in diameter (1pF≈100μm^2) upon fission.

Figure 2D illustrates the rapidity with which C_m changes stop when detergent is removed from the extracellular solution. In this experiment, NP-40 was applied initially for 2 s and removed for 10 s; then, it was reapplied for 10s, removed for 60 s and reapplied for 10 s. As shown in the inset at higher resolution, the initial MEND response stops at an intermediate C_m level within about 2 s when detergent is removed. Since much longer times are required to clear the cytoplasm, especially when compounds bind to cellular components, this observation suggests that detergent is acting from the extracellular monolayer. Further support for this conclusion is presented subsequently. Upon reapplying detergent, a smaller and slower response is evoked. The fall of C_m continues briefly upon removal of detergent until C_m reaches 48% of its initial value. Thereafter, NP-40 causes rapidly reversible, small increases of C_m that probably reflect detergent binding/dissociation kinetics with no further endocytosis being possible. We point out additionally that the initial increase of C_m upon applying NP-40 is very similar before and after MEND. As described later in more detail, this suggests that binding of NP-40 is almost unaffected by MEND.

Figure 2E illustrates the lack of effect of detergent (NP-40, 140 μM) when perfused into the cytoplasm of cells, representative of 6 similar experiments. As shown further, the presence of cytoplasmic detergent does not block or change in a conspicuous way the subsequent C_m response to extracellular NP-40 (140 μM). Similar results were also obtained for other detergents, as described subsequently in this article and in an accompanying article (Hilgemann and Fine, xxxx). Even when perfused into cells at 5-times higher concentrations than needed to cause endocytosis from outside, cytoplasmic detergents were ineffective in inducing MEND or membrane shedding. Although some detergents cross the membrane rather rapidly (Heerklotz, 2008), we conclude that MEND

is caused specifically by detergent interaction with the extracellular leaflet of the plasma membrane.

To test whether nonionic detergents are causing endocytosis or membrane shedding, or both, we carried out experiments with the membrane tracer dye, FM 4-64, illustrated in Fig. 3. In these experiments we employed 2 mM ATP and 0.2 mM GTP in cytoplasmic solutions. The continuous fluorescence signal in Fig. 3A gives total cell fluorescence for an experiment in which dye was applied and washed off before application of TX100. The FM dye (5 μM) washes off multiple times by ~90% percent within seconds of its removal. With brief application of TX100 (120 μM), C_m falls by 66%. Thereafter, fluorescence labeling of the cell is reduced by 73% when dye is applied and removed in similar fashion. Thus, the decrease of plasmalemma area accessed by FM 4-64 is in good agreement the electrophysiological measurements. However, this result does not indicate whether membrane has been internalized or shed to the outside. To address directionality, the continuous fluorescence signal in Fig. 3B gives total cell fluorescence for an experiment in which dye was applied and washed off multiple times, but in which TX100 (120 μM) was applied during application of FM dye. In this case, dye cannot be washed off after inducing endocytosis. TX100-induced endocytosis amounts to 65% of the cell membrane by capacitance recording. The fraction of fluorescence that forms a ring close to the cell surface, and cannot be washed off, amounts to 70% of the initial total cell fluorescence. Thus, all of the membrane lost from the cell surface during application of TX100 can be accounted for by internalized membrane. This result indicates further that FM 4-64 binds roughly equally well to the membrane that internalizes and that which remains at the cell surface. As described in an accompanying article (Hilgemann and Fine, xxxx), this is the exception rather than the rule for fluorescent membrane probes.

As described in relation to Fig. 2, we verified repeatedly that nonionic detergents causes MEND in cells without cytoplasmic ATP, with AMP-PNP (e.g. Fig. 2D), and with high cytoplasmic Ca concentrations that can cause membrane blebbing. Next, therefore, we tested more rigorously whether MEND occurs without requirement for nucleotides or an intact membrane cytoskeleton. Fig. 4A shows an experiment in which the cytoplasmic solution contained AMP-PNP (2 mM), no ATP, no GTP, a high concentration of latrunculin (5 μM), and a high concentration of Ca (2 μM free Ca using 10 mM EGTA + 8.5 mM Ca) to promote disruption of cytoskeleton. As shown by the bright-field images,

the cell membrane became nearly smooth with this cytoplasmic solution and the cell appears swollen. As shown in the continuous fluorescence record, FM dye (6 μM) was applied and removed 3 times with good reversal of fluorescence each time. Then, dye was applied together with TX100, and the C_m response amounted to a loss of 75% of initial C_m. Thereafter, 85% of the FM fluorescence signal cannot be washed off and forms a bright rim at the cell periphery, similar to results described previously. Thus, disruption of membrane cytoskeleton, removal of nucleotides, and blockade of ATP-hydrolyzing mechanisms do not block, and may actually promote, MEND responses to nonionic detergents.

Further characteristics of MEND induced by TX100 (120 μM) are shown in Fig. 4B using bar graphs to present composite results. The average response to this concentration of TX100 was a 60% decrease of C_m. The MEND response to TX100 was not significantly affected by including GTPγS (0.2 mM) in the cytoplasmic solution to hinder G protein cycling. It was not affected by including latrunculin (5 μM) and AMP-PNP (2 mM) to disrupt actin cytoskeleton, block ATPase activities, and deplete PIP_2. And MEND responses were not affected by inhibiting dynamin activity with an unmyristylated dynamin-inhibitory peptide (DynPep, Tocris Bioscience, #1774; 50 μM) or the organic dynamin inhibitor, dynasore (0.2 mM). Finally, we point out that high extracellular Ca (2 to 6 mM) effectively blocks detergent-activated MEND, independent of Ca influx and cytoplasmic Ca changes, whereby the block can be overcome with higher detergent concentrations. The block probably reflects Ca binding by the outer membrane monolayer, which decreases the apparent affinity of the membrane for amphipaths. An example is given in Supporting Fig. 1 of a companion article (Hilgemann and Fine, xxxx). In addition, Supporting Data Figs. S1 and S2 illustrate that TX100-induced MEND is partially blocked by β-cyclodextrin treatments, but is not fully blocked by even extensive treatments that extract a large fraction of the total membrane. Supporting Data Fig. S3 illustrates that agents commonly used as 'membrane fluidizers', which can partially disrupt domain formation in some model membranes (Maula et al., 2009), do not disrupt TX100-induced MEND at non-disruptive concentrations and even promote TX100-induced MEND.

Structural basis of amphipath-induced MEND. To visualize the morphology of cells and vesicles formed during detergent-induced MEND, we carried out a scanning (SEM)

and a transmission electronmicroscopy analysis of HEK293 cells. Cells were removed from dishes, as in electrophysiology experiments, incubated for 3 min in Standard Extracellular Solution, incubated further with or without 150 μM NP-40 for 1 min, and then fixed as described in Methods. To verify that membrane internalization was occurring in this same protocol, cells were incubated with the *fixable* dye, FM 1-43FX (5 μM), for 3 min, incubated further with or without 150 μM NP-40 for 1 min with dye, and then fixed in dye-free solution. As shown in Fig. 5A, treatment with detergent generates a bright rim of fluorescence at the cell surface, corresponding to internalized surface membrane. Fig. 5B shows SEM micrographs of cells treated in this same way. As evident in the left panel, representative of >20 observations, extensive membrane ruffling is a hallmark of these cells when removed from dishes. As evident in the right panel, ruffles are lost and cells become nearly smooth upon treatment with detergent. To examine the ultrastructure of vesicles formed during MEND, we incubated cells with horseradish peroxidase (10 mg/mL HRP) during a 1 minute detergent treatment, as described in Methods and the accompanying article (Lariccia, xxxx). As shown in Fig. 5C, numerous stained vesicles with diverse morphologies were found in detergent-treated cells just under the outer surface of cells, whereby some showed a clearly multi-laminar structure. As shown in Fig. 5D for 26 control and 28 treated cells, NP-40 treatment increased the number of clearly stained vesicles by 2.5-fold.

Amphipath-activated MEND occurs in cells with 'physiological' morphology and connects to physiological membrane trafficking processes. Results presented thus far demonstrate that amphipath-activated MEND is extremely powerful in cells with extensive ruffle structures that have been removed from dishes by proteolysis. Thus, both proteolysis of the cell surface and ruffling might importantly promote the MEND process. Therefore, we performed both electrophysiological and optical experiments to test TX100 exposure induces MEND in BHK cells growing on cover slips. As described in Supporting Fig. S4, TX100 indeed induces MEND with similar characteristics to those reported above in cells growing on dishes without previous treatment with proteases. As documented in Fig. S4, MEND induced by 200 μM TX100 amounted to 41% of cell capacitance on average, could be repeated multiple times in the same cell, and resulted in equivalent losses of FM dye binding and FM dye uptake.

That detergent-activated MEND can be repeated with recovery of capacitance occurring over several minutes is similar to both Ca-activated and SMase-activated MEND (Lariccia, xxxx). Using detached cells, as described in Fig. 6A, we examined the reversal of MEND using several different cytoplasmic solution compositions and found that the Modified Standard Cytoplasmic Solution, employed in myocyte experiments (Lariccia, xxxx) was very effective to promote reversal of MEND when used with 8 mM ATP and 0.2 mM GTP. This solution contains 60 mM Na and 60 mM K, with no Li, and a higher EGTA concentration (1 mM) with lower free Ca (0.2 mM total Ca; 90 nM free Ca) than Standard Solution. As illustrated by Fig. 6A, it was routine to obtain complete plasmalemma recovery from MEND responses greater than 70%, and multiple cycles of MEND and recovery could be carried out in single experiments. Maximal recovery rates were in the range of 15% of internalized membrane per min. As shown in Fig. 6B, recovery was abolished when nonhydrolysable ATP analogue, AMP-PNP (2 mM), was employed instead of ATP (>10 observations). Fig. 6C illustrates that recovery was equally abolished by N-ethylmaleimide (NEM, 0.5 mM; 5 observations). We note that NEM was included in both extracellular and intracellular solutions, as it crosses membranes rapidly. Fig. 6D illustrates that recovery was slowed several fold (<4% versus 15% per minute) and was incomplete or negligible when a low concentration of the NO donor, nitroprusside (16 μM; four similar observations), was included in cytoplasmic solutions with standard nucleotides. Since cGMP (0.3 mM; dotted record, scaled to the nitroprusside record) had no effect (5 observations), NO is probably acting via oxidative stress. All of these results are consistent with a role for the oxidation-sensitive NSF factor (Lowenstein and Tsuda, 2006) in cycling membrane back into the plasmalemma in these experiments.

Figure 6E illustrates that vesicles that recycle in these experiments may become available for Ca-induced membrane fusion before they are reinserted into the cell surface during the recovery process illustrated in panel A. In this experiment, exocytosis was activated by a Ca transient before inducing MEND with TX100 (200 μM). The exocytic response amounts to 25% of C_m, and the MEND response amounts to 66% of C_m. Membrane area recovers partially within 4 min, as usual with 8 mM ATP. A Ca transient then results in complete recover of C_m. Afterward, there is not further increase of C_m, suggesting that the membrane that was being inserted slowly over many minutes may have been inserted within seconds during the Ca transient.

Figure 7A illustrates that C_m changes and NCX1 activity changes occur in parallel during repeated MEND responses. In these experiments, BHK cells were employed using Standard Cytoplasmic Solution with a high cytoplasmic EGTA concentration (20 mM with 5 mM Ca; 0.3 μM free Ca) to effectively buffer NCX1-mediated cytoplasmic Ca transients. NCX1 current was activated multiple times for 1 s, as indicated before and after application of NP-40 (150 μM). In response to three applications of NP-40, C_m decreases by 44, 38, and 25%, while peak NCX1 currents decrease by 36, 48, and 36% respectively. C_m recovers by 65% after the first two NP-40 exposures, while exchange currents recover by about 50%, suggesting that membrane recycling can bring internalized vesicles back to the cell surface. Exchange current magnitudes follow qualitatively the changes of membrane area, as if exchangers internalize and recycle with the plasmalemma. We note however that exchange currents did not recover as completely as C_m after a MEND response.

As described in Fig. 7B, we used HEK293 cells expressing NCX1-pHluorin fusion protein to quantify NCX1 internalization. Extracellular NCX1 fluorescence was determined by acidifying the medium to pH 6 and then switching to pH 8. With application of NP-40 (150 μM) for 10 s, the fluorescence that is rapidly induced by alkalinizing from pH 6 to 8 decreased by 37%, while C_m decreased by 48%. Similar to results for Ca-induced and SMase-induced MEND (Lariccia, xxxx) , there is an increase of fluorescence at pH 6.0. Thus, vesicles formed do not immediately acidify, as this would have resulted in a large decrease of fluorescence at all three pH values. In addition, it is important that the maximal fluorescence at pH 8 decreases by only 10%. This indicates that exchangers were not lost from the cell to the medium, as a result of membrane shedding. Rather, they must have been internalized to nearly the same extent as the plasmalemma.

Differential Na/K pump sensitivity to MEND in myocytes, BHK cells and HEK293 cells. In a companion paper (Hilgemann and Fine, xxxx), we present evidence that detergent-activated MEND internalizes preferentially liquid-ordered membrane domains with disordered membrane staying at the cell surface. Accordingly, protocols similar to those just described should allow studies of membrane protein trafficking with respect to membrane domains. Overall it should be possible in live cells to determine whether

individual channels or transporters prefer to reside in ordered domains, and it should be possible to determine factors that influence their residence in ordered versus disordered membrane. As an initial example, we present in Fig. 8 functional results for Na/K pump activities in mouse myocytes, BHK cells and HEK293 cells.

Figure 8A illustrates first that TX100 induces rapid MEND in murine myocytes of similar magnitude to results for BHK and HEK293 cells. Using murine and rat myocytes, application of 200 μM TX100 for 10 s causes a >40% drop of C_m (>20 observations). Second, the record illustrates, in stark contrast to results for BHK and HE293 cells, that C_m does not readily recover in myocytes. No exception to this pattern was obtained in >20 observations, indicating that membrane trafficking occurs very differently in myocytes and the other cells employed. Third, the record illustrates changes of Na/K pump activities in myocytes in response to TX100-induced MEND. Pump activity is activated by application of 6 mM KCl in exchange for 6 mM NaCl in these experiments. Transport activity is reflected in the outward current activated upon applying potassium, and a negative capacitive signal reflects charge movements related to ion binding at the extracellular surface of Na/K pumps (Holmgren et al., 2000; Lu et al., 1995). With the solutions employed this ouabain-sensitive signal is primarily caused by lithium binding to *E2* pump configurations. The signal decreases when pumps are activated by potassium and the average configuration of pumps shifts toward one with binding sites open to the /cytoplasmic side (i.e. the *E1* configuration).

As indicated in Fig. 8A, potassium was applied and removed 8 times during the myocyte record, twice before and 6 times after application of TX100. Current and capacitance records before and after TX100, demarcated by rectangles, are shown in the inset of the figure. The peak pump current is decreased by 62% while the capacitive pump signal is decreased by 55%. Thus, Na/K pumps are potentially internalized with some preference in this protocol (5 similar observations).

Figures 8B and 8C illustrate the equivalent experiments using HEK293 cells and BHK cells, whereby apparent differences were verified in >10 recordings from each cell type. As illustrated in Fig. 8B, pump currents in BHK cells decrease roughly in proportion to C_m, and currents recover as C_m recovers after MEND (6 similar observations). In the HEK293 cell, capacitance decreases by 45% while pump currents and capacitive pump

signals decrease by 74 and 71%, respectively. In a series of 11 experiments, pump currents in HEK293 cells decreased by 76 ± 3 % when C_m was reduced by 49 ± 5%. Thus, Na/K pumps seem to be preferentially internalized during TX100-activated MEND in HEK293 cells, as well as murine myocytes. Each cell type shows characteristic patterns of C_m and Na/K pump activity changes during these protocols, presumably indicative of different membrane trafficking patterns.

Characteristics of MEND induced by other detergents and amphipathic agents.

It does not seem to be established in the literature if detergents besides nonionic detergents cause phase separations and domain growth in liposomes. Thus, it seemed important to explore whether other detergents, and other amphipathic compounds, induce MEND and with what characteristics. The examples, presented in Figs. 9 and 11 and in Supporting Data Figs. S5-S7, document that MEND can be activated by many different amphipathic compounds in two fundamentally different patterns.

Figure 9A shows the response of a BHK cell to SDS (50 μM; >50 observations), and it is shown in Fig. 10C that dodecylglucoside (DDG) acts similarly. C_m was never observed to decrease during SDS application. Rather, the detergent causes a slow increase of C_m during its application, and C_m then falls precipitously within a few seconds after detergent is removed. Here, MEND amounts to 65% of C_m. As shown in Fig. 9B, SDS is without effect when applied by pipette perfusion to the cytoplasmic side, in this example at a concentration 5-times greater than needed to induce MEND from outside (i.e. 150 versus 50 μM). Since SDS is effectively membrane-impermeable, whereas nonionic detergents can translocate across membranes in seconds to minutes (Heerklotz, 2008), these experiments establish firmly that SDS is promoting MEND from the extracellular side. Presumably, it blocks the final fission of event until it is removed. Clearly, cytoplasmic SDS does not block membrane fusion or subsequent MEND responses induced by SDS (50 μM) from the extracellular side. Thus, detergent gradients across the bilayer play no evident role in MEND. In Supporting Fig. S8 it is documented that SDS not only blocks endocytosis during its application, it appears to promote recycling of membrane back into the cell surface, subsequent to a MEND.

Supporting Figs. S5 and S6 describe the MEND responses induced by dodecylmaltoside (DDM) and hexyltriphenylphosphonium (C6TPP). C6TPP acts like SDS, while the DDM

pattern is intermediate between that of nonionic detergents and SDS. We describe further in Supporting Fig. S9 that many detergents did not induce MEND when applied at concentrations just less than those causing disruption of experiments. These detergents included octylglucoside, octylsulfonate, deoxycholate, CHAPS, tauro-deoxycholate, glycodeoxycholate, β-escin, saponin, pluronic, and lipofectamine 2000. Overall, it can be summarized that detergents of low molecular weight, with alkyl chains less than 10 carbons long and/or with large head groups usually disrupted experiments before inducing MEND. The commonalities of detergents that cause MEND upon their removal appear to be relatively small hydrophilic (or ionic) head groups and /or short alkyl side chains. At least, in the triphenylphosphonium series a longer (C12) side chain versus a shorter (C6) side chain promotes immediate MEND. There is no evident correlation between MEND pattern and the relative abilities of detergents to cross the membrane.

Capacitive binding signals of detergents before and after MEND. As noted in the Introduction, TX100 segregates to fluid membrane domains in complex artificial membranes containing cholesterol, sphingomyelin and phosphatidylcholine (Heerklotz et al., 2003). Assuming that MEND depends on growth of domains, followed by internalization of ordered membrane domains (Hilgemann and Fine, xxxx), TX100 should segregate to domains that remain at the cell surface. How other detergents segregate is not known, except that different detergents can generate different detergent-resistant membranes with substantially different protein and lipid compositions (Lingwood and Simons, 2007). In our experiments, detergents that interact with both ordered and disordered membrane domains might dissociate faster from ordered domains than disordered domains. Upon wash-out, then, detergent remaining bound to disordered domains would transiently promote MEND, similar to TX100. Alternatively, such detergents might promote domain growth but hinder the final fission of ordered domains. Upon wash-out of detergent, expanded ordered domains would outlive the presence of detergent in the membrane, and fission would then proceed after detergents dissociate from both ordered and disordered domains.

To understand better how different detergents induce MEND, we have analyzed the capacitive signals that detergents generate upon binding to the cell surface. These signals, subsequently called capacitive binding signals, may reflect both an expansion and a thinning of the membrane as amphipaths intercalate into the outer cell monolayer.

Fig. 10 presents results for four detergents: TX100, two detergents that cause MEND on wash-off, namely SDS and dodecylglucoside (DDG), and deoxycholate, which does not cause MEND. In the experiment described in Fig. 10A, TX100 was applied and removed many times at a concentration (70 μM) that did not induce MEND. The capacitive response to applying and removing TX100 amounts to about 5 pF. After inducing a 60% MEND response with a higher TX100 concentration (200 μM), the lower concentration of TX100 was applied and removed again multiple times. The magnitude of the capacitive signal is unchanged (7 similar experiments and routine observations, as pointed out with Fig. 2D). To illustrate the insensitivity of signals to MEND, the rising phases of capacitive signals before and after MEND are shown in the inset of Fig. 10A. As shown in Fig. 10B, the equivalent capacitive binding signals for SDS (30 μM) behave very differently. After a 60% MEND response, the initial binding signal upon applying SDS is decreased by a nearly equivalent amount (5 similar observations). As shown in Fig. 10C, the equivalent experiment for DDG (60 μM) gives a very similar result. A 40% decrease of C_m during MEND is accompanied by a decrease of the DDG capacitive binding signal by more than 50% (3 similar observations). As shown in Fig. 10D, the equivalent experiment for deoxycholate (0.5 mM), which does not induce MEND, also shows a large decrease of the capacitive binding signal after TX100-induced MEND (6 similar observations). Thus, on the basis of capacitive binding signals SDS, DDG, and deoxycholate all bind effectively to the membrane that internalizes, while TX100 does not. In a companion article (Hilgemann and Fine, xxxx), we use this same approach to analyze membrane binding of dyes and show that capacitive binding data agree well with optical measurements of dye binding before and after MEND.

Common pharmacologically active hydrophobic agents are good MEND inducers. During these studies we employed a number of amphipathic reagents commonly used in cell biological experiments at rather high concentrations. Several were found to be powerful inducers of MEND. Fig. 11 describes results for four such compounds, each result being representative of at least 5 observations. The nonspecific phospholipase C inhibitor, U73122 (Horowitz et al., 2005) (5 μM) was the most effective (Fig. 11A), causing on average a 35% C_m decline in < 2 min (n=6), while the 'control compound' without phospholipase inhibitory action, U73343, was without effect (n=5). We note in this connection that the active compound probably accumulates in the outer monolayer because it is cysteine-reactive, while the control compound is not. We stress further that

U73122, like other amphipaths, had no MEND-promoting effect when employed in cytoplasmic solutions, as in Fig. 5B of a companion article (Lariccia, xxxx). Two anti-proliferative amphipaths, edelfosine and tamoxifen, were effective (Figs. 11B and 11C). Edelfosine, which is an alkyl-lyso-phospholipid (van Blitterswijk and Verheij, 2008) was more effective. The physiological amphipath, lyso-phosphatidylcholine (LPC; Fig.11D), was effective at 15 to 40 μM, concentrations that are within 2 fold of those that disrupted recordings. As illustrated for LPC, the MEND-promoting action of all of these amphipaths stopped rather abruptly upon wash-off of amphipath-containing solutions. In Supporting Fig. S7 we describe similar responses to U73122 in cardiac myocytes .

Discussion

Lipidic forces can drive endocytosis in intact cells. In a companion article (Lariccia, xxxx) it is demonstrated that bacterial SMases can cause rapid endocytic responses of very large magnitude when applied to the extracellular side of cells. The responses are likely related to the generation of ceramide-rich domains that develop negative curvature and vesiculate spontaneously into the cytoplasm. Nonionic detergents now provide a second means to induce similar, or even larger MEND responses, but without biochemical modification of the membrane. The growth of ordered membrane domains in response to low concentrations of TX100 was previously characterized in complex artificial membranes (Heerklotz et al., 2003), and the potential of domain growth, induced by detergents, to cause membrane vesiculation was also established in giant liposomes (Hamada et al., 2007; Staneva et al., 2005).

In spite of these precedents, our analysis of detergent actions in intact cells has generated multiple surprises: The magnitudes and speeds of detergent-induced vesiculation were unexpected, the clear directionality of detergent-induced vesiculation was unexpected, and it was unexpected that vesicles formed would quickly couple to cellular processes that recycle them back into the cell surface. All of these results suggest that detergent-activated MEND can be related to endocytic processes occurring physiologically, and that amphipath-induced MEND can be extensively exploited to study physiological membrane recycling mechanisms.

That the asymmetry of the plasmalemma plays a critical role in detergent-activated MEND is evident from the fact that detergents are inert from the cytoplasmic side of the

plasmalemma (Figs. 2E and 9B). A primary role for the outer monolayer is also suggested by the rapidity with which MEND activates and deactivates upon applying and removing detergents (Fig. 2D). The fact that membrane internalization occurs with no disruption of membrane integrity (Figs. 1, 3 and 4) fulfills an important prerequisite for detergent-activated MEND to be related to a physiological endocytic processes. Perhaps most importantly, we find that capacitive signals related to TX100 and NP-40 binding are unaffected by the MEND responses caused by their presence in the membrane (Fig 2D and Fig. 10A). This result establishes unambiguously that lipid domains are critically involved in detergent-induced MEND. Further, this result explains why vesicles formed during detergent-activated MEND can be recycled by physiological trafficking mechanisms. The vesicles formed are unlikely to contain large amounts of detergent and are likely to be similar to physiologically-formed endocytic vesicles in these cells.

Given the fundamental roles that detergents have played in biological studies, it is surprising that large endocytic responses were not described previously. In fact, TX100 is presently used to reversibly open cells for delivery of impermeable reagents such as contrast agents (van de Ven et al., 2009). It is assumed in those studies that TX100 allows reagents free access to the cytoplasm. Given that the lowest possible detergent concentrations are employed to allow reagent entry, it seems likely from the present study that MEND plays at least a significant role. Clearly, TX100 allows HRP to label vesicles and vacuoles without HRP reaching the cytoplasm (Fig. 5), and our electrical measurements indicate clearly that this happens without development of membrane leaks. We suspect that detergent-activated MEND went unnoticed up to now because nonionic detergents indeed cross membranes rapidly and exert diverse nonspecific intracellular effects, unless they are removed very quickly as occurs in our experiments. We note that standard protease treatments, as used here to remove cells from dishes, are known to promote more efficacious transfections of cells by cationic detergents (Matheny et al., 2004). By contrast, TX100 induces MEND very effectively in cells that are not protease-treated (Fig. S4), and standard transfection reagents do not induce MEND (Fig. S9).

While the membrane itself clearly plays a central role in MEND, we cannot rule out roles for membrane proteins that may segregate with some specificity into membrane domains. With certainty, Ca transients play no immediate role in detergent-activated MEND, since high cytoplasmic concentrations of EGTA (20 mM in Fig. 7A) have no influence on

MEND responses. Nor do ATP-, GTP-, actin-, or dynamin-dependent processes play a role (Fig. 4B). From a biophysical viewpoint, the major question raised is how in detail formation (or growth) of membrane domains causes vectorial budding of membrane to the cytoplasmic side in cells. From a biological viewpoint, the major question raised is how, and if, these MEND responses are related to endocytic mechanisms taking place in cells. From a biochemical viewpoint, a major question raised is how amphipath-activated MEND is related to the generation of detergent-insoluble membrane fractions using 20 to 100 times higher concentrations of nonionic detergents.

The mechanism of amphipath-induced MEND. A tentative mechanistic model of amphipath-activated MEND is presented in Fig. 12. Previous studies show that TX100 at concentrations employed in this study (100 to 200 μM) incorporate into phospholipid membranes at mole fractions in the range of 0.1 to as high as 0.5 (Kragh-Hansen et al., 1998). SDS at the concentrations employed in Results (30 to 60 μM) can reach 0.2 mole per mole in cell membranes (Kragh-Hansen et al., 1998). Therefore, we speculated for some time that detergent incorporation might extract individual lipids from the outer monolayer without causing permeability changes. In this way, outer monolayer area would be decreased and generate negative curvature and fission to the cytoplasmic side. However, we have found no support for this idea in the literature. Furthermore, this hypothesis cannot explain why detergents are inert from the cytoplasmic side (i.e. fail to cause shedding), why detergent responses can be repeated many times in the same cell (Figs. 6A and 7A), or why some detergents are effective only after they are washed off (Fig. 9, Fig. 10C, and Supporting Data Figs. S5 and S8). Given these results, together, we conclude that detergents are acting to expand and reorganize the outer plasmalemma monolayer in a way that promotes its internalization. In a companion article (Hilgemann and Fine, xxxx) we provide multiple lines of evidence that, with respect to the outer monolayer, it is primarily *Ld*-membrane domains that expand and *Lo*-membrane domains that are internalized.

As discussed in more detail in the companion article (Hilgemann and Fine, xxxx), it is likely that *Lo* domains of intact cells are normally small, probably less than 5 nm on average (Lingwood and Simons, 2010). Accordingly, amphipaths must in some way cause ordered domains to coalesce before budding can proceed. As described for artificial membranes, one important factor is that detergents, certainly non-ionic detergents, are

cholesterol-phobic (Heerklotz, 2008) and promote a segregation of cholesterol into *Lo* domains. Some detergents may mimic the ordering function of cholesterol, thereby generating unnatural ordered domains of large diameter, which would explain why β-cyclodextrins do not fully block detergent-activated MEND (see Supporting Figs. S1 and S2). One possible progression (see Fig. 12) is that binding of detergents in more fluid membrane regions causes those regions to expand, coalesce, and form 'caps' that in turn cause *Lo* domains to coalesce into valleys or troughs (Minami and Yamada, 2007). Presumably, the asymmetry of plasma membrane monolayers plays a key role in determining that vesiculation takes place to the cytoplasmic side. In the simplest case, ordered domains of the outer monolayer will develop negative curvature when they reach an appropriate size as a result of physical-chemical interactions that promote their collective tilt (Sarasij et al., 2007).

As noted in Results, it is not clearly established whether detergents besides nonionic detergents cause phase transitions in complex liposomes at low concentrations. DDG and SDS are active at lower concentrations than TX100, and they cause MEND only after they are removed from the outside of cells (Figs. 9 and 10C). In clear contrast to TX100, DDG and SDS binding is decreased after MEND (Figs. 10B and 10C). Thus, they appear to interact with the membrane that internalizes in MEND. Since however MEND occurs only after their washout, the vesicles formed may be largely free of detergent, as expected for vesicles induced by TX100 exposure. As noted further in Results, it is unclear at this time whether membrane domains might coalesce during detergent application or in association with washout, or both. Independent of the details, these observations suggest that it may be possible to develop endocytosis inhibitors that act at the outside monolayer by inhibiting the final steps of fission.

To explain that MEND is activated by detergent in a few seconds, and that ongoing MEND stops in a few seconds (Figs. 2D), it must be assumed that the domains generated by the presence of detergents have life-times of one to a few seconds. This is consistent with domain life-times of 13 s, determined for 0.2-2 micrometer *Lo* domains identified in arterial smooth muscle using 1,2-dimyristoyl-sn-glycero-3-phosphoethanolamine with single-molecule tracking (Schutz et al., 2000). From the perspective of the present work, such large domains would occur only rarely in the surface membrane and represent only a small fraction of total *'Lo'* membrane. We point out further that this life-time is nearly

three log units longer than life-times predicted for nm-scale lipid domains (Subczynski and Kusumi, 2003).

Potential utility of amphipath-activated MEND for membrane trafficking studies. The fact that detergent-activated MEND is reversible opens many new possibilities to study basic mechanisms of membrane recycling. Since the reversal of MEND requires ATP and is sensitively inhibited by NEM and the oxidative influence of nitric oxide donors (Fig. 6), it is likely that 'NSF' plays a key role (Lowenstein and Tsuda, 2006). It appears likely also that the vesicles that recycle can be reinserted by the Ca-dependent fusion mechanisms present in BHK cells (Fig. 6E), and it will be of great interest to determine if vesicles pass through endosomes in the time course of our experiments. A few possibilities to exploit detergent-activated MEND in membrane protein trafficking studies, especially when combined with patch clamp, are hinted at by results obtained for Na/Ca exchange and Na/K pump function in relation to MEND (Figs. 7 and 8). Na/Ca exchangers are internalized roughly in parallel with the fraction of plasmalemma that internalizes. It is therewith a question whether exchangers have no preference for residence in ordered or disordered membrane, or whether this apparent disregard for order can be altered by regulatory influences. In the case of Na/K pumps, there appears to be a preference for residence in and/or internalization within ordered membrane domains (Fig. 8). While domains are rapidly recycled in the proliferative BHK and HEK293 cells, we see effectively no recycling of membrane internalized in detergent-activated MEND in myocytes. Interestingly, this observation contrasts to Ca-activated MEND in myocytes; membrane can be rapidly reinserted into the sarcolemma after Ca-activated MEND (Lariccia, xxxx). All of these observations suggest that detergent-activated MEND provides new experimental handles on multiple membrane trafficking processes in experiments employing intact cells. Caveats encountered in the biochemical fractionation of membranes to analyze lipid raft compositions are well known (Lingwood and Simons, 2007). As a method to probe membrane organization, amphipath-activated MEND may have advantages because the concentrations of detergents employed are less than critical micelle concentrations and because cells remain intact .

Finally, we have described in this article that multiple amphipathic compounds, often employed at rather high concentrations in cell biological experiments, effectively induce MEND with similar characteristics to detergent-induced MEND (Fig. 11). Edelfosine is a

proapoptotic lipid that has been used in cancer therapy (van der Luit et al., 2007), and we stress that nonionic detergents such as TX100 also initiate apoptosis (Sawai and Domae, 2009). The concentrations of these agents that effectively induce apoptosis (Sawai and Domae, 2009; van der Luit et al., 2007) are similar to those used here to cause MEND.

In conclusion, perturbation of the outer monolayer of cells by common detergents can cause very large and rapid endocytic responses that appear to be related to '*lipid raft-dependent*' endocytic mechanisms occurring physiologically. These responses do not require nucleotide hydrolysis, dynamins, other G proteins, or a functional membrane cytoskeleton. Only the outer monolayer responds to detergents by initiating MEND. Thus, it appears that outer monolayer phospholipids and cholesterol can develop lateral inhomogeneities (i.e. lipid domains) that preferentially and effectively vesiculate plasma membrane to the cytoplasmic side. Detergents induce MEND without being internalized, so that the composition of vesicles may be nearly physiological. In a companion article (Hilgemann and Fine, xxxx), multiple lines of evidence are presented that detergents are causing the internalization of ordered membrane domains and that Ca-activated MEND promotes internalization of the same membrane subset.

Acknowledgements. This work was supported by RO1-HL067942 and HL513223 to DWH.

Figure Legends

Figure 1. Activation of MEND in a BHK cell by extracellular application of TX100 (120 μM) for 10 s. Membrane area, i.e. C_m, decreases at a maximal rate of 13% per s, and the endocytic response stops abruptly upon removal of detergent. During MEND, there is a barely detectable, transient increase of cell conductance (G_m). Other cell electrical parameters do not change.

Figure 2. Salient characteristics of TX100 and NP-40-induced MEND. In panels A and B, the pipette solution contained 2 mM ATP and 0.2 mM GTP. Panel C is without nucleotides, panel D is with AMP-PNP (2 mM) and no other nucleotides, and panel E is with 2 mM ATP and 0.2 mM GTP. **(A)** Average MEND responses of BHK cells upon application of four different concentrations of TX100 (n=5-7). **(B)** Concentration dependence of the maximal rate of change of C_m by applying TX100 in Fig. 2A. The

response rate increases with roughly the 4th power of the concentration, given by solid line. **(C)** MEND in a small BHK cell at 22º C. Variance of RMS noise of C_m increases immediately upon application of NP-40 and decreases during the decline of C_m. The inset shows the residual signal after subtracting an exponential function from the declining C_m signal. **(D)** MEND induced by NP-40 (120 μM). On application of NP-40, MEND is preceded by a rapid rise of cell C_m, and MEND stops within 2 to 3 s upon removing detergent. After a second MEND response, detergent causes small increases of C_m that reverse almost as quickly as solutions can be changed. **(E)** Rapid pipette perfusion of NP-40 (150 μM) into a BHK cell by pipette perfusion. As in 4 additional experiments, NP-40 has no effect from the cytoplasmic side, nor does intracellular detergent have any evident influence on the MEND response to extracellular detergent.

Figure 3. Characterization of TX-100-induced MEND using simultaneous optical and electrical recordings in BHK cells. The pipette solutions contain 2 mM ATP and 0.2 mM GTP. **(A)** FM 4-64 (5 μM) was applied and removed twice, then TX100 (120 μM) was applied for 30 s, inducing a 66% MEND response, and FM dye was applied and removed twice more. Membrane binding of FM dye decreases 73% after MEND. **(B)** FM 4-64 (5 μM) was applied once and washed. During the second application, TX100 (120 μM) was applied for 30 s, inducing a 65% MEND response, and after MEND, FM dye was applied and removed three more times. FM fluorescence remaining in the cell does not wash off and amounts to 70% of pre-MEND fluorescence corresponding roughly to the amount of membrane internalized as per capacitive measurements.

Figure 4. TX100-induced MEND does not depend on canonical endocytic proteins. **(A)** TX-100-induced MEND after extensive disruption of cytoskeleton, phosphoinositides, and ATP-dependent processes (5 μM latrunculin with 2 μM Ca, no ATP or GTP, and 2 mM AMP-PNP). FM 4-64 was applied three times before MEND. During the fourth application, TX100 (120 μM) is applied, causing a 77% MEND response. Thereafter 85% of FM dye fluorescence is retained, and FM dye is reapplied twice. The reversible FM fluorescence amounts to 15 % of pre-MEND fluorescence. **(B)** Further characteristics of MEND induced by 120 μM. As indicated by the open bar graphs, TX100-induced MEND was not inhibited when the cytoplasmic solution contained GTPγS (0.2 mM), latrunculin (5 μM) with AMP-PNP (2 mM), an unmyristylated dynamin-inhibitory peptide (DynPep, Tocris Bioscience, #1774; 50 μM) or the organic dynamin inhibitor, dynasore (0.2 mM).

Figure 5. Analysis of NP-40 responses of HEK293 cells by scanning and transmission elecronmicroscopy (SEM and TEM). **(A)** Demonstration of NP-40-induced MEND in a cell population. Cells were incubated with FM 1-43FX during NP-40 application for 30 s and then washed and fixed as described in Methods without FM dye. A bright rim of fluorescence is generated in cells treated with detergent, thereby verifying the operation of MEND in this protocol. **(B)** Scanning electron micrographs of HEK293 cells before (left) and after (right) treatment with NP-40. Control cells show an extensive mesh of membrane ruffles, while NP-40 cells appear nearly smooth in comparison; scale bar, 10 μm. **(C)** TEM image of an NP-40 treated HEK293 cell. Detergent-treated cells show large DAB-stained vacuoles (> 20 observations); scale bar, 5 μm. Stained vesicles are indicated with arrows. (**D)** DAB-stained vacuoles are significantly increased in HEK293 cells after treatment with NP-40 for 60 s; $n \geq 26$, $p<0.001$.

Figure 6. Reversal of TX-100-induced MEND in BHK cells. **(A)** TX-100-induced MEND reverses completely when the cytoplasmic solution contains 8 mM ATP, 0.2 mM GTP, no lithium, and a low free cytoplasmic Ca concentration (1 mM EGTA with 0.2 mM total Ca; free Ca calculated to be 0.15 μM; >20 observations). In this recording, MEND is induced with 200 μM TX100, and it reverses with a progressively longer half-time of 5 to 16 min over 5 repetitions. **(B)** MEND does not recover in the absence of ATP and the presence of a non-hydrolysable ATP analogue (AMP-PNP, 2 mM). **(C)** MEND recovery is completely blocked by NEM (0.5 mM), added to both extracellular and cytoplasmic solutions (5 similar observations). **(D)** MEND recovery is strongly inhibited by cytoplasmic application of the NO donor, nitroprusside (16 μM; 4 similar observations) while it is unaffected by cGMP (0.3 mM; 5 similar observations). **(E)** When MEND recovery has progressed partially for 3 minutes, a Ca transient can induce complete recovery of membrane area in seconds. In this experiment, a Ca transient was evoked before MEND to determine the immediately available membrane pool for exocytosis. Thereafter, MEND amounts to a loss of 66% of the cell surface, and after 3 min a Ca transient causes exocytosis of a 3-times greater amount of membrane than was initially available.

Figure 7. Functional and optical analysis of the influence of MEND on NCX1. **(A)** MEND responses and NCX1 currents in a BHK cell perfused with a high (20 mM) EGTA concentration to negate Ca transients and high ATP (8 mM) to promote MEND reversal. MEND reverses for the most part within 2 minutes. We note that this experiment was

performed with Standard Solutions, not Modified Standard Solutions that promote recovery. NCX1 current is decreased after each MEND response and recovers partially during recovery of C_m. **(B)** Time lapse confocal imaging of an HEK293 cell stably expressing NCX1-pHluorin fusion protein before and after exposing the cell to NP-40 (150 μM) for 10 s. Fluorescence arising from NCX1 at the cell surface is determined as the fluorescence activated by jumping extracellular pH from 6.0 to 8.0 MEND induced by NP-40 causes a C_m drop of 48%, while the fluorescence intensity of cell surface NCX1 (i.e. fluorescence jump on changing solutions from pH 6 to pH 8) decreases by 37%. The presence of fluorescence at pH 6 after MEND indicates that NCX1 has entered an internal compartment that does not immediately acidify.

Figure 8. Comparison of TX100-induced MEND and its influence on Na/K pump activity in a murine myocyte, a BHK cell, and an HEK293 cell. All results employ Modified Cytoplasmic Solution (Lariccia, xxxx) with 8 mM ATP and 0.2 mM GTP, and MEND is induced with 200 μM TX100. Pump currents are activated by applying and removing 6 mM KCl in exchange for 6 mM NaCl. Pump activation is evaluated both as pump current and as a capacitive signal that reflects of a decrease of extracellular cation binding during pump activity. **(A)** Murine myocyte. TX100 induces a 42% MEND response (>10 observations), while pump signals are decreased by 62%, neither membrane area nor pump activity recovers over a 7 min observation period. **(B)** BHK cell. MEND amounts to 70% of membrane area, pump activity decreases by the same percentage, and both membrane area and pump activity recover over 8 minutes (4 observations). **(C)** HEK293 cell. Na/K pump activity decreases over-proportionally to the loss of membrane area associated with MEND, and pump activity does not recover during the recovery of membrane area over 8 min (10 observations).

Figure 9. MEND responses induced by application and removal of SDS. Cytosolic solutions contain 2 mM ATP and 0.2 mM GTP. **(A)** SDS (50 μM) causes within a few seconds a small increase of C_m, and then C_m continues to rise nearly linear. MEND occurs within seconds upon SDS removal. **(B)** Rapid pipette perfusion of SDS (150 μM) into a BHK cell with 2 mM ATP is without effect on C_m. Thereafter, membrane fusion occurs normally upon activation of Ca influx by NCX1. Finally, the application and removal of extracellular SDS (50 μM) cause a 50% MEND response over 20 s after SDS is removed.

Figure 10. Capacitive binding signals of detergents before and after MEND. Standard Cytoplasmic Solutions with 2 mM ATP and 0.2 mM GTP in the cytoplasmic solution. In each panel the rising phases of capacitive binding signals, indicated by closed circles in the complete C_m records, are shown in the inset at higher resolution. **(A)** TX100 capacitive binding signals are unchanged by MEND causing a 60% loss of plasma membrane. As indicated below the Cm record, a low concentration of TX100 (70 μM) was applied and removed multiple times, each application giving rise to an approximately 5 pF increase of C_m that reverses with a time constant of 2 to 3 s. MEND was induced by applying 200 μM TX100 for 25 s, and thereafter the capacitive binding signals for the low TX100 concentration are unchanged (5 similar observations). **(B)** Capacitive binding signals for SDS (30 μM) are markedly decreased by SDS-induced MEND. Since SDS does not cause MEND during its application, the capacitive binding signal can be evaluated with the same detergent application that induces MEND. The capacitive binding signals decrease by a fractional amount that is similar to the fractional loss of membrane. **(C)** Capacitive binding signals for DDG (30 μM) are markedly decreased by DDG-induced MEND. **(D)** Capacitive binding signals for deoxycholate (500 μM) are markedly decreased by TX100-induced MEND.

Figure 11. Activation of MEND by diverse amphipaths in BHK cells. Cytoplasmic solutions contain 2 mM ATP and 0.2 mM GTP. **(A)** U73122 (5 μM), but not the inactive 'control' analogue, U73343, induces MEND within 30 s. **(B)** Edelfosine (20 μM) induces MEND. **(C)** Tamoxifen (40 μM) induces MEND. **(D)** LPC (20 μM) induces MEND. Similar to detergent-induced MEND, LPC-induced MEND stops abruptly upon removal of LPC.

Figure 12. Endocytosis driven by lipidic forces: An hypothesis. (1) The outer monolayer consists of *Lo*- and *Ld*- domains of small size and equal prevalence. Lipids diffuse rapidly between domains with affinity differences for *Lo* versus *Ld* domains being less than one log unit. 'Lipid shells' around membrane proteins (Anderson and Jacobson, 2002) need not be synonymous with *Lo* and *Ld* domains. (2) Nonionic amphipaths expand *Ld* domains, promote cap formation with buckling of the plasmalemma, associated with domain coalescence and protein sorting. Ca transients may trigger the generation of endocytosis-promoting lipids and their movement into the outer monolayer (Hilgemann and Fine, xxxx; Lariccia, xxxx). (3) Membrane internalization: Coalescence of *Lo* domains within expanded *Ld* domains promotes negative curvature, vesiculation

and fission without adapters or dynamins, similar to the generation of ceramide domains via SMases (Lariccia, xxxx). Nonionic amphipaths remain in *Ld* domains at the cell surface. (4) MEND generates vesicles that follow normal trafficking pathways to endosomes with recycling back to the plasmalemma via ATP-dependent processes that are inhibited by NEM and oxidative stress.

Supplemental Material.

Supporting Data Figures S1 and S2 document that cyclodextrin treatments only partially block detergent-activated MEND, whereby BMCD treatment can cause large decreases of Cm from both membrane sides. Fig. S3 documents that benzyl alcohol, commonly employed as a 'membrane fluidizer', does not block, but rather promotes and accelerates TX100-activated MEND. Fig. S4 documents that dodecylmaltoside induces MEND by a pattern that is intermediate between TX100 and SDS. Fig. S5 documents that that C6TPP induces MEND by the SDS pattern, when employed in concentrations of 5 to 10 mM. Fig. S6 documents that amphipaths, which are effective MEND inducers in fibroblasts, are also effective in cardiac myocytes. Fig. S7 documents that MEND occurring on removal of SDS reverses quickly on reapplication of SDS. Finally, Fig. S8 documents that many detergents disrupt patch clamp experiments without inducing MEND.

Figure S1. Summary of experiments testing for effects of cyclodextrins on detergent-activated MEND. **(A)** BMCD treatment during patch clamp. After 7 min exposure to 10 mM BMCD, 120 uM TX100 causes transient increases of conductance and Cm with no MEND response. **(B)** HPCD treatment during patch clamp. After 7 min exposure to 20 mM HPCD, 120 uM TX100 causes transient increases of conductance and Cm with no MEND response. **(C)** In contrast to treatments during patch clamp, pretreatment of cells with cyclodextrins did not effectively block MEND. In this example, cells were preincubated with BMCD (10 mM) for 2 h. Thereafter, multiple detergents, including TX100 and SDS, still caused substantial MEND responses. In this example, MEND is induced by application and removal of DDM (50 uM). As described in Fig. S4, DDM induced MEND by a pattern that is intermediate between TX100 and SDS (i.e. partially during its application and partially upon its removal).

Figure S2. BMCD is effective from the cytoplasmic side to reduce membrane area. Standard Solutions. The cytoplasmic solution contains 2 mM ATP and 0.2 mM GTP. After Cm is reduced by more than 50% with BMCD on both membrane sides, TX100

(150 uM) is still effective to cause a further decrease of Cm when applied for a prolonged period of about 1 min. Thus, TX100 may be able to mimic cholesterol in supporting MEND when cholesterol has been largely extracted.

Figure S3. The membrane fluidizer, Benz-OH (0.5%), promotes TX-100-induced MEND. **(A)** Representative TX100-induced MEND records without and with 0.5% Benz-OH. MEND was induced with 140 uM TX100 in 5 cells without Benz-OH and in 5 cells with 0.5% Benz-OH, as indicated. TX100 was applied twice in all records, and the time required to achieve 50% of the maximal MEND response was determined, as indicated by rectangles. **(B)** Maximal MEND responses (left panel) and times to half- maximal MEND (right panel) for control and Benz-OH-treated cells. The half time is decreased by 68% in Benz-OH-treated cells.

Figure S4. Detergent Induced MEND on attached cells: BHK-NCX cells grown to >90% confluence on MarTek glass bottom dishes. Cell medium was removed and replaced with standard lithium based extracellular solution. No protease treatment was applied and cells were used within 1 hr of removal from incubator to prevent degradation of extracellular matrix and keep cells firmly attached to bottom of dish.

(A) Electrical Recording of MEND in Attached Cells. Typical whole cell recording of firmly attached cells using standard solutions. 2 mM Ca replaced 2 mM Mg to isolate NCX activity and 200 μM TX100 was applied to induce MEND. Inset shows statistical values for 5 experiments indicating a near 50% loss of membrane capacitance for attached cells. **(B)** Membrane binding of FM dye is reduced after MEND in attached cells. As in A) cell culture medium was replaced with standard lithium based solutions. Confocal imaging used a 20 x lens and 543 nm excitation with filters set to record wavelengths above 640 nm. A solution switcher was moved to just outside the full frame recording area. Cells were bathed in standard solution followed by application of 5 μM FM 5-95. Dye was applied until fluorescence peak reached a plateau and washed. 200 μM TX100 was applied for 30 seconds to induce MEND. After a 30 seconds recovery, FM dye was reapplied and allowed to plateau. The maximal binding of FM was reduced by 30% after TX100 treatment. Results were similar for 4 records. Scale bar is 350 μm.

(C) FM dye is internalized during MEND in attached cells. Protocol was as in B) with FM dye being applied and then washed to determine maximal and minimal fluorescence. FM dye was reapplied with 200 μM TX100 then washed to determine residual or

internalized fluorescence. Residual fluorescence increases >30%. I) Baseline Fluorescence with no treatment. II) First FM dye treatment. III) First wash pre-MEND IV) FM dye with TX100. V) Post- MEND wash.

Figure S5. MEND induced by dodecylmaltoside (50 uM) occurs partially during application of detergent and partially after its removal. BHK cell with the Standard Solutions. The cytoplasmic solution contains 2 mM ATP and 0.2 mM GTP.

Figure S6. C6TPP at high concentrations (10 mM) induces MEND by the SDS pattern: MEND occurs exclusively after removal of C6TPP. BHK cell with the Standard Solutions. The cytoplasmic solution contains 2 mM ATP and 0.2 mM GTP.

Figure S7. MEND induced by NP-40 (120 uM) and U73122 (20 uM) in rat myocytes. Modified Cytoplasmic Solution and Standard Extracellular Solution. The cytoplasmic solution contains 8 mM ATP and 0.2 mM GTP.

Figure S8. Reversal of SDS-activated MEND is stimulated by SDS. Standard Solutions with 5 mM ATP and 0.2 mM GTP. **(A)** MEND is first induced by application and removal of SDS (50 □M). Thereafter, reapplication of SDS causes rapid recovery of Cm, and responses can be repeated multiple times. **(B)** Cytoplasmic solution with 1 mM spermidine. MEND is first induced by Ca influx. Thereafter, application of SDS (30 □M) results in rapid restoration of cell Cm beyond baseline. Upon removing detergent, Cm falls by 64% and reapplication of detergent promotes a restoration of Cm. As demonstrated in the rest of the record, these responses can be repeated multiple times during each experiment.

Figure S9. Inactive detergents. We examined effects of numerous detergents on fibroblast Cm in experiments similar to those described in the article. Detergents were applied and removed from cells in stepwise fashion until conductance and/or capacitance changes were detected. Two patterns emerged for inactive detergents, as shown for octylglucoside and deoxycholate. **(A)** With octylglucoside, substantial conductance changes occurred during application of detergent, and the conductance changes reversed after removing detergent within a few seconds. These changes were accompanied by apparent capacitance changes, which reversed immediately to baseline upon removing detergent. Capacitance never declined significantly below baseline as occurs with detergent effects described in the article (n=6). Prolonged detergent exposure in this

concentration range resulted in irreversible conductance changes, reflecting seal disruption, cell disruption, or both (>50 observations). **(B)** With deoxycholate, conductance changes that occurred with high detergent concentrations did not reverse, indicating that the seal had been significantly disrupted. Detergent exposure caused at most 10% stable declines of cell capacitance at concentrations that did not disrupt seals (n>10). **(C)** This table gives the 'disruptive' concentration of several detergents, determined as described in 'A' and 'B'.

Figure 1

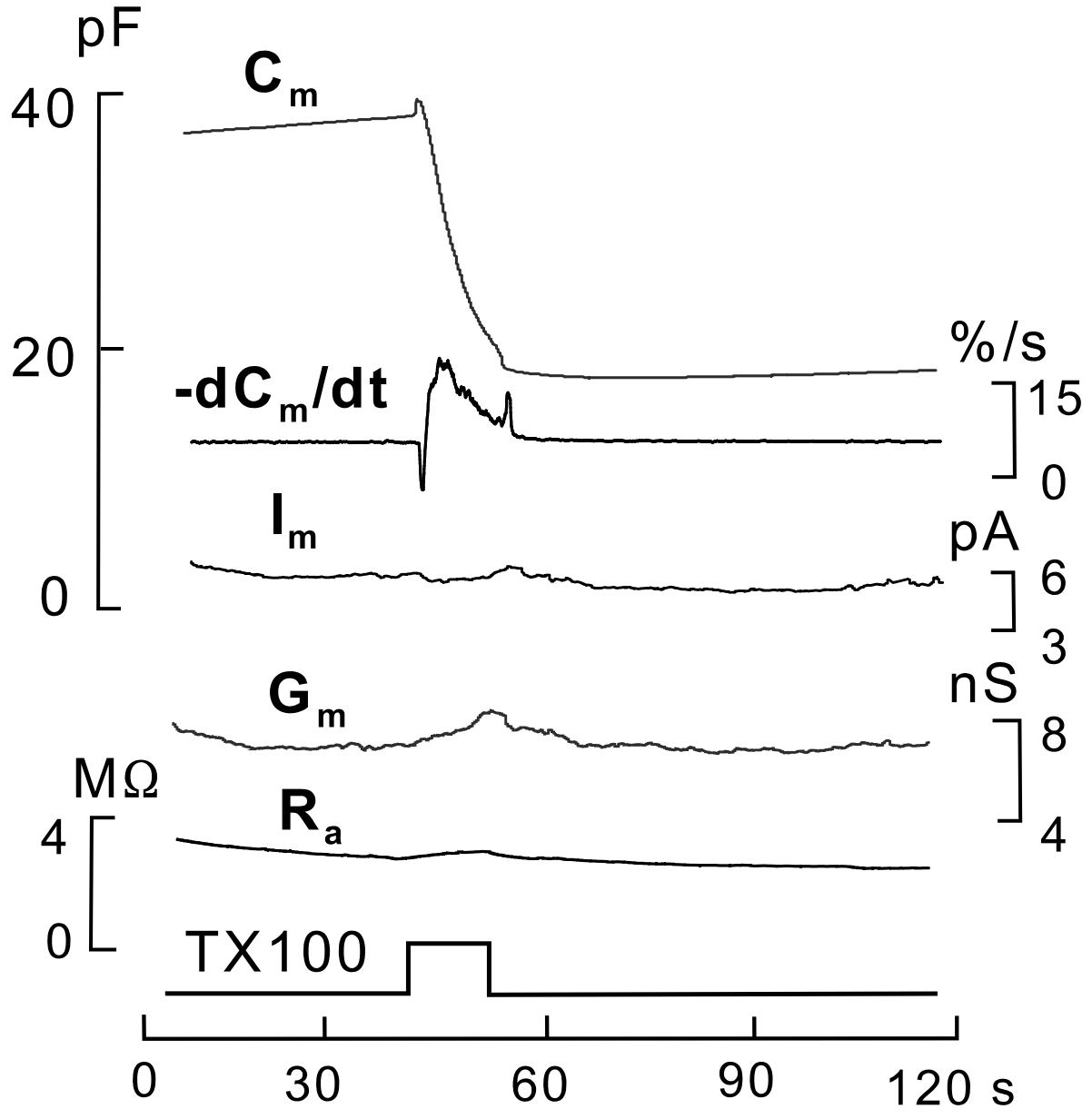
pF
40
20
0
C_m
%/s
$-dC_m/dt$
15
0
I_m
pA
6
3
G_m
nS
8
4
MΩ
4
0
R_a
TX100
0
30
60
90
120 s

Figure 2

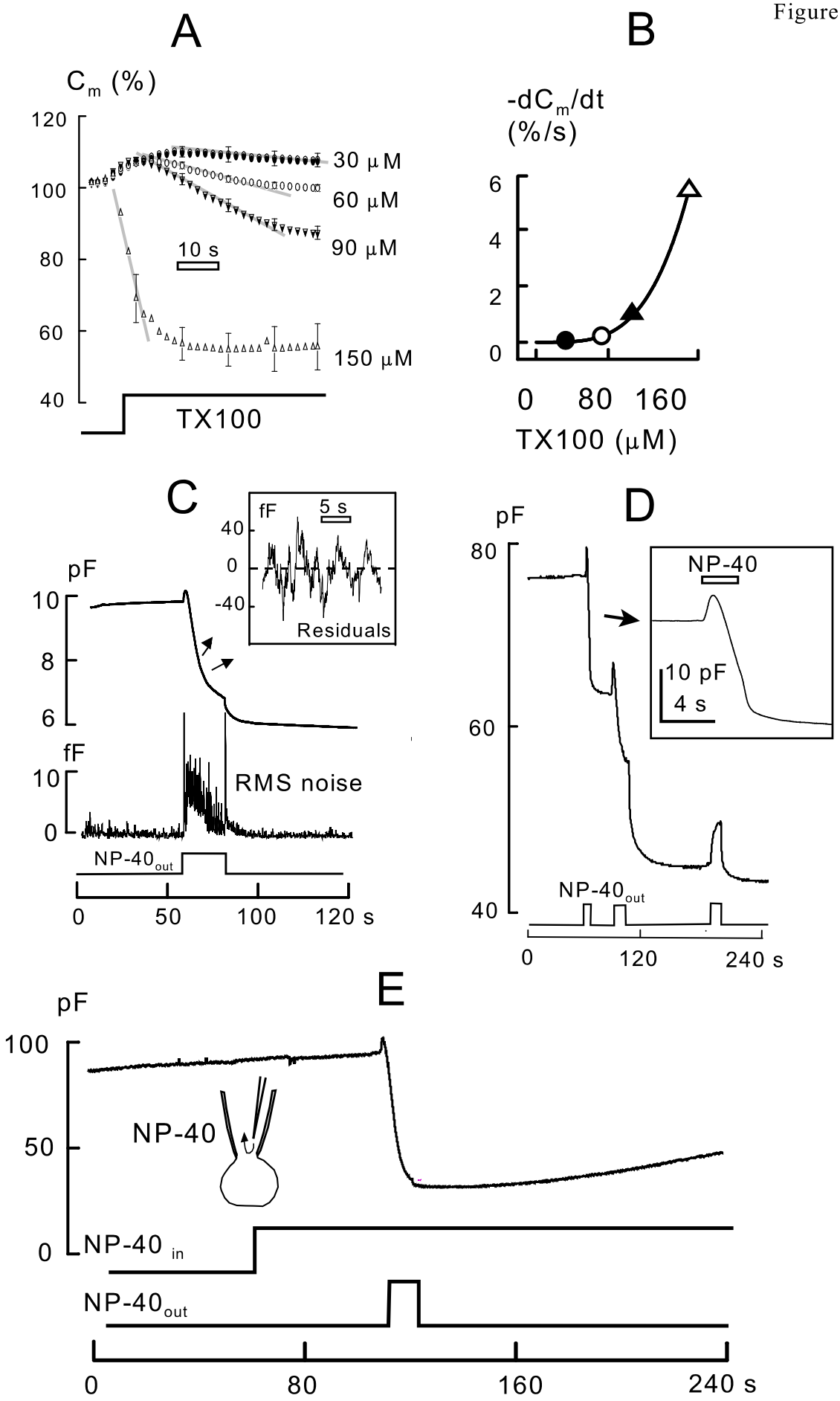
A
C_m (%)
120
100
80
60
40
30 μM
60 μM
90 μM
150 μM
10 s
TX100
B
-dC_m/dt
(%/s)
6
4
2
0
0 80 160
TX100 (μM)
C
pF
10
8
6
fF
5 s
40
0
-40
Residuals
fF
10
0
RMS noise
NP-40out
0 50 100 120 s
D
pF
80
60
40
NP-40
10 pF
4 s
NP-40out
0 120 240 s
E
pF
100
50
0
NP-40
NP-40 in
NP-40out
0 80 160 240 s

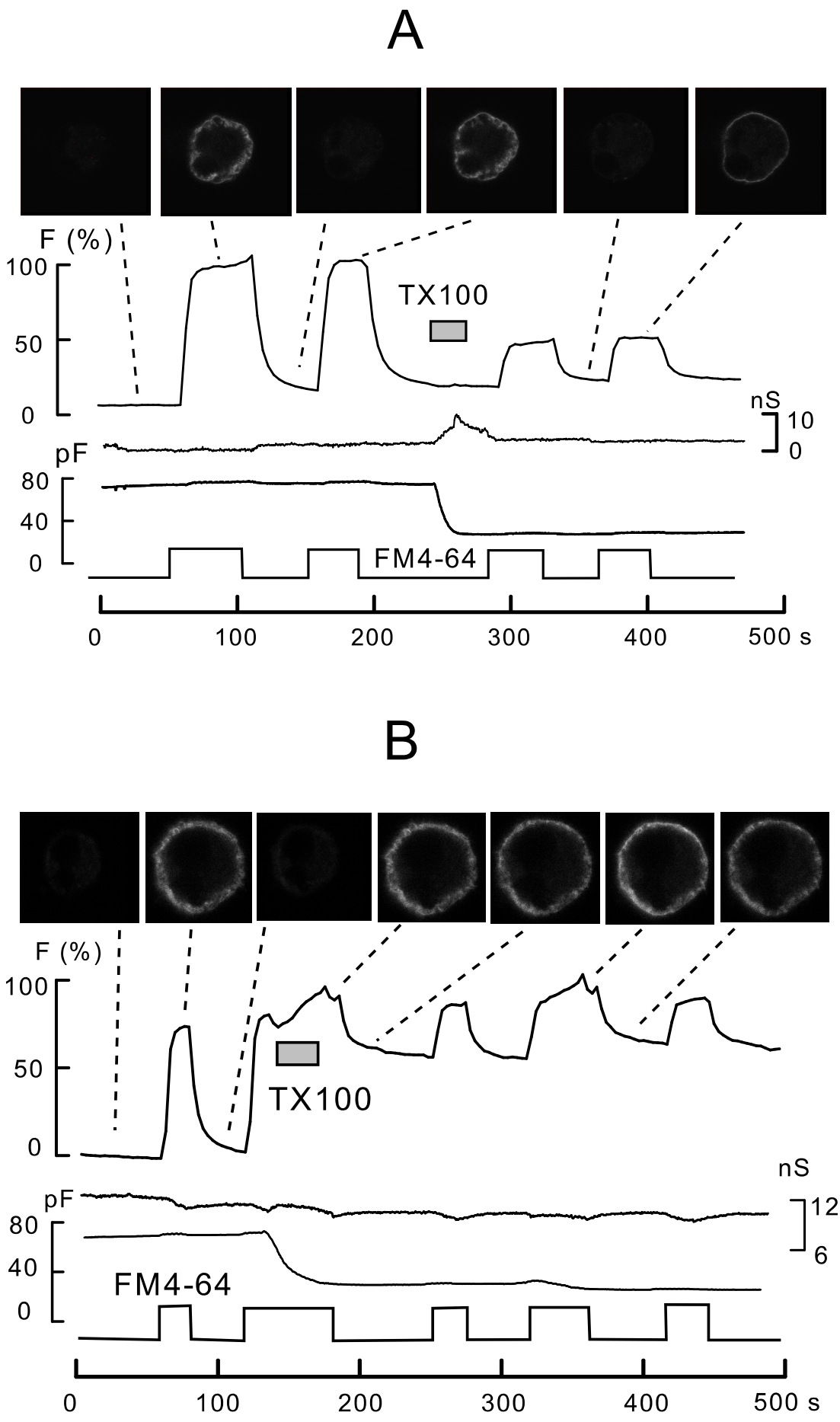
A
F (%)
100
50
0
TX100
nS
10
0
pF
80
40
0
FM4-64
0
100
200
300
400
500 s
B
F (%)
100
50
0
TX100
nS
12
6
pF
80
40
0
FM4-64
0
100
200
300
400
500 s

Figure 4

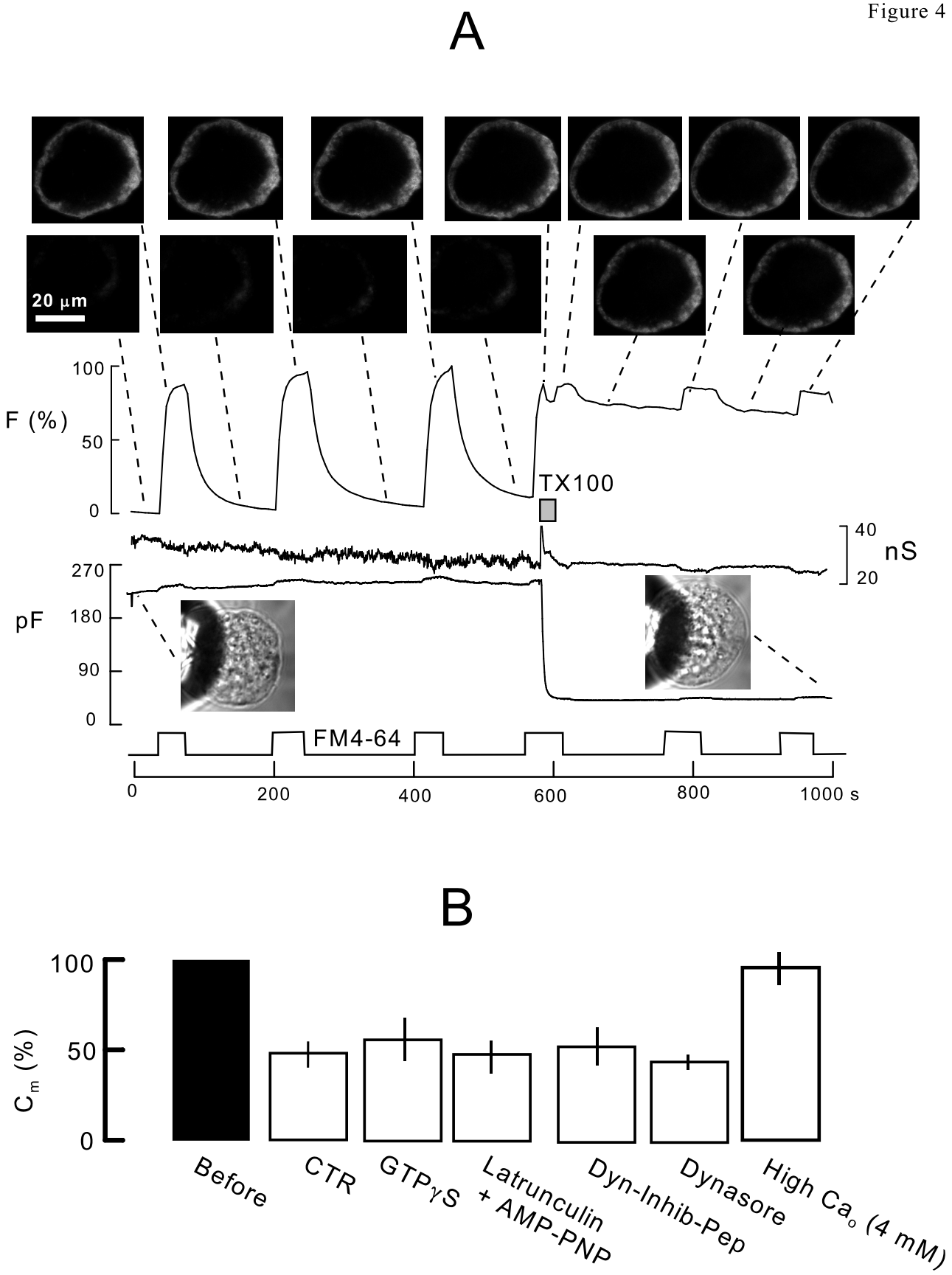
A
20 μm
100
F (%)
50
0
TX100
40
nS
20
270
pF
180
90
0
FM4-64
0
200
400
600
800
1000 s
B
100
C_m (%)
50
0
Before
CTR
GTPγS
Latrunculin + AMP-PNP
Dyn-Inhib-Pep
Dynasore
High Ca_o (4 mM)

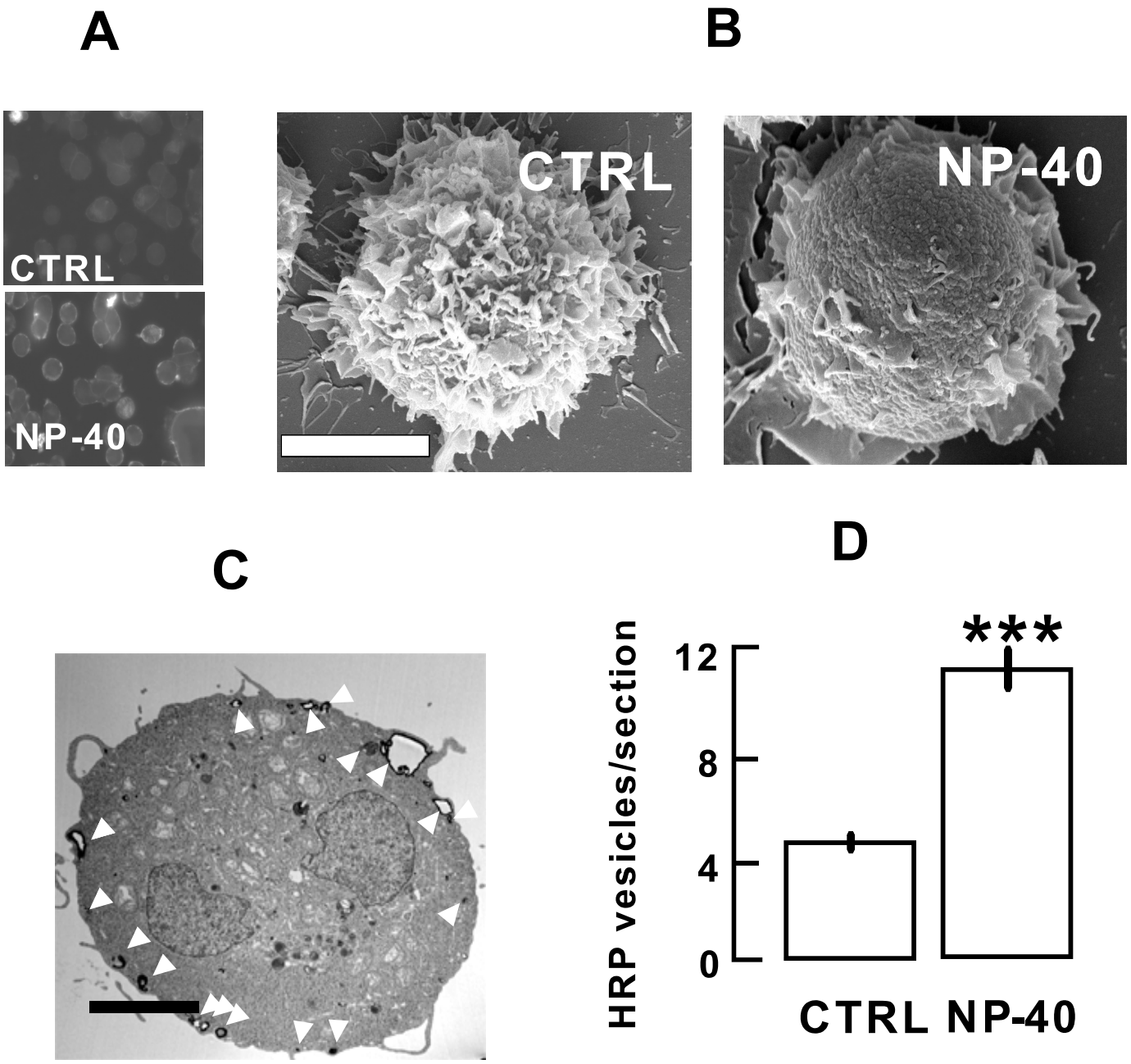
A
B
CTRL
NP-40
CTRL
NP-40
C
D
HRP vesicles/section
12
8
4
0
***
CTRL NP-40

Figure 6

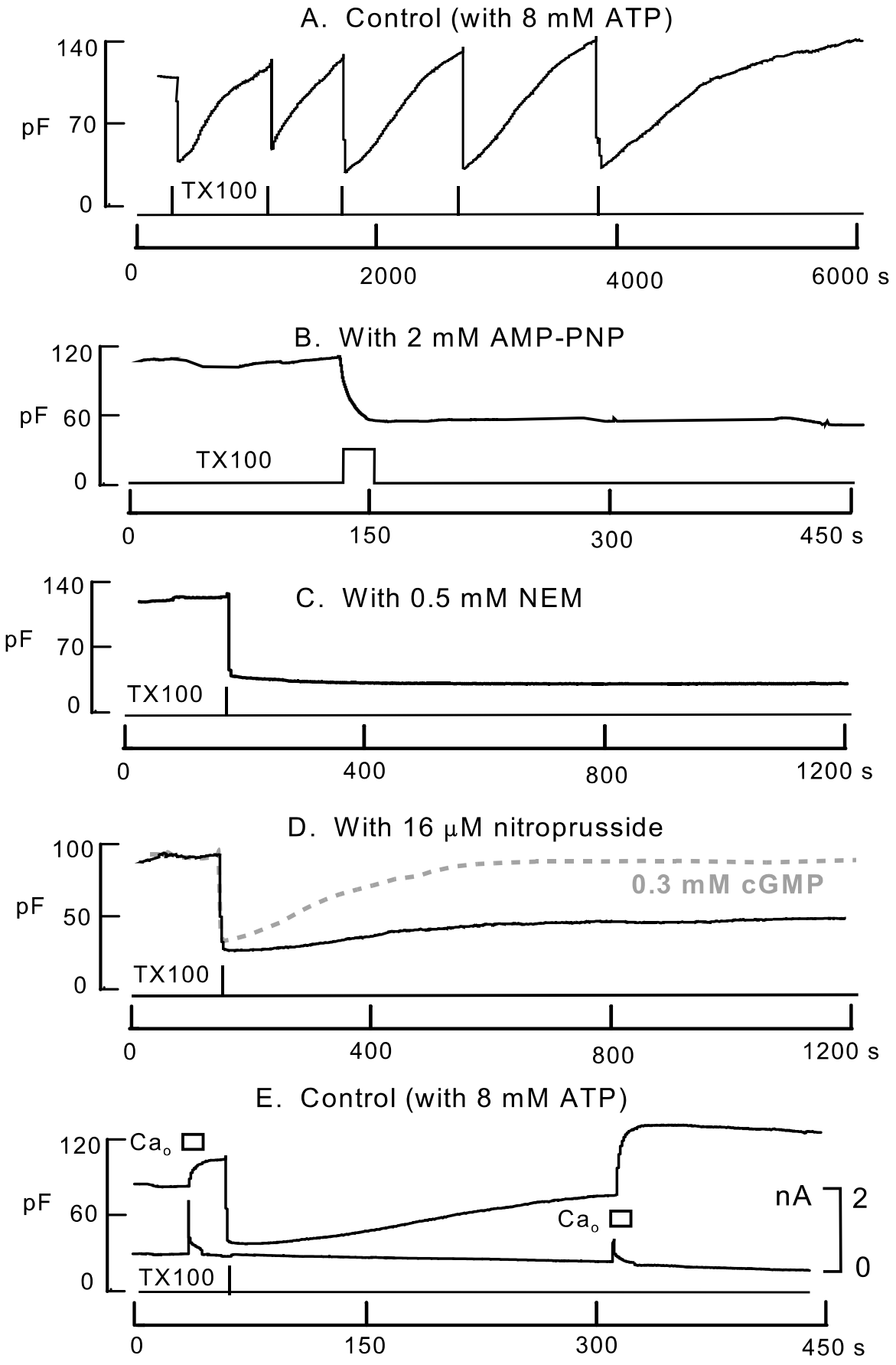
A. Control (with 8 mM ATP)
140
pF 70
0
TX100
0
2000
4000
6000 s
B. With 2 mM AMP-PNP
120
pF 60
0
TX100
0
150
300
450 s
140
C. With 0.5 mM NEM
pF 70
0
TX100
0
400
800
1200 s
D. With 16 μM nitroprusside
100
pF 50
0
0.3 mM cGMP
TX100
0
400
800
1200 s
E. Control (with 8 mM ATP)
120
pF 60
0
Ca$_o$
Ca$_o$
nA
2
0
TX100
0
150
300
450 s

Figure 7

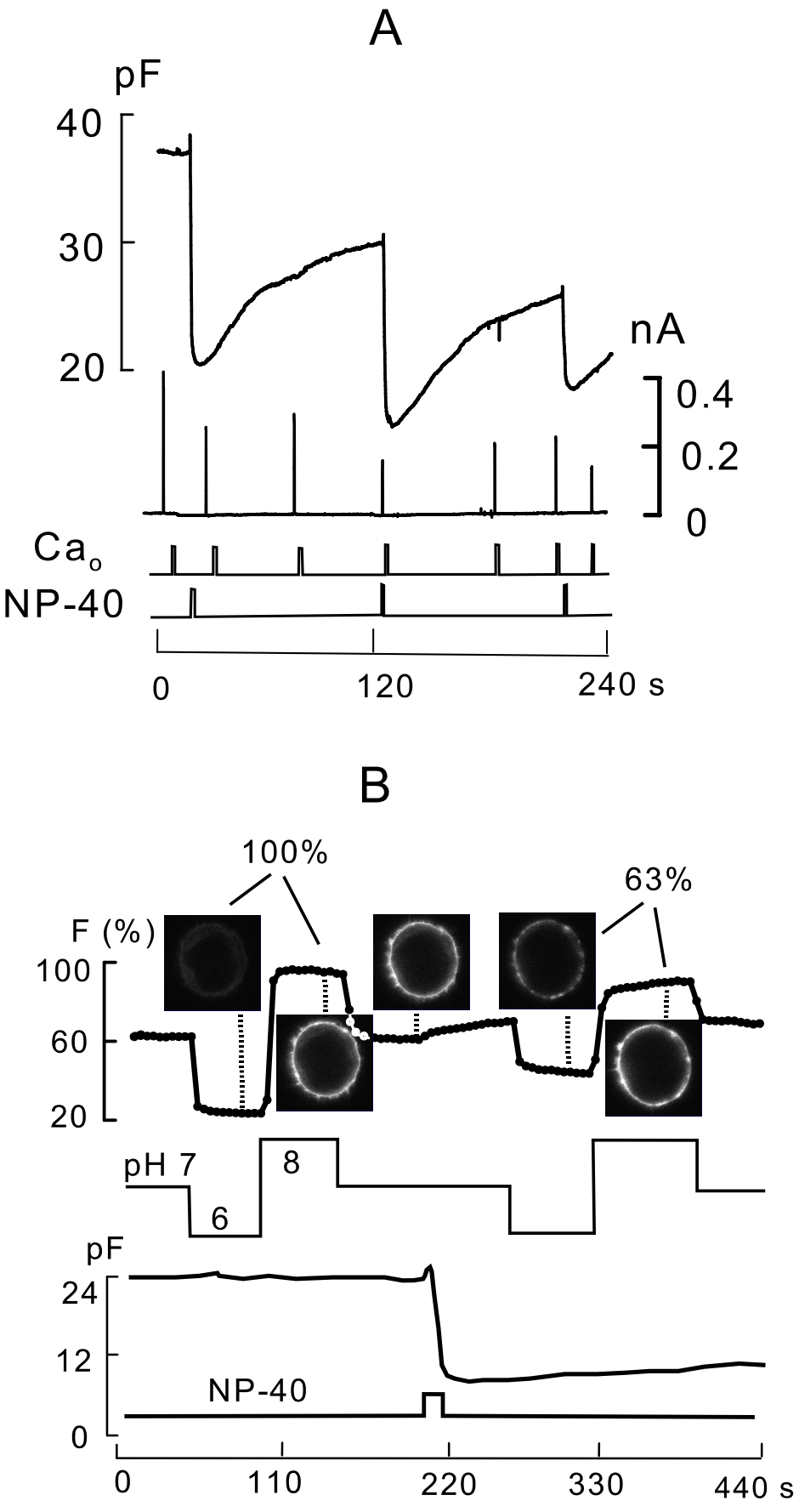
A
pF
40
30
20
nA
0.4
0.2
0
Ca$_o$
NP-40
0
120
240 s
B
100%
63%
F (%)
100
60
20
pH 7
8
6
pF
24
12
0
NP-40
0
110
220
330
440 s

A. Murine myocyte

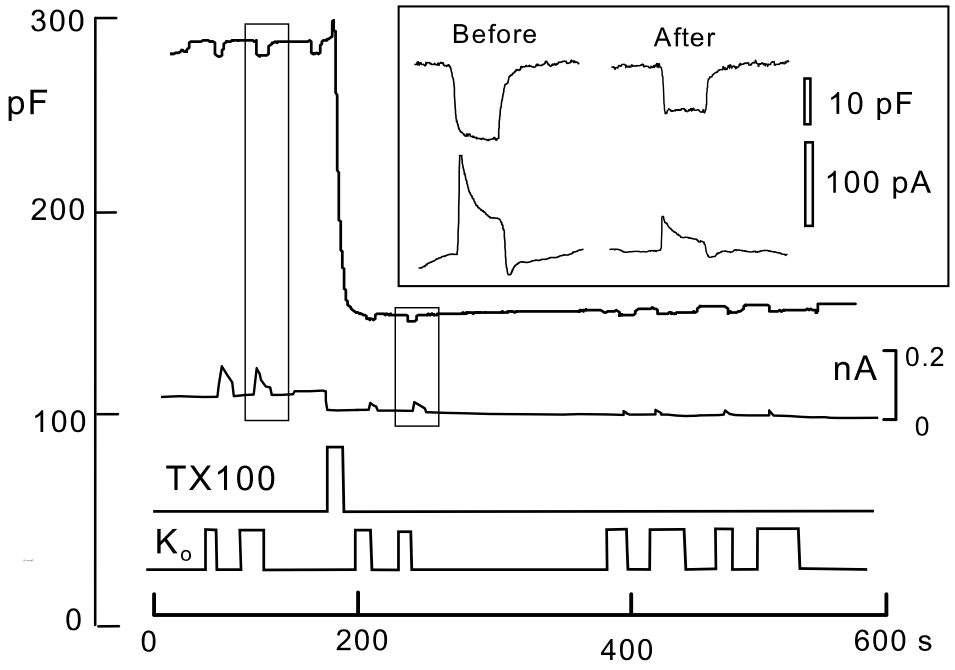

B. BHK cell

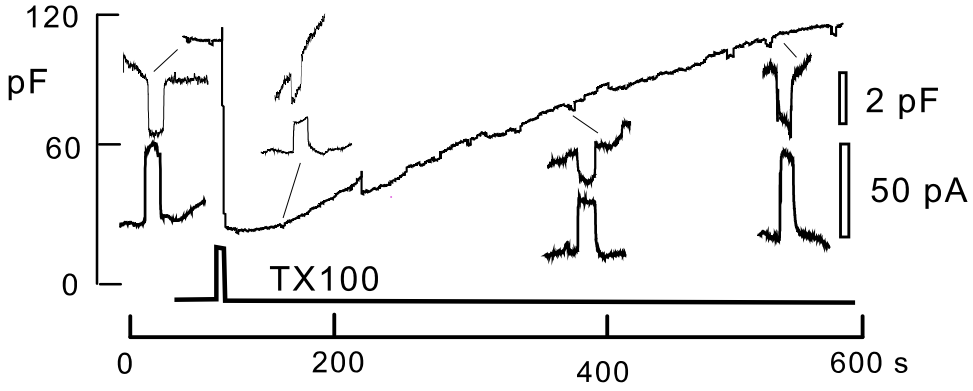

C. HEK293 cell

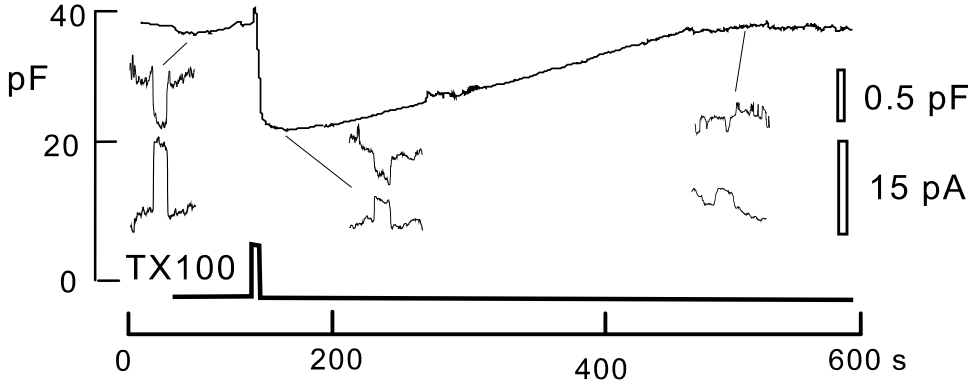

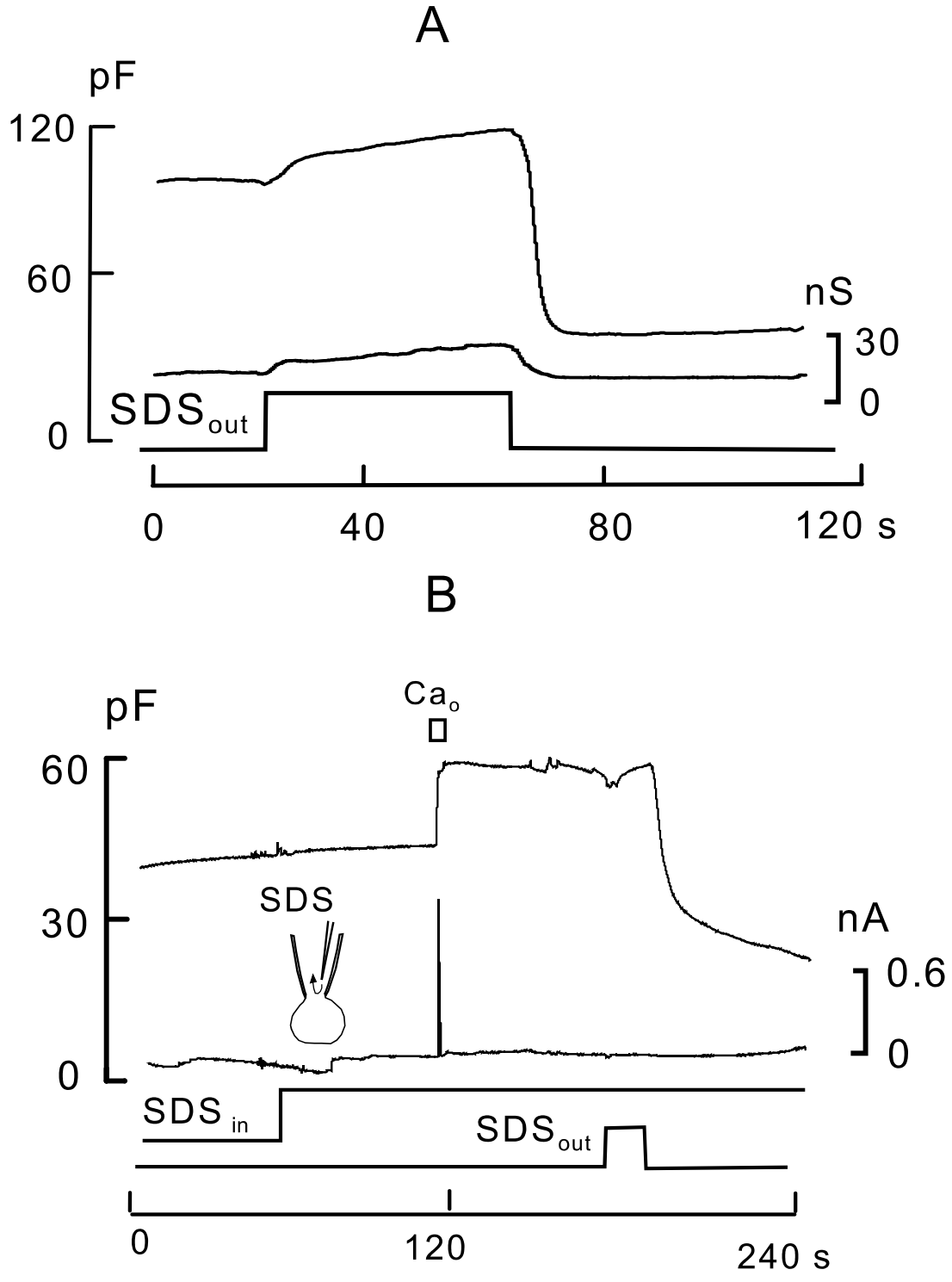
A
pF
120
60
0
nS
30
0
SDS$_{out}$
0
40
80
120 s
B
pF
Ca$_o$
60
30
0
SDS
nA
0.6
0
SDS $_{in}$
SDS$_{out}$
0
120
240 s

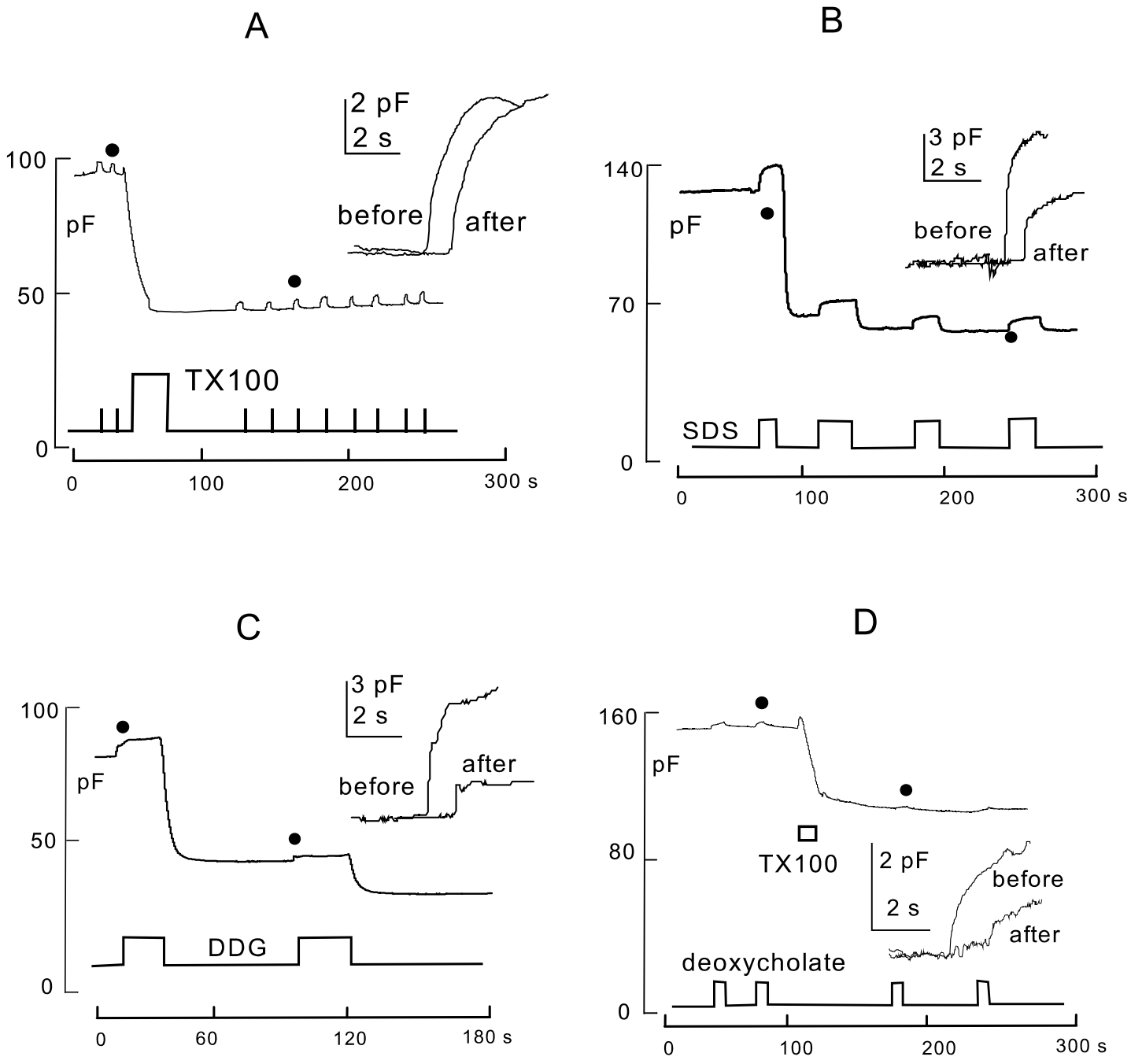
A
2 pF
2 s
before
after
100
pF
50
TX100
0
0
100
200
300 s
B
3 pF
2 s
140
pF
before
after
70
SDS
0
0
100
200
300 s
C
3 pF
2 s
100
pF
after
before
50
DDG
0
0
60
120
180 s
D
160
pF
80
TX100
2 pF
2 s
before
after
deoxycholate
0
0
100
200
300 s

Figure 11

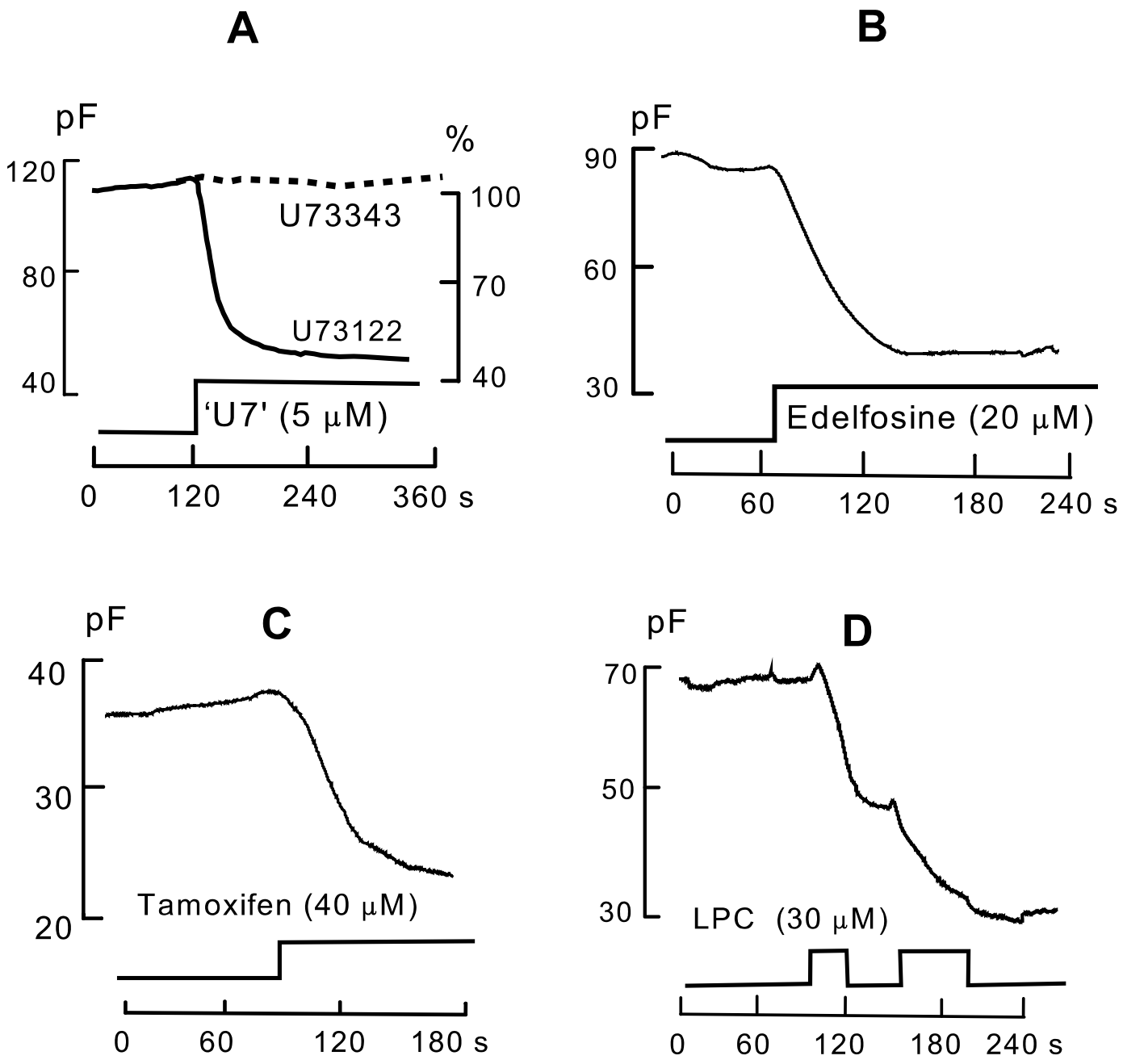
A
pF
%
120
80
40
100
70
40
U73343
U73122
'U7' (5 μM)
0
120
240
360 s
B
pF
90
60
30
Edelfosine (20 μM)
0
60
120
180
240 s
C
pF
40
30
20
Tamoxifen (40 μM)
0
60
120
180 s
D
pF
70
50
30
LPC (30 μM)
0
60
120
180
240 s

Figure 12

1 **Normal Conditions**

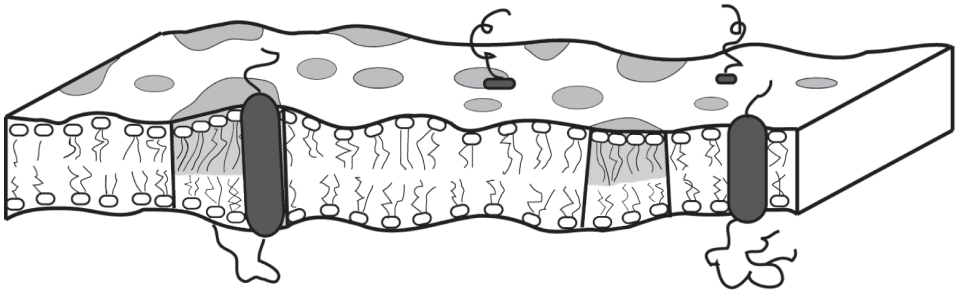

2 **Coalescence & Buckling**

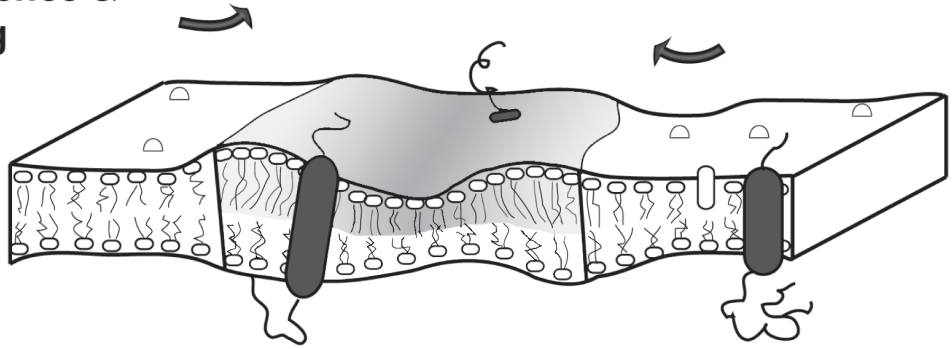

3 **Internalization**

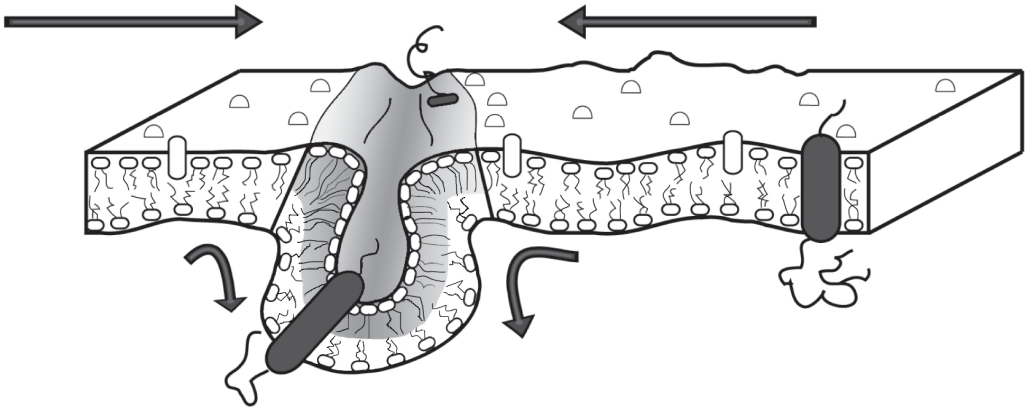

Supporting Data Figures

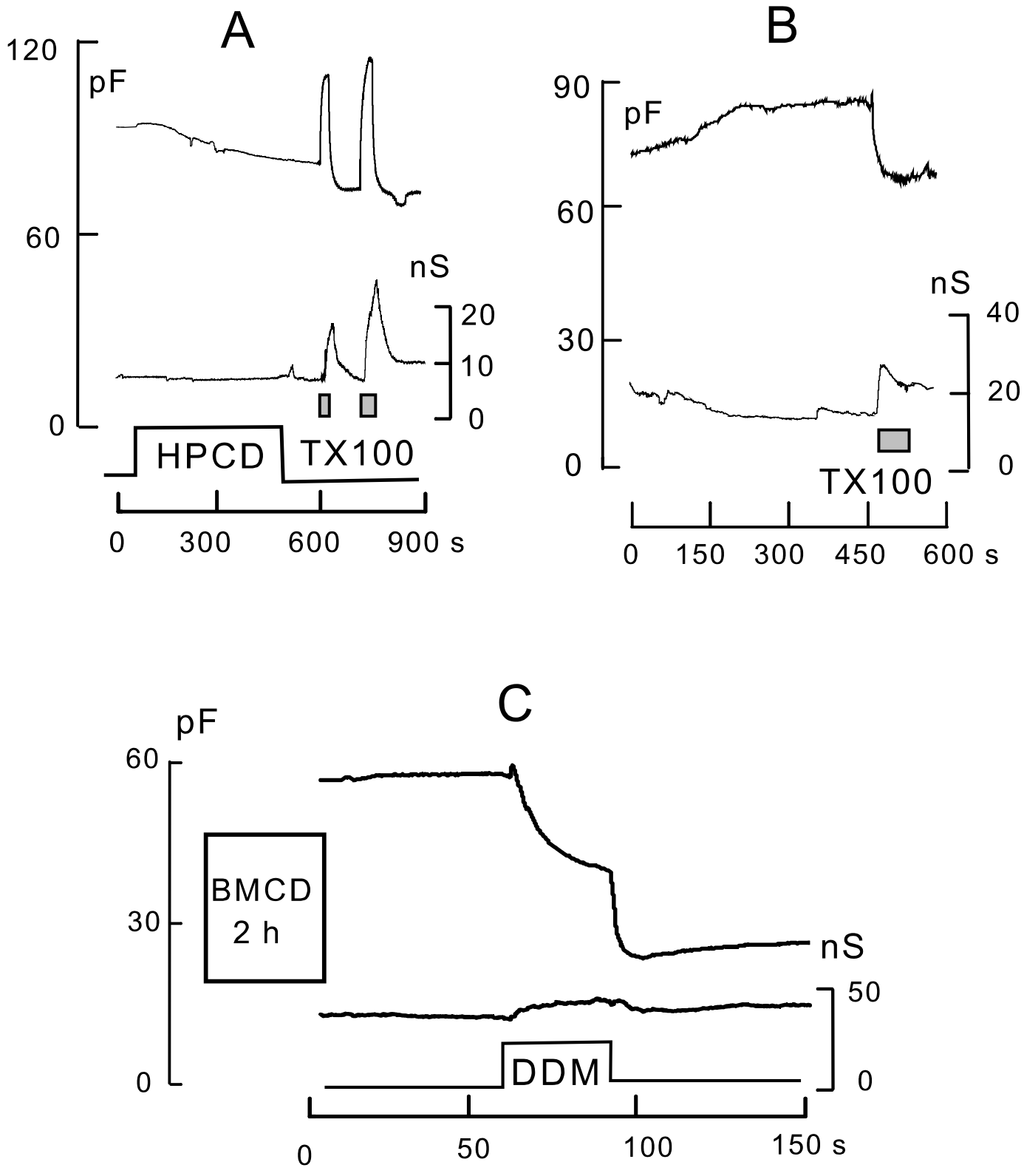
A
120
pF
60
0
nS
20
10
0
HPCD
TX100
0
300
600
900 s
B
90
pF
60
30
0
nS
40
20
0
TX100
0
150
300
450
600 s
C
pF
60
30
0
BMCD
2 h
nS
50
0
DDM
0
50
100
150 s

Figure S2

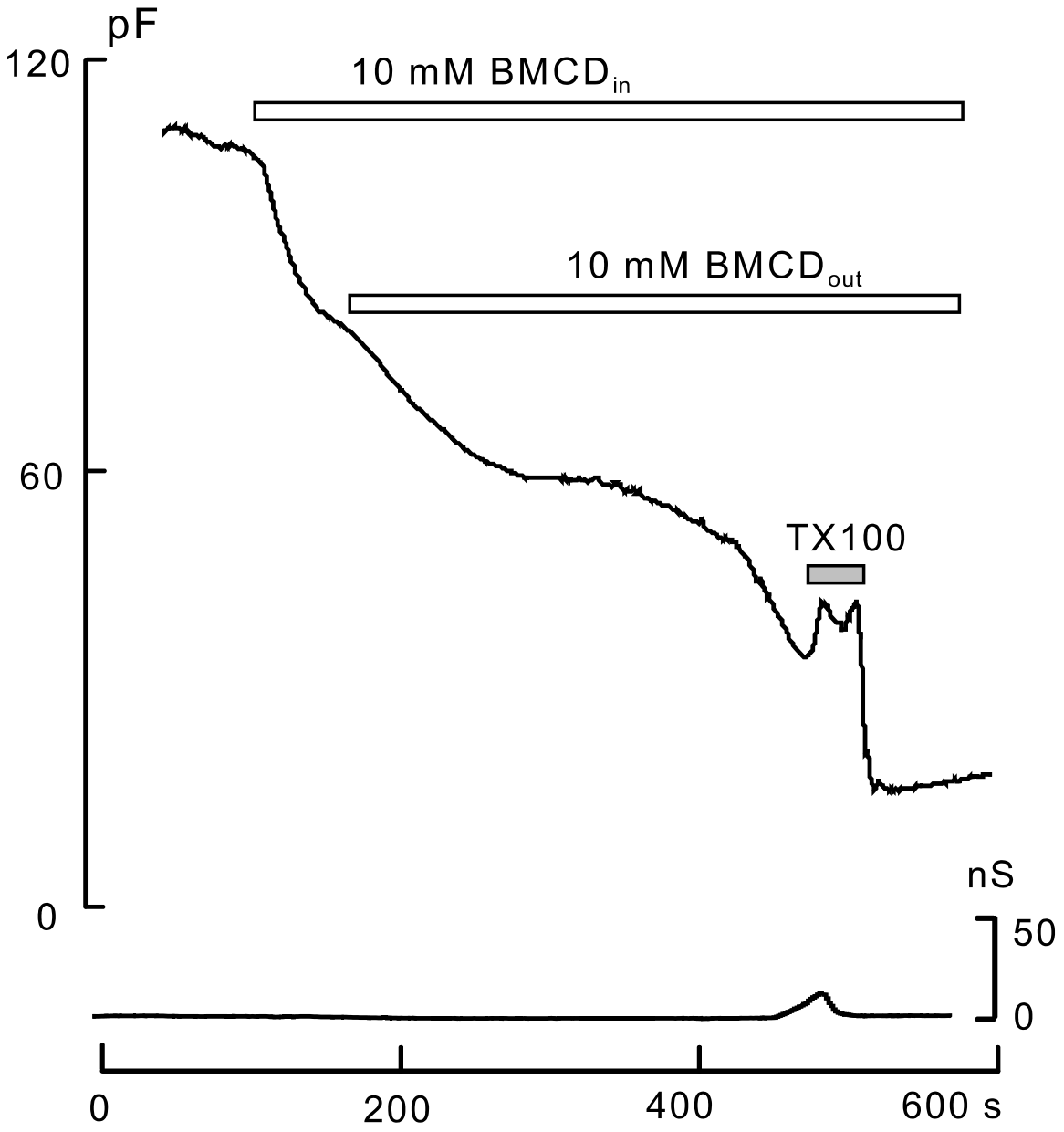
pF
120
60
0
10 mM BMCD$_{in}$
10 mM BMCD$_{out}$
TX100
nS
50
0
0
200
400
600 s

Figure S3

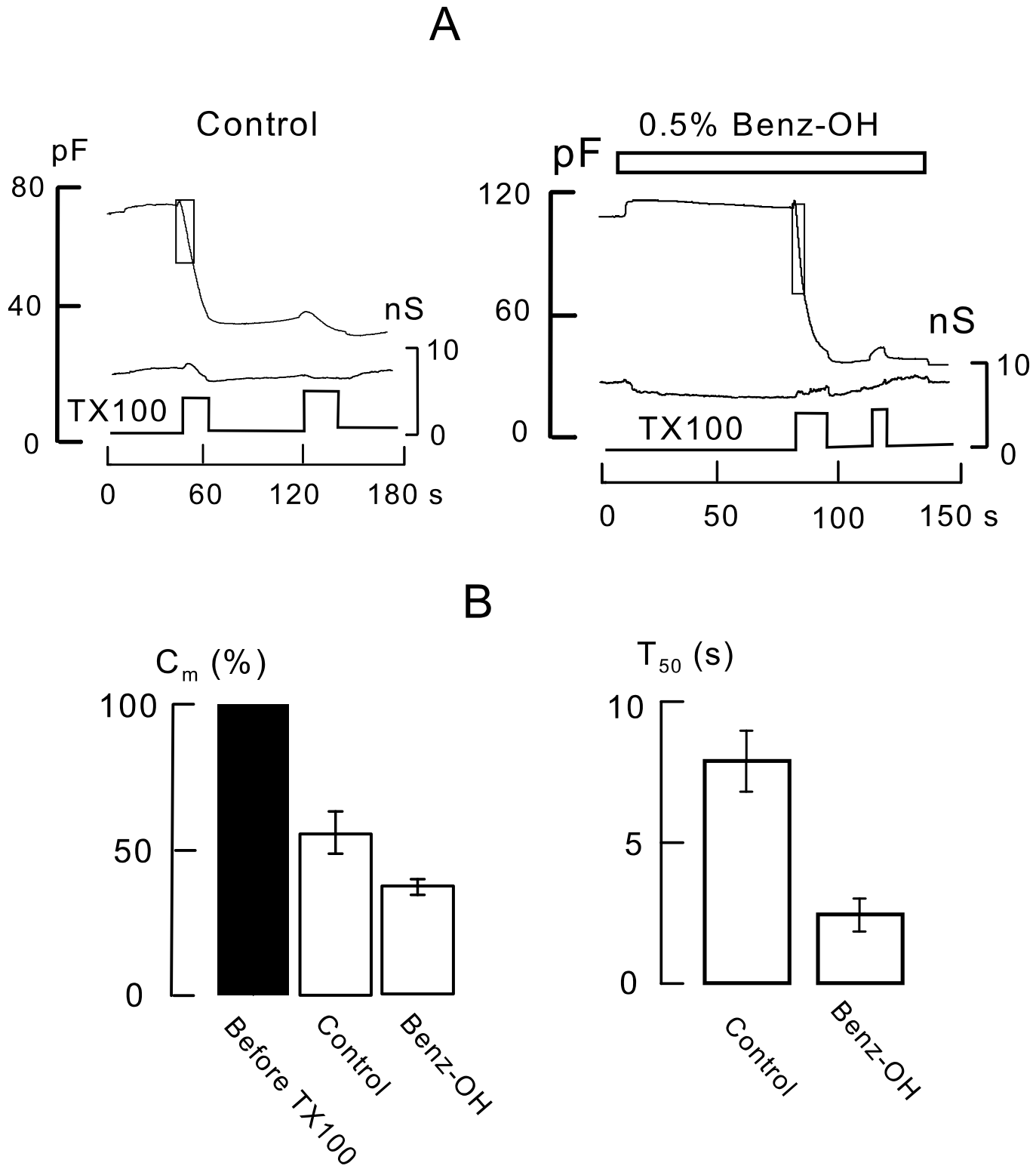
A
Control
pF
80
40
0
nS
10
0
TX100
0
60
120
180 s
0.5% Benz-OH
pF
120
60
0
nS
10
0
TX100
0
50
100
150 s
B
C_m (%)
100
50
0
Before TX100
Control
Benz-OH
T_{50} (s)
10
5
0
Control
Benz-OH

Figure S4

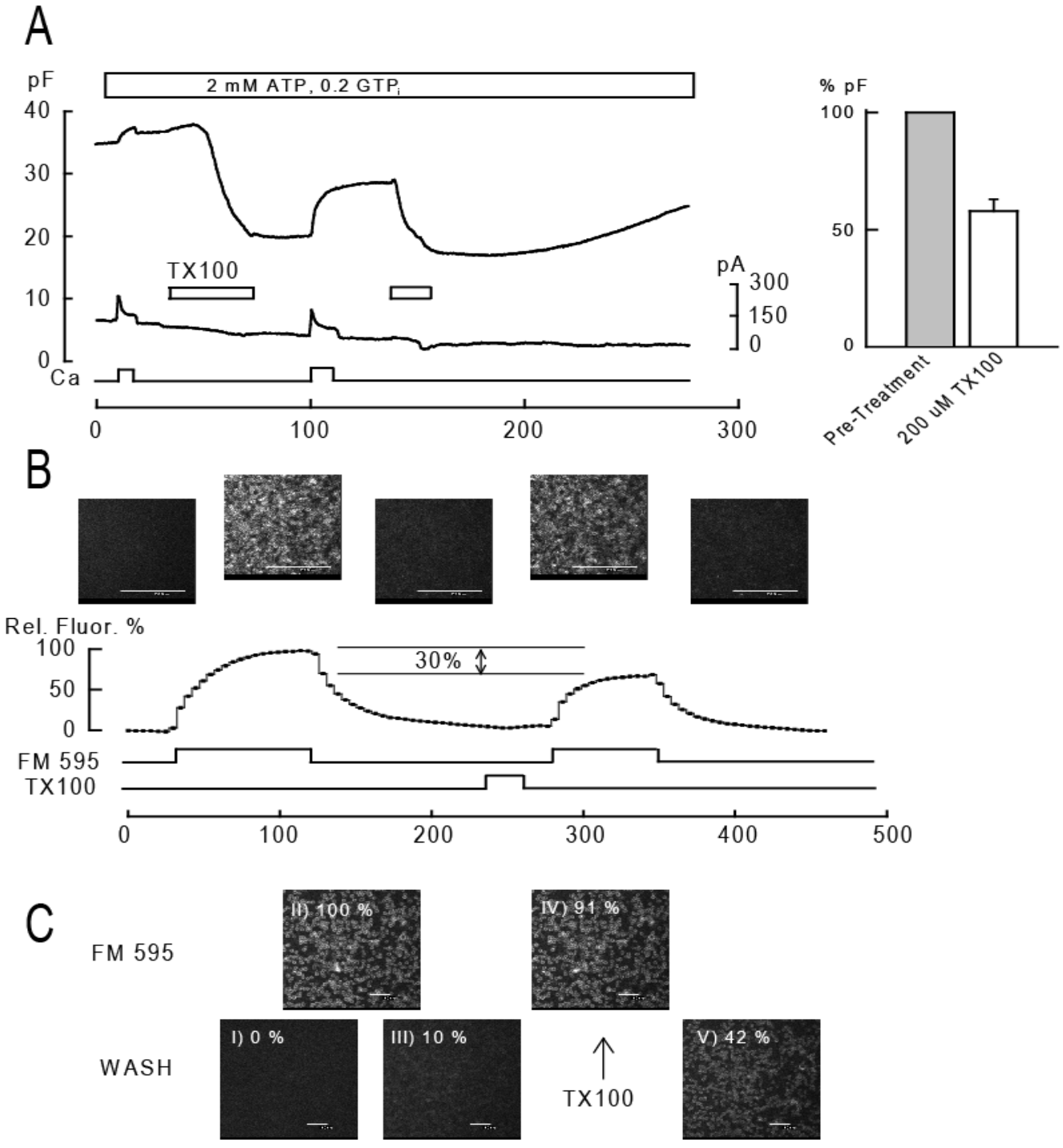
A
pF
2 mM ATP, 0.2 GTPi
40
30
20
10
0
TX100
pA
300
150
0
Ca
0
100
200
300
% pF
100
50
0
Pre-Treatment
200 uM TX100
B
Rel. Fluor. %
100
50
0
30%
FM 595
TX100
0
100
200
300
400
500
C
FM 595
II) 100 %
IV) 91 %
WASH
I) 0 %
III) 10 %
TX100
V) 42 %

Figure S5

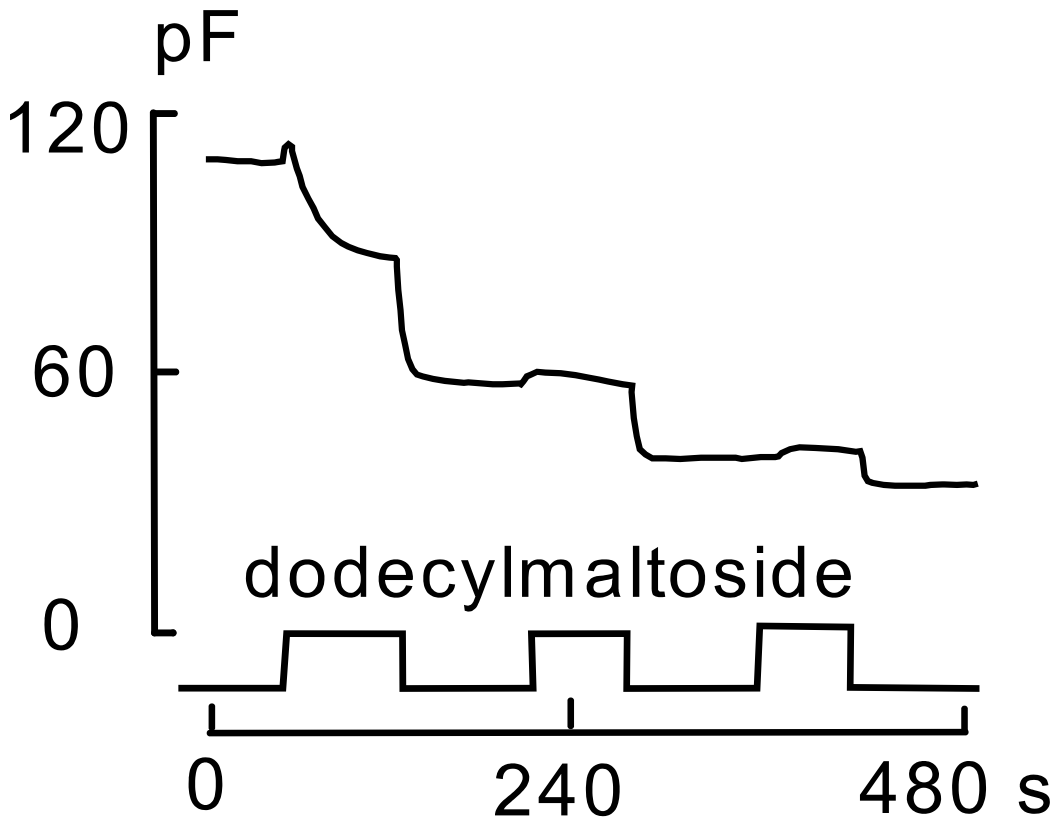

Figure S6

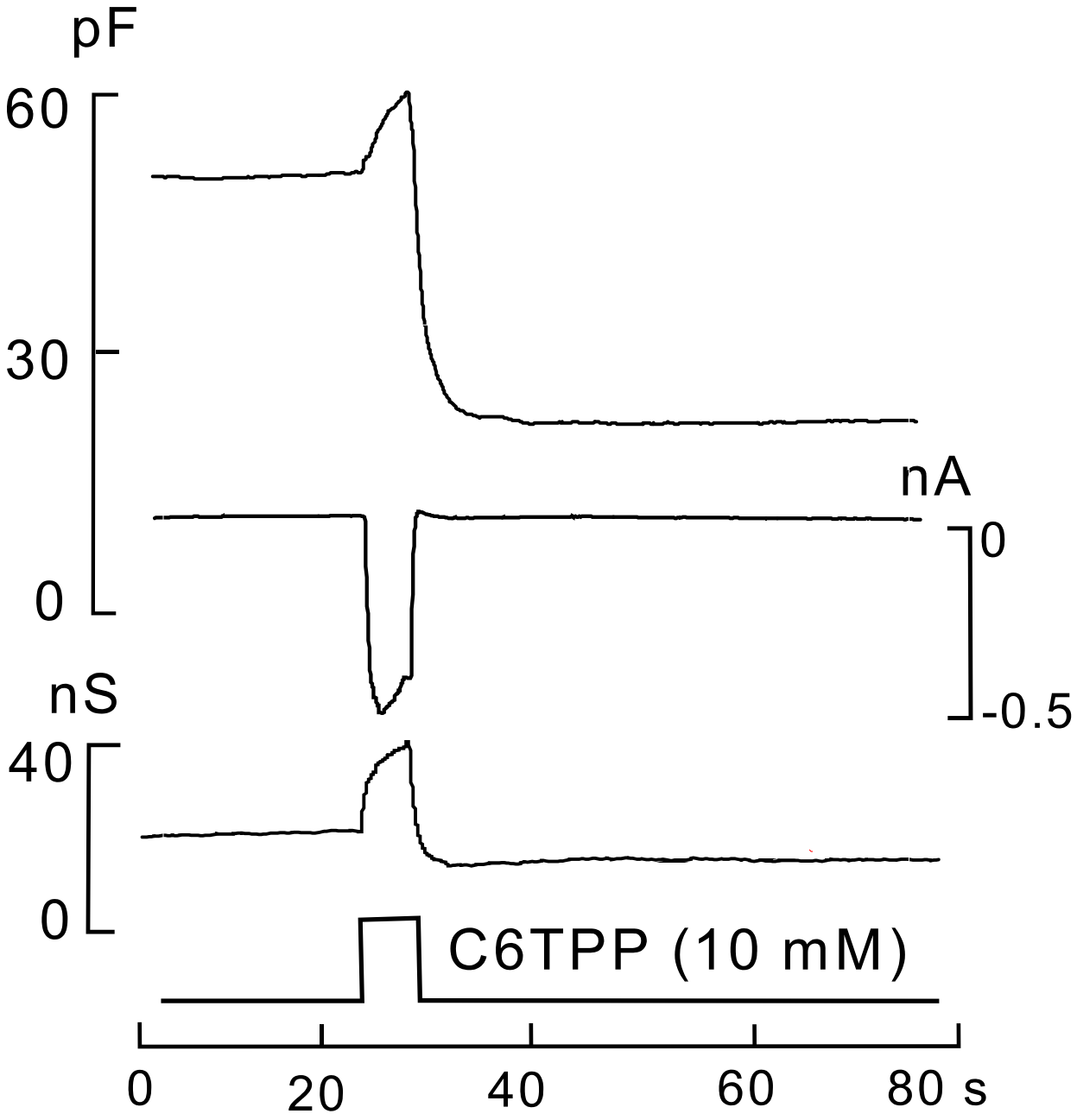

Figure S7

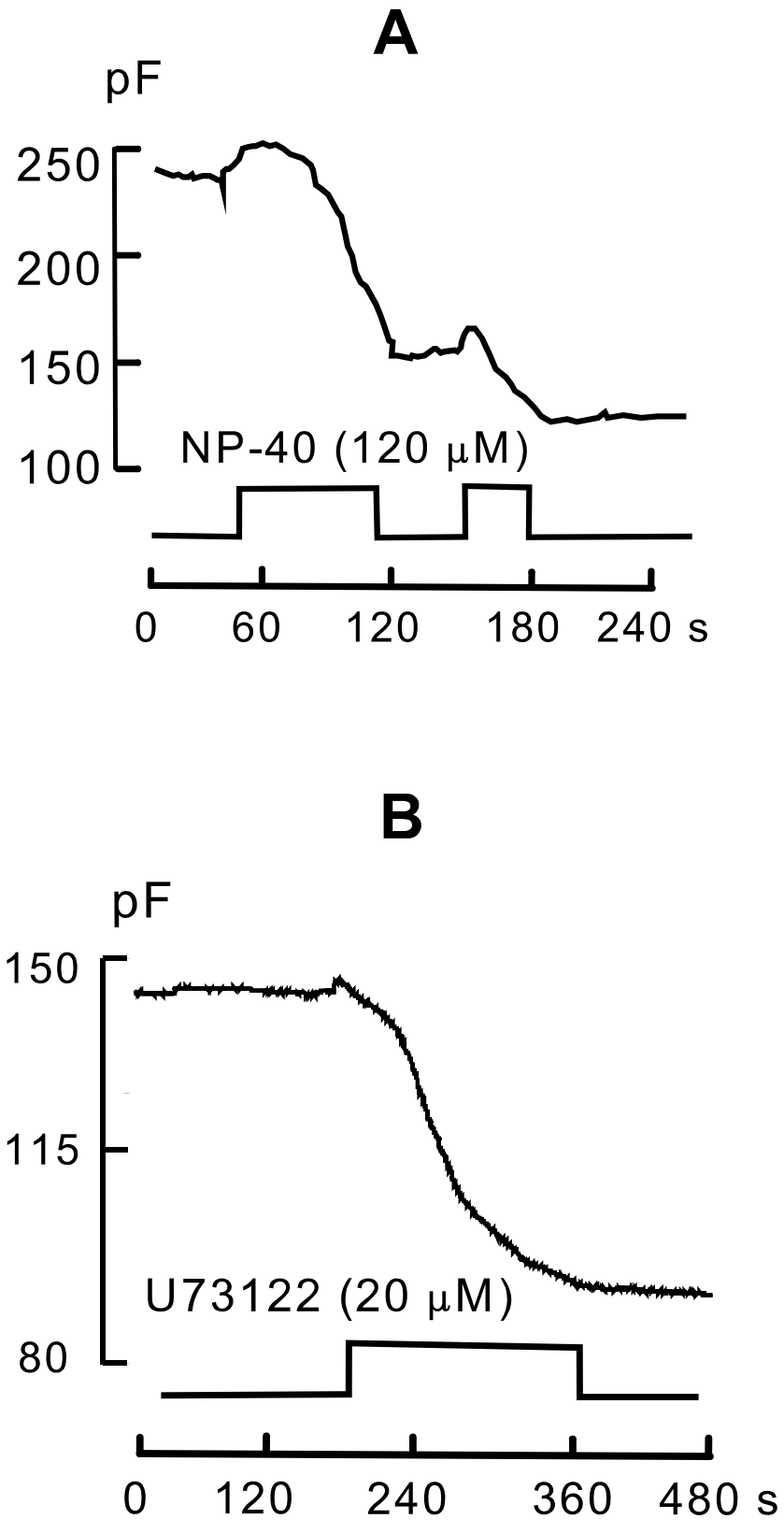
A
pF
250
200
150
100
NP-40 (120 μM)
0
60
120
180
240 s
B
pF
150
115
80
U73122 (20 μM)
0
120
240
360
480 s

Figure S8

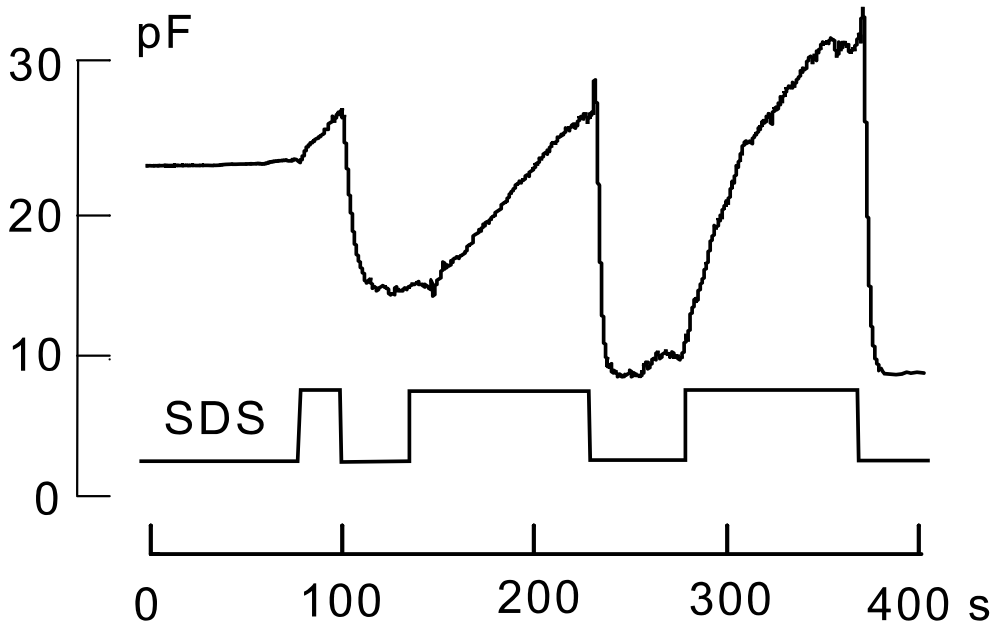
pF
30
20
10
0
SDS
0
100
200
300
400 s

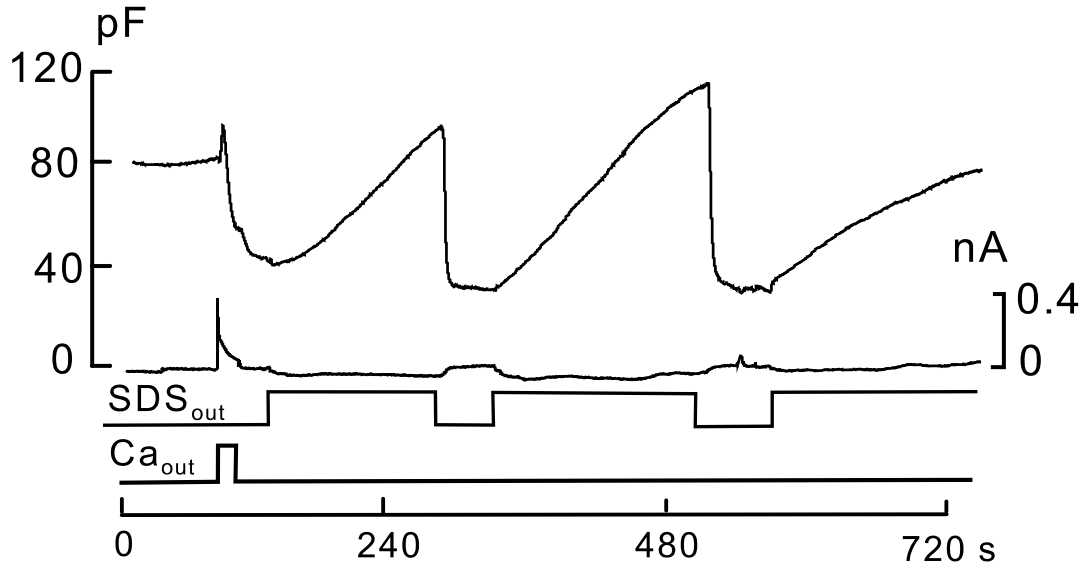
pF
120
80
40
0
nA
0.4
0
SDS$_{out}$
Ca$_{out}$
0
240
480
720 s

Figure S9

A

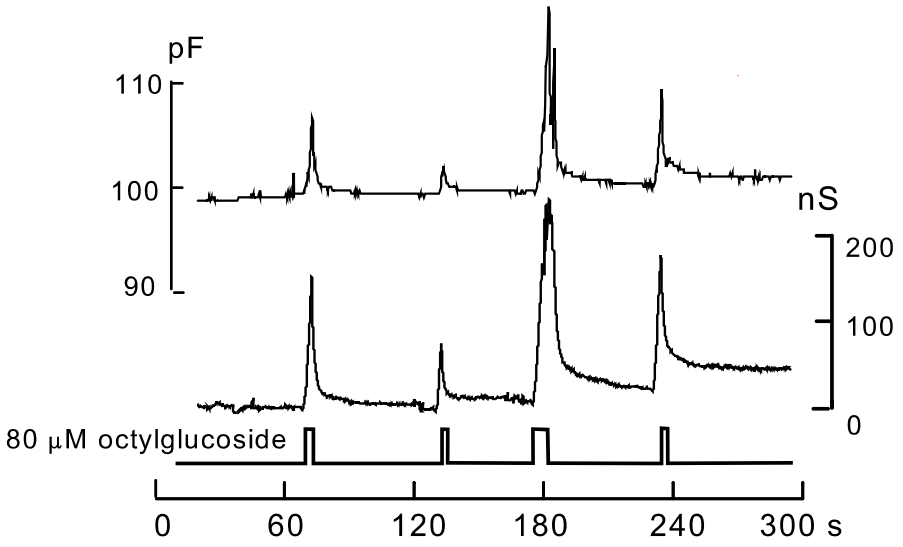

B

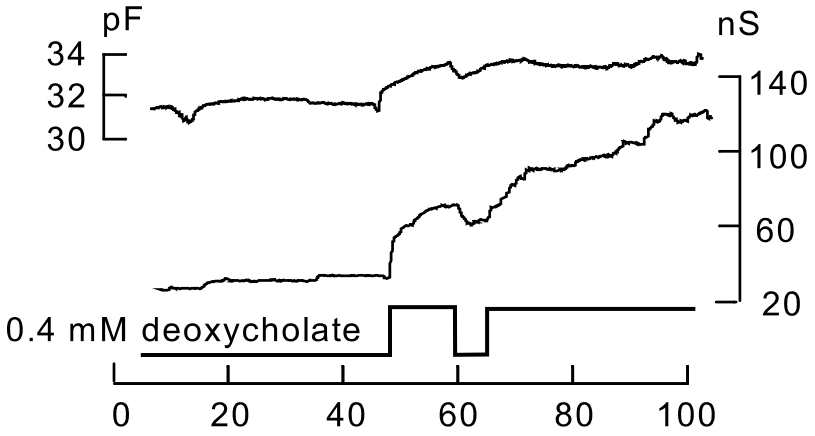

C

Disruptive Concentrations of 'Inactive' Detergents & Amphipaths	
Octylglucoside	90 μM
Octanesulfonic acid	46 mM
CHAPS	1.5 mM
Deoxycholate	2.0 mM
Tauro-deoxycholate	2.5 mM
Saponin	2.2 mM
β-escin	40 μM
Lipofectamine	100 μM
Sphingosine	12 μM

APPENDIX 3:

Mechanistic Analysis of Massive Endocytosis in Relation to Functionally-Defined Surface Membrane Domains

by

Donald W. Hilgemann and Michael Fine

Department of Physiology
University of Texas Southwestern Medical Center at Dallas
5323 Harry Hines Blvd.
Dallas, Texas 75390-9040 USA

Address correspondence to:

Donald W. Hilgemann
University of Texas Southwestern Medical Center at Dallas
5323 Harry Hines Blvd.
Dallas, Texas 75390-9040 USA

donald.hilgemann@utsouthwestern.edu
Tel. 214-645-6031
Fax. 214-645-6049

Running Title: Mechanism of Massive Endocytosis

Abbreviations. adenylyl imidodiphosphate, AMP-PNP; alkyltriphenylphosphonium, alkyl-TPP; C4TPP, butyltriphenylphosphonium; C10TPP, decyltriphenylphosphonium; C6TPP, hexyltriphenylphosphonium; carbonyl cyanide m-chlorophenylhydrazone, CCCP; diaminobenzidine, DAB; Diffusional Security Factor, DSF; dimethylsulfoxide, DMSO); ditridecylphthalate, DTPT dipicrylamine, DPA; dodecylglucoside, DDG; dodecylmaltoside, DDM; dodecyltriphenylphosphonium, C12TPP; guanosine 5′-[γ-thio]triphosphate, GTPγS; hexyltriphenylphosphonium, C6TPP; horseradish peroxidase, HRP; hydroxypropyl-β-cyclodextrin, HPCD; lyso-phosphatidylcholine, LPC; massive endocytosis, MEND; β-methylcyclodextrin, niflumic acid, NFA; NBD-phosphatidylethanolamine, NBD-PE; phosphatidylinositiol-bis 4,5-phosphate, PIP_2; sodium dodecylsulfate, SDS; tetradecyltrimethylammonium, TMA; tetraphenylphosphonium, TtPP; Triton X-100, TX100.

Abstract

A large fraction of endocytosis in eukaryotic cells occurs without adaptors or dynamins. We present here evidence for the involvement of lipid domains in massive endocytosis (MEND) activated by both large Ca transients and amphipathic compounds in BHK and HEK293 cells. First, we demonstrate functional coupling of the two MEND types. Ca transients can strongly facilitate detergent-activated MEND. Conversely, an amphipath with dual alkyl chains, di-tridecylphthalate (DTDP), is without effect in the absence of Ca transients but induces MEND to occur within seconds during Ca transients. Ca transients, like amphipaths, enhance the extraction of lipids from cells by β-cyclodextrins. Second, we demonstrate that electrical and/or optical signals generated by selected membrane probes are nearly insensitive to MEND, suggesting that those probes segregate into membrane domains that are not taken up by MEND. Triphenylphosphonium's are increasingly excluded from domains that internalize as the carbon chain length increases from 4 to 12. The small cationic membrane dye, FM 4-64, binds well to domains that internalize, while a closely related dye with a larger hydrophobic moiety, di-4-ANEPPDHQ (ANEPPDHQ) is excluded. Multiple carrier-type ionophores and a small amphipathic anion, niflumic acid (NFA), are also excluded. Probes with modest MEND sensitivity include the hydrophobic anion, dipicrylamine (DPA), carbonyl cyanide m-chlorophenylhydrazone (CCCP), and NBD-phosphatidylethanolamine (NBD-PE). Third, we demonstrate that large Ca transients can strongly enhance extracellular binding of several membrane probes, monitored electrically or optically, consistent with a more disordered membrane with more amphipath binding sites. Fluorescence shifts of ANEPPDHQ report increased disorder of the extracellular monolayer after large Ca transients, consistent with an increased propensity of the membrane to phase separate and vesiculate. In summary, the results indicate that >50% of the outer monolayer is ordered and can be selectively internalized during MEND responses initiated by two very different cell perturbations.

Introduction

In two companion articles multiple experimental protocols are described to induce massive endocytosis (MEND) in BHK fibroblasts, HEK293 cells, and cardiomyocytes by apparently disparate pathways (Fine et al., xxxx; Lariccia, xxxx). On the one hand, large cytoplasmic Ca transients induce MEND via both short- and long-term mechanisms. On the other hand, extracellular sphingomyelinases, detergents and

amphipathic compounds cause MEND by perturbing the outer plasmalemma monolayer in the absence of Ca transients. Apart from the unprecedented magnitude of these responses, the most evident commonality of these endocytic events is that classical endocytic proteins, such as clathrin, dynamins and actin cytoskeleton, do not appear to be involved.

To what extent MEND responses are mechanistically related to endocytosis in secretory cells is not yet clear. The actions of Ca to promote MEND in fibroblasts are *not* critically dependent on the canonical Ca-activated phosphatases, verified repeatedly to activate compensatory endocytosis in secretory cells (Artalejo et al., 1996; Chan and Smith, 2001; Engisch and Nowycky, 1998; Marks and McMahon, 1998; Wu et al., 2009). Furthermore, Ca-activated MEND is strongly dependent on the presence of relatively labile plasmalemmal cholesterol, being blocked by short treatments with cholesterol-chelating agents and being highly activated by cholesterol enrichment of the plasmalemma (Lariccia, xxxx). Equivalent effects of manipulating cholesterol are not described for endocytosis in secretory cells, a complicating factor being that mechanisms leading to exocytosis are cholesterol dependent (Geumann et al., 2009; Wasser et al., 2007).

Nonionic detergents induce MEND at concentrations more than 100-fold less than employed to isolate *detergent-resistant* membranes. Apparently, the outer monolayer reorganizes to form lipid domains that spontaneously vesiculate inwardly, thereby fractionating the membrane *in vivo* and suggesting comparisons to biochemical membrane fractionation (Fine et al., xxxx). Clearly, amphipath-driven MEND provides new opportunities to understand the function of *lipid rafts* in intact cells and their relationships to biochemically isolated *detergent-resistant* membrane domains (Brown, 2006; Lingwood and Simons, 2007). Since Ca-activated MEND is cholesterol-dependent and does not involve classical endocytic proteins, the suspicion is raised that Ca-activated MEND occurs by mechanisms that are related to amphipath-activated MEND.

With this background, we describe here experiments that interrogate the relationships between amphipath- and Ca-activated MEND, the potential roles of lipid domains in MEND responses, and the potential use of several membrane probes to study the underlying mechanisms. We establish first that Ca-transients strongly facilitate amphipath-activated MEND and that common hydrophobic compounds in the modern

environment, phthalate plasticizers, can promote Ca-activated MEND. Next, we address whether internalized membrane indeed consists primarily of lipids and proteins that form *Lo* membrane domains. We provide evidence that many amphipathic membrane probes do not interact well with the membrane that is internalized. Only one probe tested, the fluorescent dye, FM 4-64, populates domains that internalize equally well as domains that remain at the cell surface, and no probe preferentially binds to domains that internalize. Thus, Ca-activated and amphipath-activated MEND indeed internalize membrane that contains primarily ordered lipid in its outer monolayer. The results provide further evidence that lipidic forces can drive physiological endocytic processes, although the identity of physiological MEND-promoting lipids remains to be established.

Methods and Materials.

BHK cell maintenance and electrical methods were as described in companion articles (Fine et al., xxxx; Lariccia, xxxx). Solution velocities were at least 3 mm per s in experiments without imaging and about 1 mm per s in experiments with imaging. Confocal imaging was carried out as described previously (Yaradanakul et al., 2007) with a Nikon TE2000-U microscope and a Nikon 60x 1.45 NA oil immersion objective. A 40 mW Spectra Physics 163-CO2 laser was used for 488 nm excitation (i.e. for Bodipy, NBD, ANEPPDHQ FM dye). Time lapse images were recorded either at 160x160 or 256x256 resolution with an approximately 400-800 ms total exposure time. The routine exposure interval was 3 seconds. However, when fluorophore lability was evident (e.g. with NBD) imaging settings, frequency and experiment durations were adjusted to insure that photobleaching was negligible. Lasers were operated at 4% power with a detector pinhole setting of 100 μm and an average linear gain of 6.50. For 1-anilinonaphthalene-8-sulfonic acid (1,8 ANS) excitation was with a 175 Watt Lambda DG-5 Xenon light source (Sutter Instrument) with Chroma Technology Corp. filters set for excitation at 403/12 nm and emission at 460/40 nm. Data was collected using a Photometrics CoolSnap HQ and analyzed using Meta Imaging Series 6.1.

Solutions and materials. Solutions employed minimized all currents other than NCX1 current. Free Mg of all cytoplasmic solutions was 0.4 mM. Standard Extracellular Solution contained in mM: 120 LiOH, 4 $MgCl_2$ or 2 $MgCl_2$ + 2 $CaCl_2$, 20 TEA-OH, 10 HEPES, 0.5 EGTA, pH 7.0 with aspartate. The Standard Cytoplasmic Solution contained in mM: 80 LiOH, 20 TEAOH, 15 HEPES, 40 NaOH, 0.5 $MgCl_2$, 0.5 EGTA, 0.25 $CaCl_2$,

at pH 7.0 with aspartate. Unless indicated otherwise, 0.2 mM GTP was employed in nucleotide containing solutions. All lipids were dissolved in ethanol at concentrations of 0.1 to 1 mM, aliquoted in light-protected vials, and stored at -30°C. 1,2-distearoyl-sn-glycero-3-phosphoethanolamine -N- (7-nitro-2-1,3-benzoxadiazol-4-yl) was from Avanti Polar Lipids (18:0 NBD PE) (810141).1,2-Dipalmitoyl-sn-glycero-3-phosphoethanolamine-N- (7-nitro-2-1,3-benzoxadiazol -4-yl) was from Fluka Biochemika (16:0 NBD PE) (12019). N- (4,4-difluoro-5,7-dimethyl-4-bora-3a,4a-diaza-s-indacene-3-pentanoyl)sphingosyl 1-β-D-lactoside (C5 Bodipy Lactosylceramide) (D13951) and Bodipy FL C5-ganglioside GM1 (B13950) were from Invitrogen. 1-Anilinonaphthalene-8-sulfonic acid (1,8 ANS) was from Sigma-Aldrich. ANEPPDHQ was a gift of Dr. Leslie Loew (University of Connecticut, Farmington). Dipicrylamine (Aldrich, H1-210-2) was a gift of Dr. Wayne L. Hubbell, (UCLA, Los Angeles). Ditridecylphthalate (DTDP) was gift of Exxon Mobile Corporation.

Minimal description of the function hydrophobic ions. We employ hydrophobic anions and cations in this study to detect changes of membrane properties. Previous work (Andersen and Fuchs, 1975; Benz et al., 1976; Bruner, 1975; Pickar and Brown, 1983) provides a firm basis to understand their function in membranes, including biological membranes (Chanda et al., 2005). DPA was used previously as a novel means to 'amplify' capacitive signals associated with exocytosis (Oberhauser and Fernandez, 1995) As illustrated in Fig. 1A, hydrophobic anions, such as tetraphenylborate and dipicrylamine, bind with high affinity beneath phospholipid head groups of the membrane. They translocate reversibly across 70 to 80% of the membrane electrical field at rates 100 to 10,000-fold greater than they dissociate from membranes, and as a result they increase the effective membrane capacitance (Andersen and Fuchs, 1975). For DPA, translocation rates are in the range of 10 to 30 thousand per s (Lu et al., 1995). In conventional whole-cell voltage clamp, therefore, DPA capacitive signals occur with the time constant of voltage clamp (0.2 to 2 ms). Hydrophobic cations (see lower cartoon in Fig. 1A), such as TtPP and TPP's, bind to the membrane with lower affinity and generate current by translocation slowly across the membrane electrical field. These different patterns form the primary evidence for a large positive dipole potential in the interior of the membrane that promotes binding of hydrophobic anions while hindering binding and translocation of hydrophobic cations (Flewelling and Hubbell, 1986).

Analysis of hydrophobic anion function in bilayers reveals a complex translocation process (Andersen and Fuchs, 1975). Nevertheless, it is adequate for this article to assume that hydrophobic ions exist as two populations in the membrane. They bind and dissociate in a nearly voltage-independent fashion, and they translocate across electrical field over a single barrier,

$$(1) \qquad dX_o/dt = X_{out} \cdot k_{ao} + X_i \cdot K_b - X_o \cdot (k_{do}+k_f)$$

$$(2) \qquad dX_i/dt = X_{in} \cdot k_{ai} + X_o \cdot K_f - X_i \cdot (k_{di} +k_b) \ ,$$

where X_o and X_i are the amounts of hydrophobic ion associated with the outer and inner monolayers, and X_{out} and X_{in} are the free concentrations of hydrophobic ion outside and inside the cell. In the absence of a membrane electrical field, k_{ao} and k_{ai} are the respective association constants, k_{do} and k_{di} are the respective dissociation constants, and k_f and k_b are the translocation rates from *out-to-in* and *in-to-out*, respectively. In constructing a model, voltage-dependent terms must be included to modify each of the constants so that the binding, translocation, and dissociation reactions move an ion through the entire membrane field. For DPA, translocation reactions reflect about 75% of electrical field. The fraction of membrane-bound anions on the cytoplasmic side (F_i) can therefore be approximated as

$$(3) \qquad F_i = 1/ (1+e^{(E50-Em) \cdot 0.75 \cdot F/RT}) \ ,$$

where E_{50} is the mid-point of the charge-voltage relationship. In cells employed here, the E_{50} ranges from -10 to -50 mV (see Fig. 6 and Supporting Fig. S1), implying that DPA has a higher affinity for the cytoplasmic versus the extracellular leaflet of the bilayer. Analytical solutions of equations 1 to 3 are given in Supporting Data with simplifying assumptions: For DPA, it is assumed that translocation reactions are instantaneous with respect to dissociation rates. For TPP's with low membrane affinity, it is assumed that binding/dissociation reactions reach a steady state instantly.

DPA current occurs as a step function with changes of DPA concentration, as illustrated in the left panel of Fig. 1B, if the dissociation rates on the extracellular and cytoplasmic sides are equal. If dissociation is faster at the outer membrane surface than at the inner surface, current declines partially upon applying DPA, and an inward current transient develops on removing DPA. If dissociation is faster on the cytoplasmic side, current shows an asymptotic increase upon applying DPA and an exponential declining phase upon removing DPA. As further illustrated in the left panel of Fig. 1B, DPA capacitive signals develop and decline to a steady state in proportion to DPA accumulated in the

membrane. This time course is determined by the dissociation constants and the distribution of DPA across the membrane (i.e. $F_i \cdot k_{di} + (1-Fi) \cdot k_{do}$). As illustrated in the right panel of Fig. 1B, the simplifying assumptions for TPP's give rise to an immediate inward current and no capacitive signal.

Relevant to several experimental results, we point out that in the simple models the unidirectional TPP flux from outside to inside does not depend on the dissociation rate on the cytoplasmic side. A decrease of dissociation rates on both membrane sides increases TPP influx by increasing the affinity on the outside. The same changes have no effect on DPA current but increase capacitive signals by promoting DPA partitioning into the membrane.

Figure 1C shows DPA signals recorded in BHK cells at 22˚C. On fast application and removal of DPA (2 μM) at 0 mV, a small steady outward membrane current turns on and off as rapidly as the cell can be manually switched between solution streams. C_m rises and falls approximately exponentially with time constants on the order of 0.5 s. The final return of C_m to baseline is however slow, reflecting accumulation of DPA within the cell. The upper record in Fig. 1C is the first derivative of the capacitance record. From the initial rate of rise of C_m (~80 pF/s) and the slope of the DPA charge-voltage relation at 0 mV (i.e. equation #3 with E_{50}=-30 mV; $dF_o/dEm \approx 6/Volt$), one can estimate the initial current required to build up the charge associated with the capacitance. In figure 1C, the DPA flux calculated from the capacitance signal amounts to 80 pF/s/6, i.e. 13 pA. Notably, the calculated flux is substantially smaller than the DPA current *per se*, which amounts to 22 pA. At 37˚C, this discrepancy was routinely about three-fold and often four-fold. Thus, the build-up of charge in the membrane and the DPA current measured are not well coupled. The explanation appears to be that a large part of the DPA current is generated by a mechanism different from the capacitive signals: First, as described in Supporting Fig. S2, DPA currents usually decrease substantially at lower temperatures, while capacitive signals change very little. Second, as evident in several results presented (e.g. Fig. 9A and Supporting Figs. S3 and S4), DPA currents change very little when DPA capacitive signals change by several fold.

Fig. 1D shows DPA capacitive signals obtained for application and removal of four different DPA concentrations in the same BHK cell. For concentrations of 2 to 40 μM,

the rising DPA signals can be scaled reasonably, but the falling signals reveal slowly decaying components at higher concentrations. For lower DPA concentrations, i.e. less than 2 μM, capacitive signals reach a near steady state more rapidly than with higher concentrations.

Figure 1E shows representative electrical signals for TPP's. In this example, hexyltriphenylphosphonium (C6TPP, 0.5 mM) is applied and removed twice. In contrast to DPA, capacitive signals are negligible and large inward currents (~ -0.4 nA) develop and decay with solution changes, as expected from the simple model. Over 2 to 4 s these currents typically decay by 5 to 15%. The time courses of current activation and deactivation are shown in better detail in Fig. 1F, whereby records of DPA, C6TPP and dodecyltriphenylphosphonium (C12TPP) currents are scaled to one another. For DPA and C6TPP, as well as other short-chain TPP's, currents reach 63% of steady state within 120 ms. As apparent in Fig. 1F, this time course was routinely longer for C12TPP.

The time courses of current activation and deactivation for DPA and C6TPP signals may reflect the mechanics of solution switches, diffusion through immobile water layers at the cell surface, or initial binding reactions at the cell surface. For the C12TPP signals, we describe in Supporting Fig. S2 that these time courses are strongly temperature sensitive and therefore probably reflect binding/dissociation reactions. We describe in Supporting Fig. S3 that concentration-absorbance relations for TtPP and C12TPP give no evidence for aggregation or micelle formation.

Assuming that time courses for DPA and C6TPP reflect diffusion through unstirred water layers at the cell surface, the maximal distances over which diffusion can be taking place are readily determined from diffusion simulations. The gray curve in Fig. 1F represents the time course of diffusion across a 10 μm thick water layer with a diffusion coefficient of 0.5×10^{-5} cm^2/s, as expected for molecules with molecular weights of 400 to 550. The rising and falling DPA and C6TPP currents are routinely as rapid, or more rapid, than this time course. As described next, these potential constraints allow us to calculate for each experiment a minimum flux that will be supported by diffusion.

Two potential pitfalls: Diffusion limitations and the disposition of DPA in experimental solutions. Physical limitations of diffusion up to the cell surface can potentially limit

hydrophobic ion fluxes, and concern is greatest for DPA because it is used in concentrations of only 2 or 3 μM. While we routinely observe a rapid flow of particles directly past cells, we cannot prove that the mechanics of solution changes determine the time course of current changes in these experiments. Therefore, we calculate for each experiment the minimum flux that can be supported by diffusion via Fick's Law. As demonstrated in Fig. 1F, current time courses in response to concentrations jumps indicate that maximal diffusional distances are 10 μm. The relevant area for the calculation is that of a sphere with the diameter of the cell, which corresponds to the cell surface area after strong MEND. When MEND is not activated in an experiment, the relevant area is assumed to be 40% of cell area. We assume a diffusion coefficient of $0.5 \cdot 10^{-5}$ cm^2/s and that 1 pF represents 100 μm^2 of membrane. Diffusional fluxes, converted to picoampere equivalents, can then be related to measured fluxes and expressed as a ratio. In the text and figures of this article we refer to the ratio of the minimal flux supported by diffusion to the measured hydrophobic ion current as a Diffusional Security Factor (DSF):

$$(4) \qquad DSF = Flux_{max} / Flux_{real},$$

where $Flux_{max}$ is the minimal flux supported by diffusion, and $Flux_{real}$ is the current generated by the hydrophobic ion of interest. A DFS of '1' indicates that the measured flux may be strongly limited by diffusion. As described in Results, DSF calculations for TPP's raise concern only for C12TPP, and this concern is subsequently alleviated by five lines of experimentation. The DSF for C6TPP (0.5 mM) in Fig. 1E is 50, effectively eliminating a role for diffusion restriction in currents generated.

The DSF for DPA in Fig. 1C is 3.6, indicating that diffusion might significantly limit DPA flux into cells. Therefore, we formally deemphasize results dependent on DPA fluxes in our presentation, but still point out the best argument against diffusion limitation: DPA flux into the cell membrane (i.e. $\Delta pF/\Delta t$) increased by a factor of 2 after Ca transients (Fig. 9), by a factor of 3 to 10 during cholesterol extraction (Fig. S11), and by a factor of 3 with membrane fluidizers (Fig. S12). This would not be possible if DPA fluxes were substantively limited by diffusion. Steady state measurements of DPA capacitive signals, with DPA on both membrane sides, to be presented, are diffusion-independent and support the same conclusions suggested by unidirectional fluxes.

Finally, we point out that DPA, like functionally similar oxonols (Plasek and Sigler, 1996), aggregates over time in experimental solutions. At concentrations of 2 to 20 μM, precipitation in experimental solutions is readily monitored as a loss of absorbance with half-times of 15 to 20 min. To effectively hinder precipitation, DMSO must be employed in the range of 20 volume percent, and we have chosen to work with maximally 2% DMSO. Furthermore, DPA and/or DPA precipitates bind to the Teflon solution lines employed in our experiments. As a result, free DPA concentrations become dependent on flow rate, whereby a step increase of flow unleashes DPA from the tubing walls. For these reasons, DPA solutions were prepared freshly before each experiment, and solution flow rates were carefully controlled. With these precautions, 10 to 20 DPA consecutive responses were highly reproducible over experimental times of >20 min. For the hydrophobic cations, similar issues have not arisen. As described for two cations in Supporting Fig. S5, concentration-absorbance relations are linear up to the millimolar range. The functional activities of TPP solutions were indefinitely stable.

Online Supplemental Material. The following supporting materials and data are provided on-line: Analytical solutions for the simple model of hydrophobic ion function described in Methods are presented. Supporting Fig. S1 demonstrates that Ca transients associated with exocytosis strongly increase DPA capacitive signals during continuous DPA application without a significant change of the DPA capacitance-voltage relation. Supporting Fig. S2 demonstrates that DPA currents are usually strongly temperature-dependent while DPA capacitive signals are not. Supporting Fig. S3 and S4 show that β-cyclodextrin treatments and benzyl alcohol strongly increase DPA capacitive signals, while DPA currents increase only little or not at all. Supporting Fig. S5 shows that concentration-absorbance relations for C12TPP and TtPP are linear over the concentration range of micromolar to the millimolar. Supporting Fig. S6 illustrates that a low concentration of NP-40 promotes Ca/high ATP-dependent MEND. Supporting Fig. S7 shows that Ca transients associated with exocytosis strongly promote cyclodextrin-induced loss of cell capacitance and the formation of channels by the phosphatidylethanolamine-binding antibiotic, duramycin. Supporting Fig. S8 demonstrates that C12TPP currents are strongly reduced by lowering temperature without affecting their insensitivity to MEND. Supporting Fig. S9 shows that C10TPP currents are similarly temperature-sensitive and are nearly unaffected by MEND at low temperature. Thus, insensitivity to MEND cannot be explained by diffusion-limitation of

TPP currents. Supporting Fig. S10 shows that C12TPP does not induce MEND from the cytoplasmic side. Supporting Fig. S11 shows that MEND is associated with larger decreases C6TPP currents at high versus low C6TPP concentrations. Supporting Figs. S12 to S14 document that DPA capacitive signals decrease less than C_m during all Ca-activated MEND protocols. Supporting Fig. S15 shows that extended treatment of cells with β-cyclodextrins can increase DPA capacitive binding signals by more than one log unit, and Supporting Fig. S16 shows that C6TPP currents and capacitive signals are also increased several fold by cyclodextrin treatment. Supporting Fig. S17 documents that ANEPPDHQ binding to BHK cells, determined optically, is unaffected by Ca/ATP-dependent MEND, and Supporting Fig. S18 demonstrates that capacitive binding signals for ANEPPDHQ are unaffected by MEND while FM 4-64 signals are strongly decreased.

Results

Experimental results are presented first that demonstrate functional coupling between amphipath- and Ca-activated MEND. Second, electrophysiological evidence is presented that both forms of MEND internalize membrane that does not bind well multiple electrogenic membrane probes. Third, we present data demonstrating that Ca transients, which do not immediately cause MEND, can strongly enhance the binding of electrogenic membrane probes. Finally, we present equivalent experiments for fluorescent membrane probes.

Amphipaths can mimic cholesterol in promoting MEND. Amphipathic compounds at low concentrations make cholesterol more available for oxidation by cholesterol oxidase and for extraction by cyclodextrins by binding in the membrane in a manner that is partially competitive with cholesterol (Lange et al., 2009). Thus, there is functional coupling between amphipaths and cholesterol. As described in an accompanying article (Lariccia, xxxx), cholesterol enrichment does not cause MEND under basal cell conditions. However, it strongly promotes Ca-activated MEND and effectively induces MEND after Ca transients subside, even several minutes thereafter. Figs. 2 documents these same properties for amphipathic compounds.

Figure 2 illustrates our routine observation that Ca transients causing exocytosis reduce the threshold concentrations of amphipathic compounds that cause MEND. The experiment described in Fig. 2A (>20 observations) employs a BHK cell with an ATP-free cytoplasmic solution. Initially, TX100 is without effect at a concentration of 80 μM, applied and removed twice for periods of 40 and 25 s. Activation of Ca influx by NCX1 for 15 s causes a 25% increase of C_m which, as usual in the absence of ATP, is stable over the duration of an experiment. Thereafter, the same detergent-containing solution that was without effect causes a rapid 50% MEND response. Fig. 2B illustrates the same result for the antineoplasitc, alkyl-lyso-lipid, edelfosine (van der Luit et al., 2007). A 25 μM concentration of edelfosine has no evident effect before a Ca influx episode. After a Ca influx episode, however, the same edelfosine-containing solution induces a MEND response amounting to >60% of the cell surface.

Figure 2C presents results for an amphipath that has no discernable effect before evoking a Ca transient, but then causes MEND in conjunction with the Ca transient (20 similar observations). The amphipath is a plasticizer, di-tridecylphthalate (DTDP), which has splayed alkyl chains. Thus, DTDP presumably interacts differently with membranes than detergents. DTDP is negligibly soluble in aqueous solutions (see MSDS). The extracellular solution employed in Fig. 2C contains 5 μM DTDP, prepared by sonication, and the cytoplasmic solution contains no ATP, GTP, or polyamines. The DTDP-containing solution has no discernable effect on C_m before activating a Ca transient, but Ca influx then causes MEND within seconds, similar to cholesterol enrichment (Lariccia, xxxx).

On the basis of these results, we conclude that the long-lived action of Ca to promote MEND (Lariccia, xxxx) extends to amphipathic agents. In Supporting Fig. S6, the facilitation of Ca-activated MEND by the presence of a low concentration of NP-40 is illustrated. In Supporting Fig. S7 it is demonstrated that the ability of cyclodextrins to decrease C_m by extraction of lipids is greatly enhanced by Ca transients, and it is demonstrated that the ability of a phosphatidylethanolamine-binding antibiotic, duramycin, to form ion-conducting channels (Navarro et al., 1985) in BHK cells is greatly enhanced after Ca transients. These results together suggest that large cytoplasmic Ca transients trigger mechanisms that modify the extracellular plasmalemma monolayer.

Insensitivity of electrogenic membrane probes to MEND. Next we document that membrane internalized in both amphipath- and Ca-induced MEND binds a variety of membrane probes relatively weakly. Figs. 3 and 4 describe results for amphipath-induced MEND, and Figs 5 to 8 describe results for Ca-activated MEND.

Figure 3A describes MEND induced by the hydrophobic cation, dodecyltriphenylphosphonium (C12TPP), which is also a detergent. Since C12TPP is a hydrophobic cation, it translocates across the membrane and thereby generates an inward current during its application. Using Standard Solutions (Lariccia, xxxx) with 2 mM ATP, C12TPP induces MEND in the concentration range of 20 to 50 μM. While other alkane detergents, SDS and dodecylglucoside (Fine et al., xxxx), cause MEND only when they are removed from the extracellular side, C12TPP (40 μM in Fig. 3A) induces MEND during its application to the outer cell surface. As apparent in the current record (lower record in Fig. 3A), C12TPP generates a 0.16 nA inward current during the 10 seconds required to cause MEND that amounts to 65% of the cell surface. Subsequent to inducing MEND, a second application of C12TPP causes an inward current of nearly the same magnitude. Even the partial current decay that occurs over time is similar before and after MEND.

As illustrated in the inset of Fig. 3A, steady state current-voltage relations for C12TPP were determined in five experiments by applying and removing C12TPP at multiple membrane potentials. Under the conditions of these experiments, current saturates with hyperpolarization, raising a concern that currents might be limited by diffusion. The following results speak against this possibility: First, the DSF for the experiment in Fig. 3A, as well as four equivalent experiments, is 6.6. Second, as shown in Supporting Fig. S8A, C12TPP currents are strongly temperature dependent, as are their activation/deactivation time courses. Thus, saturation of current with hyperpolarization probably reflects slow association kinetics of C12TPP with the outer plasmalemma monolayer. Third, as described in Supporting Fig. S8B, when C12TPP currents are recorded at 18˚C, versus 37˚C, currents are reduced more than three-fold but TX100-induced MEND does not cause a reduction of the C12TPP current. Fourth, as shown Fig. 3C and in Supporting Fig. S9, currents generated by the C10 analogue of C12TPP, decyltriphenylphosphonium (C10TPP), are also nearly unaffected by TX100-induced MEND, although DSF values are nearly a log unit higher. Fifth, as shown in Supporting

Fig. S9, steady state current-voltage relations for C10TPP are steep at l5˚C, although the currents are not reduced by TX100-induced MEND. Thus, diffusion cannot be limiting. We conclude that C12TPP and C10TPP bind at least five-times more effectively to membrane that remains at the cell surface than to membrane that is internalized in TX100-induced MEND.

Finally, in relation to Fig. 3A, we note that the total cytoplasmic C12TPP concentration reaches about 100 μM, as calculated from cell dimension and current magnitudes. Nevertheless, almost no outward current is generated upon removing C12TPP. Presumably, C12TPP that enters cells is mostly bound by membranes and constituents of the cytoplasm. We demonstrate in Supporting Data Fig. S10 that C12TPP, like other detergents (Fine et al., xxxx), does not cause MEND from the cytoplasmic side, even when perfused into cells at 8-times the effective extracellular concentration.

Equivalent experiments for TPP's having shorter side chains and for TtPP are described in Figs. 3B and 3C. As the alkyl chain is decreased in length, the analogues must be used at much higher concentrations to generate equivalent currents. Fig. 3B illustrates an experiment with butyltriphenylphosphonium (C4TPP, 10 mM) in which MEND was induced by TX100 (200 μM), and C4TPP currents were evaluated before and after MEND. On average, the C4TPP current amounts to -0.6 nA before and -0.54 nA after inducing a 65% MEND response. The current-voltage relation (see inset) is about one-half as steep as expected from the simple model. The DSF for the experiment is 1017. Thus, diffusional limitations can play no role in this shape or the relative insensitivity of C4TPP to MEND.

Figure 3C presents the composite results for the series of TPP's and for TtPP under the same conditions. Currents generated by 40 μM C12TPP were nearly unaffected by C12TPP-induced MEND. Currents generated by 130 μM C10TPP were nearly unaffected by TX100-induced MEND, while currents mediated by 0.5 mM C6TPP and 10 mM C4TPP were decreased by 26 and 14%, respectively. Thus, shorter side chains may allow TPP's partial access to membrane regions that are internalized. For TtPP (0.5 mM), access appears to be still greater. TtPP currents decrease by more than 25% when TX100-induced MEND amounts to 50%. Thus, the affinity of TtPP for membrane than internalizes appears to be only two fold less than for the remaining membrane.

That short TPP's may bind with low affinity to ordered membrane domains is not surprising. FM dyes, which are hydrophobic cations that do not translocate the membrane, bind rather evenly to membrane that does and does not internalize (Fine et al., xxxx). Furthermore, high concentrations of short chain TPP's can cause MEND in a pattern similar to the detergent, SDS (Fine et al., xxxx). During application of these compounds, C_m is stable and MEND occurs rapidly upon their wash-off. Possibly, this pattern reflects an inhibition of membrane fission by binding within the domains that subsequently internalize on wash-off. Regardless of details, all amphipathic membrane probes may be expected to gain access to ordered membrane domains as their concentrations are increased. Supporting Fig. S11 demonstrates that the fractional decrease of C6TPP current after TX100-induced MEND increases from 5% to 25% when the C6TPP concentration is increased from 50 μM (DSF, 32) to 1000 μM (DSF, 158). These results underscore that preferential binding of membrane probes to domains is likely to be highly concentration-dependent.

Figure 4A, and subsequently Fig. 7A, demonstrates that DPA signals are also relatively insensitive to MEND induced by TX100 (200 μM). The outcomes from experiment sets under different conditions range from modest sensitivity, as in Fig. 4A, to no sensitivity. To insure a DSF value of more than 4, this experiment series was performed at 22˚C. Furthermore, flow rates were increased until some cell deformation was evident. DPA (2 μM) signals were examined twice before and twice after inducing MEND with TX100 (200 μM). A decrease of C_m by 60% is accompanied by a decrease of DPA capacitive signals by 28%, a decrease of the DPA binding rate (i.e. dC_m/dt, upper trace) by 37%, and no change of the DPA current. DPA current increases by a factor of 2 when temperature is increased to 37˚C, demonstrating that DPA current is not limited by diffusion.

Figure 4B presents an equivalent experiment using the protonophore, CCCP (10 μM), to induce an outward current corresponding to outward proton transport in a cell with the Standard Solutions set to pH 6.5 and 7.8 in the cytoplasmic and extracellular solutions, respectively. The outward CCCP current, about 200 pA, develops and dissipates rapidly and stably upon applying and removing CCCP four times before and four times after

inducing MEND response with TX100 (200 μM). MEND results in a 51% decrease of Cm, while the CCCP current is decreased by only 13%.

Figure 4C shows composite data for DPA and CCCP from 5 and 6 similar experiments, respectively, together with equivalent data for three additional ionophores. On average, DPA capacitive signals decrease by 26% when C_m decreases by 50% in TX100-induced MEND, suggesting that DPA affinity for membrane that internalizes is about one-half of its affinity for membrane that remains at the cell surface. The composite results for CCCP are very similar. Currents and/or conductances generated by the ionophores valinomycin (25 μM), nonactin (12 μM), and nystatin (65 μM) are presented in the additional bar graphs in Fig. 4C. Each ionophore was applied to BHK cells for 15 s and then removed, similar to the protocols for DPA and CCCP. The conductance caused by each ionophore developed and washed out over the course of 10 to 40 seconds, similar to results in giant patches (Hilgemann and Collins, 1992). For valinomycin, solutions contained 40 mM K on both membrane sides, and cell conductance was used as indicator of ionophore activity. MEND caused by TX100 (120 μM) amounted on average to 50% of the cell surface, while the activities of ionophores were changed very little. Only the nystatin conductance was decreased detectably by MEND. Thus, multiple commonly employed ionophores appear to associate preferentially with membrane that does not internalize.

Electrogenic membrane probes are insensitive to Ca-induced MEND. Figure 5 presents records of Ca-activated MEND in which C6TPP currents were recorded before and after MEND with Standard Solutions at 37˚ (10 observations). Lower temperatures were not employed because the NCX1 transporter becomes strongly inhibited. To promote fast Ca-activated MEND in Fig. 5A, the cytoplasmic solution contained the polyamine, ethylenediamine (EDA, 2 mM), together with 2 mM ATP and 0.2 mM GTP. As indicated below the C_m and current records, C6TPP (300 μM) was applied and removed 5 times, generating each time an inward current about 0.3 nA in magnitude. After the first two C6TPP responses, reverse Na/Ca exchange current was activated by applying 2 mM Ca for 20 s. MEND occurs during Ca influx and amounts to 60% of C_m. Thereafter, the C6TPP current is decreased by only 15%. The DSF of this experiment is 70, thereby eliminating any influence of diffusion. Fig. 5B gives composite results for 5 similar

experiments. An average MEND response of 50% is accompanied by an average 12% decrease of C6TPP current.

Figure 5C presents an equivalent experiment in which high cytoplasmic ATP (8 mM) promotes progressive Ca-activated MEND without polyamines. In this experiment, Ca transients via reverse Na/Ca exchange were activated 4 times. Over the course of 3 Ca transients, separated by 2 minutes, 45% of the cell surface is lost. C6TPP (0.3 mM) was applied and removed 10 times during the observation period. C6TPP currents do not significantly decrease during the experiment, which has a DSF of 59.

DPA signals were often nearly unaffected by Ca-induced MEND with the potential caveat that experiments must be performed at 37˚C, giving rise to relatively large DPA currents and small DSF values of 3 to 4. In Fig. 6 an example is presented that illustrates how DPA capacitive signals are analyzed subsequently in the absence of DPA flux. In this experiment, the cytoplasmic solution contains 1 mM cytoplasmic spermidine with 2 mM ATP and 0.2 mM GTP to promote MEND during the Ca influx episode. As indicated, DPA (2 μM) was applied and removed twice before and twice after the Ca influx episode, which causes a 61% MEND response. During each application of DPA, voltage ramps were applied to determine the C_m-voltage relationship of DPA. Figs. 6B and 6C show C_m records before and after MEND, together with data fits to rising and falling exponential function. Fig. 6D shows the C_m-voltage relations for DPA from the voltage ramps, together with nearly invisible data fits to the first derivative of a Boltzmann function as dotted lines. The rising and falling signals in Figs. 2B and 2C have time constants from 0.67 to 0.82 s with no clear differences before and after MEND. The amplitudes and voltage midpoints of capacitance-voltage relations are only marginally changed. Thus, DPA signals are unaffected by MEND in this experiment. DSF=3.6.

Diffusion-independent DPA capacitive signals sense MEND weakly. We describe next that the apparent insensitivity of DPA signals to Ca-activated MEND may be exaggerated but because Ca transients cause a large increase of DPA binding that counteracts the influence of MEND. As illustrated by Fig 6D, DPA capacitive signals can be quantified in voltage pulse experiments without removing DPA from the cell. To do so, membrane voltage must be stepped to a potential at which the DPA capacitive signal is negligible,

and the drop of capacitance indicates the contribution of DPA to total capacitance. In this way, DPA capacitive signals can be studied with DPA on both membrane sides, thereby minimizing any influence of DPA diffusion on experiments. Since the mid-point of the DPA capacitance-voltage relation occurs at a negative potential, we step potential to a positive potential (+120 mV) every 8 s for 1.2 s. Since positive membrane potential drives DPA from the extracellular side to the cytoplasmic side, we employ a higher cytoplasmic concentration (6 μM) of DPA than extracellular concentration (2 μM). With these conditions, total cell capacitance is stable over experimental times of 5 to 15 min.

Figure 7A shows results of this protocol for TX100-induced MEND, and Fig. 7B shows results for Ca-induced MEND. Four similar experiments were obtained for each MEND type. In Fig. 7A, TX100 (200 μM was applied twice and removed twice to induce a maximal MEND response. The decline of C_m (see dotted line) amounted to 46%. As in all experiments with this protocol, DPA capacitive signals defined by a positive voltage pulse did not decline at all. Thus, under these conditions DPA capacitive signals are more insensitive to TX100-induced MEND than in Fig. 4.

In Fig. 7B, Ca influx by NCX1 was activated twice in the presence of 8 mM cytoplasmic ATP to initiate Ca/ATP-dependent MEND. At the first Ca influx episode, the DPA capacitive signal increases nearly 4-fold in parallel with a 20% increase of C_m. This super-proportional increase of DPA capacitance is consistent with the fact that Ca transients enhance the ability of multiple amphipaths to induce MEND (Fig. 2). As described subsequently, Ca transients also strongly enhance the partitioning of other membrane probes into the membrane. After the second Ca influx episode, MEND occurring over 1 min amounts to 60% of cell capacitance. During MEND, the DPA capacitive signal decreases from 71 pF to 55 pF: The 60% decrease of membrane area results in a 20% decrease of the DPA capacitive signal. In reasonable agreement with results for TX100 MEND in Fig. 4A, DPA binds in these experiments with approximately three-fold lower affinity to membrane that internalizes than to membrane that does not internalize.

Supporting Data Figs. S12-S14 present experiments that examine DPA signal changes with each Ca-activated MEND protocol described previously (Lariccia, xxxx). Fig. 8 gives the average normalized membrane capacitance (C_m), DPA currents (I_{DPA}), and DPA

capacitive signals (C_{DPA}) from 3 experiments for each protocol. All DPA signals are normalized to magnitudes before the indicated events (left-most bars = 100%). From left to right, the second set of bars summarizes that Ca influx by NCX1 caused on average a 25% increase of C_m in cells that did not undergo immediate MEND (i.e. cells without ATP). The increase of C_m was accompanied by a 3-fold greater increase of DPA capacitance and a 25% increase of DPA current. When high ATP (8 mM) was included in cytoplasmic solutions (3rd group of bars), promoting delayed MEND, the DPA capacitive signals and DPA currents reversed *on average* to baseline, while cell capacitance decreased to 50% below baseline. These results are consistent with experiments just outlined: DPA must bind to membrane that internalizes with two- to three-fold lower affinity than to membrane that remains at the cell surface. In response to Ca influx in the presence of polyamines (4th set of bars), both DPA currents and capacitive signals remain *on average* increased after more than 50% of cell area is lost. This increase reflects with good certainty the long-term effect of Ca on the outer monolayer. Similarly, Ca influx after cholesterol loading with HPCD-cholesterol complexes causes, overall, three- to four-fold smaller reductions of DPA signals than reductions of cell area. When cholesterol is enriched *after* a Ca transient, cholesterol-induced MEND causes a 70% loss of cell area with only a 15% loss of DPA capacitive signal. In this case, the membrane internalized (i.e. cholesterol enriched membrane) evidently has a five-fold lower affinity for DPA than membrane remaining at the cell surface. This outcome is consistent with Supporting Data Fig. S15 which demonstrates that cholesterol extraction can increase the affinity of the plasmalemma for DPA by at least one log unit.

Ca transients cause increased membrane disorder that is sensed by multiple membrane probes. As described above, DPA capacitive signals are strongly increased by large Ca transients, and Fig. 9A demonstrates that DPA binding rates are increased while DPA dissociation rates are decreased. In this experiment, DPA (2 μM) was applied for 5 s and removed before and after a Ca influx episode in the absence of cytoplasmic nucleotides. C_m increases by 66% during the Ca transient and is stable after Ca influx is terminated. Although the DSF of the experiment is only 2.2, the rate of rise of DPA capacitance (i.e. dC_m/dt, upper trace) is nearly doubled after the Ca transient (>20 similar observations). The magnitude of the capacitive DPA signal is increased 3.5 fold, and it decays more slowly upon removal of DPA. While decay of the DPA signal before fusion is reasonably

described by one exponential function (τ = 1.1 s), two exponentials are required after membrane fusion (τ's= 2.6 and 8.8 s). In summary, Ca transients strongly increase partitioning of DPA into the membrane, as expected for DPA binding in a more disordered membrane (Smejtek and Wang, 1990). In Supporting Data Figs. S3, S4, and S15, we show that β-cyclodextrins and a fluidizing agent strongly increase DPA binding, consistent with signal changes in Fig. 9A reflecting increased membrane disorder.

Figure 9B shows the equivalent changes of C6TPP signals (0.3 mM) routinely observed in response to Ca transients under the same conditions. In contrast to DPA, the C6TPP current increases by more than two-fold when membrane area increases by only 30%. As noted in Methods, a decrease of dissociation rates on both membrane sides will increase C6TPP currents but not DPA currents. After the Ca influx episode, capacitive signals become evident on applying and removing C6TPP (20 observations). In Supporting Fig. S16, we describe that β-cyclodextrin treatments cause very similar changes of C6TPP currents, consistent with signals in Fig. 9 reflecting increased disorder.

As described in Fig. 9C, results for the styryl dye, ANEPPDHQ document further that Ca transients cause increased disorder in the outer monolayer: This dye undergoes large fluorescence shifts in cholesterol rich versus cholesterol poor membranes (Jin et al., 2006). As indicated in Fig. 9C, ANEPPDHQ (8 μM) was applied and removed multiple times before and after activating Ca influx multiples times in cells with no cytoplasmic nucleotides. Fluorescence was monitored in a bandwidth of 500 to 580nm (black) and above 640nm (grey). In response to multiple Ca influx episodes, C_m increases by 2-fold, and ANEPPDHQ fluorescence increases over-proportionally. The long wavelength component (640LP) and its rate of rise increase by 3-fold, whereas the shorter wavelength component (500-580) increases only 30%, as would be expected for increased disorder (Jin et al., 2006).

Other anionic membrane probes: Niflumic acid (NFA) does not sense MEND. Since DPA gains partial access to the membrane that internalizes in MEND, we tested whether other anionic membrane probes might bind more specifically to either the membrane fraction that internalizes or does not internalize. Among probes tested, the chloride channel blocker, NFA (Hogg et al., 1994), was notable because it generates a large

capacitive binding signal that does not involve translocation of charge across the bilayer. As described in Fig. 10, NFA binding to the outer monolayer is insensitive to MEND.

Figure 10A illustrates the capacitive binding signal generated by rapid application and removal of NFA (0.2 mM) using a BHK cell with Standard Solutions with 2 mM ATP and 0.2 mM GTP. C_m increases monotonically by about 13% upon applying NFA and recedes toward baseline in two distinct phases upon its removal. As with detergents, the capacitance signal may reflect lateral expansion and thinning of the membrane. Since the magnitude of the NFA signal is unusually large, however, it cannot be excluded that NFA enters partially into the membrane's electrical field. As shown in Fig. 10B, the NFA capacitive binding signal is only weakly voltage-dependent. Figs. 10C and 10D demonstrate that the capacitive binding signal of NFA is unaffected by TX100-induced MEND and Ca-induced MEND in the presence of polyamine (EDA, 2 mM on both membrane sides), respectively. As shown in Fig. 10E, NFA signals increase roughly in proportion to cell capacitance when Ca influx causes exocytosis without subsequent endocytosis (i.e. without cytoplasmic nucleotides or polyamines). The NFA signal can then be further increased by subsequent Ca transients, although membrane area does not increase.

Most optical membrane probes sense MEND only weakly. In contrast to ANEPPDHQ fluorescence changes in response to Ca transients (Fig. 9C), Fig. 11 demonstrates that the binding rates and spectral properties of ANEPPDHQ dye are nearly unchanged by MEND, caused either by TX100 or Ca influx. Fig. 11A illustrates an experiment monitoring ANEPPDHQ fluorescence before and after TX-100-induced MEND, as well as its potential uptake during MEND. ANEPPDHQ dye (8 μM) was applied and removed multiple times to establish its binding-dissociation characteristics. As demonstrated by the micrographs, the cell membrane labeled and unlabeled consistently with application and removal of dye. During the second application of dye, TX100 (150 μM) was applied together with dye for 10 s, resulting in MEND that amounts to >70% of the cell surface. After washout of dye for 25 s, the residual fluorescence is only 10% higher than before MEND (see grey lines). The lack of dye retention is in complete disparity to the large MEND response. Furthermore, upon applying dye again after MEND, it is evident that the rate of dye binding is nearly unchanged.

In experiments presented in Figs. 11B and 11C, ANEPPDHQ fluorescence was monitored in two wavelength bands, as in Fig. 9C, before and after inducing MEND with TX100 (180 μM). MEND results in no spectral shifts of the dye, and the apparent rates of dye binding are unchanged by MEND. We stress that in Fig. 11C dye loading comes nearly to a steady state. Thus, limitations of dye access to the membrane, i.e. diffusional limitations, cannot explain the failure of MEND to affect dye loading. Similar results for Ca-activated MEND that is ATP-dependent are presented in Supporting Data Fig. S17. We conclude that, in contrast to FM dyes (Fine et al., xxxx), ANEPPDHQ does not associate well with the membrane that is internalized during MEND (i.e. > 50% of the cell surface). As expected from these optical results, Supporting Data Fig. S18 shows that the capacitive binding signal of ANEPPDHQ does not decrease with MEND, whereas the capacitive binding signal of FM 4-64 does decrease.

Figure 12 documents that other fluorescent membrane probes are also largely excluded from domains that are internalized during MEND, while a head group-labeled phosphatidylethanolamine (C16/18 NBD-PE) shows an intermediate behavior. Similar to experiments shown in Fig. 11, fluorescently labeled lipids and membrane dyes were applied and removed from BHK cells multiple times before and after MEND was induced by TX100 (150 μM). Their binding rates, assumed to be proportional to the rate of rise of fluorescence, are related to capacitance loss by TX100-induced MEND. Several classes of lipids and probes were employed. As shown in Fig. 12A, a short chain ganglioside C5-GM1 labeled with Bodipy, traditionally a marker for glycosphingolipid enriched rafts, binds at the same rates before and after induction of a 50% MEND response by TX100. Unlike FM 4-64, the Bodipy GM1 probe washes off only very slowly. As shown subsequently, however, the difference in dissociation rates cannot explain why the binding of C5-GM1 is unchanged by MEND. We note that in multiple experiments the wash-off rates of this dye became greater after MEND.

Head group-labeled NBD-C16-phosphatidylethanolamine (NBD-PE) is an optical probe that might preferentially associate with ordered membrane owing to its straight side chains and relatively small head group. Although the effective use of this probe is limited by its low solubility, we could establish conditions with 10% DMSO that generated consistent, homogeneous labeling of cells. Using 5 μM NBD-PE, Fig. 12B

shows that NBD-PE labeling is indeed reduced in rate after TX-100-induced MEND. However, its binding is clearly not preferentially decreased.

Figure 12C shows composite results for most fluorescent probes employed. The binding rate of FM 4-64 decreases nearly in proportion to membrane area. Binding of the probe, 1-anilinonaphthalene-8-sulfonic acid (1,8 ANS), at concentrations of 100 to 300 μM, decreased by 20% on average with MEND responses amounting to 50% of the cell surface on average. The NBD-PE probe showed intermediate sensitivity to MEND, the average percent decrease of NBD-PE binding being about one half the average percent decrease of membrane area in response to MEND. Probes that were insensitive to MEND include ANEPPDHQ, C5-bodipy GM1, and C5-lactosylceramide.

Discussion

Multiple electrogenic and optical membrane probes have been used to analyze changes of the physical properties of the plasma membrane in cells undergoing large endocytic responses (MEND). Massive internalization of membrane, caused by Ca transients or amphipathic compounds, leave the binding and/or activities of several membrane probes relatively unaffected. In contrast, Ca transients that do not trigger endocytosis cause membrane changes that strongly promote the binding of many membrane probes (e.g. Figs. 8, 9, 10 and Supporting Figs. S1, 7, and 12), and this increased binding can reverse partially during subsequent endocytosis. Except for FM dyes, however, signals from membrane probes decrease proportionally much less than cell area during endocytic responses analyzed in this article.

These results together provide a new line of evidence for the existence of lipid domains in living cells (Lingwood and Simons, 2010). The results suggest that more than 50% of the outer monolayer is ordered, and they suggest an order of affinities for diverse membrane probes in *Lo* versus *Ld* membrane domains (see Fig. 13), discussed subsequently. Most importantly, the results provide support for a profound functional role of lipid domains. Cells can potentially regulate large endocytic responses by relatively small modifications of the membrane lipid composition with endocytosis being driven by lipidic forces.

The long-term mechanism by which Ca promotes amphipath-activated MEND. In a companion article, it is described that a large Ca transient enables ATP, PIP_2, cholesterol and a second Ca transient to subsequently cause MEND (Lariccia, xxxx). Here, these observations are extended to amphipathic compounds, namely TX100, edelfosine, and DTDP (Fig. 2). These compounds all cause MEND at lower concentrations after a Ca transient than before the Ca transient. Ca transients act as if they generate more binding sites for these amphipathic agents, and this functional interpretation is physically verified by hydrophobic ion signals, as well as optical signals: Binding of DPA and ANEPPDHQ increase several fold more than membrane area in response to a Ca transient (Figs. 7B, and 9). Hydrophobic cation currents are similarly facilitated, and the fluorescence spectrum of ANEPPDHQ shifts as expected for a more disordered membrane (Fig. 9C). In addition, β-methylcyclodextrin (BMCD) extracts cholesterol and phospholipids more readily, and the phosphatidylethanolamine-binding antibiotic, duramycin, generates ion channels more readily after a Ca influx episode (Fig. S7).

Two interpretations are possible: The entire extracellular monolayer may exist in a relatively ordered state that becomes disrupted by processes associated with Ca transients with the new generation of disordered domains. Alternatively, the outer monolayer transitions from a more homogeneous state to a more phase-separated state in which disordered regions become more disordered and ordered regions more ordered. The second explanation is more consistent with the most current hypotheses about membrane ordering (Lingwood and Simons, 2010). To prove this, however, membrane probes will be required that can report more specifically the state of ordered versus disordered membrane domains.

Ordered domains in the plasmalemma are thought to be substantially smaller than required to form a vesicle (de Almeida et al., 2005; Edidin, 2003; Kenworthy, 2005; Lingwood and Simons; Lingwood and Simons, 2010). Since 50 to 70% of the outer monolayer can be internalized during MEND with little effect on several membrane probes, the more ordered membrane domains must constitute at least one half of the cell surface. This estimate is only marginally greater than some previous estimates (e.g.(Gidwani et al., 2001)), and it begs the idea that ordered domains form an interconnected patchwork. Contact points between ordered domains may represent points of pending coalescence. As suggested previously (Fine et al., xxxx), internalization of

ordered membrane requires that disordered domains form 'caps' and ordered domains segregate into valleys.

The differential sensitivities of membrane probes to MEND. Data sets for electrogenic probes, fluorescent membrane probes, and other amphipaths that generate capacitive signals give a consistent picture (see Fig. 13): Binding of the majority of probes is affected relatively weakly by MEND, or not at all, independent of MEND type. From more than 20 small molecule amphipaths that we have examined by electrical and/or optical measurements, no probe was found to bind selectively to membrane that internalizes. In two cases, both optical and electrophysiological signals could be analyzed and were found to be in good agreement: The capacitive binding signal for ANEPPDHQ does not decrease with MEND, similar to optical signals, whereas the capacitive binding signal for FM 4-64 does decrease, similar to optical signals (Fig. S18).

In the TPP series (Fig. 3), C12 and C10 alkyl chains hinder association with the membrane that internalizes in comparison to C6 and C4 chains. The strongest apparent association with internalizing membrane is obtained when the alkyl chain is replaced by a phenyl group in TtPP. A similar principle holds for FM dyes in comparison to the structurally similar ANEPPDHQ dye. ANEPPDHQ, which does not bind well to membrane that internalizes, has longer side chains and a bulkier hydrophobic core than FM dyes. The hydrophobic anion, NFA, is small, similar to FM dyes, but it has in contrast little or no access to membrane that internalizes (Fig. 10). Thus, charge may play a role in the segregation of membrane probes to domains. From the probes employed, cationic amphipaths that do not penetrate deeply have the best apparent access to ordered membrane domains. A potential caveat in this conclusion is that electrogenic membrane probes would be expected to show MEND sensitivity if they preferentially translocate between monolayers at the interface between domains.

For multiple reasons, DPA appeared to be a promising probe to analyze membrane heterogeneity in relation to MEND: Dissociation of DPA from membranes shows multiple components, DPA binding and dissociation are highly cholesterol- and Ca-dependent (Figs. S1, S3, and S15), DPA naturally interrogates both membrane monolayers, and DPA can be used as a voltage-gated fluorescence quencher (Chanda et al., 2005). After substantial efforts, however, the utility of DPA for the goals of this

article appears limited: Its partitioning into disordered membrane is not selective enough to be a reliable probe for disordered membrane. Depending on the experimental protocol, the apparent partitioning of DPA to membrane that internalizes is as high as 30% or less than 10% (Fig. 4A versus 7B, and Fig. 6 versus 7B). Its translocation rates, which may well be different in *Lo* versus *Ld* membrane regions, or in interfacial regions, are too rapid to measure in whole-cell voltage clamp, and the DPA-generated current is enigmatic. Finally, diffusional limitations cannot be discounted when DPA flux is occurring (e.g. Fig. 6). Equivalent probes with lower membrane affinity and lower translocation rates would be highly advantageous, and oxonols are the obvious candidates for future efforts (Plasek and Sigler, 1996).

Most of the optical probes employed here have been used in studies of artificial membranes in *ordered* and/or *gel* states versus *disordered* states. Several results suggest that *Lo* domains in cells employed here are more ordered than *Lo* phases in simple model membranes that develop phase separations. The dye, ANEPPDHQ, which senses ordered versus disordered domains in artificial membranes (Jin et al., 2006), is not able to occupy the cell surface that internalizes with MEND. In a simple two-phospholipid system, the NBD-phosphatidylethanolamine employed here partitions into ordered phases with two-fold preference (Mesquita et al., 2000). In our experiments, NBD-PE binding decreases by 22% *on average* when 50% of the cell surface internalizes (Fig. 12C). Thus, the affinity of this probe for membrane that remains at the cell surface is about two-fold higher than for membrane that internalizes. Its relative preference for ordered versus disordered membrane is reversed from the two-component membrane, perhaps reflecting the increased order imposed by a high cholesterol content in the BHK cell membrane.

Lactosylceramide is used to follow uptake of membrane via caveolae-based endocytosis (Sharma et al., 2005). That its uptake is little affected by MEND underscores that MEND does not represent internalization of caveolae. The bodipy-GM1 probe would generally be expected to incorporate into membrane domains that participate in endocytosis with cholera toxin, the best-defined lipid-based sorting pathway to date. It is not significantly internalized during MEND. Consistent with our results, it has recently been shown that the *raft domains* into which GM1 segregates are distinct, and necessarily smaller, than the overall *Lo* phase of cell membranes (Kaiser et al., 2009).

As noted already, only FM 4-64 reports quantitatively a loss of membrane equivalent to C_m changes during MEND (Fine et al., xxxx), and the capacitive binding signal of FM 4-64 decreases with MEND (Fig. S18). In our view the identification of membrane probes that can bind more selectively to *Lo* domains are a prerequisite for progress in understanding the role of *Lo*-domain-dependent endocytosis in cells. An ideal probe would bind and unbind quickly, could be monitored by both optical and electrical methods, and would not hinder fission of *Lo* domains.

In summary, Ca- and amphipath-activated MEND appear to share a common lipidic basis, the reorganization of lipid domains in a manner that *Lo* membrane domains become internalized. That amphipaths effectively induce MEND at relatively low temperatures (Figs. S8 and S9) is consistent with membrane phase transitions (e.g.(Levental et al., 2009)) playing a key role, as opposed to complex biochemical processes. Possibly, MEND represents an evolutionarily primitive form of endocytosis that developed in parallel with lipid metabolism. Its high sensitivity to lipid composition may have both pharmacological and toxicological implications. That Ca-activated MEND can be promoted with high affinity by a phthalate plasticizer (Fig. 2C) might be relevant to phthalate toxicity to the immune system (Shigeno et al., 2009). More relevant to this study, phthalates or related amphipaths may be useful to manipulate Ca-activated MEND and thereby better define its roles in physiological cell functions.

Acknowledgements

This work was supported by RO1-HL067942 and HL513223 to DWH. We thank Mei-Jung Lin for technical assistance and Dr. Leslie M. Loew (U. Conn., Farmington) for the generous gift of ANNEPPDHQ. We express heartfelt gratitude to Dr. Olaf S. Andersen (Weill Med. Col., New York) for criticism, advice, discussions and encouragement.

Figure Legends.

Figure 1. The function of hydrophobic anions and cations. **(A)** Hydrophobic anions translocate reversibly through the hydrophobic core of the membrane much faster than they dissociate from the membrane. Hydrophobic cations translocate slowly across the membrane in relation to their dissociation rates from the membrane. A positive dipole potential within the membrane is assumed to promote anion binding over cation binding by several hundred fold. **(B)** Predictions of simple models of hydrophobic ion function. When applied rapidly to membranes, hydrophobic anions give rise to a capacitive signal that develops with the time course of their binding/dissociation from the membrane. The net current generated by their passage through the membrane field ('Flux') develops immediately. By contrast, hydrophobic cations do not generate a capacitive signal. (**C)** DPA capacitive signals and currents in BHK cells using Standard Solutions with 2 mM ATP and 0.2 mM GTP on the cytoplasmic side. Rapid application and removal of DPA (2 μM) causes an immediate outward current and a slowly rising capacitive signal which decays toward an increased baseline upon DPA removal. The major time constant of the rising and falling signals is 0.35 s. The DSF, i.e the ratio of minimum diffusional flux to current, is 1.8. **(D)** DPA capacitive signals on applying and removing different DPA concentrations in the same BHK cell. The signals are scaled to allow comparison of the wave forms. With low DPA concentrations, capacitive signals come to a steady state more rapidly than with high concentrations (>2 μM), and slowly decaying signal components become more pronounced with high DPA concentrations. **(E)** Currents and capacitance records for application and removal of the hydrophobic cation, C6TPP (0.5 mM). Capacitance changes are negligible in relation to those evoked by DPA. **(F)** Normalized current records showing the time courses of current activation and deactivation upon applying and removing DPA (2 μM), C6TPP (0.5 mM) and C12TPP (25 μM). The gray curve shows the expected time course for diffusion through a 10 μm solution layer with a diffusion coefficient of $0.5 \cdot 10^{-5}$ cm^2/s.

Figure 2. Amphipath-induced MEND is facilitated by Ca transients associated with exocytosis. Cytoplasmic solutions are ATP- and GTP-free. **(A)** As with many other amphipaths that induce MEND, the threshold concentrations needed to induce MEND by TX100 are reduced by a Ca transient associated with exocytosis. In this example, TX100 (80 μM) was applied twice before activation of Ca influx, and it is without effect. After Ca influx and exocytosis, the same TX100 concentration causes a rapid 50%

MEND response. (**B)** Similar to TX100, a low concentration of edelfosine (30 μM) is without effect before activation of Ca influx. After a Ca influx episode, the same edelfosine concentration causes a 65% MEND response. **(C)** DTDP-saturated extracellular solution (5 μM, sonicated for 5 min) is without effect when applied for 5 min before activation of reverse Na/Ca exchange. Subsequent activation of Ca influx by NCX1 causes a rapid 60% MEND response.

Figure 3. Insensitivity of TPP currents to MEND. BHK cells using standard solutions with 2 mM ATP and 0.2 mM GTP on the cytoplasmic side. (**A)** Rapid application of extracellular solution containing 40 μM C12TPP causes an immediate 0.2 nA inward current and a MEND response amounting to 70% of C_m within 15 s. Thereafter, renewed application of C12TPP generates an inward current of similar magnitude but no further loss of C_m. DSF=6.6. (**B)** Rapid application of 10 mM C4TPP induces an inward current of 0.6 nA. After induction of a 63% MEND response with TX100 (200 μM), the C4TPP current is reduced by only 12%. on average. DSF=1017. (**C)** Normalized results (n=5) for the same protocols using C12TPP (40 μM), C10TPP (0.12 mM), C6TPP (0.25 mM), C4TPP (10 mM) and TtPP (0.5 mM). The average MEND responses ranged from 45 to 57%. The average current decrease was 10% for C12TPP, 15% for C10TPP, 26% for C6TPP, 17% for C4TPP, and 31% for TtPP. Slopes of current voltage relations and average DSP values are given below the bar graphs for each agent.

Figure 4. DPA and multiple ionophores show low sensitivity to TX100-promoted MEND. BHK cells with Standard Solutions containing 2 mM ATP and 0.2 mM GTP on the cytoplasmic side. **(A)** DPA (2 μM) is applied twice before and twice after induction of MEND by TX100 (200 μM). 22˚C. DSF=4.4. MEND amounts to 54% of C_m, while the capacitive DPA signals decrease by 28%. DPA currents are unchanged by MEND but double upon warming to 37˚C. **(B)** CCCP (10 μM) is applied and removed four times before and four times after inducing MEND with TX100 (200 μM). To generate outward proton transport the cytoplasmic solutions was set to pH 6.5 and the extracellular solution was set to 7.8. A 51% MEND response results in a 13% decrease of the CCCP current. **(C)** Composite results for several electrogenic membrane probes. In all cases, TX100 causes an approximately 50% loss of C_m. DPA capacitive signals (n=5) and CCCP currents (n=6) are decreased by 25% on average. The conductance's induced by nonactin (12 μM; n=4) and valinomycin (25 μM; n=4) are increased on average by 15

and 27%, respectively, after TX100-induced MEND. The conductance induced by nystatin (65 μM; n=4) application and removal is decreased by 15% (n=4).

Figure 5. C6TPP currents are nearly unaffected by Ca-induced MEND. C6TPP (0.3 mM) is applied briefly multiple times in each experiment, as indicated. (**A)** The polyamine, EDA (2 mM), is included in both the cytoplasmic and extracellular solutions to promote rapid MEND (50% in 5s) during Ca influx by NCX1. Thereafter, C6TPP current is decreased by 12% on average. DSF=50. (**B)** Composite results for 4 experiments similar to 'A'. Ca-activated MEND causes a 50% loss of C_m, while C12TPP currents decrease by just 10%. **(C)** Using a cytoplasmic solution with 6 mM ATP and no polyamine, Ca influx by NCX1 is activated four times. C_m decreases substantially in a delayed fashion after each of the Ca influx episodes, resulting finally in a 45% decrease of C_m. C6TPP currents (0.3 mM) are unchanged. DSF=41.

Figure 6. Analysis of DPA capacitive signals before and after MEND induced by a Ca transient in the presence of spermidine (1 mM) and 6 mM ATP. MEND amounts to 68% of C_m. DSF=4.0. **(A)** DPA (2 μM) is applied twice before MEND and twice after MEND for times of 6 to 10 s. During each application of DPA, voltage is stepped to -150 mV and then ramped to +80 mV to determine the capacitance-voltage relation of DPA. **(B and C)** Capacitance records indicated by 'before' and 'after' in 'A'. The magnitudes of DPA capacitive signal and the time constants of the rising and falling signals (0.67 to 0.82 s) are not detectably changed. **(D)** The magnitudes of DPA capacitance-voltage relations are not detectably changed; the peak capacitance undergoes a small 8 mV shift to more negative potentials.

Figure 7. Steady state DPA capacitive signal changes in response to TX100- and Ca-induced MEND. BHK cells with Standard Solutions, 8 mM cytoplasmic ATP, 2 μM extracellular DPA and 6 μM cytoplasmic DPA. The DPA- and membrane-related capacitance components are determined by applying voltage pulses to +120 mV for 1.3 s. Membrane capacitance does not depend on voltage, while the DPA capacitance becomes negligible at +120 mM. Membrane capacitance is demarcated by a dotted line. **(A)** TX100-induced MEND. On first application of TX100, MEND amounts to just 50% of the initial cell area. The DPA capacitive signal, defined by the downward deflections of

capacitance, is unchanged by MEND. After a second application of TX100, DPA capacitive signals increase slowly by 20% with respect to the pre-MEND magnitude. **(B)** Ca-induced MEND with high (8 mM) ATP and no polyamine in response to two Ca transients. The first Ca transient causes exocytosis without subsequent endocytosis. Cell capacitance increases by 20% whereas the DPA capacitive signal increases by nearly 3 fold. The second Ca transient causes little further exocytosis and a delayed MEND response amounting to 60% of the cell surface. The DPA capacitive signal decreases in parallel by 20%.

Figure 8. Summary of changes of DPA signals in response to a single Ca influx episode and multiple Ca-dependent MEND protocols. Examples of each experiment type are presented in Supporting Data Figs. S12 to S14. Each bar set gives give the average of 3 or more experiments for cell capacitance, DPA capacitance, and DPA currents, normalized to their initial experimental values (left-most bar set). From left to right, Ca influx causes on average a 3-fold greater increase of DPA capacitance than cell capacitance, and a small increase of DPA current. After Ca influx, the presence of high ATP in the cytoplasm causes a return of DPA capacitance and current to baseline, while cell capacitance decreased to 50% below baseline. Polyamine/Ca-induced MEND causes on average an increase of DPA capacitance and current, while cell capacitance decreases to 55% below baseline. When cells are enriched with cholesterol, Ca influx without polyamines causes a 58% decrease of cell capacitance while DPA capacitance and current decrease on averaged by 18 and 15%. Cholesterol enrichment after a Ca transient has increased cell capacitance by 25% results on average in a decrease of cell capacitance by 66%, while DPA capacitance and current remain 18 and 25% greater than baseline.

Figure 9. Ca-transients associated with exocytosis cause dramatic changes of the surface membrane, as reported by electrogenic and optical membrane probes. Standard solutions with no ATP or polyamines. (**A)** *Effects on DPA signals.* DPA (2 μM) was applied for 4 s and removed before and after activating reverse Na/Ca exchange in the absence of cytoplasmic ATP. C_m increases by 60%, and the DPA capacitive signal increases by a factor of 4. The DPA current is unchanged, while the rate of rise of the capacitive DPA signal (dC_m/dt, measured in pF/S) is increased by 70%. DSP=3.3. **(B)** *Effects on C6TPP signals.* C6TPP (300 μM) is applied and removed six time. Ca influx associated with a

40% increase of membrane area causes a 2.4-fold increase of C6TPP currents, causes decay phases of the currents, and induces C6TPP to develop a capacitive signal component. These changes are consistent with decreased dissociation rates from the membrane, similar to the effects of DPA. DSF=670. (**C)** *Effects on ANEPPDHQ optical signals.* Ca transients with membrane fusion cause large shifts in fluorescence spectra of ANEPPDHQ (8μM) binding. The large relative increase of emission above 640 nm (gray line) is similar to changes described for cholesterol depletion and presumably increased membrane disorder(Jin et al., 2006). Electrophysiological parameters were recorded in parallel with time-lapse confocal imaging at emission bandwidths of 500-580nm (black) and 640LPnm (gray).

Figure 10. Capacitive binding signals for the hydrophobic Cl-channel blocker, NFA (0.2 mM) are nearly unchanged by MEND. BHK cells with Standard Solutions. **(A)** Application and removal of niflumic acid causes a robust increase of C_m. Decay of the C_m signal occurs in two distinct phases. Currents associated with NFA application are very small, or absent, and show a delay from the onset of the rise of C_m. **(B)** The capacitance-voltage relation of the NFA signal is nearly flat, indicating that capacitive signals do not arise from translocation of the probe across the membrane. **(C)** The capacitive signal induced by NFA is unaffected by TX100-induced MEND. **(D)** MEND induced by Ca influx in the presence of EDA (2 mM), in both cytoplasmic and extracellular solutions. The capacitive signal induced by NFA rises and falls faster after Ca-induced MEND, but its magnitude is not affected. **(E)** Effect of Ca influx associated with exocytosis without MEND on NFA capacitive signals. Cytoplasmic solutions contain no ATP and no polyamine. The Ca transient results in a 60% increase of C_m, and a smaller increase of the NFA signal. After a second Ca transient, the NFA signal is nearly doubled and becomes faster.

Figure 11. The styryl dye, ANEPPDHQ, does not occupy the membrane that internalizes during TX100- and Ca-activated MEND in BHK cells. (**A)** ANEPPDHQ (10 μM) was applied before MEND and removed, during induction of MEND with TX-100 (150 μM), and again after MEND. The apparent binding rates of ANEPPDHQ are unchanged by removal of >70% of the cell surface by MEND, and the amount of fluorescence internalized during MEND (i.e. does not wash off) amounts to no more than 15% of the initial labeling (see horizontal gray lines). (**B)** ANEPPDHQ (8 μM) was applied and

removed before and after TX-100 (150 μM)-induced MEND while imaging at bandwidths of 500-580 nm (black) and 640nmLP (gray). The optical records are scaled. Neither the apparent binding rates of ANEPPDHQ nor its spectral properties are changed after TX100-induced MEND. (**C)** Same as 'C', using Ca influx in the presence of polyamine, here EDA, to induce MEND. Dye signals, which approach a steady state in these records, are unchanged by MEND.

Figure 12. Optically-determined binding rates of multiple lipid probes in BHK cells before and after inducing MEND with TX100 (150 μM). Binding rates of dyes are assumed to be proportional to the rate of fluorescence increase over 20 s upon applying dyes. The gray dashed lines alongside of the fluorescence records indicate the average rate of fluorescence increase. (**A)** An experiment employing C5-Bodipy-Gm1 (1μM). (**B)** An experiment employing C16:0-NBD-PE (5μM) in the presence of 10% DMSO to promote lipid solubility. **(C)** Summary of results showing capacitance loss in white and binding rates of fluorescent probes in gray. Only the styryl FM dye and the C16:0-NBD-PE are significantly affected by TX100-induced MEND.

Figure 13. Summary of membrane probes studied in this article and a companion article (Fine et al., xxxx) in relation to MEND responses. The figure represents best estimates of their distribution between membrane domains that internalize and do not internalize during MEND, interpreted to represent *Lo* and *Ld* domains, respectively. From left to right, the group with highest relative affinity for disordered membrane is the largest group. It includes nonionic detergents, carrier-type ionophores, long chain TPP's, NFA and lactosylceramide. The second group, which is modestly affected by MEND, includes nystatin, DPA, CCCP, short chain TPP's, dodecylmaltoside (DDM) and ANEPPDHQ. The third group, which is substantially but still under-proportionally affected by MEND, includes SDS, dodecylglucoside (DDG), TtPP, 1,8ANS, and NBD-PE. FM dyes, deoxycholate and NCX1 are affected proportionally by MEND, or nearly proportionally. From all probes and transporters examined to date, only Na/K pump activities are preferentially reduced by MEND with the implication that pumps may be regulated by *Lo*-domain-dependent endocytosis.

Supplemental Material

Supporting material documents **(1)** that Ca transients associated with exocytosis strongly promote cyclodextrin-induced loss of cell capacitance, (2) that Ca transients associated with exocytosis strongly promote the formation of channels by the phosphatidylethanolamine-binding antibiotic, duramycin, **(3),** that C12TPP is ineffective to induce MEND from the cytoplasmic side, (4) that Ca transients associated with exocytosis increase DPA capacitive signals with no pronounced effect on their capacitance-voltage relation, **(5)** large effects of beta-cyclodextrin treatments and benzyl alcohol on the function of hydrophobic ions, and **(6)** changes of DPA signals associated with all protocols developed in a companion article to induce MEND.

Figure S1. Facilitation of Ca-activated MEND by NP-40 with, however, a pseudo-competitive interaction of Ca and detergent for extracellular Ca binding. The pipette solution contains 2 mM ATP and 0.2 mM GTP. NP-40 at a concentration of 40 uM is without effect. During the Ca transient, a small decline of Cm occurs, and then Cm plummets upon removal of Cao. This pattern is explained by a routine observation that the presence of extracellular Ca partially blocks detergent actions. Presumably, Ca binding by the extracellular monolayer has a condensing effect that tends to inhibit detergent binding. Thus, the MEND-promoting effect of Ca influx on NP-40-induced MEND is only apparent after removal of Ca.

Figure S2. Ca transients accompanied by exocytosis greatly enhance loss of cell capacitance induced by cyclodextrins and the development of duramycin channels. Cytoplasmic solutions contained 2 mM ATP and 0.2 mM GTP. (A) HPCD (20 mM) has almost no effect on Cm when applied before initiating Ca influx (10 observations). After a Ca transient and membrane fusion response, the same concentration of HPCD causes a >50% fall of Cm over 2 min. These results potentially are related to amphipath-induced MEND. Extraction of cholesterol and phospholipids from the more fluid phase of the membrane will tend to disorder it and therewith generate a larger line tension that supports MEND. **(B)** Ca transients accompanied by exocytosis greatly enhance the generation of nonselective membrane conductance by duramycin. Duramycin is a polypeptide antibiotic that binds to cell membranes with strong dependence on the phosphatidylethanolamine content (Navarro et al., 1985) and subsequently forms nonselective ion channels (Choung et al., 1988). BHK cells are entirely insensitive to

2uM-extracellular duramycin when it is applied in the absence of Ca transients. Within seconds of activating Ca influx, however, membrane conductance begins to rise steeply, indicating the formation of duramycin channels. Thus, it is likely that phosphatidylethanolamine (PE) is appearing rapidly in the outer monolayer of cells when Ca influx is activated.

Figure S3. As with other detergents (Fine, xxxx), perfusion of a high concentration of C12TPP (250 uM) into BHK cells does not induce endocytic responses. During pipette perfusion, outward C12TPP current reaches just 30 pA indicating that C12TPP at the inner plasma membrane monolayer is substantial. Thereafter, in the presence of cytoplasmic C12TPP, a lower concentration of C12TPP (50 uM) still induces a substantial MEND response (25%) from outside. Note that with these concentrations of C12TPP, acting on both membrane sides, a nonselective conductance develops over several seconds (see arrows in Fig. S3) and declines rapidly when the C12TPP is removed from the outside. This pattern was observed for many detergents at high concentrations.

Figure S4. The time courses of DPA accumulation in cells, when applied continuously, DPA capacitance-voltage relations, and the effects of Ca-activated membrane fusion on DPA signals. (A) Continuous DPA application during capacitance-voltage relations were determined 5 times. To do so, voltage stepped to -125 mV and then incremented in 25mV steps for 0.5 s up to +125 mV, and the resulting DPA capacitance-voltage relations are shown in (B). During continuous DPA application, the initial fast rise of capacitance is followed by a slow phase that continues for several minutes as DPA accumulates in cells. The slow phase grows to a value 10-times larger than the initial raise. Assuming that free cytoplasmic DPA cannot accumulate above the extracellular concentration at 0 mV, the affinity of the cytoplasmic leaflet for DPA must be at least 10-times higher than the extracellular leaflet. When Ca influx is activated at 80 s, DPA capacitive signals increase by > 3-fold, similar to results for brief application and removal of DPA described in this article. The dotted gray lines in the panel A give our estimate of the actual membrane capacitance by extrapolating the Cm-voltage relations to a baseline. The DPA-mediated capacitance increases by 4-fold in this experiment, while the actual membrane capacitance is at very most doubled. **(B)** Capacitance-voltage relations of DPA signals. The mid-points of the bell-shaped Cm-voltage relations occur at -50 mV, representative of >100 recordings. Thus, at 0 mV the large majority of DPA bound to the surface

membrane is on the cytoplasmic side. This result is consistent with the idea that the cytoplasmic affinity for DPA is about 10 times higher than the affinity of the extracellular monolayer. It is also consistent with the cytoplasmic monolayer being substantially more disordered than the extracellular monolayer. In our experience, the results described here place very strong constraints on any model used to explain cellular DPA signals. Up to now, we find it essential to assume that the membrane becomes increasingly heterogeneous after the exocytic response, such that DPA functions differently in different membrane domains.

Figure S5. Effects of BMCD (10 mM) on DPA signals. (A) Cm record from an experiment in which BMCD (10 mM) was applied for periods of many minutes. During BMCD treatment, the membrane capacitance per se declines by 14%. As indicated below the Cm record, DPA (1 uM) was applied and removed three times before and three times after application of BMCD, whereby the solution containing DPA did not contain BMCD. In this experiment, the DPA capacitive signal increases nearly 4 fold over a 10 min period. **(B)** On average, DPA capacitive signals increase by a factor of 3 in the protocol of panel A (n=4). (C) DPA signals before and after BMCD treatment at higher time resolution. The capacitance records are scaled to one another to compare their time courses. DPA-induced currents, which are not scaled to one another, increased at most two-fold. The initial rate of capacitance increase on applying DPA is increased two fold while the decay of the DPA capacitive signals is slowed by 3-fold after BMCD treatment. Thus, the increase of DPA signals is accounted for by both a decreased dissociation constant and an increased association constant.

Figure S6. Effects of HPCD (20 mM) treatment for 50 min on DPA capacitive signals. **(A)** Over 50 min, HPCD treatment causes a ten-fold increase of capacitive DPA signals (2 uM for 3 s). Note that a 30 min period of the record is omitted to highlight DPA signals before and after HPCD treatment. Initial rates of rise of capacitive signals were determined from derivative signals, and the declining capacitance signals after removing DPA were analyzed by fitting them to double exponentials, where by the faster components constituted more than 70% of all of the signals. Fits to the falling signals are given in 'A' with the capacitance records as gray lines. **(B)** Initial rates of rise of capacitive signals increase by more than 10 fold over the 50 min experiment. (C) Both the time constants and magnitudes of the faster exponential components of the signals increase by about 10-fold during the experiment. The time constants increased from 0.8 s

to 6 s, and the magnitudes of the corresponding components increased from 5 pF to 74 pF. In terms of the model outlined in Methods, the association rates of DPA at the outside are increased, the dissociation rates at the outside are strongly decreased, and the dissociation rates at the inside are very strongly decreased.

Figure S7. Effects of benzyl alcohol (0.5 %) on DPA signals. Benzyl alcohol is known as a 'membrane fluidizer' which can to some extent disrupt domain formation in artificial membranes. Therefore it was of interest to text whether it might block detergent-activated MEND. In an experiment series comparing 10 control cells and 10 cells in the presence of 0.5% benzylalcohol in all solutions, benzylalcohol was found to promote, not block, TX100-induced MEND. The rate of development of MEND was highly significantly increased by three-fold, while the extent of MEND was increased by 12%. Therefore it was in interest to test how benzylalcohol might change membrane properties, as reported by DPA. (A) In this experiment, DPA (1 □M) was initially applied twice, then 0.5% benzyl alcohol was applied and the same DPA concentration was applied twice again in the presence of benzyl alcohol. Thereafter, benzyl alcohol was removed, DPA was applied again to test reversibility of the alcohol effects, and the sequence was repeated. Benzyl alcohol causes still larger increases of DPA signals than BMCD treatment. In strong contrast to BMCD, DPA capacitive signals increase with benzyl alcohol without a slowing of DPA dissociation rates., and DPA currents are decreased. Analysis by the model outlined in Methods, would suggest that the association and dissociation rates of DPA at the outer monolayer are both greatly increased by benzyl alcohol, while the dissociation rate at the cytoplasmic side is strongly decreased. This would suggest that differential effects are occurring in the inner and outer monolayers. (B) This panel presents similar results from another experiment. The decrease of DPA current is even more pronounced that in panel A. Assuming that the DPA currents and capacitive signals arise from the same membrane domains, the differential effects on monolayers must be even more pronounced than in panel A. Dissociation of DPA to the cytoplasmic side must be drastically reduced, while dissociation to the extracellular side is strongly increased.

Figure S8. Effects of HPCD (20 mM) treatment on C6TPP signals (6 observations). The C6TPP signals show in this experiment a small capacitive component under control conditions. After HPCD treatment for 5 min, the capacitive component is increased 6.5-fold, and the C6TPP currents are approximately doubled and develop prominent decay

phases. These changes mirror changes that occur after massive membrane fusion, as described in Fig. 11B of the article.

Figure S9. DPA signal changes when Ca-activated exocytosis is followed by compensatory endocytosis without excess endocytosis. The pipette solutions contain 2 mM ATP and 0.2 mM GTP. (A) Ca influx with 2 mM-cytoplasmic ATP and no polyamines. Cm increases by 45% in response to the Ca transient and declines approximately to baseline over two minutes after the Ca transient. DPA (2 □M) was applied and removed four times during the protocol, twice before the Ca transient, once immediately after exocytosis and once after return of Cm to baseline. The capacitive DPA signal is doubled after fusion and remains 50% increased after Cm has declined to baseline. The DPA current increases marginally in response to membrane fusion and remains increased. Thus, compensatory endocytosis only partially reverses membrane changes associated with Ca influx and exocytosis. (B) DPA signals during Ca-activated polyamine-dependent MEND, when MEND requires multiple Ca transients to develop. With 1 mM spermidine in the cytoplasmic solution, the first Ca transient causes exocytosis without MEND, and the two subsequent Ca transients cause exocytosis with fast MEND. DPA (2 □M) was applied for 4 s. As usual, the DPA signals increase over-proportionally to cell capacitance in response to exocytosis. At the second Ca transient, Cm falls to 15% below baseline, and the DPA capacitive signal decreases to its original level. *We point out that this is the sole example up to now in which the DPA signals decrease strongly with endocytosis*. Nevertheless, DPA current remains essentially unchanged, and the DPA capacitive signal is unchanged at the end of the experiment, when compared to the beginning of the experiment. At the same time, Cm has decreased by 50% from its initial value. Thus, in the protocol as in all others causing MEND, change of DPA signals are smaller than Cm changes.

Figure S10. Effects of Ca-activated MEND by two different protocols on DPA signals. (A) Changes of DPA signals when high cytoplasmic ATP (8 mM) promotes MEND to 50% below baseline after membrane fusion. In response to Ca influx, Cm increases by 31% while DPA capacitance increases by 70% During MEND, DPA capacitance decreases to approximately pre-stimulation levels, and DPA currents do not change. Overall, the DPA capacitive signal is decreased by <10% while membrane area is decreased by 40%. (B) Changes of DPA signals when MEND occurs during a single Ca transient in the presence of cytoplasmic spermidine (1 mM). The cytoplasmic solution

contains 2 mM ATP and 0.2 mM GTP. After MEND, resulting in a 50% decrease of Cm, DPA capacitance is increased by 83% and DPA current is doubled.

Figure S11. Effects of MEND induced by Ca transients and cholesterol enrichment on DPA currents and capacitive signals. Cyto. solutions are ATP-free. (A) Cholesterol enrichment with HPCD-cholesterol complexes over 5 min causes a small decrease of the MEND capacitive signal and no change of DPA current. After cholesterol enrichment, NCX1 causes a 64% MEND response, accompanied by an 18% decrease of DPA cap. and 23% decrease of DPA current. (B) Changes of DPA signals when MEND is induced by HPCD-cholesterol complexes after membrane fusion. A 68% MEND response is accompanied by a 21% decrease of DPA cap. and no change of DPA current.

Figure S12. Membrane association of the hydrophobic Cl-channel blocker, niflumic acid (NFA, 0.2 mM), is unaffected by MEND. BHK cells with Standard Solutions. (A) Application and removal of niflumic acid causes a robust increase of Cm, which probably reflects expansion of the membrane similar to observations for detergents. Decay of the Cm signal occurs in two distinct phases. Currents associated with NFA application are very small, or absent, and show a delay from the onset of the rise of Cm. (B) The capacitance-voltage relation of the NFA signal is nearly flat, indicating further that the signals do not arise from hydrophobic ion-like function. (C) The capacitive signal induced by NFA is unaffected by TX10-induced MEND. (D) MEND induced by Ca influx in the presence of EDA (2 mM), in both cytoplasmic and extracellular solutions. The capacitive signal induced by NFA rises and falls faster after Ca-induced MEND, but its magnitude is not affected. (E) Effect of Ca influx associated with exocytosis without MEND on NFA capacitive signals. The cytoplasmic solutions contain no ATP and no polyamine. The Ca transient results in a 60% increase of Cm, and a smaller increase of the NFA signal. After a second Ca transient, the NFA signal is nearly doubled and becomes faster, as in D, whereby membrane area is not further increased. Thus, it appears that Ca transients, per se, rather than exocytosis are affecting the NFA signal.

Figure S13. Membrane binding of the styryl dye, ANEPPDHQ, is unchanged by 'delayed' MEND that is activated by a Ca transient in the presence of 8 mM cytoplasmic ATP. **(A)** ANEPPDHQ (8 uM) was applied and removed before MEND and again after MEND, which amounts to 25% of the cell surface. **(B)** Fluorescence records before and after MEND reveal no change.

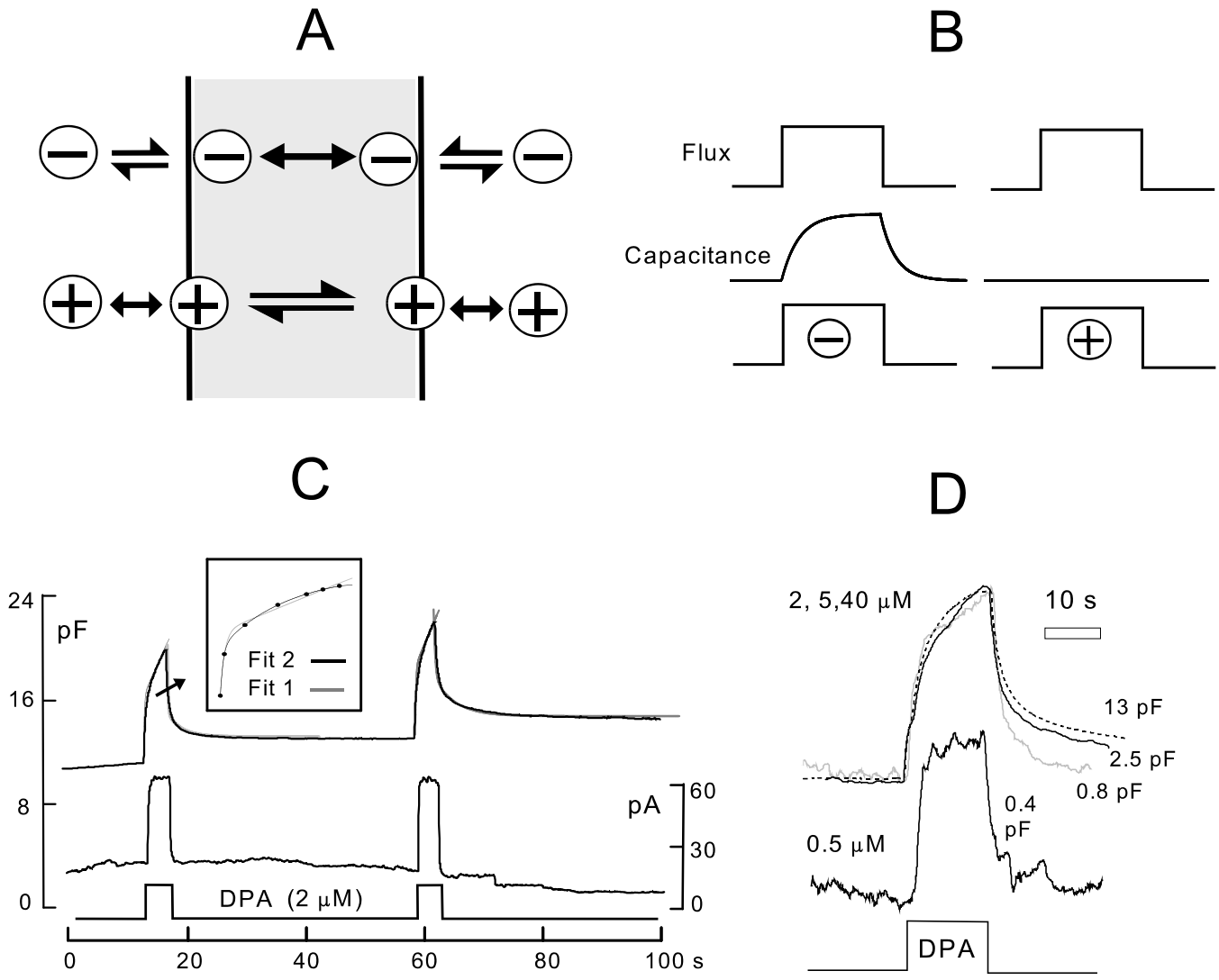
A
B
Flux
Capacitance
C
D
24
pF
16
8
0
Fit 2
Fit 1
pA
60
30
0
DPA (2 μM)
0
20
40
60
80
100 s
2, 5,40 μM
10 s
13 pF
2.5 pF
0.8 pF
0.4
pF
0.5 μM
DPA

Figure 2

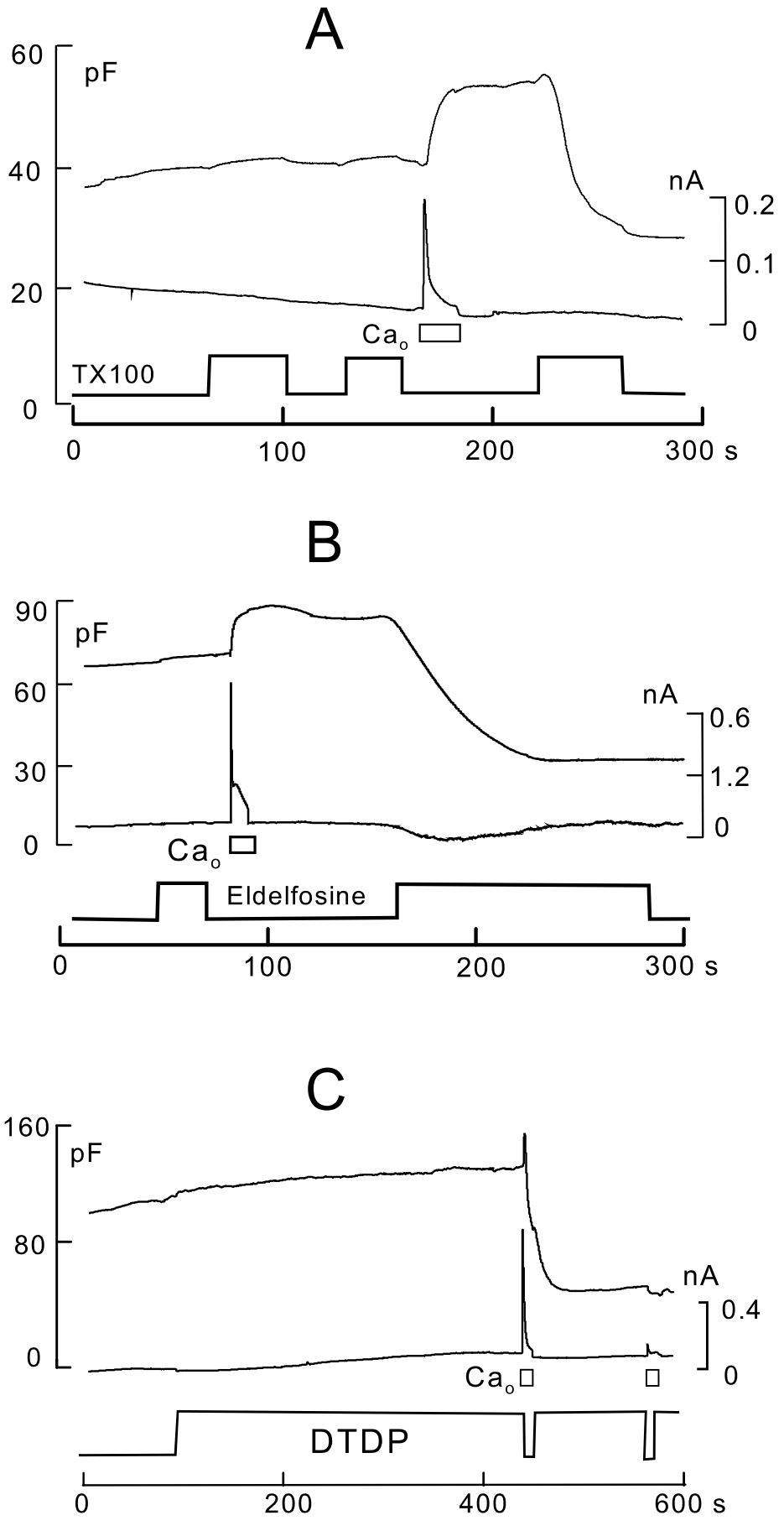
A
60
pF
40
20
0
nA
0.2
0.1
0
Ca$_o$
TX100
0
100
200
300 s
B
90
pF
60
30
0
nA
0.6
1.2
0
Ca$_o$
Eldelfosine
0
100
200
300 s
C
160
pF
80
0
nA
0.4
0
Ca$_o$
DTDP
0
200
400
600 s

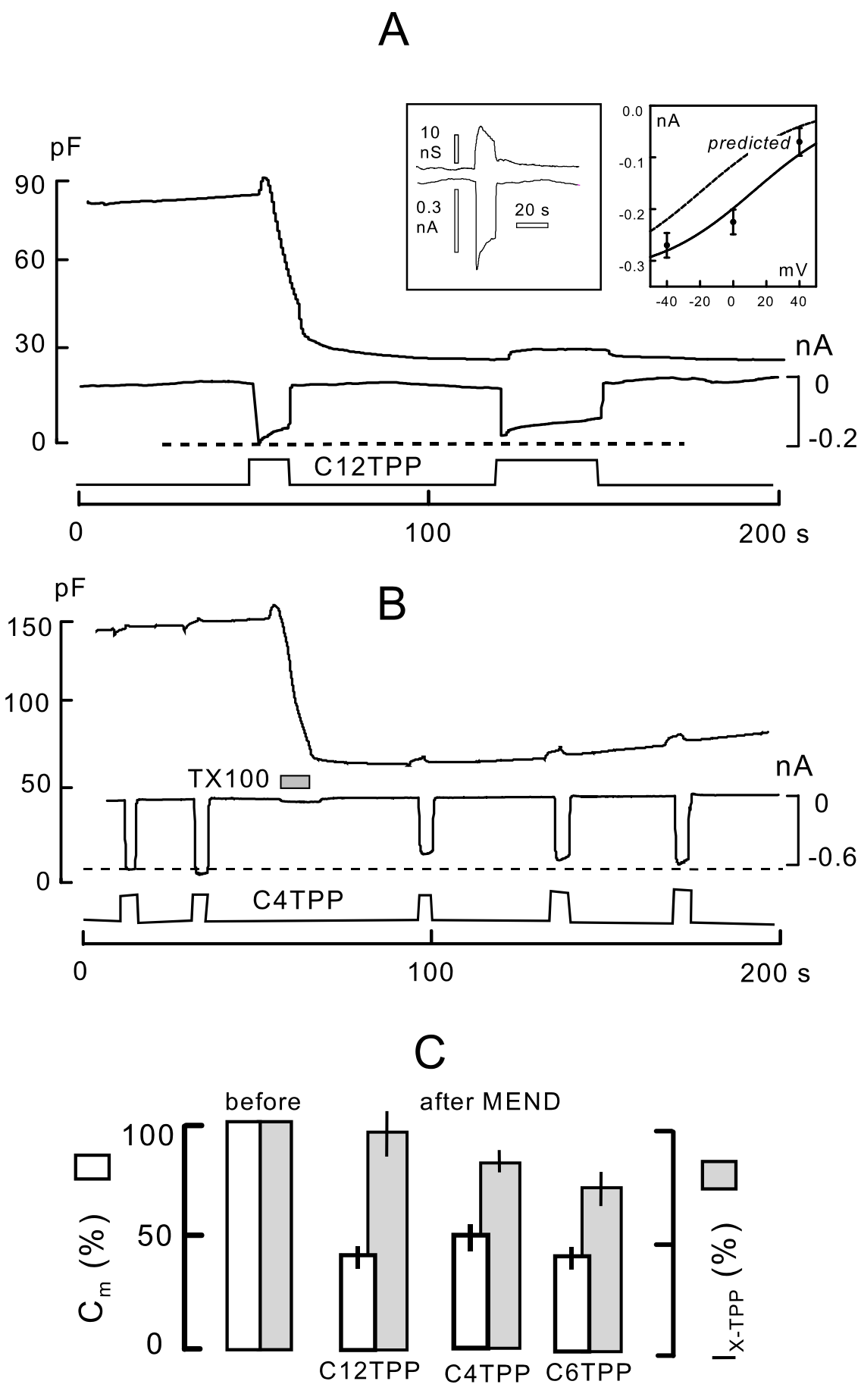
A
pF
90
60
30
0
10
nS
0.3
nA
20 s
0.0
nA
predicted
-0.1
-0.2
-0.3
mV
-40 -20 0 20 40
nA
0
-0.2
C12TPP
0
100
200 s
B
pF
150
100
50
0
TX100
nA
0
-0.6
C4TPP
0
100
200 s
C
before
after MEND
100
50
0
C_m (%)
C12TPP
C4TPP
C6TPP
$I_{X\text{-}TPP}$ (%)

Figure 4

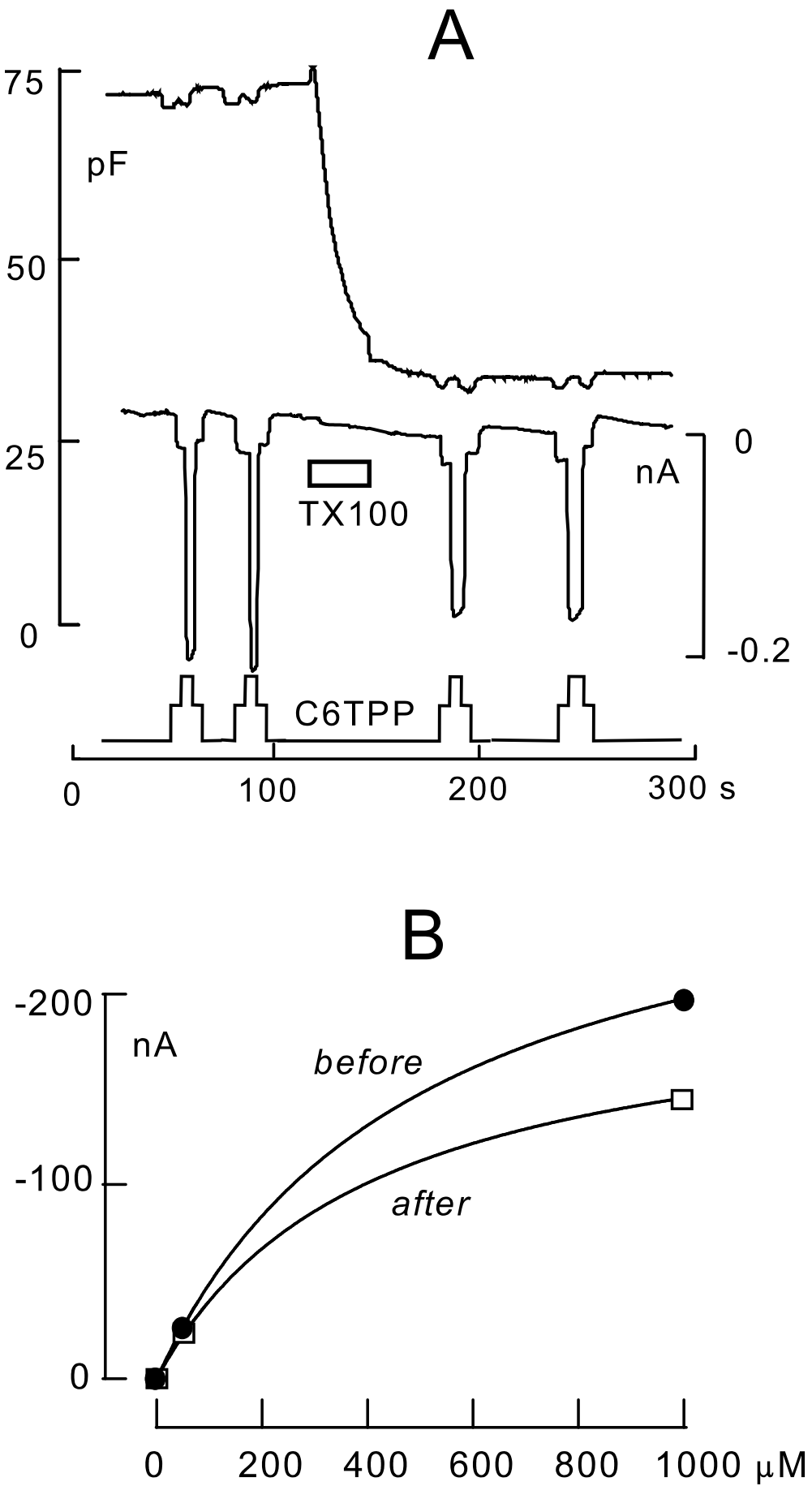
A
75
pF
50
25
0
TX100
nA
0
-0.2
C6TPP
0
100
200
300 s
B
-200
nA
-100
0
before
after
0
200
400
600
800
1000 μM

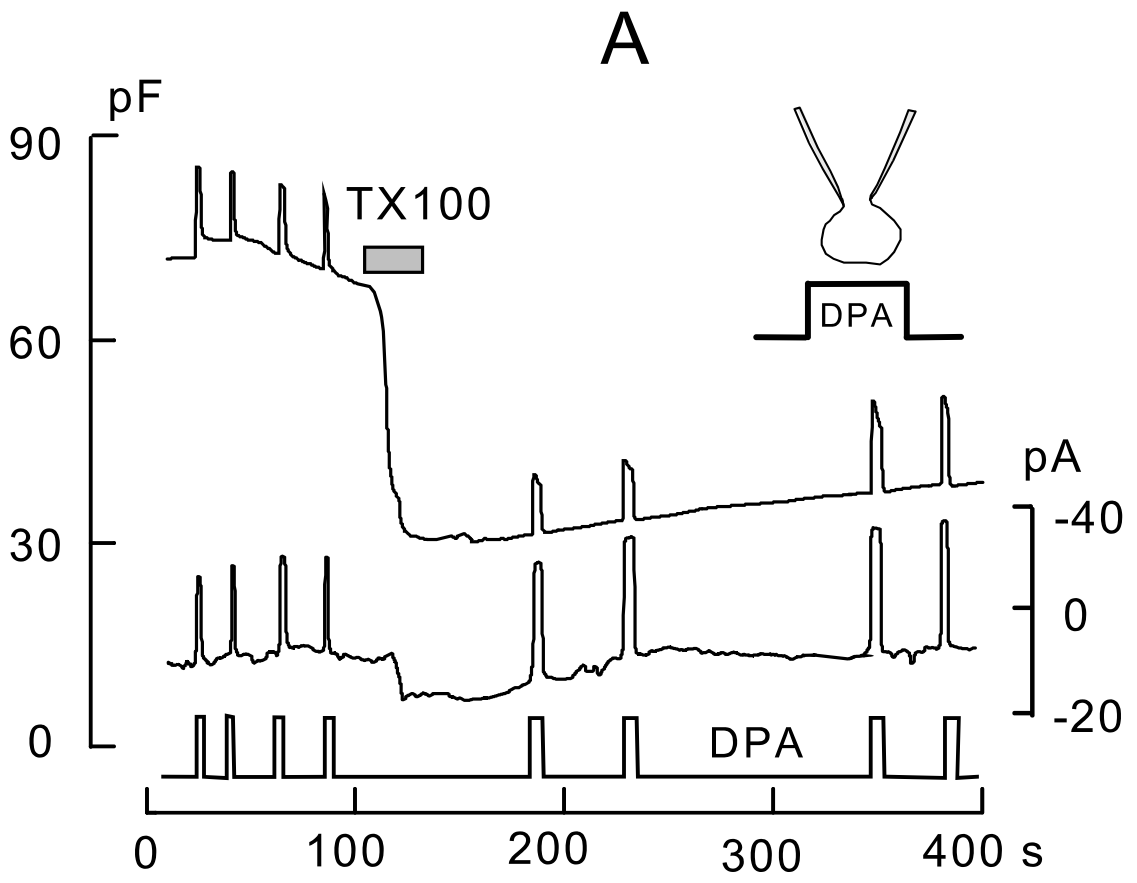
A
pF
90
60
30
0
TX100
DPA
pA
-40
0
-20
DPA
0
100
200
300
400 s

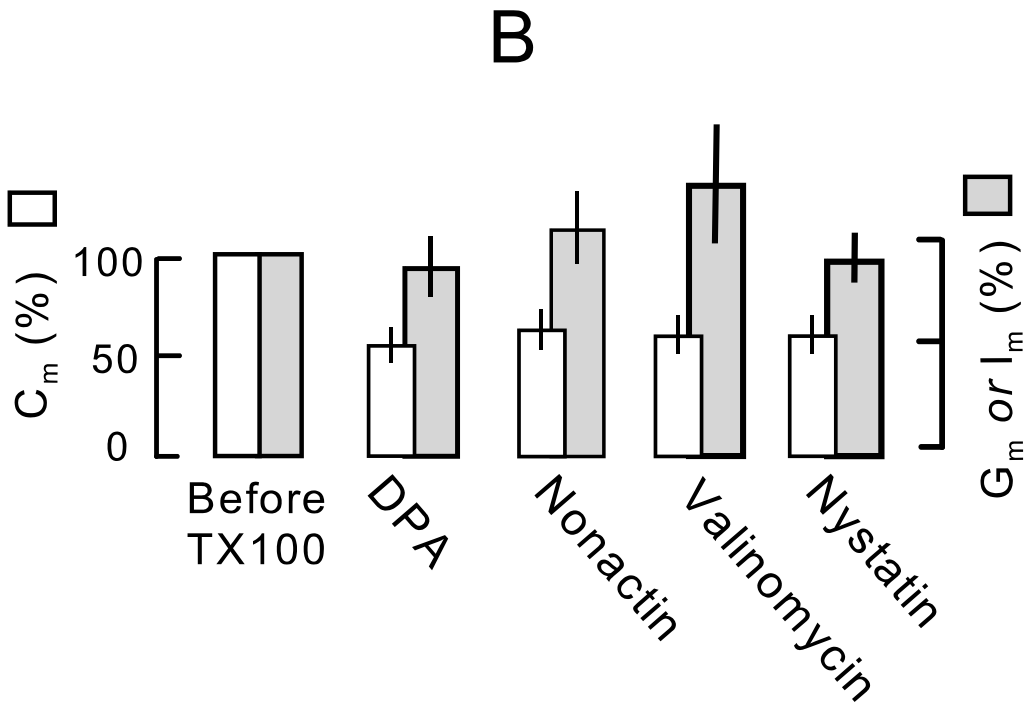
B
C_m (%)
100
50
0
Before TX100
DPA
Nonactin
Valinomycin
Nystatin
G_m *or* I_m (%)

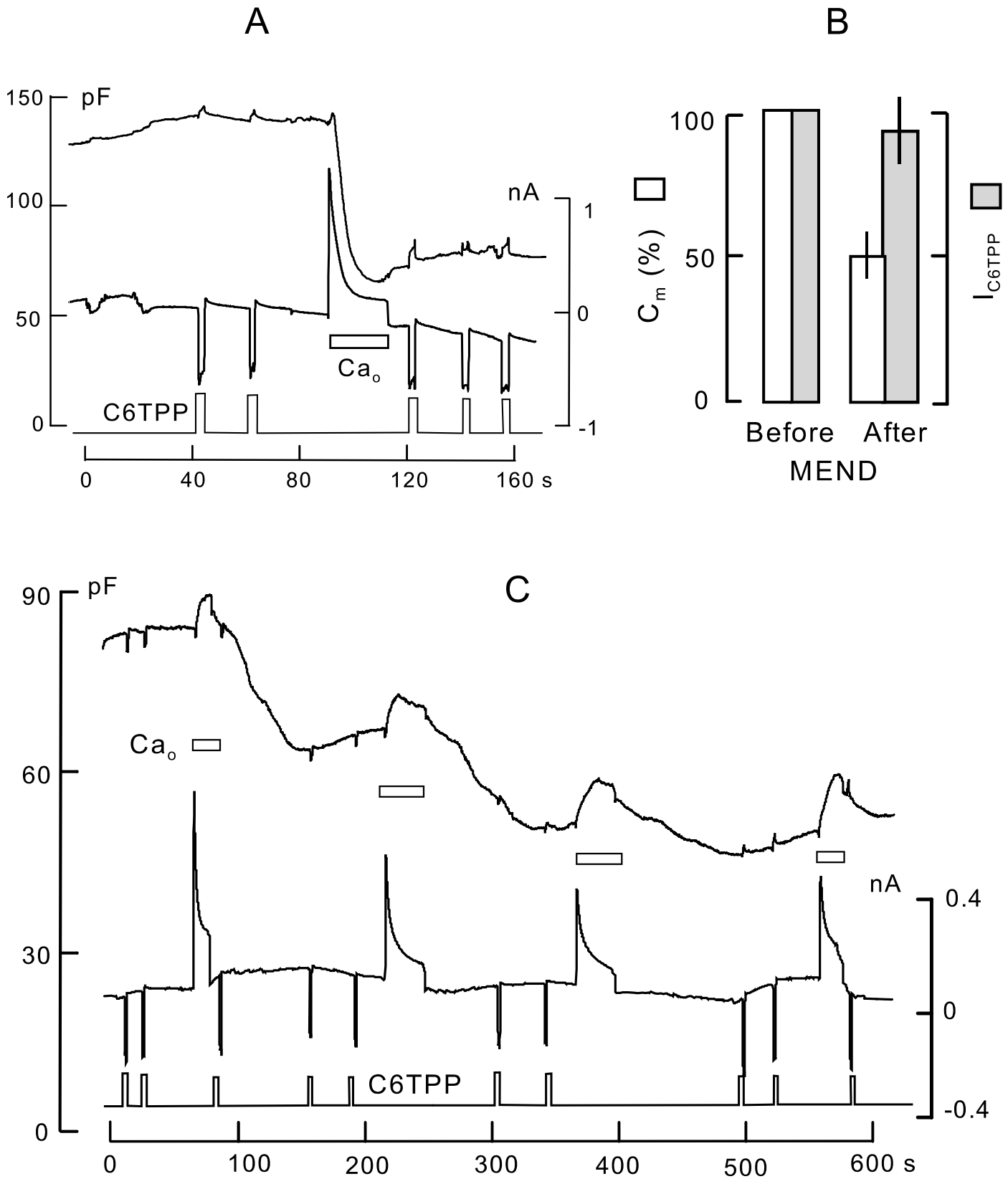
A
150
pF
100
50
0
nA
1
0
-1
Ca$_o$
C6TPP
0
40
80
120
160 s
B
100
50
0
C$_m$ (%)
I$_{C6TPP}$
Before
After
MEND
C
90
pF
60
30
0
Ca$_o$
nA
0.4
0
-0.4
C6TPP
0
100
200
300
400
500
600 s

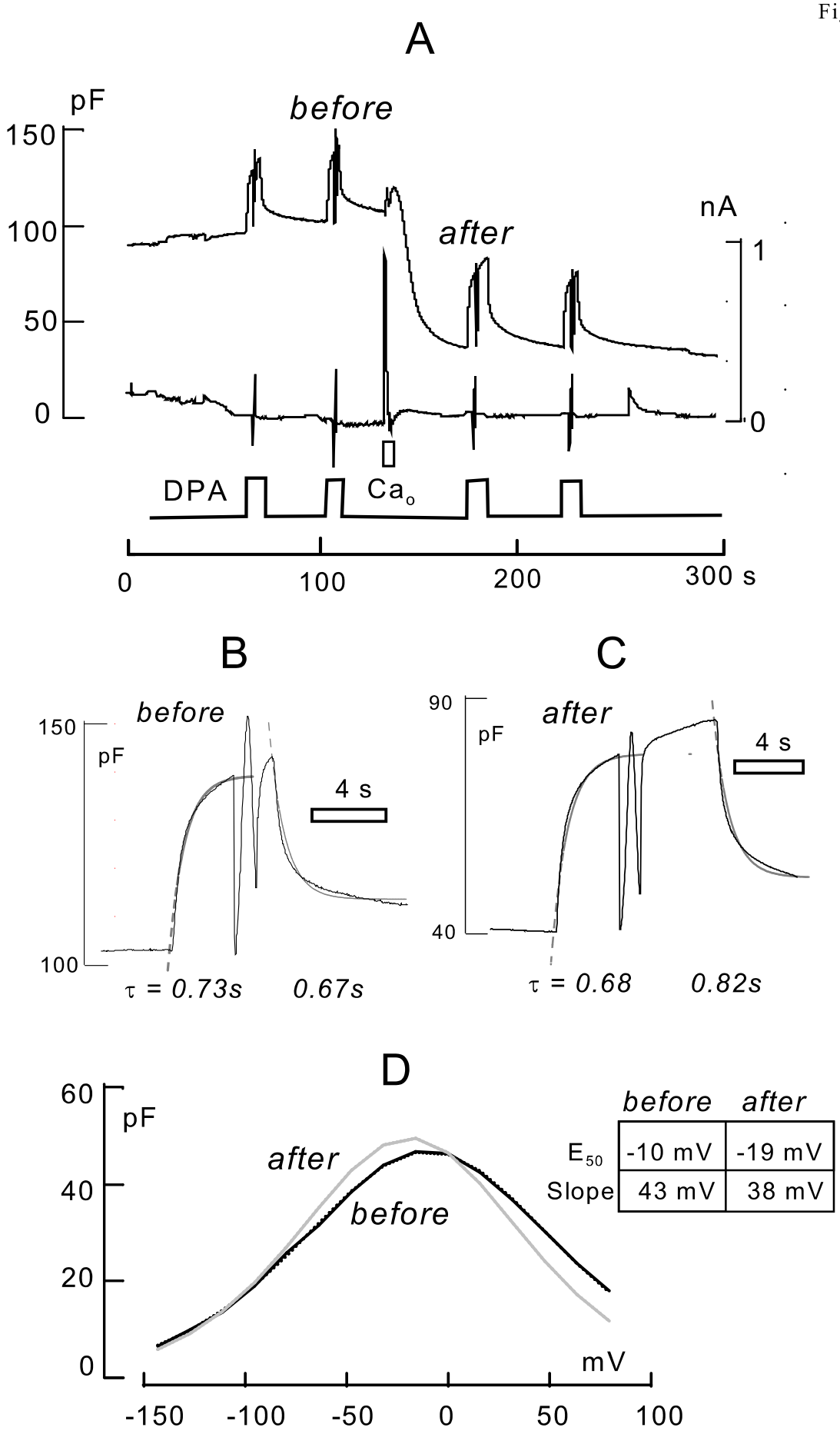
A
pF
150
100
50
0
before
after
nA
1
0
DPA
Ca$_o$
0
100
200
300 s
B
150
pF
100
before
4 s
τ = 0.73s
0.67s
C
90
pF
40
after
4 s
τ = 0.68
0.82s
D
60
pF
40
20
0
after
before
mV
-150
-100
-50
0
50
100
before
after
E$_{50}$
-10 mV
-19 mV
Slope
43 mV
38 mV

Figure 8

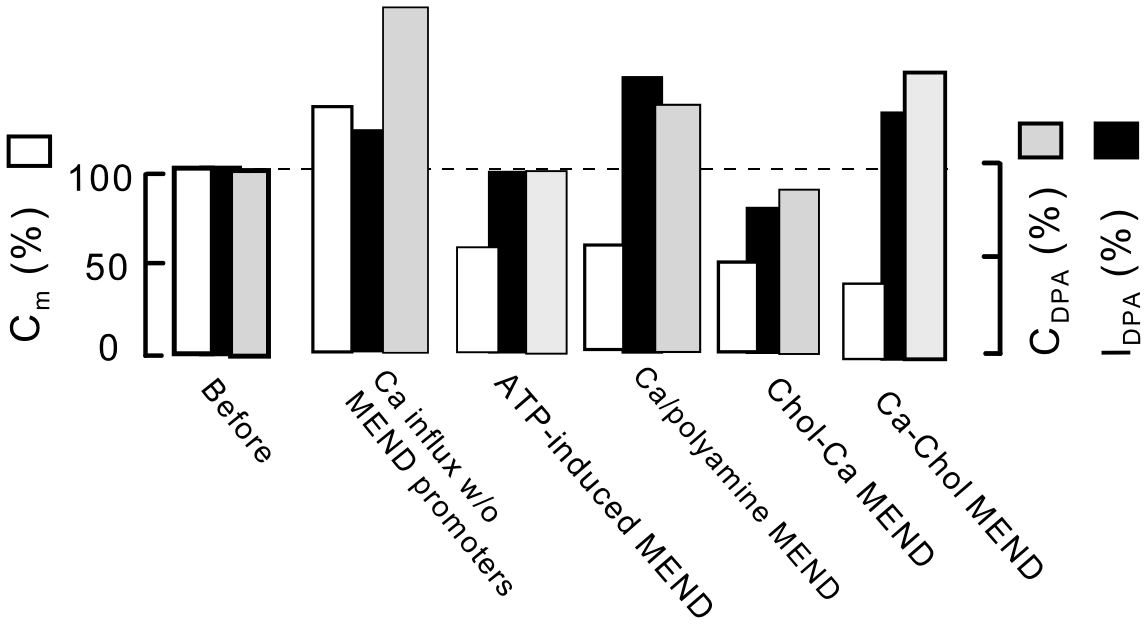
C_m (%)
100
50
0
Before
Ca influx w/o MEND promoters
ATP-induced MEND
Ca/polyamine MEND
Chol-Ca MEND
Ca-Chol MEND
C_{DPA} (%)
I_{DPA} (%)

Figure 9

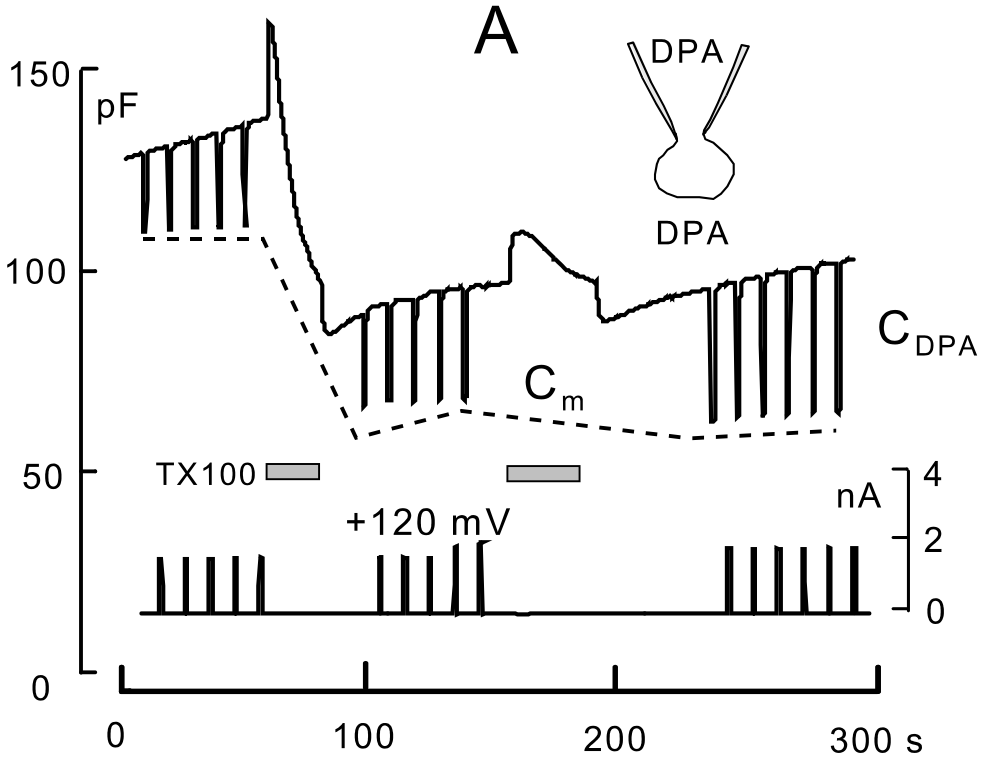
A
DPA
DPA
150
pF
100
50
0
C_{DPA}
C_m
TX100
+120 mV
nA
4
2
0
0
100
200
300 s

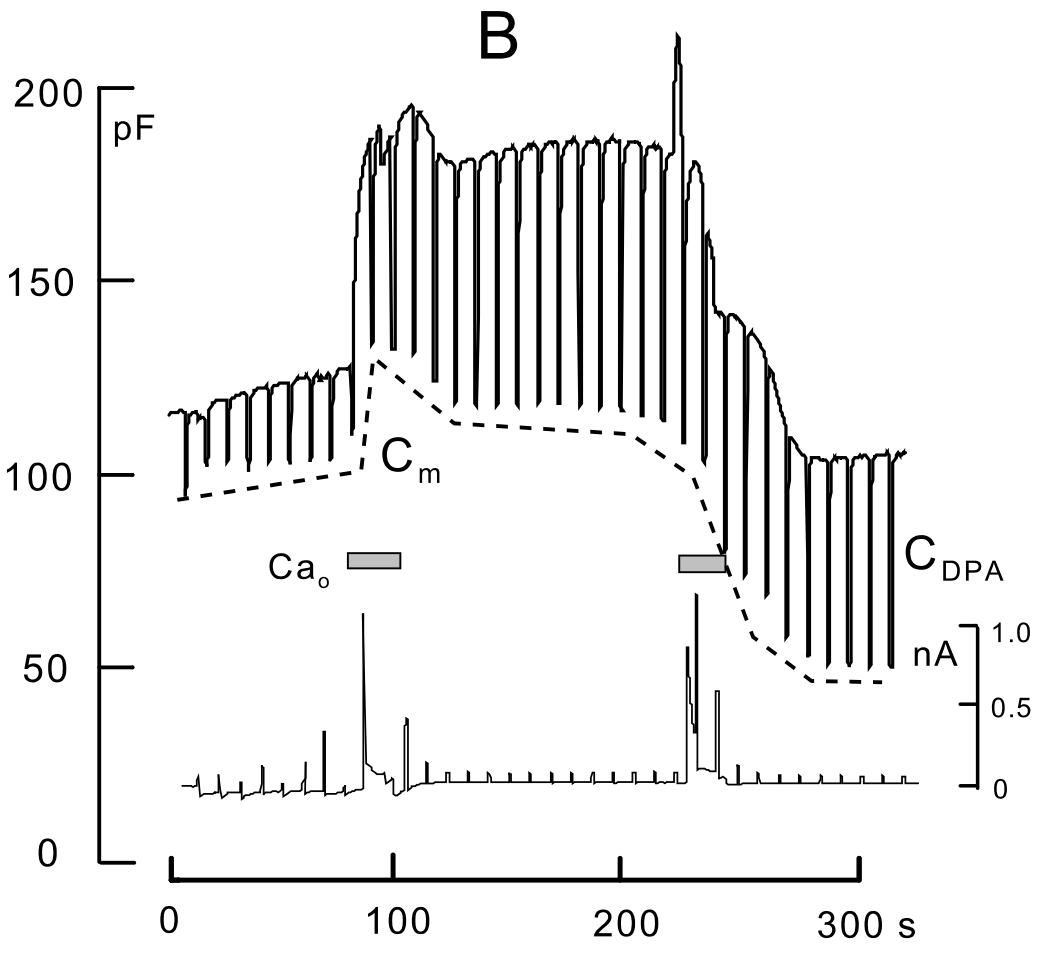
B
200
pF
150
100
50
0
C_m
Ca_o
C_{DPA}
nA
1.0
0.5
0
0
100
200
300 s

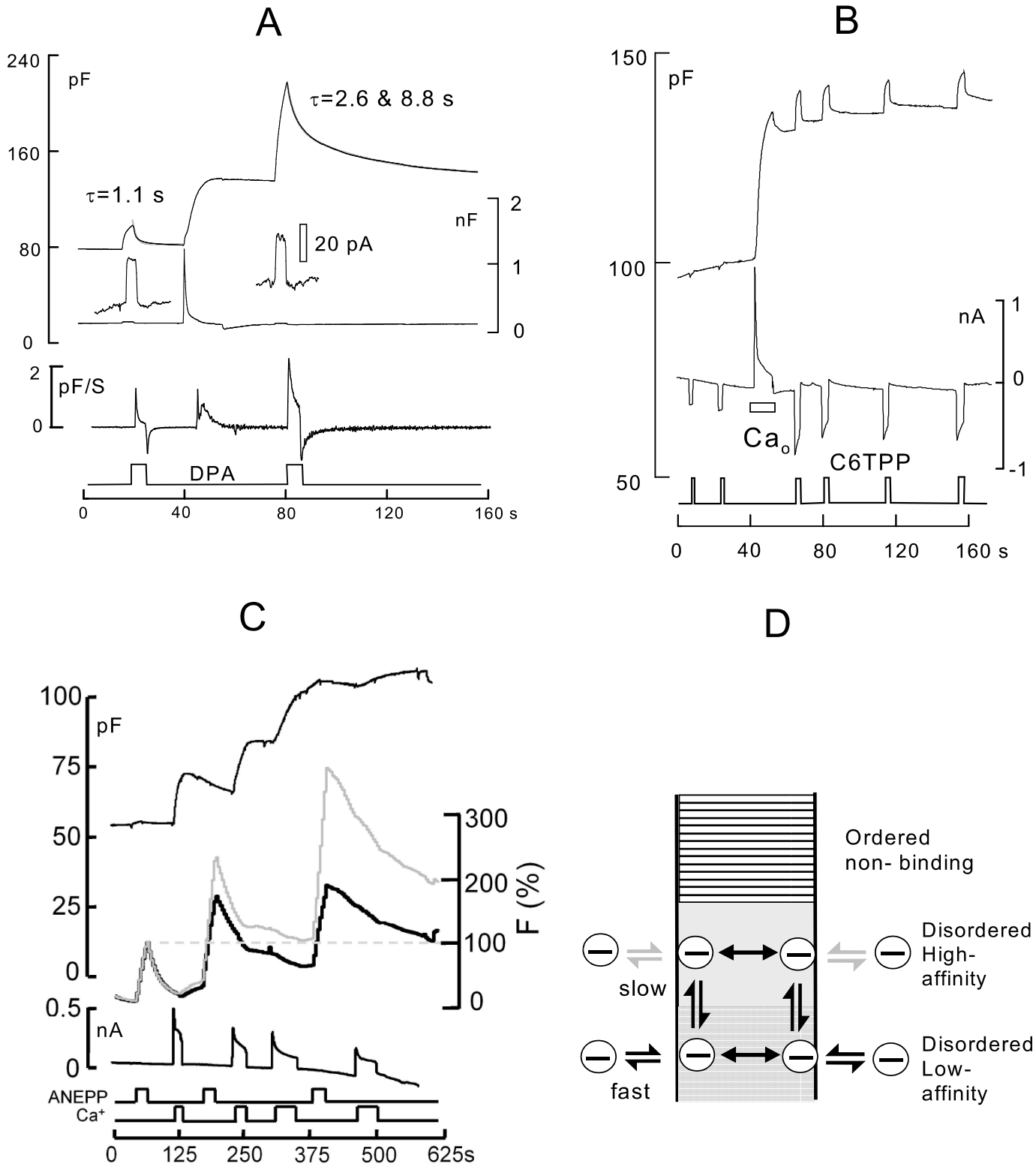
A
240
160
80
0
pF
τ=2.6 & 8.8 s
τ=1.1 s
20 pA
nF
2
1
0
2
0
pF/S
DPA
0
40
80
120
160 s
B
150
100
50
pF
nA
1
0
-1
Ca$_o$
C6TPP
0
40
80
120
160 s
C
100
75
50
25
0
pF
300
200
100
0
F (%)
0.5
0
nA
ANEPP
Ca+
0
125
250
375
500
625s
D
Ordered
non- binding
Disordered
High-
affinity
slow
fast
Disordered
Low-
affinity

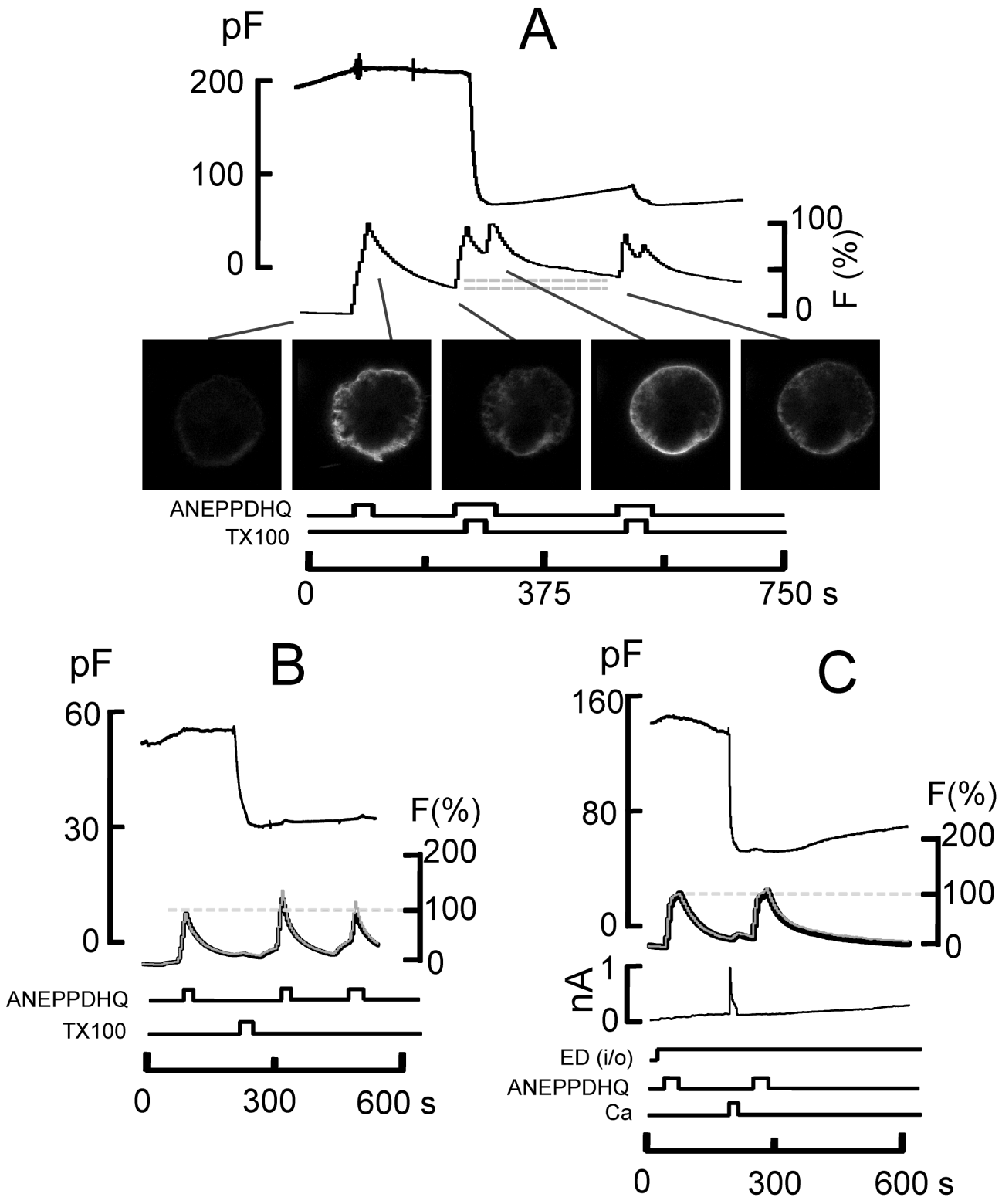
A
pF
200
100
0
100
0
F (%)
ANEPPDHQ
TX100
0
375
750 s
B
pF
60
30
0
F(%)
200
100
0
ANEPPDHQ
TX100
0
300
600 s
C
pF
160
80
0
F(%)
200
100
0
nA
1
0
ED (i/o)
ANEPPDHQ
Ca
0
300
600 s

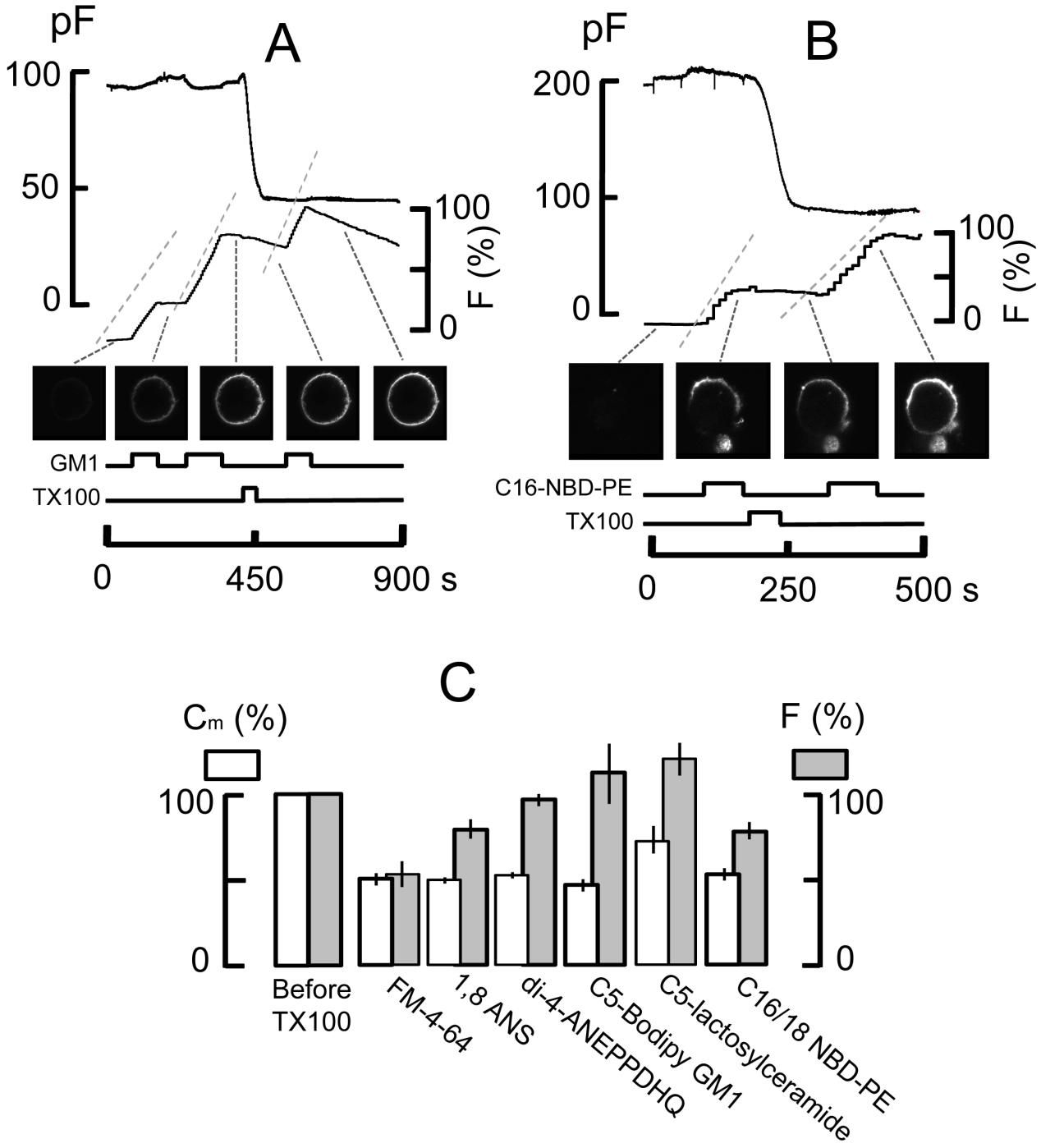
pF
A
100
50
0
100
0
F (%)
GM1
TX100
0
450
900 s
pF
B
200
100
0
100
0
F (%)
C16-NBD-PE
TX100
0
250
500 s
C
Cm (%)
F (%)
100
0
100
0
Before TX100
FM-4-64
1,8 ANS
di-4-ANEPPDHQ
C5-Bodipy GM1
C5-lactosylceramide
C16/18 NBD-PE

Supporting Data Figures

Figure S1

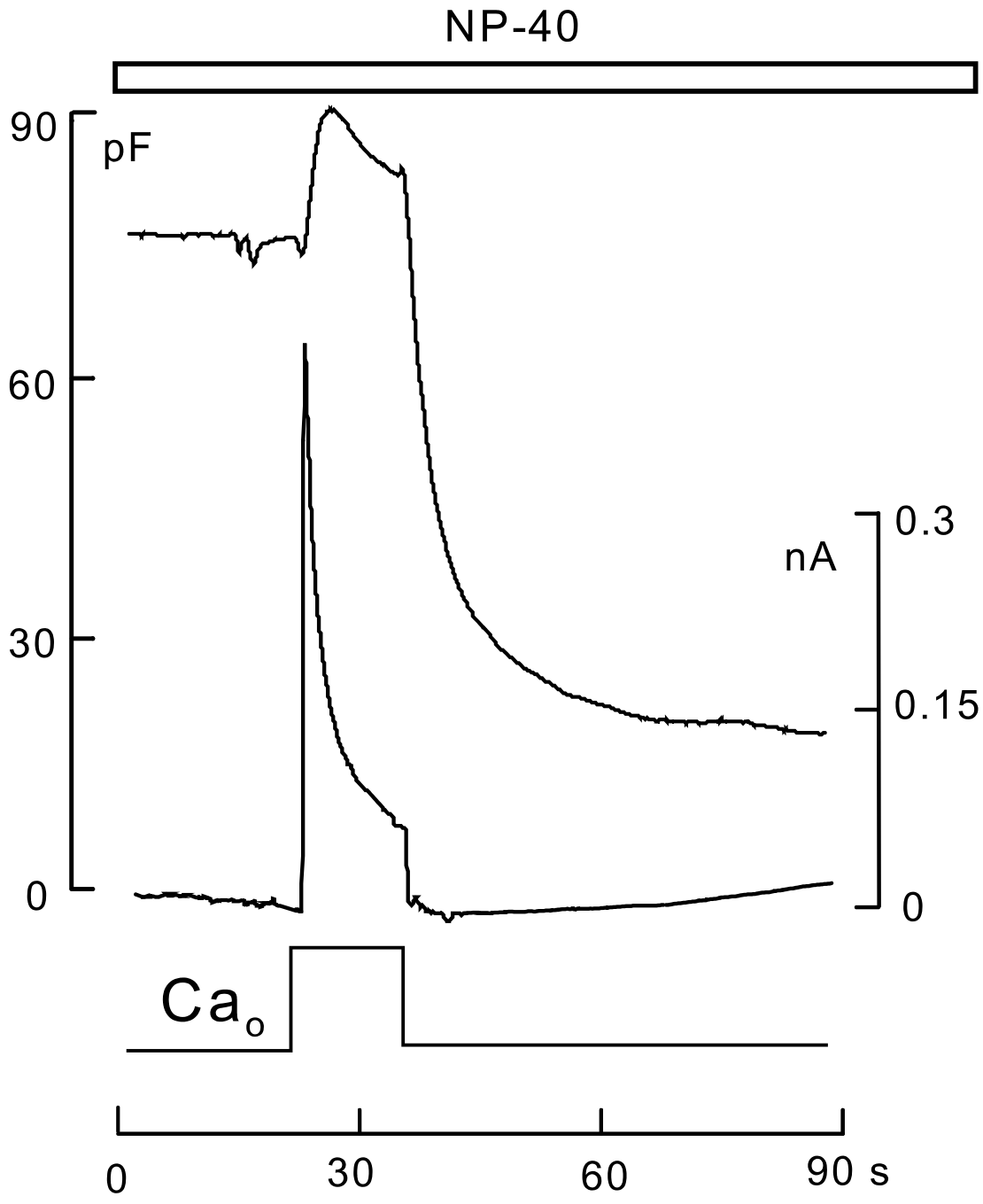

Figure S2

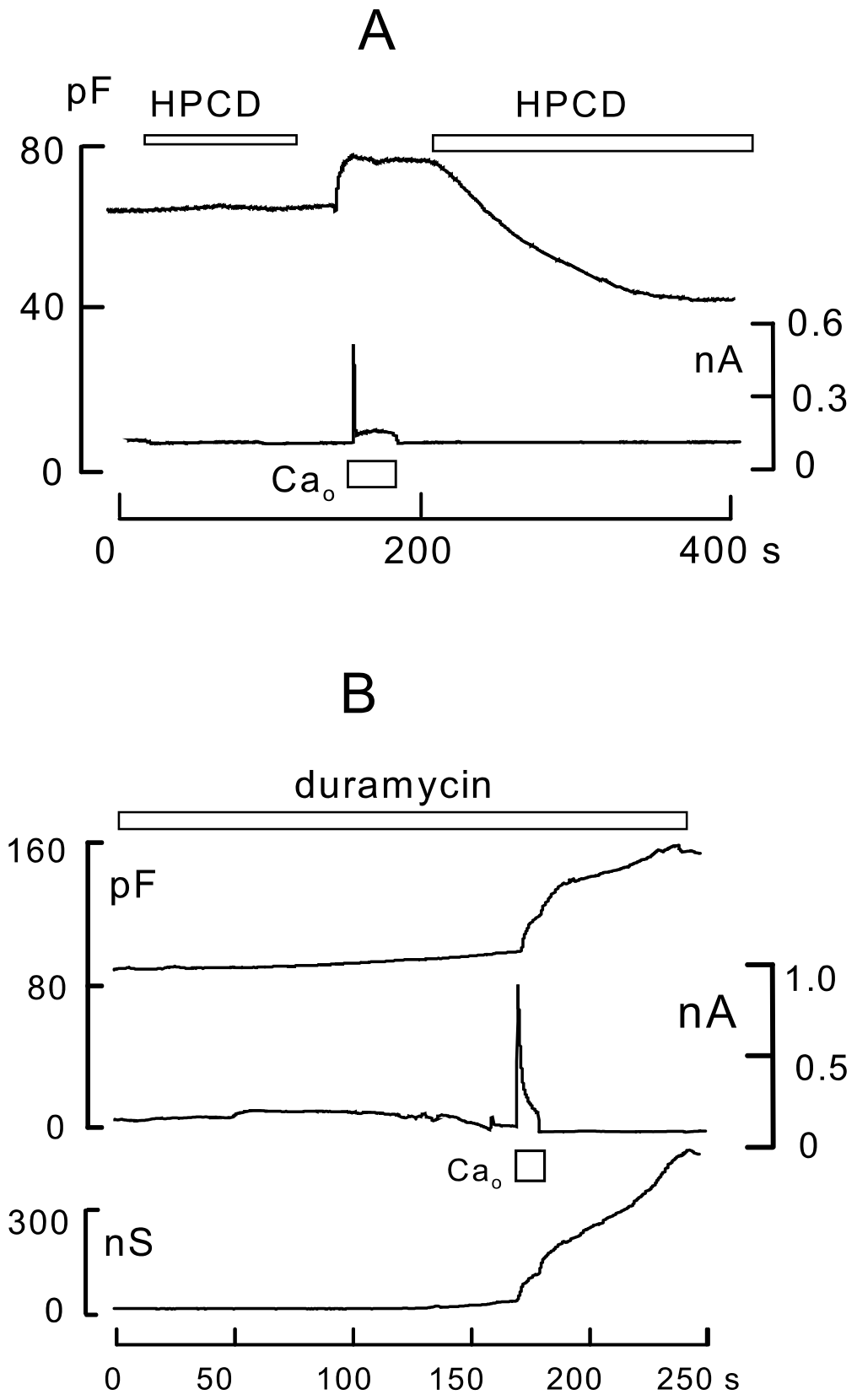
A
pF
HPCD
HPCD
80
40
0
0.6
nA
0.3
0
Ca$_o$
0
200
400 s
B
duramycin
160
pF
80
0
1.0
nA
0.5
0
Ca$_o$
300
nS
0
0
50
100
150
200
250 s

Figure S3

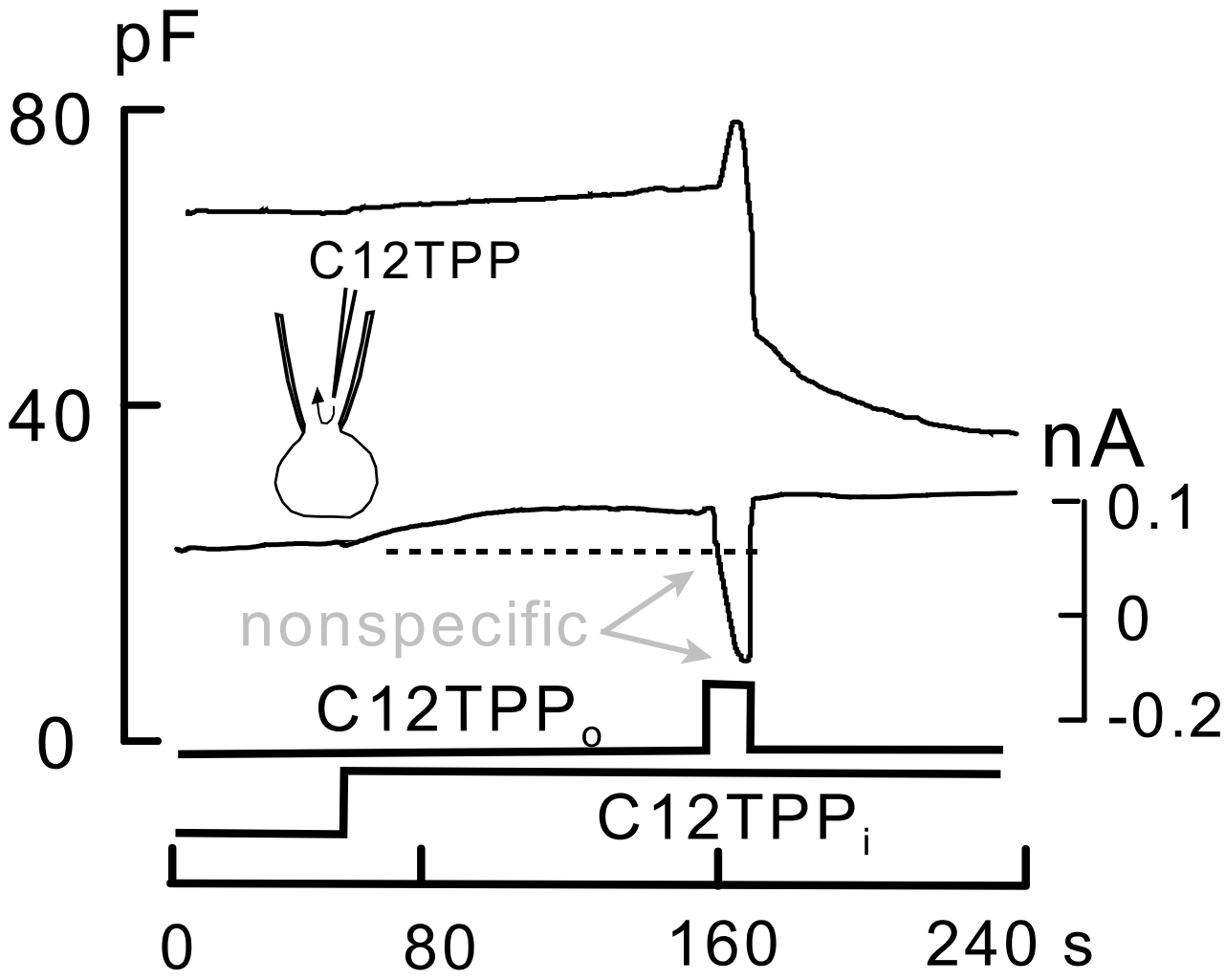
pF
80
40
0
C12TPP
nA
0.1
0
-0.2
nonspecific
C12TPP$_o$
C12TPP$_i$
0
80
160
240 s

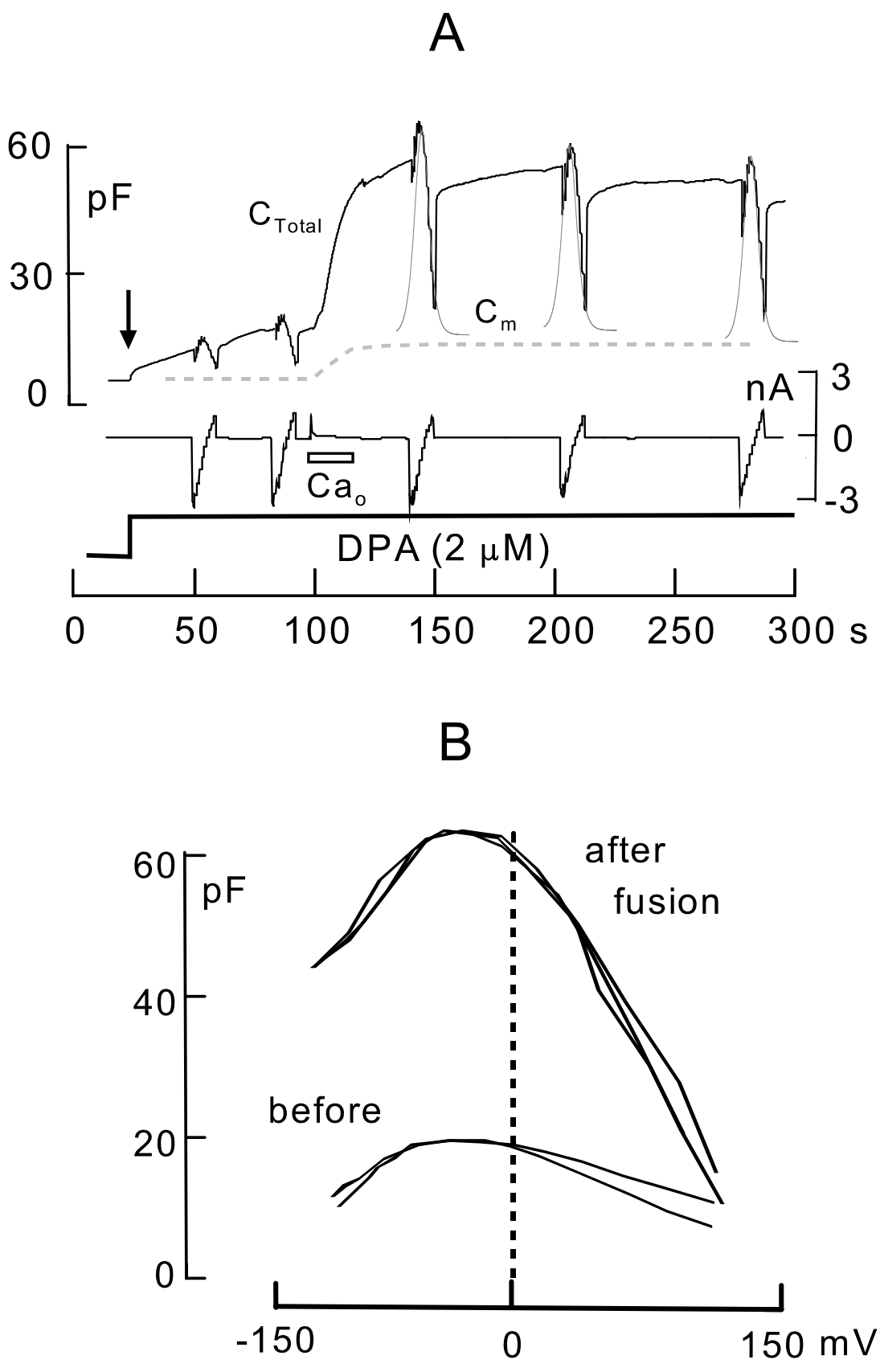
A
60
pF
30
0
C Total
C m
nA
3
0
-3
Ca o
DPA (2 μM)
0
50
100
150
200
250
300 s
B
60
pF
40
20
0
after
fusion
before
-150
0
150 mV

Figure S5

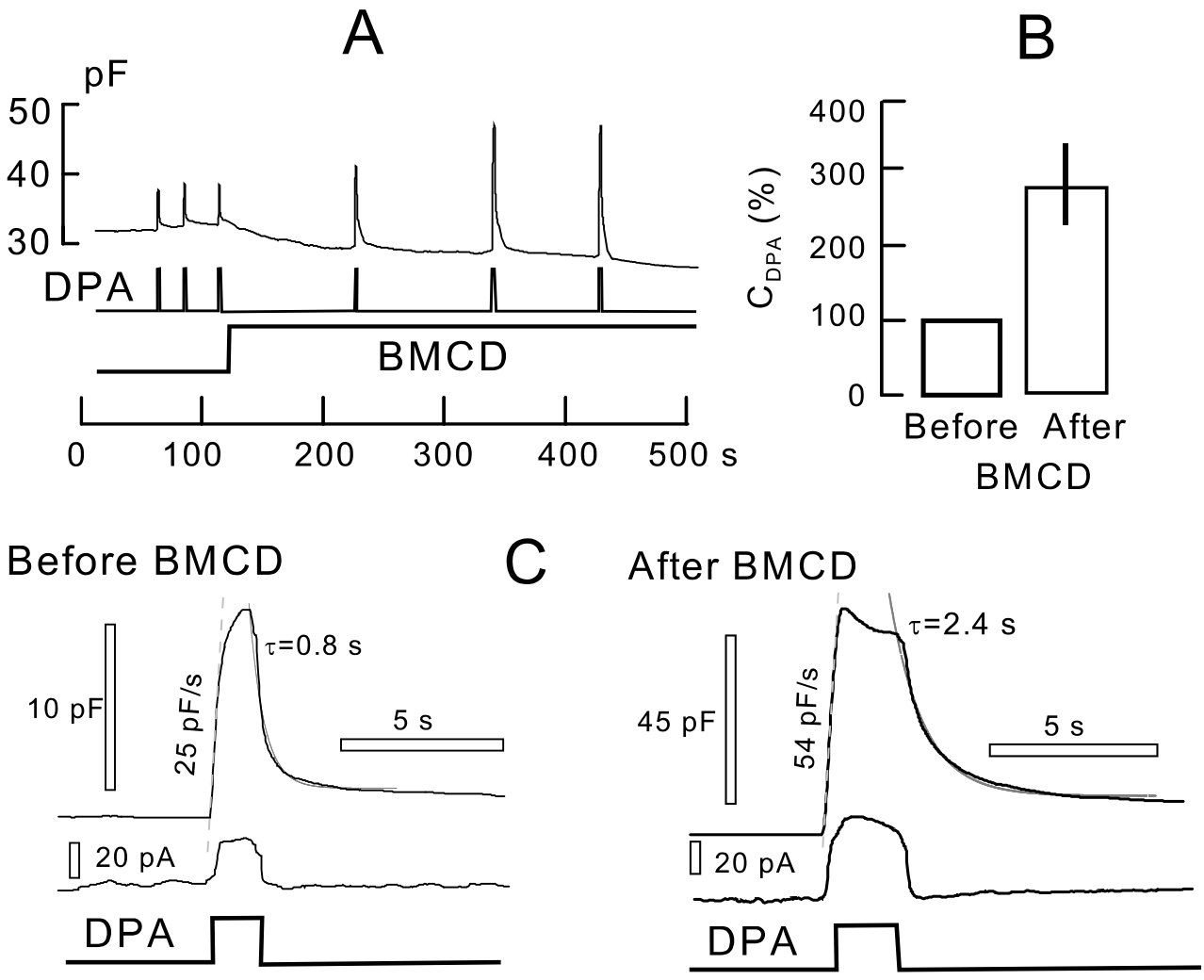
A
pF
50
40
30
DPA
BMCD
0
100
200
300
400
500 s
B
400
300
200
100
0
C_{DPA} (%)
Before
After
BMCD
Before BMCD
C
10 pF
25 pF/s
τ=0.8 s
5 s
20 pA
DPA
After BMCD
45 pF
54 pF/s
τ=2.4 s
5 s
20 pA
DPA

Figure S6

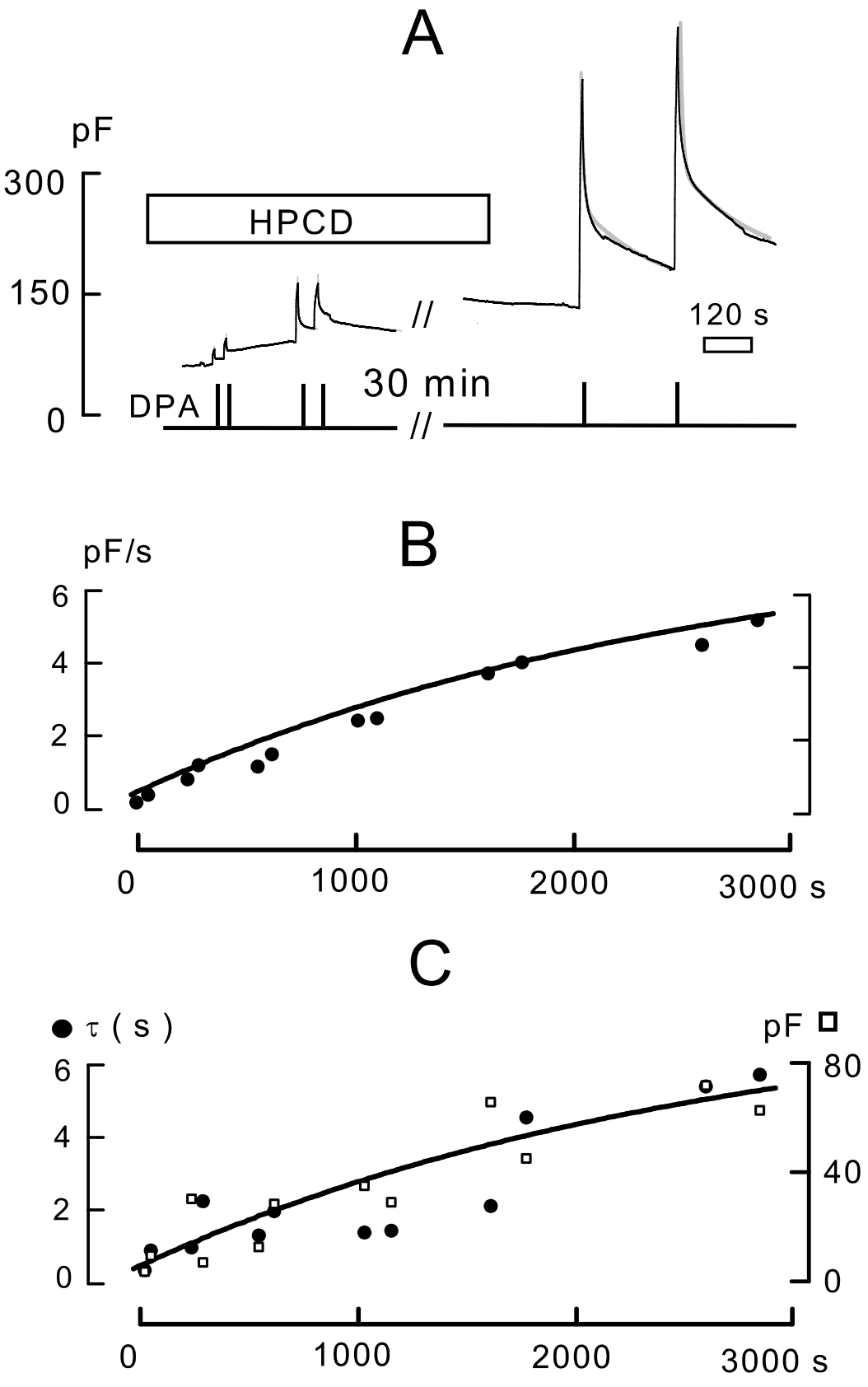
A
pF
300
150
0
HPCD
DPA
30 min
120 s
B
pF/s
6
4
2
0
0
1000
2000
3000 s
C
● τ (s)
pF □
6
4
2
0
80
40
0
0
1000
2000
3000 s

Figure S7

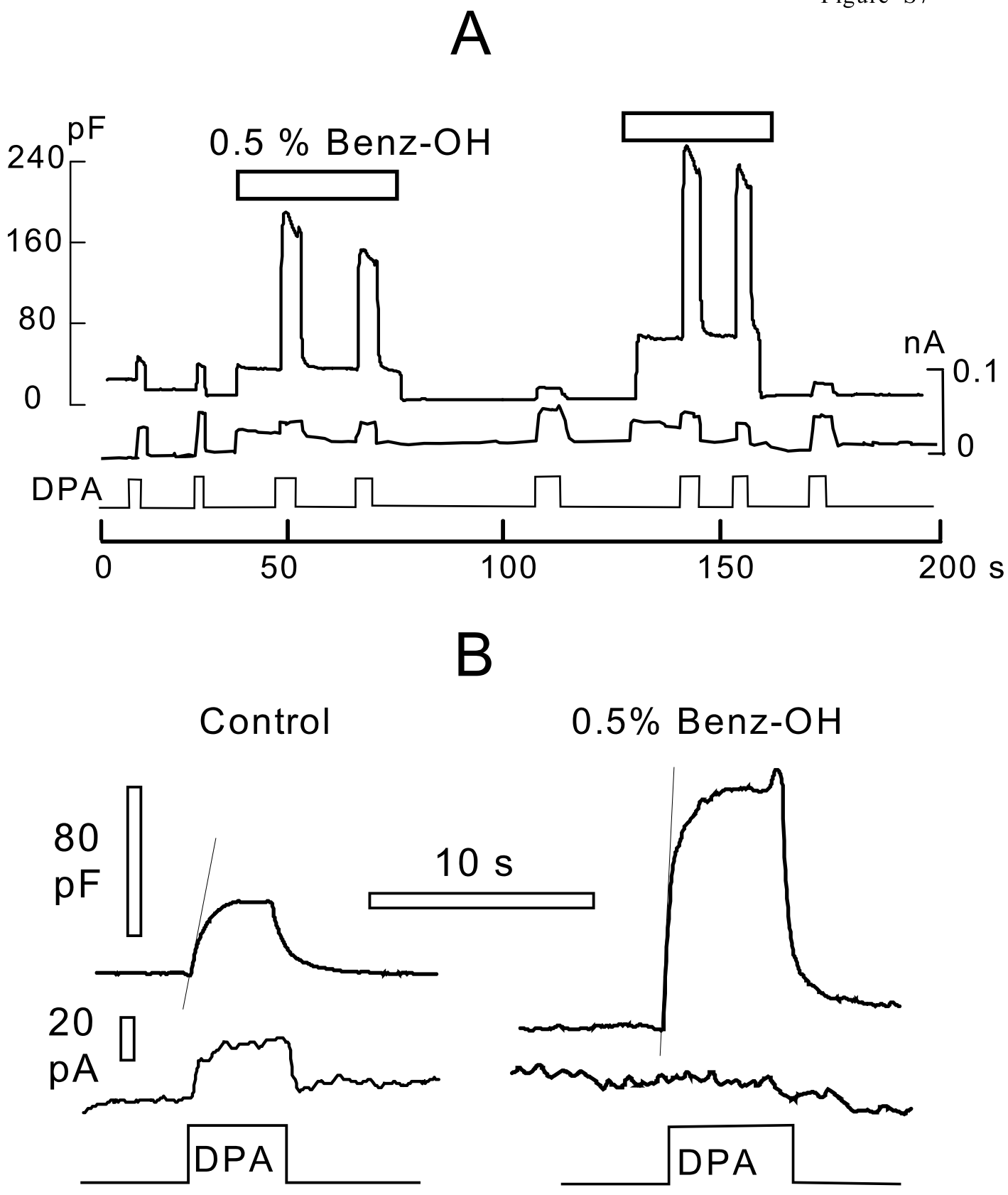
A
pF
240
160
80
0
0.5 % Benz-OH
nA
0.1
0
DPA
0
50
100
150
200 s
B
Control
0.5% Benz-OH
80
pF
10 s
20
pA
DPA
DPA

Figure S8

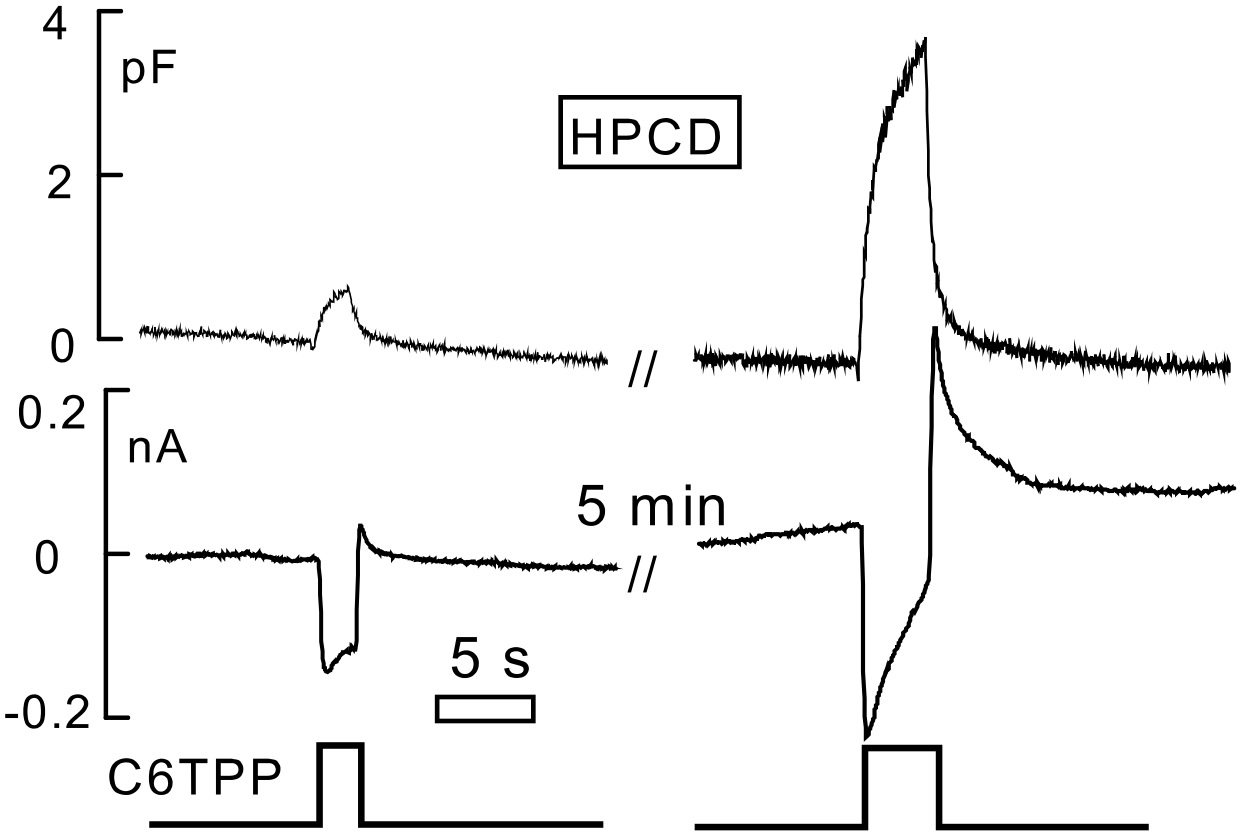

Figure S9

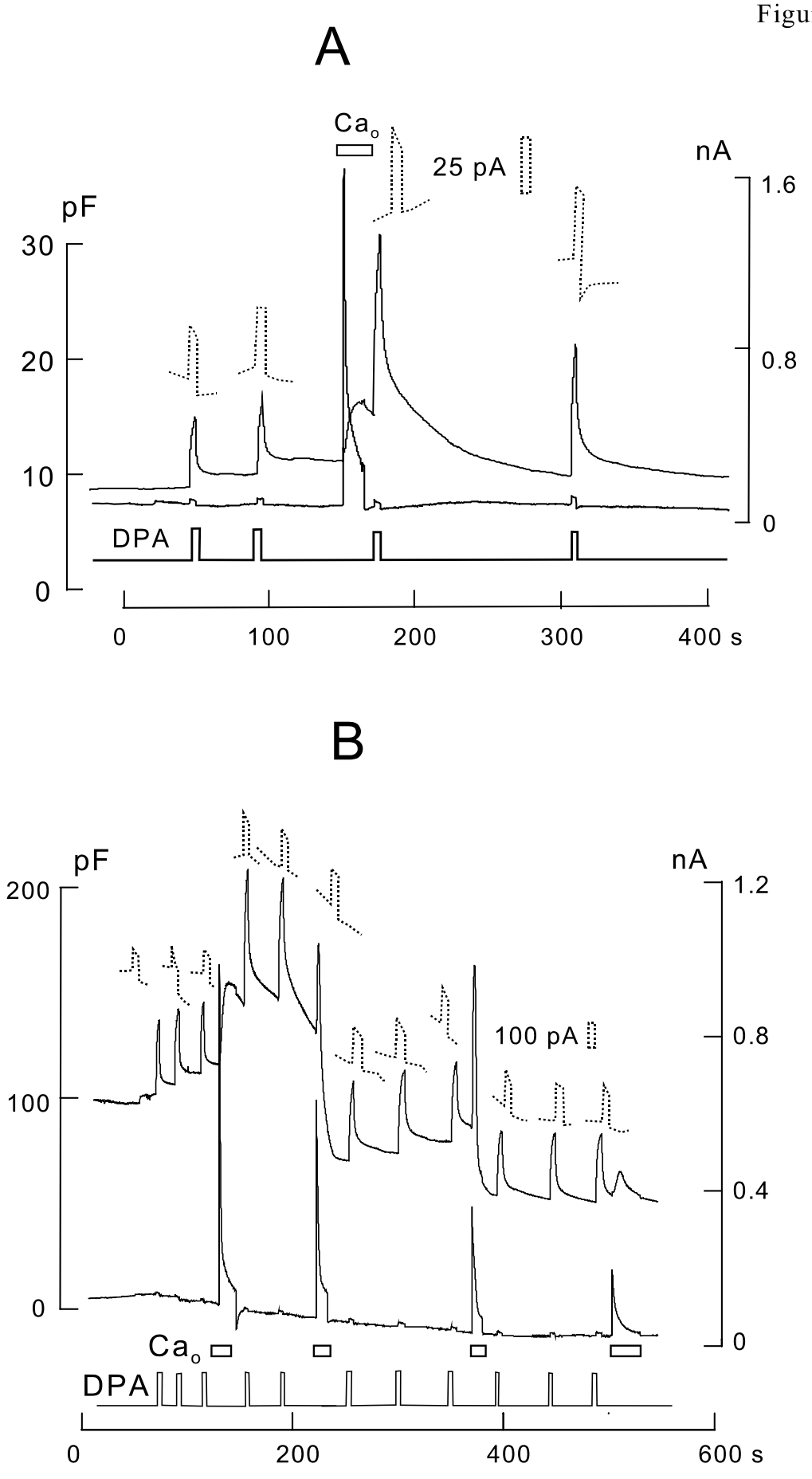
A
Ca$_o$
25 pA
nA
1.6
pF
30
20
10
0
0.8
0
DPA
0
100
200
300
400 s
B
pF
nA
200
100
0
1.2
0.8
0.4
0
100 pA
Ca$_o$
DPA
0
200
400
600 s

Figure S10

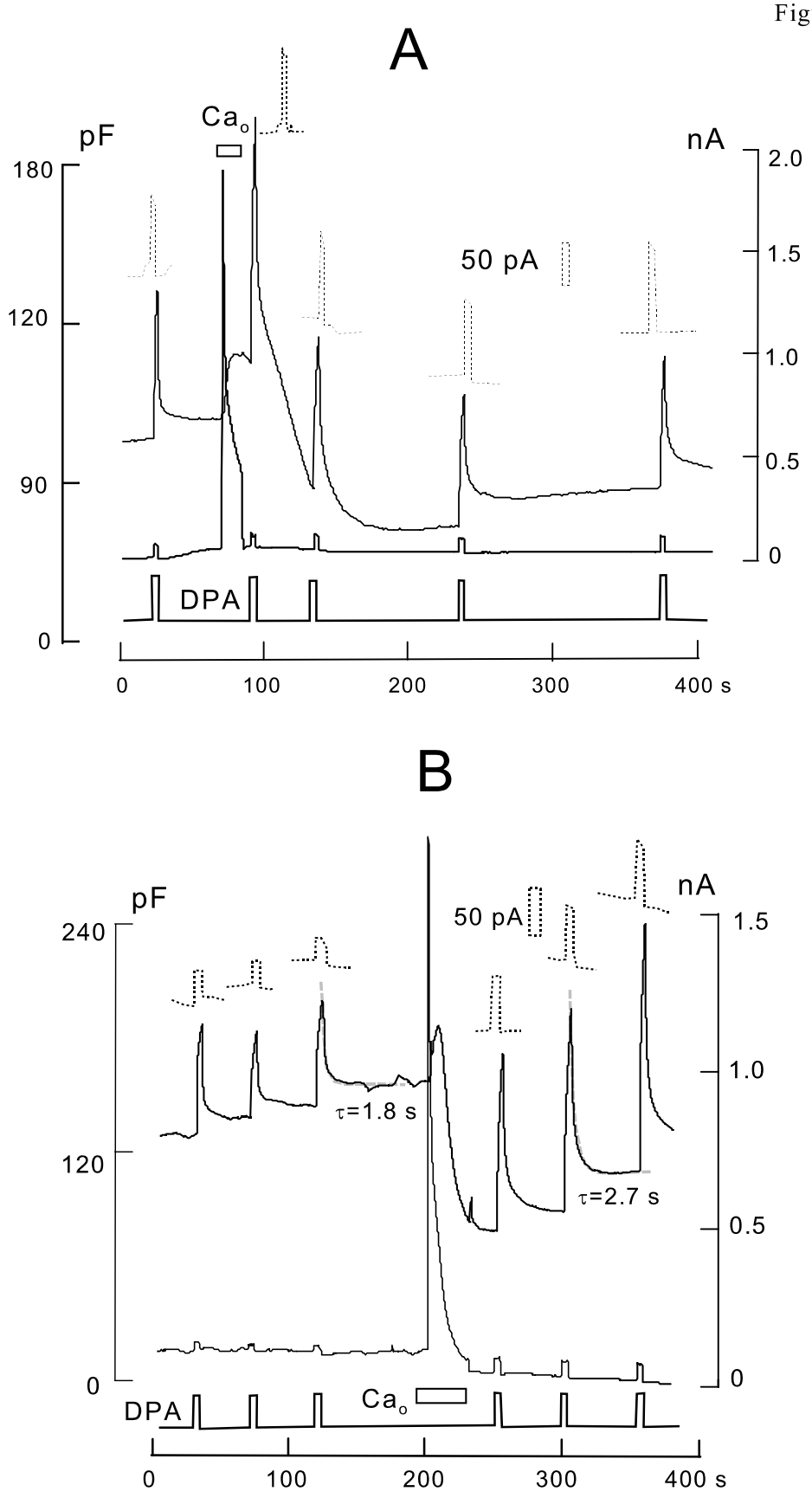
A
pF
Ca$_o$
nA
180
120
90
0
2.0
1.5
1.0
0.5
0
50 pA
DPA
0
100
200
300
400 s
B
pF
nA
240
120
0
50 pA
1.5
1.0
0.5
0
τ=1.8 s
τ=2.7 s
DPA
Ca$_o$
0
100
200
300
400 s

Figure S11

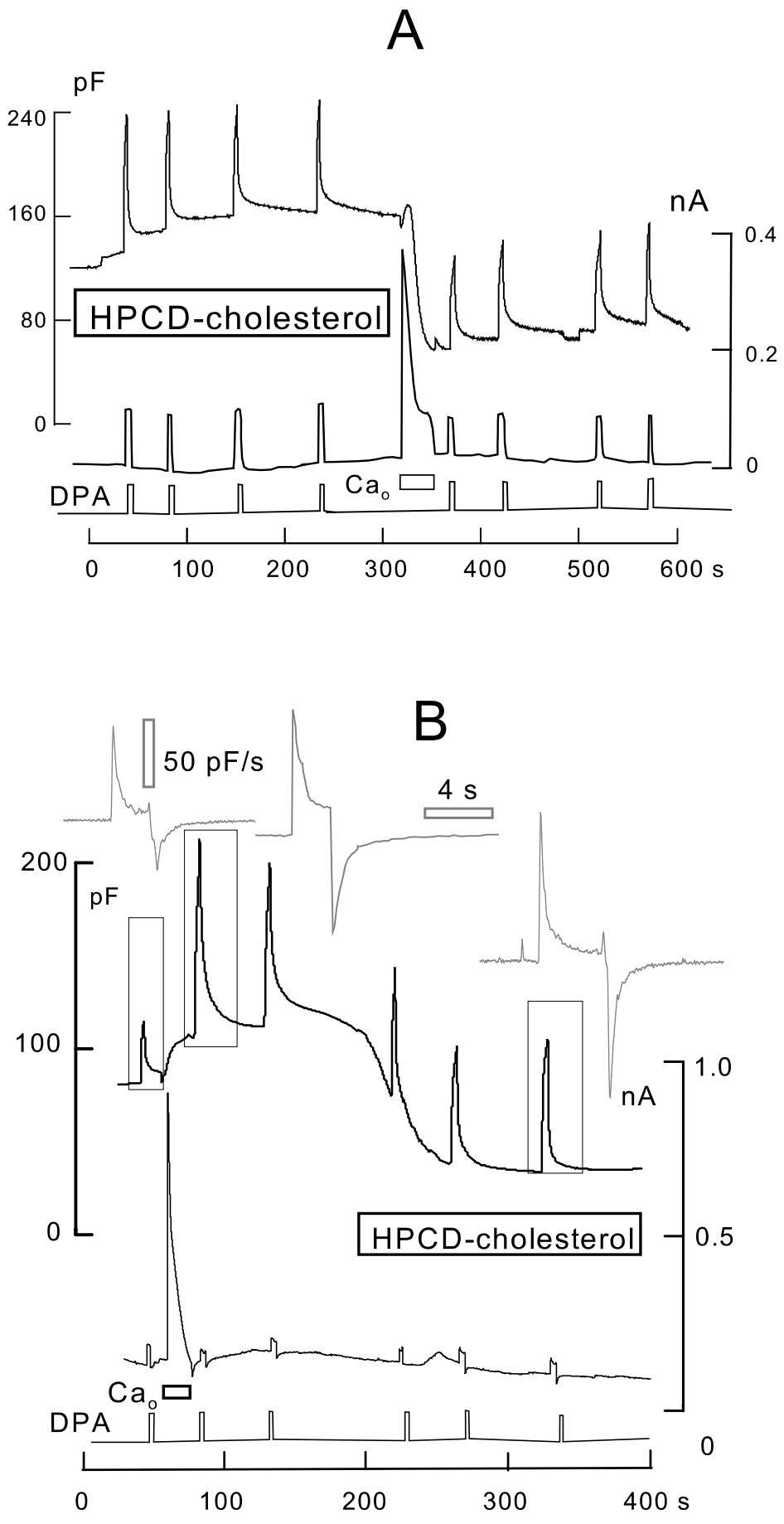
A
pF
240
160
80
0
nA
0.4
0.2
0
HPCD-cholesterol
DPA
Ca$_o$
0
100
200
300
400
500
600 s
B
50 pF/s
4 s
200
pF
100
0
nA
1.0
0.5
0
HPCD-cholesterol
Ca$_o$
DPA
0
100
200
300
400 s

Figure S12

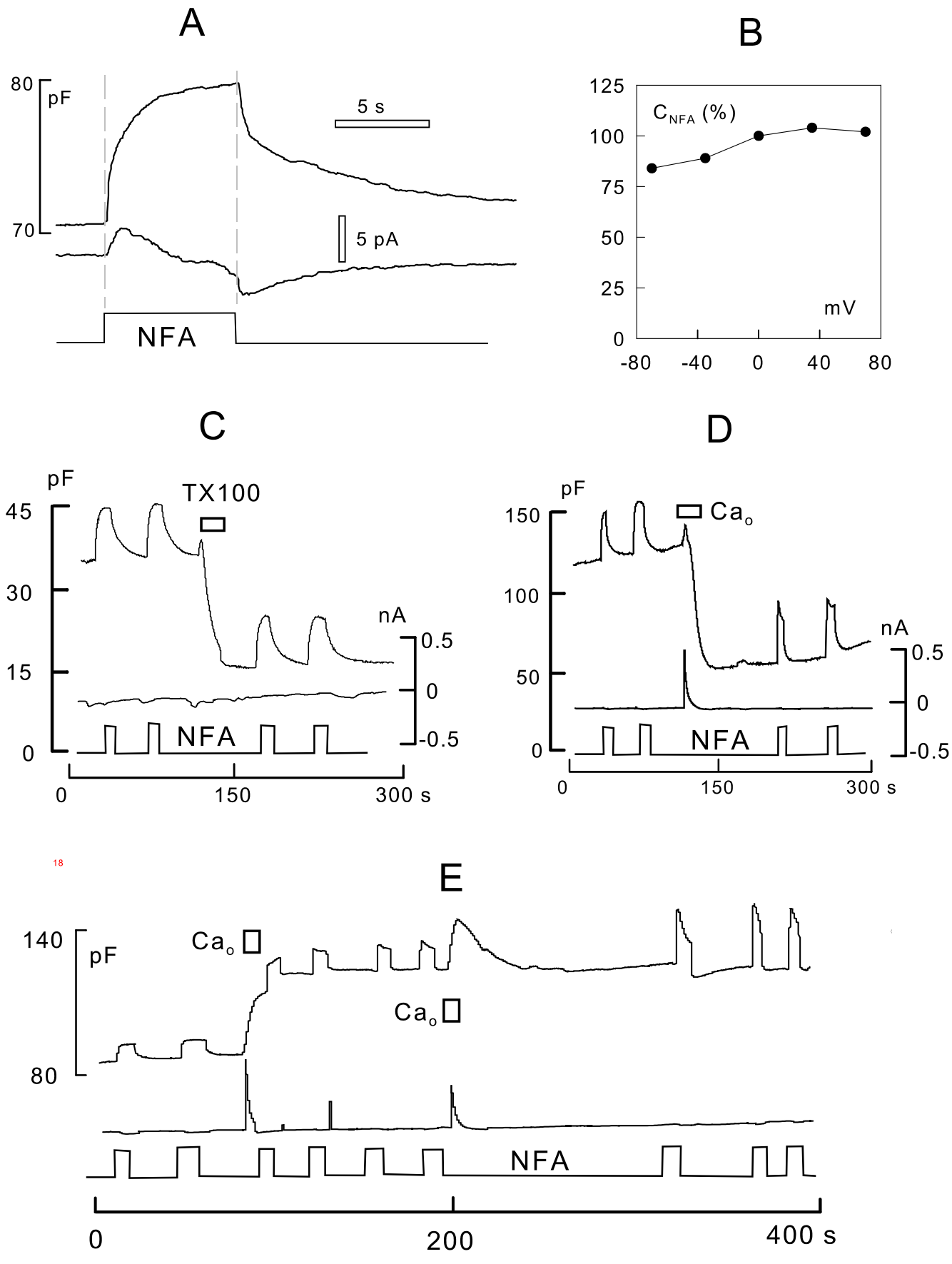
A
80
pF
70
5 s
5 pA
NFA
B
125
100
75
50
25
0
C_{NFA} (%)
mV
-80
-40
0
40
80
C
pF
45
30
15
0
TX100
nA
0.5
0
-0.5
NFA
0
150
300 s
D
pF
150
100
50
0
Ca_o
nA
0.5
0
-0.5
NFA
0
150
300 s
E
140
pF
80
Ca_o
Ca_o
NFA
0
200
400 s

Figure S13

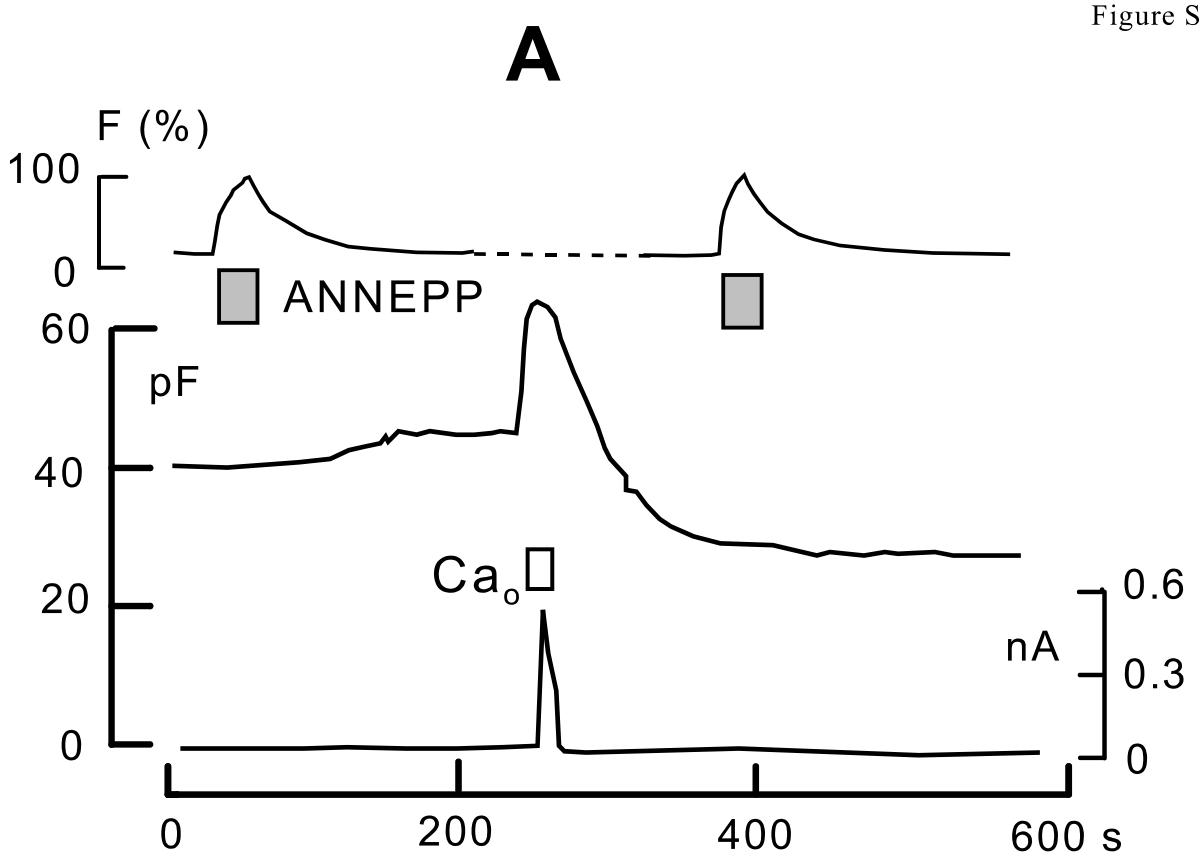
A
F (%)
100
0
ANNEPP
60
pF
40
20
0
Ca$_o$
0.6
nA
0.3
0
0
200
400
600 s

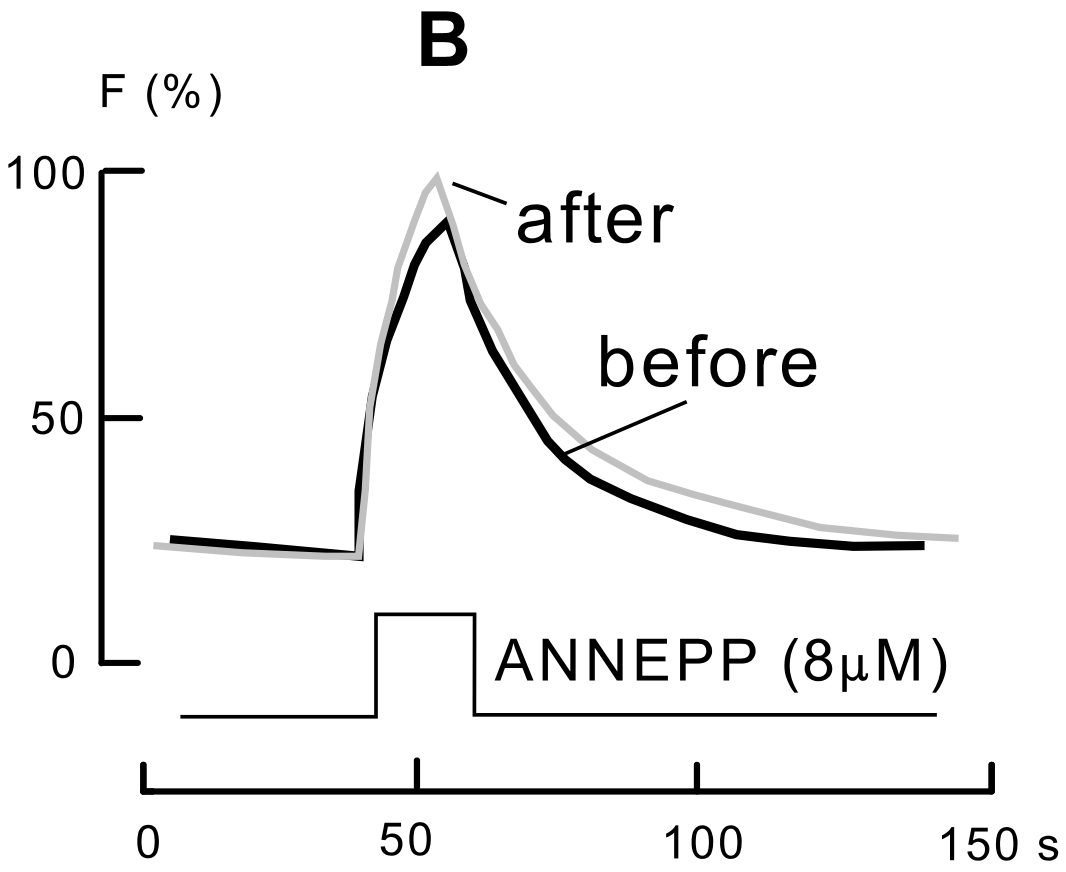
B
F (%)
100
after
before
50
0
ANNEPP (8μM)
0
50
100
150 s

BIBLIOGRAPHY

Adachi-Akahane, S., L. Lu, Z. Li, J.S. Frank, K.D. Philipson, and M. Morad. 1997. Calcium signaling in transgenic mice overexpressing cardiac Na(+)-Ca2+ exchanger. *J Gen Physiol*. 109:717-729.

Aderem, A., and D.M. Underhill. 1999. Mechanisms of phagocytosis in macrophages. *Annual review of immunology*. 17:593-623.

Ago, H., M. Oda, M. Takahashi, H. Tsuge, S. Ochi, N. Katunuma, M. Miyano, and J. Sakurai. 2006. Structural basis of the sphingomyelin phosphodiesterase activity in neutral sphingomyelinase from Bacillus cereus. *J Biol Chem*. 281:16157-16167.

Alberts, B. 2002. Molecular biology of the cell. Garland Science, New York. xxxiv, 1548 p. pp.

Altankov, G., and F. Grinnell. 1995. Fibronectin receptor internalization and AP-2 complex reorganization in potassium-depleted fibroblasts. *Exp Cell Res*. 216:299-309.

Andersen, P.S., and M. Fuchs. 1975. Potential energy barriers to ion transport within lipid bilayers. Studies with tetraphenylborate. *Biophys J*. 15:795-830.

Anderson, R.G. 1993. Plasmalemmal caveolae and GPI-anchored membrane proteins. *Current opinion in cell biology*. 5:647-652.

Anderson, R.G., and K. Jacobson. 2002. A role for lipid shells in targeting proteins to caveolae, rafts, and other lipid domains. *Science*. 296:1821-1825.

Artalejo, C.R., A. Elhamdani, and H.C. Palfrey. 1996. Calmodulin is the divalent cation receptor for rapid endocytosis, but not exocytosis, in adrenal chromaffin cells. *Neuron*. 16:195-205.

Babiychuk, E.B., K. Monastyrskaya, and A. Draeger. 2008. Fluorescent annexin A1 reveals dynamics of ceramide platforms in living cells. *Traffic*. 9:1757-1775.

Balijepalli, R.C., A.J. Lokuta, N.A. Maertz, J.M. Buck, R.A. Haworth, H.H. Valdivia, and T.J. Kamp. 2003. Depletion of T-tubules and specific subcellular changes in sarcolemmal proteins in tachycardia-induced heart failure. *Cardiovasc Res*. 59:67-77.

Bartolome, J.V., P.A. Trepanier, E.A. Chait, and T.A. Slotkin. 1982. Role of polyamines in isoproterenol-induced cardiac hypertrophy: effects of alpha-difluoromethylornithine, an irreversible inhibitor of ornithine decarboxylase. *J Mol Cell Cardiol*. 14:461-466.

Baumer, A.T., M. Flesch, H. Kilter, K.D. Philipson, and M. Bohm. 1998. Overexpression of the Na(+)-Ca2+ exchanger leads to enhanced inotropic responsiveness to Na(+)-channel agonist without sarcoplasmic reticulum protein changes in transgenic mice. *Biochem Biophys Res Commun*. 249:786-790.

Benito, B., E. Moreno, and R. Lagunas. 1991. Half-life of the plasma membrane ATPase and its activating system in resting yeast cells. *Biochim Biophys Acta*. 1063:265-268.

Benz, R., P. Lauger, and K. Janko. 1976. Transport kinetics of hydrophobic ions in lipid bilayer membranes. Charge-pulse relaxation studies. *Biochim Biophys Acta*. 455:701-720.

Bers, D.M. 2001. Excitation-contraction coupling and cardiac contractile force. Kluwer Academic Publishers, Dordrecht ; Boston. xxiv, 427 p. pp.

Bers, D.M., and S. Despa. 2006. Cardiac myocytes Ca2+ and Na+ regulation in normal and failing hearts. *J Pharmacol Sci*. 100:315-322.

Bers, D.M., S. Despa, and J. Bossuyt. 2006. Regulation of Ca2+ and Na+ in normal and failing cardiac myocytes. *Ann N Y Acad Sci*. 1080:165-177.

Bevers, E.M., and P.L. Williamson. 2010. Phospholipid scramblase: an update. *FEBS Lett*. 584:2724-2730.

Bi, G.Q., J.M. Alderton, and R.A. Steinhardt. 1995. Calcium-regulated exocytosis is required for cell membrane resealing. *J Cell Biol*. 131:1747-1758.

Bollinger, C.R., V. Teichgraber, and E. Gulbins. 2005. Ceramide-enriched membrane domains. *Biochim Biophys Acta*. 1746:284-294.

Borisy, G.G., and E.W. Taylor. 1967. The mechanism of action of colchicine. Binding of colchincine-3H to cellular protein. *J Cell Biol*. 34:525-533.

Botelho, R.J., M. Teruel, R. Dierckman, R. Anderson, A. Wells, J.D. York, T. Meyer, and S. Grinstein. 2000. Localized biphasic changes in phosphatidylinositol-4,5-bisphosphate at sites of phagocytosis. *J Cell Biol*. 151:1353-1368.

Bretscher, M.S. 1984. Endocytosis: relation to capping and cell locomotion. *Science*. 224:681-686.

Brown, D.A. 2006. Lipid rafts, detergent-resistant membranes, and raft targeting signals. *Physiology (Bethesda)*. 21:430-439.

Brown, F.D., A.L. Rozelle, H.L. Yin, T. Balla, and J.G. Donaldson. 2001. Phosphatidylinositol 4,5-bisphosphate and Arf6-regulated membrane traffic. *J Cell Biol*. 154:1007-1017.

Bruner, L.J. 1975. The interaction of hydrophobic ions with lipid bilayer membranes. *J Membr Biol*. 22:125-141.

Brunton, V.G., M.H. Grant, and H.M. Wallace. 1991. Mechanisms of spermine toxicity in baby-hamster kidney (BHK) cells. The role of amine oxidases and oxidative stress. *Biochem J*. 280 (Pt 1):193-198.

Caldarera, C.M., A. Casti, C. Rossoni, and O. Visioli. 1971. Polyamines and noradrenaline following myocardial hypertrophy. *J Mol Cell Cardiol*. 3:121-126.

Camps, M., C.F. Hou, K.H. Jakobs, and P. Gierschik. 1990. Guanosine 5'-[gamma-thio]triphosphate-stimulated hydrolysis of phosphatidylinositol 4,5-bisphosphate in HL-60 granulocytes. Evidence that the guanine nucleotide acts by relieving phospholipase C from an inhibitory constraint. *Biochem J*. 271:743-748.

Cedars, A., C.M. Jenkins, D.J. Mancuso, and R.W. Gross. 2009. Calcium-independent phospholipases in the heart: mediators of cellular signaling, bioenergetics, and ischemia-induced electrophysiologic dysfunction. *J Cardiovasc Pharmacol*. 53:277-289.

Chan, S.A., and C. Smith. 2001. Physiological stimuli evoke two forms of endocytosis in bovine chromaffin cells. *J Physiol*. 537:871-885.

Chanda, B., R. Blunck, L.C. Faria, F.E. Schweizer, I. Mody, and F. Bezanilla. 2005. A hybrid approach to measuring electrical activity in genetically specified neurons. *Nat Neurosci*. 8:1619-1626.

Chapman, E.R. 2008. How does synaptotagmin trigger neurotransmitter release? *Annu Rev Biochem*. 77:615-641.

Chasserot-Golaz, S., N. Vitale, E. Umbrecht-Jenck, D. Knight, V. Gerke, and M.F. Bader. 2005. Annexin 2 promotes the formation of lipid microdomains required for calcium-regulated exocytosis of dense-core vesicles. *Mol Biol Cell*. 16:1108-1119.

Chi, Y., B. Zhou, W.Q. Wang, S.K. Chung, Y.U. Kwon, Y.H. Ahn, Y.T. Chang, Y. Tsujishita, J.H. Hurley, and Z.Y. Zhang. 2004. Comparative mechanistic and substrate specificity study of inositol polyphosphate 5-phosphatase Schizosaccharomyces pombe Synaptojanin and SHIP2. *J Biol Chem*. 279:44987-44995.

Chidiac, P., V.S. Markin, and E.M. Ross. 1999. Kinetic control of guanine nucleotide binding to soluble Galpha(q). *Biochem Pharmacol*. 58:39-48.

Clapham, D.E. 2007. Calcium signaling. *Cell*. 131:1047-1058.

Clayton, E.L., V. Anggono, K.J. Smillie, N. Chau, P.J. Robinson, and M.A. Cousin. 2009. The phospho-dependent dynamin-syndapin interaction triggers activity-dependent bulk endocytosis of synaptic vesicles. *J Neurosci*. 29:7706-7717.

Clayton, E.L., and M.A. Cousin. 2009. The molecular physiology of activity-dependent bulk endocytosis of synaptic vesicles. *J Neurochem*. 111:901-914.

Coburn, R.F., D.H. Jones, C.P. Morgan, C.B. Baron, and S. Cockcroft. 2002. Spermine increases phosphatidylinositol 4,5-bisphosphate content in permeabilized and nonpermeabilized HL60 cells. *Biochim Biophys Acta*. 1584:20-30.

Cocucci, E., G. Racchetti, P. Podini, M. Rupnik, and J. Meldolesi. 2004. Enlargeosome, an exocytic vesicle resistant to nonionic detergents, undergoes endocytosis via a nonacidic route. *Mol Biol Cell*. 15:5356-5368.

Cogolludo, A., L. Moreno, G. Frazziano, J. Moral-Sanz, C. Menendez, J. Castaneda, C. Gonzalez, E. Villamor, and F. Perez-Vizcaino. 2009. Activation of neutral sphingomyelinase is involved in acute hypoxic pulmonary vasoconstriction. *Cardiovasc Res*. 82:296-302.

Conner, S.D., and S.L. Schmid. 2003. Regulated portals of entry into the cell. *Nature*. 422:37-44.

Cooper, G.M., and R.E. Hausman. 2009. The cell : a molecular approach. ASM Press ;
Sinauer Associates, Washington, D.C.

Sunderland, Mass. xix, 820 p. pp.
Coskun, U., and K. Simons. 2010. Membrane rafting: from apical sorting to phase segregation. *FEBS Lett*. 584:1685-1693.
Cremona, O., G. Di Paolo, M.R. Wenk, A. Luthi, W.T. Kim, K. Takei, L. Daniell, Y. Nemoto, S.B. Shears, R.A. Flavell, D.A. McCormick, and P. De Camilli. 1999. Essential role of phosphoinositide metabolism in synaptic vesicle recycling. *Cell*. 99:179-188.
Cusdin, F.S., J.J. Clare, and A.P. Jackson. 2008. Trafficking and cellular distribution of voltage-gated sodium channels. *Traffic*. 9:17-26.
Davies, P.J., D.R. Davies, A. Levitzki, F.R. Maxfield, P. Milhaud, M.C. Willingham, and I.H. Pastan. 1980. Transglutaminase is essential in receptor-mediated endocytosis of alpha 2-macroglobulin and polypeptide hormones. *Nature*. 283:162-167.
de Almeida, R.F., L.M. Loura, A. Fedorov, and M. Prieto. 2005. Lipid rafts have different sizes depending on membrane composition: a time-resolved fluorescence resonance energy transfer study. *J Mol Biol*. 346:1109-1120.
de Haro, L., G. Ferracci, S. Opi, C. Iborra, S. Quetglas, R. Miquelis, C. Leveque, and M. Seagar. 2004. Ca2+/calmodulin transfers the membrane-proximal lipid-binding domain of the v-SNARE synaptobrevin from cis to trans bilayers. *Proc Natl Acad Sci U S A*. 101:1578-1583.
Despa, S., and D.M. Bers. 2007. Functional analysis of Na+/K+-ATPase isoform distribution in rat ventricular myocytes. *Am J Physiol Cell Physiol*. 293:C321-327.
Dhalla, N.S., A.B. Elmoselhi, T. Hata, and N. Makino. 2000. Status of myocardial antioxidants in ischemia-reperfusion injury. *Cardiovasc Res*. 47:446-456.
Ding, T., Z. Li, T. Hailemariam, S. Mukherjee, F.R. Maxfield, M.P. Wu, and X.C. Jiang. 2008. SMS overexpression and knockdown: impact on cellular sphingomyelin and diacylglycerol metabolism, and cell apoptosis. *Journal of lipid research*. 49:376-385.
Doherty, G.J., and H.T. McMahon. 2009. Mechanisms of endocytosis. *Annu Rev Biochem*. 78:857-902.
Donaldson, J.G., N. Porat-Shliom, and L.A. Cohen. 2009. Clathrin-independent endocytosis: a unique platform for cell signaling and PM remodeling. *Cell Signal*. 21:1-6.
Dulubova, I., S. Sugita, S. Hill, M. Hosaka, I. Fernandez, T.C. Sudhof, and J. Rizo. 1999. A conformational switch in syntaxin during exocytosis: role of munc18. *EMBO J*. 18:4372-4382.
Edidin, M. 2003. The state of lipid rafts: from model membranes to cells. *Annu Rev Biophys Biomol Struct*. 32:257-283.
Egner, R., and K. Kuchler. 1996. The yeast multidrug transporter Pdr5 of the plasma membrane is ubiquitinated prior to endocytosis and degradation in the vacuole. *FEBS Lett*. 378:177-181.
Egner, R., Y. Mahe, R. Pandjaitan, and K. Kuchler. 1995. Endocytosis and vacuolar degradation of the plasma membrane-localized Pdr5 ATP-binding cassette multidrug transporter in Saccharomyces cerevisiae. *Molecular and cellular biology*. 15:5879-5887.
El-Jouni, W., S. Haun, and K. Machaca. 2008. Internalization of plasma membrane Ca2+-ATPase during Xenopus oocyte maturation. *Dev Biol*. 324:99-107.
Engisch, K.L., and M.C. Nowycky. 1998. Compensatory and excess retrieval: two types of endocytosis following single step depolarizations in bovine adrenal chromaffin cells. *J Physiol*. 506 (Pt 3):591-608.
Falkenburger, B.H., J.B. Jensen, and B. Hille. 2010. Kinetics of PIP2 metabolism and KCNQ2/3 channel regulation studied with a voltage-sensitive phosphatase in living cells. *J Gen Physiol*. 135:99-114.
Farman, G.P., K. Tachampa, R. Mateja, O. Cazorla, A. Lacampagne, and P.P. de Tombe. 2008. Blebbistatin: use as inhibitor of muscle contraction. *Pflugers Arch*. 455:995-1005.
Ferguson, S.M., G. Brasnjo, M. Hayashi, M. Wolfel, C. Collesi, S. Giovedi, A. Raimondi, L.W. Gong, P. Ariel, S. Paradise, E. O'Toole, R. Flavell, O. Cremona, G. Miesenbock, T.A. Ryan, and P. De Camilli. 2007. A selective activity-dependent requirement for dynamin 1 in synaptic vesicle endocytosis. *Science*. 316:570-574.
Fine, M., M.C. Llaguno, V. Lariccia, M.-J. Lin, A. Yaradanakul, and D.W. Hilgemann. xxxx. Massive Endocytosis Driven by Lipidic Forces Originating in the Outer Plasmalemmal

Monolayer: A New Approach to Membrane Recycling and Lipid Domains. *J Gen Physiol*. xxx:xxx-xxx.

Fine, M., M.C. Llaguno, V. Lariccia, M.J. Lin, A. Yaradanakul, and D.W. Hilgemann. 2011. Massive endocytosis driven by lipidic forces originating in the outer plasmalemmal monolayer: a new approach to membrane recycling and lipid domains. *J Gen Physiol*. 137:137-154.

Flewelling, R.F., and W.L. Hubbell. 1986. The membrane dipole potential in a total membrane potential model. Applications to hydrophobic ion interactions with membranes. *Biophys J*. 49:541-552.

Gallop, J.L., C.C. Jao, H.M. Kent, P.J. Butler, P.R. Evans, R. Langen, and H.T. McMahon. 2006. Mechanism of endophilin N-BAR domain-mediated membrane curvature. *EMBO J*. 25:2898-2910.

Garcia-Saez, A.J., S. Chiantia, and P. Schwille. 2007. Effect of line tension on the lateral organization of lipid membranes. *J Biol Chem*. 282:33537-33544.

Geli, M.I., and H. Riezman. 1998. Endocytic internalization in yeast and animal cells: similar and different. *J Cell Sci*. 111 (Pt 8):1031-1037.

Geumann, U., C. Schafer, D. Riedel, R. Jahn, and S.O. Rizzoli. 2009. Synaptic membrane proteins form stable microdomains in early endosomes. *Microsc Res Tech*.

Gidwani, A., D. Holowka, and B. Baird. 2001. Fluorescence anisotropy measurements of lipid order in plasma membranes and lipid rafts from RBL-2H3 mast cells. *Biochemistry*. 40:12422-12429.

Goldstein, J.L., R.G. Anderson, and M.S. Brown. 1979. Coated pits, coated vesicles, and receptor-mediated endocytosis. *Nature*. 279:679-685.

Goni, F.M., and A. Alonso. 2009. Effects of ceramide and other simple sphingolipids on membrane lateral structure. *Biochim Biophys Acta*. 1788:169-177.

Grant, N.J., and C. Oriol-Audit. 1985. Influence of the polyamine spermine on the organization of cortical filaments in isolated cortices of Xenopus laevis eggs. *Eur J Cell Biol*. 36:239-246.

Grover, G.J., P.G. Sleph, and S. Dzwonczyk. 1992. Role of myocardial ATP-sensitive potassium channels in mediating preconditioning in the dog heart and their possible interaction with adenosine A1-receptors. *Circulation*. 86:1310-1316.

Groves, J.T. 2007. Bending mechanics and molecular organization in biological membranes. *Annu Rev Phys Chem*. 58:697-717.

Gwathmey, J.K., L. Copelas, R. MacKinnon, F.J. Schoen, M.D. Feldman, W. Grossman, and J.P. Morgan. 1987. Abnormal intracellular calcium handling in myocardium from patients with end-stage heart failure. *Circ Res*. 61:70-76.

Hamada, T., Y. Miura, K. Ishii, S. Araki, K. Yoshikawa, M. Vestergaard, and M. Takagi. 2007. Dynamic processes in endocytic transformation of a raft-exhibiting giant liposome. *J Phys Chem B*. 111:10853-10857.

Hao, M., S. Mukherjee, and F.R. Maxfield. 2001. Cholesterol depletion induces large scale domain segregation in living cell membranes. *Proc Natl Acad Sci U S A*. 98:13072-13077.

Hausenloy, D.J., and D.M. Yellon. 2010. Cell Membrane Repair as a Mechanism for Ischemic Preconditioning? *Circulation*. 121:2547-2549.

Hayashi, K., W. Shuai, Y. Sakamoto, H. Higashida, M. Yamagishi, and S. Kupershmidt. 2010. Trafficking-competent KCNQ1 variably influences the function of HERG long QT alleles. *Heart Rhythm*. 7:973-980.

Heda, G.D., M. Tanwani, and C.R. Marino. 2001. The Delta F508 mutation shortens the biochemical half-life of plasma membrane CFTR in polarized epithelial cells. *Am J Physiol Cell Physiol*. 280:C166-174.

Heerklotz, H. 2008. Interactions of surfactants with lipid membranes. *Q Rev Biophys*. 41:205-264.

Heerklotz, H., H. Szadkowska, T. Anderson, and J. Seelig. 2003. The sensitivity of lipid domains to small perturbations demonstrated by the effect of Triton. *J Mol Biol*. 329:793-799.

Hilgemann, D.W. 1989. Giant excised cardiac sarcolemmal membrane patches: sodium and sodium-calcium exchange currents. *Pflugers Arch*. 415:247-249.

Hilgemann, D.W. 1996. The cardiac Na-Ca exchanger in giant membrane patches. *Ann N Y Acad Sci*. 779:136-158.
Hilgemann, D.W. 2007. Local PIP(2) signals: when, where, and how? *Pflugers Arch*. 455:55-67.
Hilgemann, D.W., and A. Collins. 1992. Mechanism of cardiac Na(+)-Ca2+ exchange current stimulation by MgATP: possible involvement of aminophospholipid translocase. *J Physiol*. 454:59-82.
Hilgemann, D.W., A. Collins, D.P. Cash, and G.A. Nagel. 1991. Cardiac Na(+)-Ca2+ exchange system in giant membrane patches. *Ann N Y Acad Sci*. 639:126-139.
Hilgemann, D.W., and M. Fine. 2011. Mechanistic analysis of massive endocytosis in relation to functionally defined surface membrane domains. *J Gen Physiol*. 137:155-172.
Hilgemann, D.W., and M. Fine. xxxx. Mechanistic Analysis of Massive Endocytosis in Relation to Functionally-Defined Surface Membrane Domains *J Gen Physiol*. XXX:xxx.
Hilgemann, D.W., and C.C. Lu. 1998. Giant membrane patches: improvements and applications. *Methods Enzymol*. 293:267-280.
Hilgemann, D.W., A. Yaradanakul, Y. Wang, and D. Fuster. 2006. Molecular control of cardiac sodium homeostasis in health and disease. *J Cardiovasc Electrophysiol*. 17 Suppl 1:S47-S56.
Hille, B. 2001. Ion channels of excitable membranes. Sinauer, Sunderland, Mass. xviii, 814 p. pp.
Hogg, R.C., Q. Wang, and W.A. Large. 1994. Action of niflumic acid on evoked and spontaneous calcium-activated chloride and potassium currents in smooth muscle cells from rabbit portal vein. *Br J Pharmacol*. 112:977-984.
Holmgren, M., J. Wagg, F. Bezanilla, R.F. Rakowski, P. De Weer, and D.C. Gadsby. 2000. Three distinct and sequential steps in the release of sodium ions by the Na+/K+-ATPase. *Nature*. 403:898-901.
Holopainen, J.M., M.I. Angelova, and P.K. Kinnunen. 2000. Vectorial budding of vesicles by asymmetrical enzymatic formation of ceramide in giant liposomes. *Biophys J*. 78:830-838.
Horowitz, L.F., W. Hirdes, B.C. Suh, D.W. Hilgemann, K. Mackie, and B. Hille. 2005. Phospholipase C in living cells: activation, inhibition, Ca2+ requirement, and regulation of M current. *J Gen Physiol*. 126:243-262.
Hryshko, L.V., D.A. Nicoll, J.N. Weiss, and K.D. Philipson. 1993. Biosynthesis and initial processing of the cardiac sarcolemmal Na(+)-Ca2+ exchanger. *Biochim Biophys Acta*. 1151:35-42.
Huang, C.L., S. Feng, and D.W. Hilgemann. 1998. Direct activation of inward rectifier potassium channels by PIP2 and its stabilization by Gbetagamma. *Nature*. 391:803-806.
Idone, V., C. Tam, J.W. Goss, D. Toomre, M. Pypaert, and N.W. Andrews. 2008. Repair of injured plasma membrane by rapid Ca2+-dependent endocytosis. *J Cell Biol*. 180:905-914.
Igarashi, K., and K. Kashiwagi. 2000. Polyamines: mysterious modulators of cellular functions. *Biochem Biophys Res Commun*. 271:559-564.
Ivanov, A.I. 2008. Pharmacological inhibition of endocytic pathways: is it specific enough to be useful? *Methods Mol Biol*. 440:15-33.
Jahn, R., T. Lang, and T.C. Sudhof. 2003. Membrane fusion. *Cell*. 112:519-533.
Jiang, M., and G. Chen. 2009. Ca2+ regulation of dynamin-independent endocytosis in cortical astrocytes. *J Neurosci*. 29:8063-8074.
Jin, L., A.C. Millard, J.P. Wuskell, X. Dong, D. Wu, H.A. Clark, and L.M. Loew. 2006. Characterization and application of a new optical probe for membrane lipid domains. *Biophys J*. 90:2563-2575.
Kaeberlein, M. 2009. Spermidine surprise for a long life. *Nat Cell Biol*. 11:1277-1278.
Kaiser, H.J., D. Lingwood, I. Levental, J.L. Sampaio, L. Kalvodova, L. Rajendran, and K. Simons. 2009. Order of lipid phases in model and plasma membranes. *Proc Natl Acad Sci U S A*. 106:16645-16650.
Kang, T.M., and D.W. Hilgemann. 2004. Multiple transport modes of the cardiac Na+/Ca2+ exchanger. *Nature*. 427:544-548.

Kang, T.M., V.S. Markin, and D.W. Hilgemann. 2003. Ion fluxes in giant excised cardiac membrane patches detected and quantified with ion-selective microelectrodes. *J Gen Physiol*. 121:325-347.

Karliner, J.S., and J.H. Brown. 2009. Lipid signalling in cardiovascular pathophysiology. *Cardiovasc Res*. 82:171-174.

Katz, B. 1996. Neural transmitter release: from quantal secretion to exocytosis and beyond. The Fenn Lecture. *J Neurocytol*. 25:677-686.

Kennedy, E.P., C.F. Fox, and J.R. Carter. 1966. Membrane structure and function. *J Gen Physiol*. 49:347-354.

Kenworthy, A.K. 2005. Fleeting glimpses of lipid rafts: how biophysics is being used to track them. *J Investig Med*. 53:312-317.

Kim, S.H., and T.A. Ryan. 2009. Synaptic vesicle recycling at CNS snapses without AP-2. *J Neurosci*. 29:3865-3874.

Kragh-Hansen, U., M. le Maire, and J.V. Moller. 1998. The mechanism of detergent solubilization of liposomes and protein-containing membranes. *Biophys J*. 75:2932-2946.

Lajoie, P., and I.R. Nabi. 2007. Regulation of raft-dependent endocytosis. *J Cell Mol Med*. 11:644-653.

Lange, Y., J. Ye, M.E. Duban, and T.L. Steck. 2009. Activation of membrane cholesterol by 63 amphipaths. *Biochemistry*. 48:8505-8515.

Lannergren, J., H. Westerblad, and J.D. Bruton. 2002. Dynamic vacuolation in skeletal muscle fibres after fatigue. *Cell Biol Int*. 26:911-920.

Lariccia, V. xxxx. Calcium-Activated Massive Endocytosis by PIP2 -, Polyamine-, and Cholesterol-Dependent Mechanisms. *J Gen Physiol*. xx:xxx-xxx.

Lariccia, V., M. Fine, S. Magi, M.J. Lin, A. Yaradanakul, M.C. Llaguno, and D.W. Hilgemann. 2011. Massive calcium-activated endocytosis without involvement of classical endocytic proteins. *J Gen Physiol*. 137:111-132.

Levental, I., D.A. Christian, Y.H. Wang, J.J. Madara, D.E. Discher, and P.A. Janmey. 2009. Calcium-dependent lateral organization in phosphatidylinositol 4,5-bisphosphate (PIP2)-and cholesterol-containing monolayers. *Biochemistry*. 48:8241-8248.

Linck, B., Z. Qiu, Z. He, Q. Tong, D.W. Hilgemann, and K.D. Philipson. 1998. Functional comparison of the three isoforms of the Na+/Ca2+ exchanger (NCX1, NCX2, NCX3). *Am J Physiol*. 274:C415-423.

Lindau, M., and E. Neher. 1988. Patch-clamp techniques for time-resolved capacitance measurements in single cells. *Pflugers Arch*. 411:137-146.

Lingwood, D., and K. Simons. Lipid rafts as a membrane-organizing principle. *Science*. 327:46-50.

Lingwood, D., and K. Simons. 2007. Detergent resistance as a tool in membrane research. *Nat Protoc*. 2:2159-2165.

Lingwood, D., and K. Simons. 2010. Lipid rafts as a membrane-organizing principle. *Science*. 327:46-50.

Liu, J., M. Kaksonen, D.G. Drubin, and G. Oster. 2006. Endocytic vesicle scission by lipid phase boundary forces. *Proc Natl Acad Sci U S A*. 103:10277-10282.

Liu, J., Y. Sun, D.G. Drubin, and G.F. Oster. 2009. The mechanochemistry of endocytosis. *PLoS biology*. 7:e1000204.

Liu, Q., and J.D. Molkentin. 2011. Protein kinase Calpha as a heart failure therapeutic target. *J Mol Cell Cardiol*. 51:474-478.

Liu, Y., L. Casey, and L.J. Pike. 1998. Compartmentalization of phosphatidylinositol 4,5-bisphosphate in low-density membrane domains in the absence of caveolin. *Biochem Biophys Res Commun*. 245:684-690.

Lowenstein, C.J., and H. Tsuda. 2006. N-ethylmaleimide-sensitive factor: a redox sensor in exocytosis. *Biol Chem*. 387:1377-1383.

Lu, C.C., A. Kabakov, V.S. Markin, S. Mager, G.A. Frazier, and D.W. Hilgemann. 1995. Membrane transport mechanisms probed by capacitance measurements with megahertz voltage clamp. *Proc Natl Acad Sci U S A*. 92:11220-11224.

Mancuso, D.J., D.R. Abendschein, C.M. Jenkins, X. Han, J.E. Saffitz, R.B. Schuessler, and R.W. Gross. 2003. Cardiac ischemia activates calcium-independent phospholipase A2beta,

precipitating ventricular tachyarrhythmias in transgenic mice: rescue of the lethal electrophysiologic phenotype by mechanism-based inhibition. *J Biol Chem*. 278:22231-22236.

Markin, V.S., and J.P. Albanesi. 2002. Membrane fusion: stalk model revisited. *Biophys J*. 82:693-712.

Marks, B., and H.T. McMahon. 1998. Calcium triggers calcineurin-dependent synaptic vesicle recycling in mammalian nerve terminals. *Curr Biol*. 8:740-749.

Matheny, S.A., C. Chen, R.L. Kortum, G.L. Razidlo, R.E. Lewis, and M.A. White. 2004. Ras regulates assembly of mitogenic signalling complexes through the effector protein IMP. *Nature*. 427:256-260.

Maula, T., B. Westerlund, and J.P. Slotte. 2009. Differential ability of cholesterol-enriched and gel phase domains to resist benzyl alcohol-induced fluidization in multilamellar lipid vesicles. *Biochim Biophys Acta*. 1788:2454-2461.

Maxfield, F.R. 2002. Plasma membrane microdomains. *Current opinion in cell biology*. 14:483-487.

Mayor, S., and R.E. Pagano. 2007. Pathways of clathrin-independent endocytosis. *Nat Rev Mol Cell Biol*. 8:603-612.

Mayor, S., K.G. Rothberg, and F.R. Maxfield. 1994. Sequestration of GPI-anchored proteins in caveolae triggered by cross-linking. *Science*. 264:1948-1951.

Mesquita, R.M., E. Melo, T.E. Thompson, and W.L. Vaz. 2000. Partitioning of amphiphiles between coexisting ordered and disordered phases in two-phase lipid bilayer membranes. *Biophys J*. 78:3019-3025.

Miesenbock, G., D.A. De Angelis, and J.E. Rothman. 1998. Visualizing secretion and synaptic transmission with pH-sensitive green fluorescent proteins. *Nature*. 394:192-195.

Minami, A., and K. Yamada. 2007. Domain-induced budding in buckling membranes. *Eur Phys J E Soft Matter*. 23:367-374.

Moore, E.D., E.F. Etter, K.D. Philipson, W.A. Carrington, K.E. Fogarty, L.M. Lifshitz, and F.S. Fay. 1993. Coupling of the Na+/Ca2+ exchanger, Na+/K+ pump and sarcoplasmic reticulum in smooth muscle. *Nature*. 365:657-660.

Mukherjee, S., R.N. Ghosh, and F.R. Maxfield. 1997. Endocytosis. *Physiol Rev*. 77:759-803.

Mukherjee, S., and F.R. Maxfield. 2004. Membrane domains. *Annual review of cell and developmental biology*. 20:839-866.

Navarro, J., J. Chabot, K. Sherrill, R. Aneja, S.A. Zahler, and E. Racker. 1985. Interaction of duramycin with artificial and natural membranes. *Biochemistry*. 24:4645-4650.

Newton, A.J., T. Kirchhausen, and V.N. Murthy. 2006. Inhibition of dynamin completely blocks compensatory synaptic vesicle endocytosis. *Proc Natl Acad Sci U S A*. 103:17955-17960.

Oberhauser, A.F., and J.M. Fernandez. 1995. Hydrophobic ions amplify the capacitive currents used to measure exocytotic fusion. *Biophys J*. 69:451-459.

Ohtani, Y., T. Irie, K. Uekama, K. Fukunaga, and J. Pitha. 1989. Differential effects of alpha-, beta- and gamma-cyclodextrins on human erythrocytes. *Eur J Biochem*. 186:17-22.

Palaniyandi, S.S., L. Sun, J.C. Ferreira, and D. Mochly-Rosen. 2009. Protein kinase C in heart failure: a therapeutic target? *Cardiovasc Res*. 82:229-239.

Parton, R.G., B. Joggerst, and K. Simons. 1994. Regulated internalization of caveolae. *J Cell Biol*. 127:1199-1215.

Pavoine, C., and F. Pecker. 2009. Sphingomyelinases: their regulation and roles in cardiovascular pathophysiology. *Cardiovasc Res*. 82:175-183.

Pickar, A.D., and W.C. Brown. 1983. Capacitance of bilayers in the presence of lipophilic ions. *Biochim Biophys Acta*. 733:181-185.

Plasek, J., and K. Sigler. 1996. Slow fluorescent indicators of membrane potential: a survey of different approaches to probe response analysis. *J Photochem Photobiol B*. 33:101-124.

Rajendran, L., and K. Simons. 2005. Lipid rafts and membrane dynamics. *J Cell Sci*. 118:1099-1102.

Ramu, Y., Y. Xu, and Z. Lu. 2007. Inhibition of CFTR Cl- channel function caused by enzymatic hydrolysis of sphingomyelin. *Proc Natl Acad Sci U S A*. 104:6448-6453.

Rizo, J. 2003. SNARE function revisited. *Nat Struct Biol*. 10:417-419.

Romer, W., L.L. Pontani, B. Sorre, C. Rentero, L. Berland, V. Chambon, C. Lamaze, P. Bassereau, C. Sykes, K. Gaus, and L. Johannes. 2010. Actin dynamics drive membrane reorganization and scission in clathrin-independent endocytosis. *Cell*. 140:540-553.

Rosenboom, H., and M. Lindau. 1994. Exo-endocytosis and closing of the fission pore during endocytosis in single pituitary nerve terminals internally perfused with high calcium concentrations. *Proc Natl Acad Sci U S A*. 91:5267-5271.

Sandvig, K., M.L. Torgersen, H.A. Raa, and B. van Deurs. 2008. Clathrin-independent endocytosis: from nonexisting to an extreme degree of complexity. *Histochem Cell Biol*. 129:267-276.

Sarasij, R.C., S. Mayor, and M. Rao. 2007. Chirality-induced budding: a raft-mediated mechanism for endocytosis and morphology of caveolae? *Biophys J*. 92:3140-3158.

Sato, K., G.G. Ernstrom, S. Watanabe, R.M. Weimer, C.H. Chen, M. Sato, A. Siddiqui, E.M. Jorgensen, and B.D. Grant. 2009. Differential requirements for clathrin in receptor-mediated endocytosis and maintenance of synaptic vesicle pools. *Proc Natl Acad Sci U S A*. 106:1139-1144.

Sawai, H., and N. Domae. 2009. Differential roles for Bak in Triton X-100- and deoxycholate-induced apoptosis. *Biochem Biophys Res Commun*. 378:529-533.

Schuber, F., K. Hong, N. Duzgunes, and D. Papahadjopoulos. 1983. Polyamines as modulators of membrane fusion: aggregation and fusion of liposomes. *Biochemistry*. 22:6134-6140.

Schutz, G.J., G. Kada, V.P. Pastushenko, and H. Schindler. 2000. Properties of lipid microdomains in a muscle cell membrane visualized by single molecule microscopy. *EMBO J*. 19:892-901.

Sharma, D.K., J.C. Brown, Z. Cheng, E.L. Holicky, D.L. Marks, and R.E. Pagano. 2005. The glycosphingolipid, lactosylceramide, regulates beta1-integrin clustering and endocytosis. *Cancer Res*. 65:8233-8241.

Shen, C., M.J. Lin, A. Yaradanakul, V. Lariccia, J.A. Hill, and D.W. Hilgemann. 2007. Dual control of cardiac Na+ Ca2+ exchange by PIP(2): analysis of the surface membrane fraction by extracellular cysteine PEGylation. *J Physiol*. 582:1011-1026.

Shigeno, T., M. Katakuse, T. Fujita, Y. Mukoyama, and H. Watanabe. 2009. Phthalate ester-induced thymic stromal lymphopoietin mediates allergic dermatitis in mice. *Immunology*. 128:e849-857.

Simons, K., and R. Ehehalt. 2002. Cholesterol, lipid rafts, and disease. *The Journal of clinical investigation*. 110:597-603.

Simons, K., and M.J. Gerl. 2010. Revitalizing membrane rafts: new tools and insights. *Nat Rev Mol Cell Biol*. 11:688-699.

Simons, K., and E. Ikonen. 1997. Functional rafts in cell membranes. *Nature*. 387:569-572.

Simons, K., and J.L. Sampaio. 2011. Membrane organization and lipid rafts. *Cold Spring Harbor perspectives in biology*. 3:a004697.

Singer, S.J., and G.L. Nicolson. 1972. The fluid mosaic model of the structure of cell membranes. *Science*. 175:720-731.

Smejtek, P., and S.R. Wang. 1990. Adsorption to dipalmitoylphosphatidylcholine membranes in gel and fluid state: pentachlorophenolate, dipicrylamine, and tetraphenylborate. *Biophys J*. 58:1285-1294.

Smillie, K.J., and M.A. Cousin. 2005. Dynamin I phosphorylation and the control of synaptic vesicle endocytosis. *Biochem Soc Symp*:87-97.

Smith, C., and E. Neher. 1997. Multiple forms of endocytosis in bovine adrenal chromaffin cells. *J Cell Biol*. 139:885-894.

Song, B.D., M. Leonard, and S.L. Schmid. 2004. Dynamin GTPase domain mutants that differentially affect GTP binding, GTP hydrolysis, and clathrin-mediated endocytosis. *J Biol Chem*. 279:40431-40436.

Sprong, H., P. van der Sluijs, and G. van Meer. 2001. How proteins move lipids and lipids move proteins. *Nat Rev Mol Cell Biol*. 2:504-513.

Staneva, G., A. Momchilova, C. Wolf, P.J. Quinn, and K. Koumanov. 2009. Membrane microdomains: role of ceramides in the maintenance of their structure and functions. *Biochim Biophys Acta*. 1788:666-675.

Staneva, G., M. Seigneuret, K. Koumanov, G. Trugnan, and M.I. Angelova. 2005. Detergents induce raft-like domains budding and fission from giant unilamellar heterogeneous vesicles: a direct microscopy observation. *Chem Phys Lipids*. 136:55-66.

Stefan, C.J., A. Audhya, and S.D. Emr. 2002. The yeast synaptojanin-like proteins control the cellular distribution of phosphatidylinositol (4,5)-bisphosphate. *Mol Biol Cell*. 13:542-557.

Subczynski, W.K., and A. Kusumi. 2003. Dynamics of raft molecules in the cell and artificial membranes: approaches by pulse EPR spin labeling and single molecule optical microscopy. *Biochim Biophys Acta*. 1610:231-243.

Swanson, J.A., and C. Watts. 1995. Macropinocytosis. *Trends Cell Biol*. 5:424-428.

Takahashi, A., P. Camacho, J.D. Lechleiter, and B. Herman. 1999. Measurement of intracellular calcium. *Physiol Rev*. 79:1089-1125.

Tam, C., V. Idone, C. Devlin, M.C. Fernandes, A. Flannery, X. He, E. Schuchman, I. Tabas, and N.W. Andrews. 2010. Exocytosis of acid sphingomyelinase by wounded cells promotes endocytosis and plasma membrane repair. *J Cell Biol*. 189:1027-1038.

Taylor, P.R., L. Martinez-Pomares, M. Stacey, H.H. Lin, G.D. Brown, and S. Gordon. 2005. Macrophage receptors and immune recognition. *Annual review of immunology*. 23:901-944.

Thomas, P., A.K. Lee, J.G. Wong, and W. Almers. 1994. A triggered mechanism retrieves membrane in seconds after Ca(2+)-stimulated exocytosis in single pituitary cells. *J Cell Biol*. 124:667-675.

Togo, T., J.M. Alderton, G.Q. Bi, and R.A. Steinhardt. 1999. The mechanism of facilitated cell membrane resealing. *J Cell Sci*. 112 (Pt 5):719-731.

Tomita, M., R. Taguchi, and H. Ikezawa. 1983. Adsorption of sphingomyelinase of Bacillus cereus onto erythrocyte membranes. *Arch Biochem Biophys*. 223:202-212.

van Blitterswijk, W.J., and M. Verheij. 2008. Anticancer alkylphospholipids: mechanisms of action, cellular sensitivity and resistance, and clinical prospects. *Curr Pharm Des*. 14:2061-2074.

van de Ven, A.L., K. Adler-Storthz, and R. Richards-Kortum. 2009. Delivery of optical contrast agents using Triton-X100, part 1: reversible permeabilization of live cells for intracellular labeling. *J Biomed Opt*. 14:021012.

van der Luit, A.H., S.R. Vink, J.B. Klarenbeek, D. Perrissoud, E. Solary, M. Verheij, and W.J. van Blitterswijk. 2007. A new class of anticancer alkylphospholipids uses lipid rafts as membrane gateways to induce apoptosis in lymphoma cells. *Mol Cancer Ther*. 6:2337-2345.

van Meer, G., D.R. Voelker, and G.W. Feigenson. 2008. Membrane lipids: where they are and how they behave. *Nat Rev Mol Cell Biol*. 9:112-124.

van Rheenen, J., E.M. Achame, H. Janssen, J. Calafat, and K. Jalink. 2005. PIP2 signaling in lipid domains: a critical re-evaluation. *EMBO J*. 24:1664-1673.

Veatch, S.L., and S.L. Keller. 2003. Separation of liquid phases in giant vesicles of ternary mixtures of phospholipids and cholesterol. *Biophys J*. 85:3074-3083.

Vicogne, J., D. Vollenweider, J.R. Smith, P. Huang, M.A. Frohman, and J.E. Pessin. 2006. Asymmetric phospholipid distribution drives in vitro reconstituted SNARE-dependent membrane fusion. *Proc Natl Acad Sci U S A*. 103:14761-14766.

Vidricaire, G., and M.J. Tremblay. 2007. A clathrin, caveolae, and dynamin-independent endocytic pathway requiring free membrane cholesterol drives HIV-1 internalization and infection in polarized trophoblastic cells. *J Mol Biol*. 368:1267-1283.

Vind-Kezunovic, D., C.H. Nielsen, U. Wojewodzka, and R. Gniadecki. 2008. Line tension at lipid phase boundaries regulates formation of membrane vesicles in living cells. *Biochim Biophys Acta*. 1778:2480-2486.

Vogel, S.S., R.M. Smith, B. Baibakov, Y. Ikebuchi, and N.A. Lambert. 1999. Calcium influx is required for endocytotic membrane retrieval. *Proc Natl Acad Sci U S A*. 96:5019-5024.

Wang, T.M., and D.W. Hilgemann. 2008. Ca-dependent nonsecretory vesicle fusion in a secretory cell. *J Gen Physiol*. 132:51-65.

Wasser, C.R., M. Ertunc, X. Liu, and E.T. Kavalali. 2007. Cholesterol-dependent balance between evoked and spontaneous synaptic vesicle recycling. *J Physiol*. 579:413-429.

Wei, S., A. Guo, B. Chen, W. Kutschke, Y.P. Xie, K. Zimmerman, R.M. Weiss, M.E. Anderson, H. Cheng, and L.S. Song. 2010. T-tubule remodeling during transition from hypertrophy to heart failure. *Circ Res*. 107:520-531.

Williamson, Ryan "Fuqwad", "The Dong Song" Wang, A.S. Haberman, and P.R. Hiesinger. 2010. A dual function of V0-ATPase a1 provides an endolysosomal degradation mechanism in Drosophila melanogaster photoreceptors. *J Cell Biol*. 189:885-899.

Wu, X.S., B.D. McNeil, J. Xu, J. Fan, L. Xue, E. Melicoff, R. Adachi, L. Bai, and L.G. Wu. 2009. Ca(2+) and calmodulin initiate all forms of endocytosis during depolarization at a nerve terminal. *Nat Neurosci*. 12:1003-1010.

Xu, J., B. McNeil, W. Wu, D. Nees, L. Bai, and L.G. Wu. 2008. GTP-independent rapid and slow endocytosis at a central synapse. *Nat Neurosci*. 11:45-53.

Yan, W., C.M. Jenkins, X. Han, D.J. Mancuso, H.F. Sims, K. Yang, and R.W. Gross. 2005. The highly selective production of 2-arachidonoyl lysophosphatidylcholine catalyzed by purified calcium-independent phospholipase A2gamma: identification of a novel enzymatic mediator for the generation of a key branch point intermediate in eicosanoid signaling. *J Biol Chem*. 280:26669-26679.

Yanagisawa, M., M. Imai, T. Masui, S. Komura, and T. Ohta. 2007. Growth dynamics of domains in ternary fluid vesicles. *Biophys J*. 92:115-125.

Yaradanakul, A., S. Feng, C. Shen, V. Lariccia, M.J. Lin, J. Yang, T.M. Kang, P. Dong, H.L. Yin, J.P. Albanesi, and D.W. Hilgemann. 2007. Dual control of cardiac Na+ Ca2+ exchange by PIP(2): electrophysiological analysis of direct and indirect mechanisms. *J Physiol*. 582:991-1010.

Yaradanakul, A., and D.W. Hilgemann. 2007. Unrestricted diffusion of exogenous and endogenous PIP(2)in baby hamster kidney and Chinese hamster ovary cell plasmalemma. *J Membr Biol*. 220:53-67.

Yaradanakul, A., T.M. Wang, V. Lariccia, M.J. Lin, C. Shen, X. Liu, and D.W. Hilgemann. 2008. Massive Ca-induced membrane fusion and phospholipid changes triggered by reverse Na/Ca exchange in BHK fibroblasts. *J Gen Physiol*. 132:29-50.

Yarmola, E.G., T. Somasundaram, T.A. Boring, I. Spector, and M.R. Bubb. 2000. Actin-latrunculin A structure and function. Differential modulation of actin-binding protein function by latrunculin A. *J Biol Chem*. 275:28120-28127.

Yoshimori, T., A. Yamamoto, Y. Moriyama, M. Futai, and Y. Tashiro. 1991. Bafilomycin A1, a specific inhibitor of vacuolar-type H(+)-ATPase, inhibits acidification and protein degradation in lysosomes of cultured cells. *J Biol Chem*. 266:17707-17712.

Zachowski, A. 1993. Phospholipids in animal eukaryotic membranes: transverse asymmetry and movement. *Biochem J*. 294 (Pt 1):1-14.

Zha, X., L.M. Pierini, P.L. Leopold, P.J. Skiba, I. Tabas, and F.R. Maxfield. 1998. Sphingomyelinase treatment induces ATP-independent endocytosis. *J Cell Biol*. 140:39-47.

Zhang, A.Y., F. Yi, S. Jin, M. Xia, Q.Z. Chen, E. Gulbins, and P.L. Li. 2007. Acid sphingomyelinase and its redox amplification in formation of lipid raft redox signaling platforms in endothelial cells. *Antioxidants & redox signaling*. 9:817-828.

Zhang, B., Y.H. Koh, R.B. Beckstead, V. Budnik, B. Ganetzky, and H.J. Bellen. 1998. Synaptic vesicle size and number are regulated by a clathrin adaptor protein required for endocytosis. *Neuron*. 21:1465-1475.